Understanding roles for PARP1 in skeletal muscle

By

Arnold Tan

A thesis submitted to the Nottingham Trent University

for the degree of

DOCTOR OF PHILOSOPHY

Interdisciplinary Science and Technology Centre (ISTeC)

School of Science and Technology

Nottingham Trent University

January 2023

Abstract

Depletion of Nicotinamide adenine dinucleotide (NAD^+), a critical cofactor in biochemical reactions, is ascribed to metabolic dysfunction and poor quality of life. The NAD^+ consuming enzyme Poly-(ADP-ribose) polymerase 1 (PARP1) generates ADP-ribose (ADPR), applied as a form of post-translational modification termed Poly (ADP-ribosyl)ation (PARylation), crucial for genome maintenance. However, recent work has ascertained further roles including energy homeostasis and cellular identity.

This work aimed to identify PARP1 mediated PARylation within skeletal muscle myoblast cell lines that undergo myogenesis into myotubes. PARP1 PARylation was inhibited at the start of myogenesis to ascertain its dynamics and impacts throughout myogenesis. Further downstream impacts of PARP1 inhibited differentiated myotubes were investigated using proteomic and transcriptomic approaches. PARP1 and PAR dynamics within tissues of mice subjected to various metabolic challenges were also assessed.

While not fundamental for myotube development, myotubes subjected to PARP1 inhibition at the start of myogenesis exhibited impacts on expression of genes and proteins key for structure and function, and additionally, the transcriptional response to glucocorticoids. These underscore PARP1 impacts in pathways mutual to actions of glucocorticoids, which act as regulators of skeletal muscle mass, myogenesis and atrophy, as well as protein metabolism.

Overall, this work highlights how PARP1 mediated PARylation impacts skeletal muscle homeostasis – mechanisms crucial to mass maintenance and endocrine response.

For Mum and Dad,

who have both assiduously raised me

into the best version of myself

Acknowledgements

First and foremost, I would like to express heartfelt gratitude to my supervisor Craig for his immeasurable advice and support be it scientific or personally, throughout my PhD journey. These were most evident throughout the stages of the pandemic which proved to be some of the toughest, challenging and crestfallen times of my life where I felt like giving up on this journey altogether. Craig, it's the biggest privilege to have been your first PhD student, thank you.

My gratitude also goes to my co-supervisors, Amanda Coutts and Prof. Craig Sale for their valuable feedback on this work throughout. Additionally, I would like to extend appreciation to Prof. Gareth Lavery at the University of Birmingham for his influence on my scientific development, and his kindness in making the *in vivo* work to supplement this thesis possible. Also at the University of Birmingham, I couldn't be more grateful to Yu-Chiang Lai for his support and mentorship from my early days as a scientist. I also extend my indebtedness to David Boocock and Clare Coveney at NTU, for which the omics work within this thesis wouldn't be possible without their expertise.

Unequivocally, I would like to express gratitude for past and present members of the Doig lab including Alex, Jade and Awais for making the environment lively which helped the daily lab work not feel like a grind. I also want to thank the diverse and brilliant colleagues at ISTeC (Cristina, Tameille, Abha, Nikoletta, Satinder, Alice, Jess, Rhianna, Dan), as well as those who have had influence in my PhD and career development, including Rich and Sam. Particularly, Nikky, Jade and Lydia – Nikky, thank you for being there from day one to listen to all of my life problems throughout and the gossip which is now

essentially part of my daily macros. Jade, having mentored and watched you develop into the scientist you are today couldn't have made me any more proud and I'm sure you will go on to write a great thesis and move on to do great things. Lydia, thank you for all of the car rides to places I never thought I'd get to see.

6760 miles away, I am also immensely grateful for my friends Joshua, Clarence and Vanan – while few in number, I can trust all of you with my life, although I hope one of them (you know who you are) doesn't disappear if it ever got down to that! Wei Lee, while we're just 570 miles away from each other now, I'm grateful for the opportunity to work together back then and your teachings in the lab as well as our close friendship which not many people will get with former co-workers. Also, special appreciation to the 6am workout crew at Gymmboxx for spotting me miles away during this journey.

To my family – Aaron, thank you for keeping everyone together throughout my absence. Ariel, I couldn't be more proud of you as a brother and having a more trustworthy brother-in-law in Joo to care for you for the rest of your life. Also the doggos, Aries, Ashley, Kobee and now Bagel, I look forward to visiting all of you and giving some overdue belly rubs and cuddles!

Lastly, Mum and Dad. The two strongest pillars in my life. Thank you for instilling onto me the values I will always hold close to my heart. Thank you for being there to celebrate my proudest moments, as well as being there to soothe my mistakes, my pain and my tears during my lowest. And thank you for giving me life and love. I love both of you and I hope as proud as I am to be your son you would both be equally proud of the man I have become.

Table of Contents

List of Figures

List of Tables

List of Publications

Tan, A., Younis, A. Z., Evans, A., Creighton, J. V., Coveny, C., Boocock, D. J., Sale, C., Lavery, G. G., Coutts, A. S., & Doig, C. L. (2023). PARP1 mediated PARylation contributes to myogenic progression and glucocorticoid transcriptional response. *Cell Death Discovery 2023* 9:1, 9(1), 1–13.

Tan, A., & Doig, C. L. (2021). NAD^+ Degrading Enzymes, Evidence for Roles During Infection. *Frontiers in Molecular Biosciences*, *8*, 803.

Lavilla, C. J., Billacura, M. P., Hanna, K., Boocock, D. J., Coveney, C., Miles, A. K., Foulds, G. A., Murphy, A., **Tan, A.**, Jackisch, L., Sayers, S. R., Caton, P. W., Doig, C. L., McTernan, P. G., Colombo, S. L., Sale, C., & Turner, M. D. (2021). Carnosine protects stimulus-secretion coupling through prevention of protein carbonyl adduction events in cells under metabolic stress. *Free Radical Biology and Medicine*, *175*, 65–79.

Abbreviations

Acetyl CoA	Acetyl coenzyme A
ADP	Adenosine diphosphate
ADPR	ADP-ribose
AMP	Adenosine monophosphate
AMPK	AMP-activated protein kinase
ANOVA	Analysis of Variance
ARH3	ADP-ribosylhydrolase 3
ART	ADP-ribosyltransferase
ARTC	ecto-ADPR transferase
ATF2	Activating transcription factor 2
ATP	Adenosine triphosphate
BRCT	Breast Cancer Associated 1 C-terminal domain
BSA	Bovine serum albumin
Ca^{2+}	Calcium
cADPR	Cyclic ADP-ribose
CBG	Corticosteroid-binding globulins
CBX6	Chromobox 6
cDNA	Complementary DNA
CHD1L	Chromodomain Helicase DNA Binding Protein 1
ChIP	Chromatin immunoprecipitation
CO_2	Carbon dioxide
CoA	Coenzyme A
CREB	cAMP response element-binding protein
Ct	Threshold cycle
DBD	DNA binding domain
DM	Differentiation media
DMEM	Dulbecco's Modified Eagle's Medium
DMSO	Dimethyl sulfoxide
DNA	Deoxyribonucleic acid
dNTP	Deoxynucleotide triphosphate
dsDNA	Double stranded DNA
ECL	Enhanced chemiluminescence
FADH	Flavin adenine dinucleotide
FBS	Foetal bovine serum
FDR	False discovery rate
FGF2	Fibroblast growth factor 2
FOXO1	Forkhead box protein O1
FPKM	Fragments per kilobase of transcript per million reads mapped
GAPDH	Glyceraldehyde 3-phosphate dehydrogenase
GLUT	Glucose transporter

GM	Growth media
GR	Glucocorticoid Receptor
GRE	Glucocorticoid response element
GRP78/BiP	Glucose-regulated protein of 78 kDa/ immunoglobulin heavy-chain-binding protein
GYS1	Glycogen synthase 1
H6PD	Hexose-6-phosphate dehydrogenase
HD	Helical subdomain
HDAC6	Histone deacetylase 6
HIF1α	Hypoxia-inducible factor 1-alpha
HIPK2	Homeodomain-interacting protein kinase 2
HPA	Hypothalamus–pituitary–adrenal axis
HPF1	Histone PARylation factor 1
HRP	Horseradish peroxidase
HS	Horse serum
HSD11β1	11β-hydroxysteroid dehydrogenase 1
HSD11β2	11β-hydroxysteroid dehydrogenase 2
HSP70	Heat shock protein 70 kDa
IDA	Information-dependent acquisition
IL1/6	Interleukin 1/6
IP	Immunoprecipitation
KO	Knockout
KOH	Potassium hydroxide
LBD	Ligand binding domain
LC-MS	Liquid chromatography coupled with mass spectrometry
LKLF	Lung Krüppel-like Factor
MAR	Mono ADP-ribose
MARylation	Mono-ADP-ribosylation
MR	Mineralocorticoid receptor
MRFs	Myogenic regulatory factors
MT2	Metallothionein 2
mtDNA	Mitochondrial DNA
MYF5/6	Myogenic factor 5/6
MYL1/4	Myosin light chain 1/4
MYMK	Myomaker, Myoblast Fusion Factor
MyoD	Myogenic differentiation protein 1
NA	Nicotinic acid
NaAD	Nicotinate adenine dinucleotide
NAD(H)	Nicotinamide adenine dinucleotide
NADase	Nicotinamide adenine dinucleotide glycohydrolase
NADP(H)	Nicotinamide adenine dinucleotide phosphate
NADS	Nicotinamide adenine dinucleotide synthase

NAM	Nicotinamide
NAMN	Nicotinic Acid Mononucleotide
NAMPT	Nicotinamide phosphoribosyltransferase
NAPRT	Nicotinate phosphoribosyltransferase
NES	Normalized enrichment score
NFAT	Nuclear factor of activated T cell
NF-kB	Nuclear factor kappa B
NFW	Nuclease free water
NMN	Nicotinamide mononucleotide
NMNAT	Nicotinamide mononucleotide adenylyl transferase
NMRK	Nicotinamide riboside kinase
NR(H)	Nicotinamide riboside
NRF	Nuclear respiratory factor
NRK2.Tg	NRK2 transgenic
NTD	N-terminal domain
OAADPr	O-Acetyl-ADP-ribose
OGG1	8-oxoguanine-DNA glycosylase
P/S	Penicillin/Streptomycin
p38 MAPK	p38 mitogen-activated protein kinase
PAR	Poly-ADP-ribose
PARG	Poly-ADP-ribose glycohydrolase
PARP	Poly-(ADP-ribose) polymerase
PARylation	Poly (ADP-ribosyl)ation
PBS	Phosphate buffered saline
PCR	Polymerase chain reaction
PCr	Creatine phosphate
PDGF-BB	Platelet-derived growth factor BB
PFA	Paraformaldehyde
PGC1α	Peroxisome proliferator-activated receptor gamma coactivator 1-alpha
Pi	Inorganic phosphate
PPAR	Peroxisome proliferator-activated receptor
PTF1	Pancreas transcription factor 1
PTMA	Prothymosin Alpha
PVDF	Polyvinylidene fluoride
qPCR	Quantitative polymerase chain reactionm
QPRT	Quinolinate phosphoribosyltransferases
RGB	Red-green-blue
RNA	Ribonucleic Acid
RNase	Ribonuclease
RNAseq	RNA sequencing
ROS	Reactive oxygen species
RPM	Rotations per minute

RT	Room temperature
SARM1	Sterile alpha and Toll/Interleukin 1 receptor motif-containing 1
SCD2	Stearoyl-Coenzyme A desaturase 2
SDS	Sodium dodecyl sulfate
SDS-PAGE	Sodium dodecyl sulfate–polyacrylamide gel electrophoresis
SEM	Standard error of mean
siPARP1	siRNA transient knockdown of PARP1
SIR2	Silent Information Regulator 2
siRNA	Small interfering ribonucleic acid
SIRT	Sirtuin
Sox2	Sex determining region Y box 2
STIM2	Stromal interaction molecule 2
SWATH-MS	Sequential window acquisition of all theoretical mass spectra
TA	Tibialis anterior
TBST	Tris-buffered saline with Tween 20
TCA cycle	Tricarboxylic acid cycle
TIR	Toll interleukin 1 receptor
TNFα	Tumour necrosis factor alpha
TNNT	Troponin type
TRPM2	Transient receptor potential cation channel subfamily M member 2
v/v	Volume/volume
VEGF	Vascular endothelial growth factor
w/v	Weight/volume
WT	Wild-type
XRCC1	X-ray Cross Complementing Group 1
YY1	Yin Yang 1
ZF	Zinc finger
ΔCt	Delta Ct
ΔΔCt	Delta ΔCt

Amino Acid Code

Amino Acid	Three letter symbol	Single letter symbol
Alanine	Ala	A
Arginine	Arg	R
Asparagine	Asn	N
Aspartic acid	Asp	D
Cysteine	Cys	C
Glutamic acid	Glu	E
Glutamine	Gln	Q
Glycine	Gly	G
Histidine	His	H
Isoleucine	Ile	I
Leucine	Leu	L
Lysine	Lys	K
Methionine	Met	M
Proline	Pro	P
Serine	Ser	S
Threonine	Thr	T
Tryptophan	Trp	W
Tyrosine	Tyr	Y
Valine	Val	V
Any other amino acid	Xaa	X

Chapter 1

General Introduction

This thesis will investigate molecular mechanisms of the nicotinamide adenine dinucleotide (NAD) consuming enzyme Poly-(ADP-ribose) polymerase 1 (PARP1) within skeletal muscle tissue and cells. Fundamental roles of skeletal muscle include contributions to overall metabolic health and whole-body homeostasis. It helps determine basal energy metabolism and organism locomotion. NAD is an enzyme cofactor and REDOX molecule present mainly as oxidized (NAD^+) or reduced (NADH) and is a rate-limiting cofactor for critical processes including glycolysis and formation of the post-translational modification ADP-ribosylation. Ratios of NAD^+/NADH have been reported within skeletal muscle subcellular components and impacts on cellular bioenergetics, REDOX states and substrate utilization in response to stress have been described [1]. Declines in NAD^+ have been ascribed to aging and age-associated metabolic disorder phenotypes [2]. Given that PARP1 levels and activity are increased in aging tissues [3], it has been implicated in the exacerbation of cellular NAD^+ decline. Whilst PARP1 roles in genome repair and stability are well-studied, elucidation of any nongenomic roles PARP1 plays in skeletal muscle would help provide new avenues for PARP1 targeted therapeutic development in ameliorating skeletal muscle decline.

1.1. Skeletal Muscle

Skeletal muscle is a contractile tissue composed of an intricate mix of multi-nucleated fibres known as myofibres, embedded within a connective tissue matrix and subsequently integrated within neural and vascular networks [4]. Accounting for up to 50% of total body mass and 50 to 75% of all body proteins in healthy adult individuals, skeletal muscle is for most humans, the largest organ in the human body. Amongst the plethora of functions such as

locomotion and glucose metabolism, skeletal muscle has crucial implications for whole body metabolic homeostasis. This is a result of its contributions to nutrient storage, basal metabolic rate and thermogenesis for maintenance of core body temperature [5]. Its functional significance is evident in aging individuals who experience natural declines in skeletal muscle mass and contractile force of these tissue, which can be clinically diagnosed as sarcopenia or further exacerbated by a whole-body wasting condition known as cachexia [6]. Consequently, skeletal muscle is a sensitive organ whereby its health is dependent on a multitude of factors such as diet and lifestyle, as well as exposure to endocrine/paracrine hormones such as glucocorticoids, androgens and estrogens. Therefore, maintenance of healthy skeletal muscle mass and function is necessary for an optimal quality of life. Currently, nearly 1.7 billon people experience musculoskeletal dysfunction alongside non-communicative chronic ill health. This makes preservation of muscle function and tissue mass a key health priority across the globe. However, no current medication exists that can positively impact muscle mass. There is therefore, an urgent unmet need to generate new potential therapies to intervene.

1.1.1. Structure and function

Skeletal muscle is one of the three main muscle types that typically exhibit as multi-nucleated and cylindrical shaped cells called myofibres. These are proximally attached to bones to enable voluntary movement controlled by the somatic nervous system [7], with the other two types being smooth and cardiac muscle. Within skeletal muscle, each individual myofibre is coated with a layer of connective tissue known as the endomysium. These fibres are further bundled tightly as fascicles which are subsequently wrapped by another layer

of tissue known as the perimysium. An outer layer of connective tissue, the epimysium, surrounds the entire muscle structure and is responsible for the reduction of friction against other muscles and bones [4,8] (Fig. 1.1).

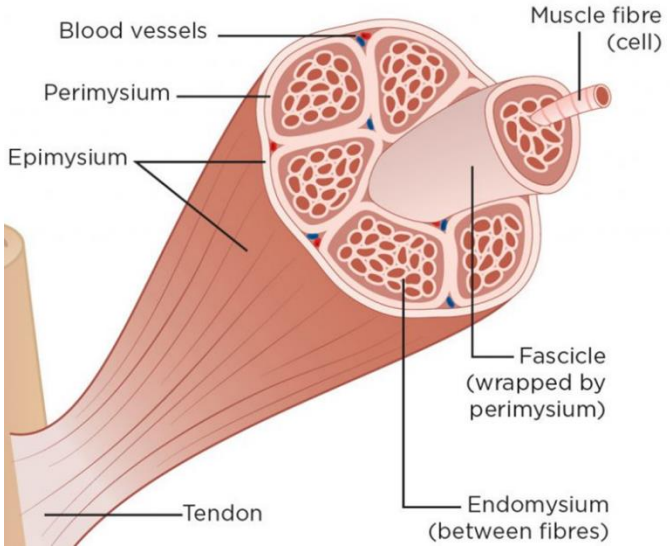

Figure 1.1. Overview of skeletal muscle structure
The epimysium is a layer of connective tissue which wraps around each muscle in the body that is tightly bundled into muscle fibres within the perimysium. Individual fibres are then sheathed within the endomysium. Subsequently, these connective tissues are proximally attached to bones via the muscle tendon [403].

Myofibres are further composed of filaments termed myofibrils that subsequently extend across the entire fibre. Myofibrils are further composed of myofilaments which are subdivided into either thin or thick filaments. Thin filaments are composed of an actin-tropomyosin-troponin muscle protein complex, while thick filaments are predominantly composed of myosin [9,10]. Each of these filaments are surrounded by the sarcoplasmic reticulum that is fundamental for skeletal muscle contraction and other signalling process through their calcium (Ca^{2+}) ion storage capacity [11]. The subsequent parallel arrangement of thin and thick filaments within the myofibrils forms the sarcomere, and repeated alignments of sarcomeres gives rise to the characteristic striated appearance of skeletal muscle and collectively entails

muscle contraction [4]. The sarcomere is then further split into regions based on appearance – the A-band, also known as the anisotropic region and the I-band, which is a lighter isotropic region. Each individual sarcomere unit is then divided by a Z-line (Fig. 1.2).

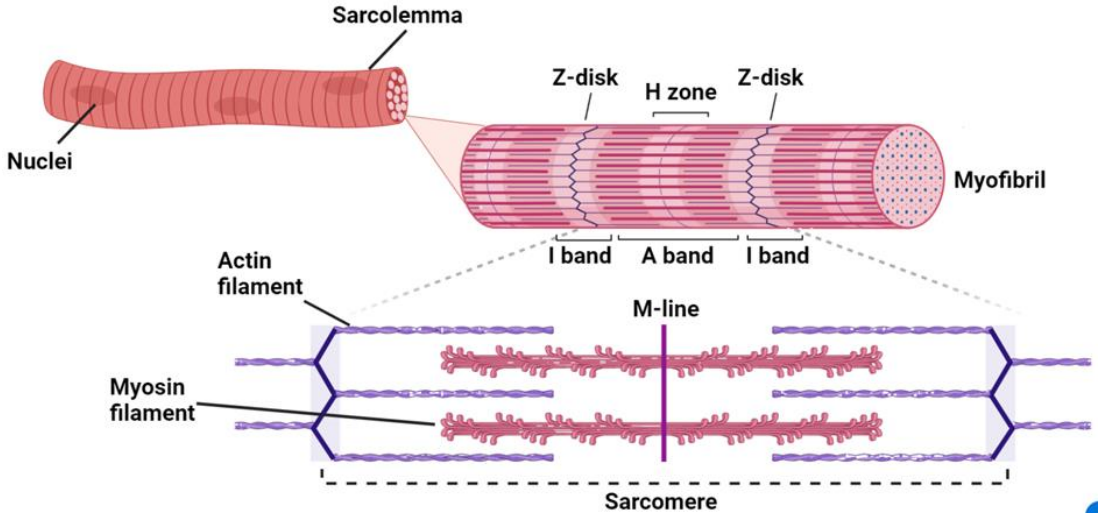

Figure 1.2. Simplified representation of individual myofibres
Myofibres are arranged in an intricate matrix. Individual myofibrils are composed of thick and thin myofilaments that are aligned in parallel to one another forms the sarcomere which is fundamental for voluntary muscle contraction.

Skeletal muscle is the predominant component of the musculoskeletal system that is fundamental for whole body locomotion, physiological respiration, posture and stability. These functions are dependent on voluntary muscle contraction, which occurs through a series of excitation-coupling events mediated by motor neuron inputs from the somatic nervous system [12]. Action potentials travel across the span of the muscle cell membrane known as the sarcolemma induces the depolarisation of t-tubules and release of Ca^{2+} ions from the sarcoplasmic reticulum into the sarcoplasm of muscle cells [13]. Within the sarcoplasm, Ca^{2+} ions interact with Troponin C, causing a conformational change in the actin-tropomyosin-troponin complex filaments that exposes actin for interaction with head groups of myosin filaments to form an actin-myosin cross bridge [12]. Adenosine triphosphate (ATP) binds to the myosin

heads, causing dissociation of the cross bridge and hydrolyses ATP into adenosine diphosphate (ADP) and inorganic phosphate (Pi). This induces a further conformational change in the angle of the myosin head and formation of an actin-myosin bond, which enables movement along the actin filament and shortening of the sarcomere in an event termed as the power stroke to ultimately result in muscle contraction. Subject to further ATP and Ca^{2+} availability within the sarcoplasm, ATP binds to the actin-myosin cross bridge and this event is repeated, allowing filaments to slide over each other. This molecular mechanism of muscle contraction is known as the 'sliding filament theory', processes highly conserved across mammalians [14–16] (Fig. 1.3).

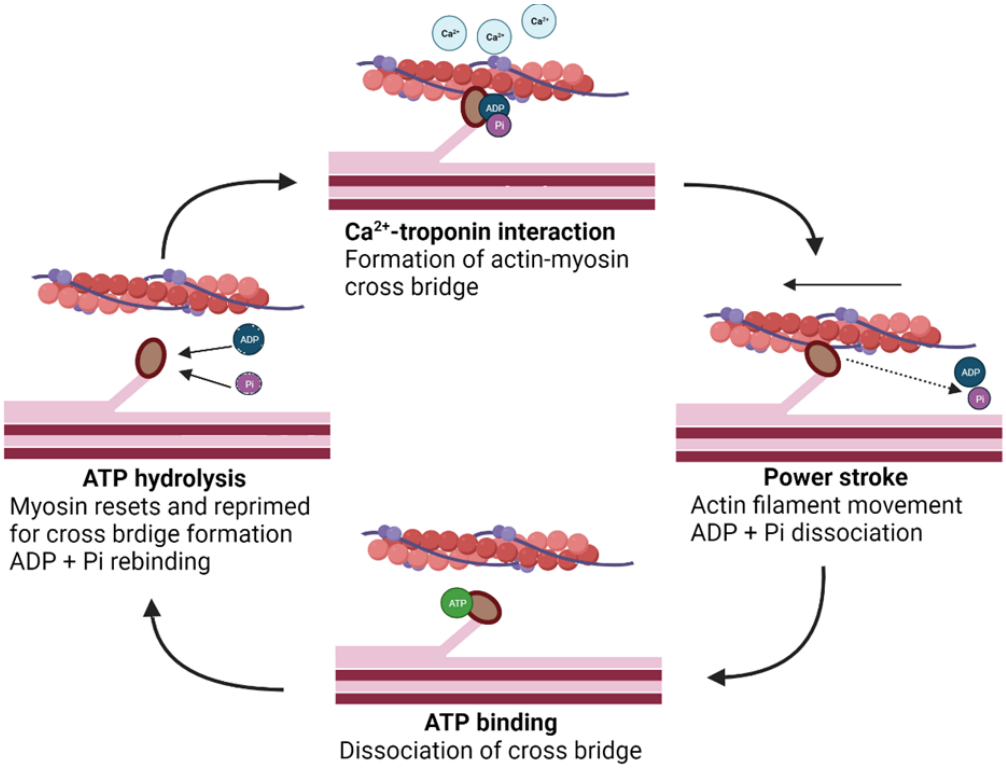

Figure 1.3. The sliding filament theory
Interaction of actin and myosin units occur via a cross bridge following the binding of Ca^{2+} ions to troponin C. Confirmational changes within myosin heads and sarcomere shortening following the release of ADP and Pi causes the power stroke which allows movement of actin filaments relative to myosin to drive muscle contraction. Subject to availability, ATP can bind and dissociate the cross bridge to reset the contraction cycle.

1.1.2. Skeletal muscle fibre types

Skeletal muscle exhibits distinct cell and fibre types with differing structural, functional and energetic properties for adaptions to day to day activities [17]. Fibre types are classified based on the differential expression profiles of the myosin heavy chain (MYH) isoforms, MYH1, MYH2, MYH4 or MYH7 [18,19] (Table 1.1). Subsequently, three fibre types have been described in humans: Type 1, Type 2A and Type 2X (or Type 2B in rodents). Type 1 fibres, commonly referred as slow-twitch oxidative fibres, derive energy from oxidative metabolism and aerobic respiration [20]. In contrast, Type 2X or 2B fibres, also known as fast-twitch glycolytic fibres, rely primarily on glycolysis for energy generation, and Type 2A fibres are fast-twitch oxidative fibres that are an intermediate between that of Type 1 and Type 2X or 2B fibres [17] (Table 1.1). Generally, fibre types are mixed within an individual muscle, which is dependent on a variety of factors such as activity. For example, postural muscles are mainly comprised of slow-twitch fibres that are involved in low intensity steady state activities such as walking and maintenance of posture. On the other hand, phasic muscles are comprised of a higher composition of the glycolytic fast twitch Type 2X or 2B fibres and are involved in activities of greater intensities and explosive movements including weightlifting and sprinting [21]. Type 2A intermediate fibres pre-dominantly make up muscles involved in activities that require more energy than posture maintenance but less than that of explosive movements (Table 1.1).

Subsequently, the fibre type with the highest contribution to an individual muscle defines the metabolic profile of that muscle. For example, Type 1 slow-twitch oxidative fibres have a greater degree of mitochondria and aerobic

respiratory enzymes, increased myoglobin concentrations and greater capillary supply for oxidative phosphorylation [19,22,23], and are slow to fatigue. On the other hand, the Type 2X or 2B fast-twitch glycolytic fibres possess greater levels of glycogen due to their dependence on glycolysis as an energy source. Consequently, these fibres fatigue quickly in comparison to Type 1 slow-twitch oxidative fibres due to their lower mitochondria content and myoglobin concentration [24] (Table 1.1). Factors including dietary, lifestyle and age can influence the outcome of fibre type composition within the muscle [25,26] and fibre types can undergo switching [19,27,28].

	Fibre type			
Properties	**Type 1**	**Type 2A**	**Type 2X**	**Type 2B**
Major storage fuel	Triglycerides	Creatine phosphate, glycogen, triglycerides	Creatine phosphate, glycogen	Creatine phosphate, glycogen
Fatigue resistance	High	Fairly high	Intermediate	Low
Myosin heavy chain isoform	MYH7	MYH2	MYH1	MYH4
Force production	Weak	Moderate	Strong	Very strong
Contraction time	Slow	Intermediately fast	Fast	Very fast
Mitochondria	High	High	Low	Low
Capillary supply	Good	Good	Poor	Poor
Oxidative capacity	High	High	Intermediate	Low
Glycolytic capacity	Low	Intermediate	High	High
Activity type	Oxidative / aerobic	Oxidative-glycolytic / long-term anaerobic	Glycolytic/ acute anaerobic	Glycolytic / acute anaerobic

Table 1.1. Muscle fibre types in humans and rodents [19]

1.1.3. Myogenesis

During mammalian embryonic development, the development of skeletal muscle begins in the lateral plate and paraxial somatic mesoderm [29,30]. This is succeeded by a cascade of events where the somite segregates to form the dermomyotome where subsequent involution of these cells gives rise to the myotome [29]. Skeletal muscle myogenesis is a differentiation process where myofibres are formed, beginning from the initial commitment of mesodermal progenitor cells to myoblasts. This is succeeded by the terminal differentiation of myoblasts into myotubes and finally, myofibres (Fig. 1.4). This is dependent on differential expression of myogenic regulatory factors (MRFs) such as myogenic factor 5 (MYF5), myogenic differentiation protein 1 (MyoD) and paired box transcription factors Pax3 and Pax7, which are initially expressed at the early myoblast stage and fundamental for muscle differentiation commitment. Subsequent myogenic progression results in the decreased expression of these factors while terminal skeletal muscle differentiation factors such as myogenin, MRF4 and MYH3, as well as muscle proteins such as Troponin Type 1 (TNNT1), begin to increase in expression (Fig. 1.4). Additional studies have demonstrated that the MRFs themselves are not the sole mediators of successful myogenesis and subsequent skeletal muscle phenotype [31], and the process itself is also mediated by input from other signalling pathways such as Notch [32]. These suggest the dynamic nature of myogenesis as well as the presence of compensatory mechanisms and proteins in sustaining proper myogenic trajectory following loss of MRFs [33].

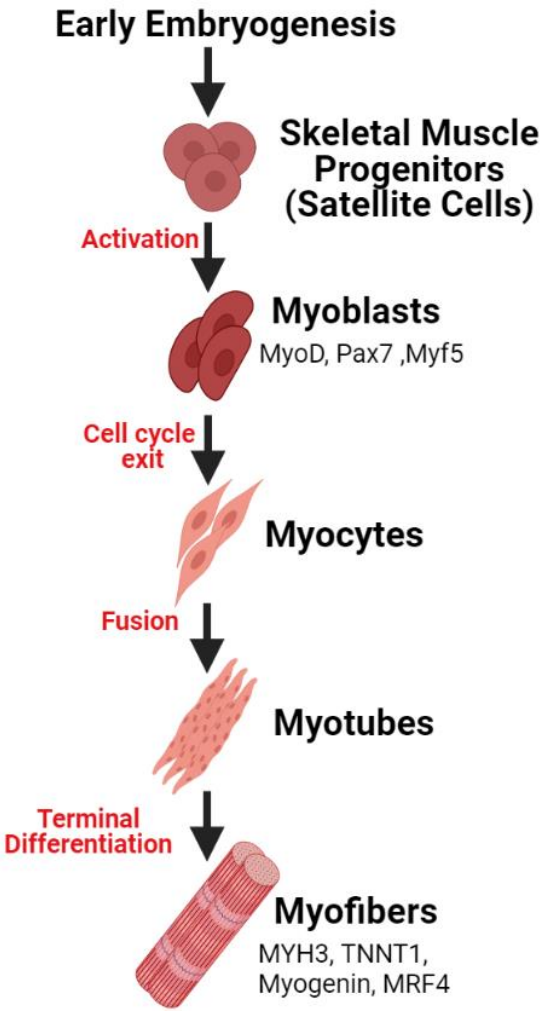

Figure 1.4. Myogenesis
An overview of skeletal myogenesis. The process is tightly regulated through the MRFs from the initiation of the commitment of progenitor cells into myoblasts to the alignment, fusion and terminal differentiation into multi-nucleated myotubes.

Formation of individual myofibres is dependent on alignment and fusion of multiple progenitor myoblasts that themselves, are products of muscle residing, self-renewing myogenic precursors called satellite cells [34]. These cells are capable of re-entering proliferative cycles, entailing regenerative repair in response to skeletal muscle injury, disease or exercise in the adult skeletal muscle through fusion with damaged myofibres [34]. In healthy adults, these satellite cells, derived from Pax3/Pax7 embryonic progenitors [35], reside within the basal lamina, a membrane composed of laminin and collagen proteins,

where they remain predominately quiescent until activation [34,36]. Activated satellite cells subsequently express MRFs and myogenic proteins [37,38], enabling them to proliferate and generate myoblasts (Fig. 1.4).

1.1.4. Energy metabolism in skeletal muscle

Skeletal muscle contributes to approximately 30% of resting metabolic rate [5,39], which can increase to 90% in response to intense activities such as exercise. This underscores its ability to mediate metabolic adaptions in response to duration and intensity of activities or other energetic demands and metabolic stress [39,40]. Examples of metabolic adaptions include modulated mitochondrial biogenesis and function, glucose mobilisation, blood flow and muscle fibre type switching [25,41]. In events of high energy demand, efficient replenishment of energy stores within the skeletal muscle to sustain contraction and activity performance is required. Within humans, skeletal muscle possess glycogen stores [42,43] that can be tapped upon for maintenance of energy balance and mediating adaptions in response to perturbation events such as exercise, varying food intake and fasting through processes such as glucose uptake, glycogenolysis and gluconeogenesis [42,43].

Skeletal muscle mainly derives energy from three substrates: glucose, amino acids and fatty acids. Fatty acids are the preferential source of energy in sedentary adult skeletal muscle. During sustained increased energetic demands, glucose is primarily used as the first line of energy source, followed by fatty acids and amino acids [44,45]. Additional factors including hormonal and neuronal stimuli can also alter the type of substrate utilised [46,47] (Fig. 1.5). Depending on individual substrate availability, interchangeable utilization is possible – this is termed as metabolic flexibility.

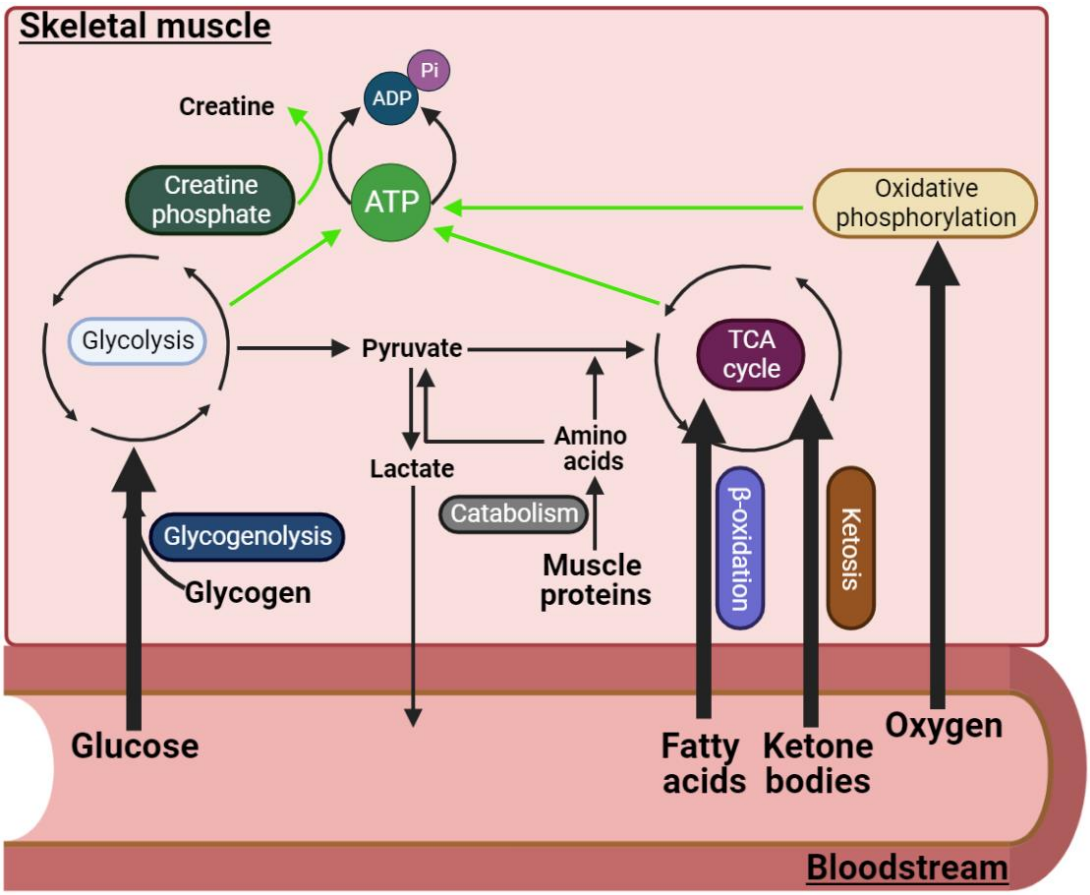

Figure 1.5. Processes of substrate utilisation within skeletal muscle
Skeletal muscle derives energy from three main substrates. In response to energetic demand, ATP can be generated rapidly via creatine phosphate. Energy can also be derived from three main substrates 1) glycogen through glycogenolysis, 2) glucose from the bloodstream through uptake by glucose transporters into muscle or directly from glycogenolysis, which enters glycolysis to produce pyruvate and 3) fatty acid uptake from the bloodstream that is β-oxidised to form acetyl-CoA. Collectively, pyruvate and acetyl-CoA serves as substrates for the TCA cycle to yield additional ATP. In response to sustained physical activities, greater quantities of ATP can be produced via aerobic respiration in a process termed oxidative phosphorylation. In prolonged exercise and caloric restriction, ketone bodies produced via ketosis and amino acids from muscle catabolism serve as substrates to continuously fuel the TCA cycle.

1.1.4.1. Creatine phosphate breakdown

Increased energetic demand causes ATP utilisation to exceed production. Creatine kinase is an ADP sensor enzyme that catalyses the reversible transfer of phosphate groups from ATP to creatine to yield creatine phosphate (PCr), which serves as an energy store to support short-term energy supplementation during initial stages of increased activity demand [48]. Constant hydrolysis of ATP yields ADP that is consequently detected by creatine kinase

which catalyses hydrolysis of PCr to yield phosphate groups that are added to ADP to form ATP [49]. During reduced energy demand, creatine kinase catalyses the re-phosphorylation of creatine to regenerate creatine phosphate [1.]. Consequently, high creatine kinase levels serve as a marker for brain as well as skeletal and cardiac muscle damage/dysfunction [50].

1.1.4.2. Glycogenolysis

Sustained periods of intensive activity diminishes PCr stores. In response, a switch over to glucose metabolism for energy source occurs. Glycogenolysis is the process where glycogen stores are broken down to yield glucose for supplement of energy demand. First, PCr diminishment causes the activation of glycogen phosphorylase, which catalyses the breakdown of glycogen branches to release glucose-1-phopshate. Glucose-1-phosphate is subsequently converted into glucose-6-phosphate by phosphoglucomutase which is used as a substrate for glycolysis. Periods of prolonged intense activities eventually causes depletion of glycogen stores, resulting in reliance on alternative sources of fuel such as fatty acids and amino acids [51].

1.1.4.3. Glycolysis

Anaerobic glycolysis within the cytosol results in the generation of ATP via the sequential degradation of glucose into pyruvate that is catalysed by a series of enzymes (Fig. 1.6). Subsequently, two molecules of ATP are generated following glycolysis of a single glucose molecule. Lactate dehydrogenase further catalyses the conversion of pyruvate into lactate and NAD^+, entailing a glycolytic flux that is essential for constant ATP generation [52]. Additionally, pyruvate can alternatively be used as a substrate for construction of the amino

acid alanine in a reaction that is catalysed by alanine transaminases as well as being a substrate for hepatic gluconeogenesis [53].

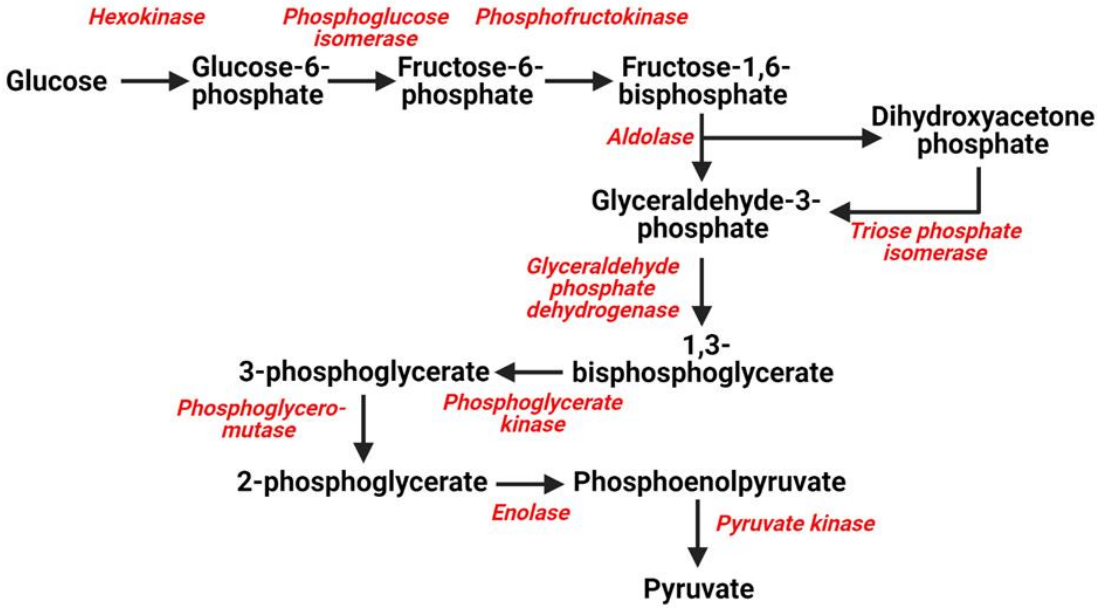

Figure 1.6. Glycolysis
Glycolysis is a multi-step process catalysed by a series of enzymes to ultimately result in the breakdown of glucose into pyruvate. Pyruvate then serves as substrates for energy generation either via the TCA cycle or is conversion into lactate that is dependent on oxygenated conditions.

In contrast, aerobic glycolysis takes place predominantly within the mitochondria. Fundamentally, this process sees pyruvate being converted into acetyl coenzyme A (Acetyl-CoA) by the pyruvate dehydrogenase complex or alternatively, carboxylated into oxaloacetate by pyruvate carboxylases. Subsequently, both Acetyl-CoA and oxaloacetate are used as substrates for the tricarboxylic acid (TCA) cycle, where NAD^+ is reduced to NADH and flavin adenine dinucleotide ($FADH_2$) is produced [54,55]. NADH is paramount for oxidative phosphorylation to subsequently yield greater ATP generation, with approximately 30 molecules being generated per molecule of glucose [56].

1.1.4.4. Fatty acid oxidation

Fatty acids can also be utilized as a source of energy, initiated by the catabolism of triglycerides stored in adipose tissues, catalysed by lipases in a process termed lipolysis to yield glycerol and free fatty acids. Subsequently, these free fatty acids enter circulation where they are transported in plasma lipoproteins to skeletal muscle and other cells, where they can be directed towards oxidation, esterified into complex lipids or remain in their free state within cells [57]. The process of fatty acid oxidation begins with fatty acids reacting with coenzyme A (CoA) to yield acyl-CoA. This is succeeded by formation and elongation of acyl-CoA chains which then get broken down in a process termed β-oxidation, subsequently yielding acetyl-CoA [58]. Concomitantly, $FADH_2$ and NADH are also produced as by-products of this process and subsequently utilized in the electron transport chain, while acetyl-CoA enters and fuels the TCA cycle for energy generation.

1.1.4.5. Ketosis and protein catabolism of muscle

Ketosis is a metabolic state elevated during periods of prolonged caloric restriction, exercise or low carbohydrate intake. Within the liver, a diversion of oxaloacetate to gluconeogenic pathways occurs, causing formation and release of ketone bodies such as acetoacetate, β-hydroxybutyrate and acetone for energy generation via the TCA cycle [59]. When carbohydrates and fatty acids are depleted, amino acids such as alanine are then derived from muscle proteins to serve as substrates for gluconeogenesis and TCA cycle for energy generation [60,61]. Prolonged protein catabolism is detrimental for overall health due to resulting skeletal muscle atrophy [62], and indicates the presence of disorders such as cancer-associated cachexia [63].

1.1.5. Oxidative phosphorylation

Oxidative phosphorylation is the process of ATP generation that occurs through the mitochondrial electron transport chain [56]. Glucose or pyruvate products obtained following the metabolism of the aforementioned substrates described are first metabolised in the TCA cycle to yield carbon dioxide (CO_2), NADH and $FADH_2$. This is succeeded by a cascade of step-wise mechanisms in which electron donors and acceptor intermembrane protein complexes located within the inner mitochondrial membrane mediate the transfer of electrons from NADH and $FADH_2$, and eventually onto oxygen where water is produced. The constant generation of hydrogen ions throughout this process across the membrane and into the intermembrane space causes a build-up of a potential energy gradient after which hydrogen ions flow down via this gradient, back into the membrane, and through ATP synthase to drive the activity of this enzyme to produce ATP through the phosphorylation of ADP [64] (Fig. 1.7). This flow of hydrogen ions is known as the proton-motive force and serves to maintain constant ATP synthase activity. Subsequently, oxidative phosphorylation yields approximately 36 ATP molecules per molecule of glucose [65].

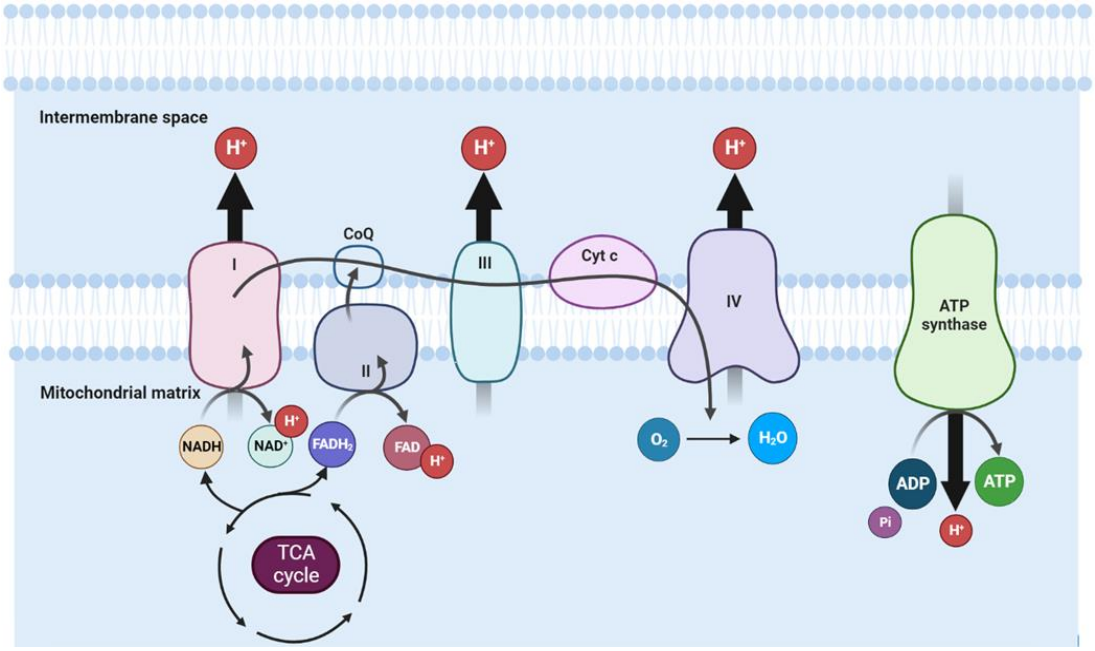

Figure 1.7. Oxidative phosphorylation
The inner mitochondrial membrane possess a variety of intermembrane complexes: Complex I (NADH dehydrogenase, ubiquinone, complex II (succinate dehydrogenase), complex III (ubiquinol-cytochrome C reductase), complex IV (cytochrome C oxidase) and ATP synthase. These complexes work to drive oxidative phosphorylation through the step-wise transfer and donation of electrons for reduction of O_2 into H_2O. Throughout, hydrogen ions are generated into the intermembrane space that creates an energy gradient resulting in the backflow of hydrogen ions into the inner mitochondrial membrane and through ATP synthase that drives the energy generation of ATP via ADP phosphorylation.

Although oxidative phosphorylation is a fundamental metabolic process, one of the by-products produced is reactive oxygen species (ROS). ROS accumulation is detrimental to cellular stability due to protein oxidization and inducing Deoxyribonucleic Acid (DNA) mutations. Generally, ROS is rapidly cleared through its conversion to hydrogen peroxide and subsequently water, as well as through antioxidant defences within the cell such as the peroxidases and superoxide dismutase enzymes, as well as the vitamins C and E [66]. Consequently, ROS accumulation has been associated to a multitude of conditions including chronic inflammation and poor aging [67,68].

1.1.6. Molecular adaptations to exercise in skeletal muscle

Amongst improvements in mental health, bone health, sleep improvement, cardiovascular health and basal metabolic rate, exercise promotes protein synthesis, thus reducing age-associated decline of skeletal muscle [69,70]. This translates into reduced risk and better management of metabolic disorders including type 2 *diabetes mellitus*, sarcopenia and obesity. Exercise induces whole proteome and genome changes associated with metabolism within skeletal muscle. These include players involved in key signalling pathways associated with myogenesis (MyoD, myogenin), glucose (Glucose transporter (GLUT) 4 (GLUT4), cAMP response element-binding protein (CREB)) and lipid (Forkhead box protein O1 (FOXO1), Peroxisome proliferator-activated receptor (PPAR) gamma coactivator 1-alpha (PGC1α)) metabolism, angiogenesis (Vascular endothelial growth factor (VEGF), Hypoxia-inducible factor 1-alpha (HIF1α)), as well as mitochondrial transcriptional genes (PPAR, (Nuclear Respiratory Factor) (NRF) [39]. Additionally, global metabolome changes with regards to metabolites associated with ATP, NAD, branched chain and ketogenic amino acid and glucose metabolism pathways have been demonstrated – more importantly, trained versus untrained state muscle exhibited differential metabolite changes [71]. Roles for the skeletal muscle secretome in mediating training adaptations, including myokines and cytokines, have also been described [72]. These illustrate the metabolic plasticity and adaptive processes in skeletal muscle following repeated stimulation and underlie the significance of exercise in general health and wellbeing (Fig. 1.8).

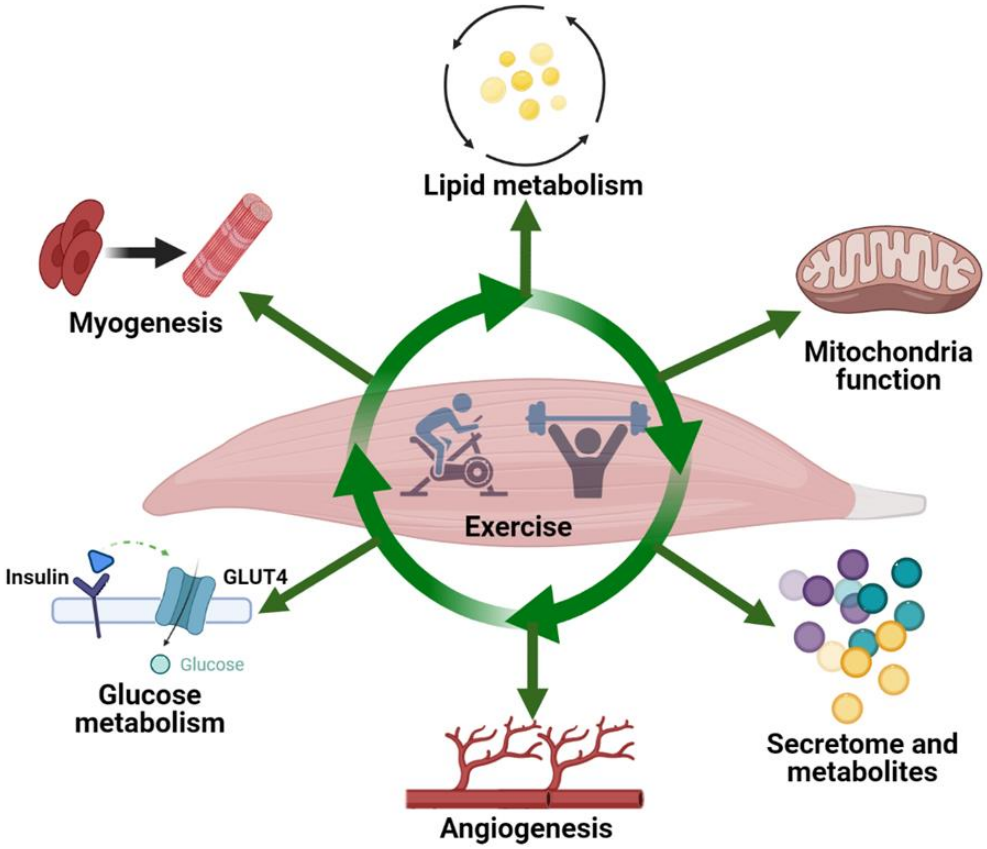

Figure 1.8. Adaptations of skeletal muscle to exercise
Skeletal muscle exhibits plasticity and initiates adaptative responsiveness to exercise. These can modulate global proteome and genome expression changes in regulators of pathways including include repair and building of muscle through increased myogenesis, enhanced basal metabolic rate and blood vessel formation. Additionally, metabolite and secretome profiling identifies changes in response to exercise which are predominantly associated with energy associated pathways.

One major molecular adaption of skeletal muscle in response to exercise is via the modulation of mitochondria function. Mitochondria possess their own DNA (mtDNA), coding for 37 genes and 13 subunit proteins crucial for overall function and oxidative phosphorylation [73,74]. Events such as caloric restriction and exercise have been shown to influence overall mitochondria number within skeletal muscle [75–77], implying presence of adaptions through mitochondrial modulation. Mechanistically, mitochondria biogenesis induced in response to exercise or caloric restriction within skeletal muscle occurs through post-transcriptional and translational modifications of PGC1α, the

primary transcriptional coactivator regulating a plethora of mitochondria biogenesis genes [78]. PGC1α can be induced by 1) the transcriptional factors p38 mitogen-activated protein kinase (MAPK) and Activating transcription factor 2 (ATF2) [79], 2) phosphorylation by AMP-activated protein kinase (AMPK) [80] and, 3) deacetylation by the NAD^+ consuming enzyme sirtuin 1 (SIRT1) [81]. Subsequently, PGC1α deacetylation causes nuclear activation of Mitochondrial transcription factor A (TFAM), NRF1 and NRF2 to initiate mitochondrial biogenesis [82] (Fig. 1.9).

Dysfunctional mitochondria as a result of mtDNA damage by ROS accumulation or declines in oxidative capacity are selectively cleared in a process termed mitophagy. This necessitates replacement of lost mitochondria, making mitochondria biogenesis a fundamental process in mitochondrial homeostasis. An imbalance in healthy and functional mitochondria are large contributors into the aetiologies of aging and other aberrant conditions including Parkinson's, autoimmune disease, diabetes and cardiovascular diseases [83–87]. It is therefore paramount that cofactors and molecules such as NAD^+ and $FADH_2$ crucial for driving fundamental energy generating processes including the TCA cycle and oxidative phosphorylation are constantly available and replenished via the metabolism of substrates and regulation of their consumption by consuming enzymes.

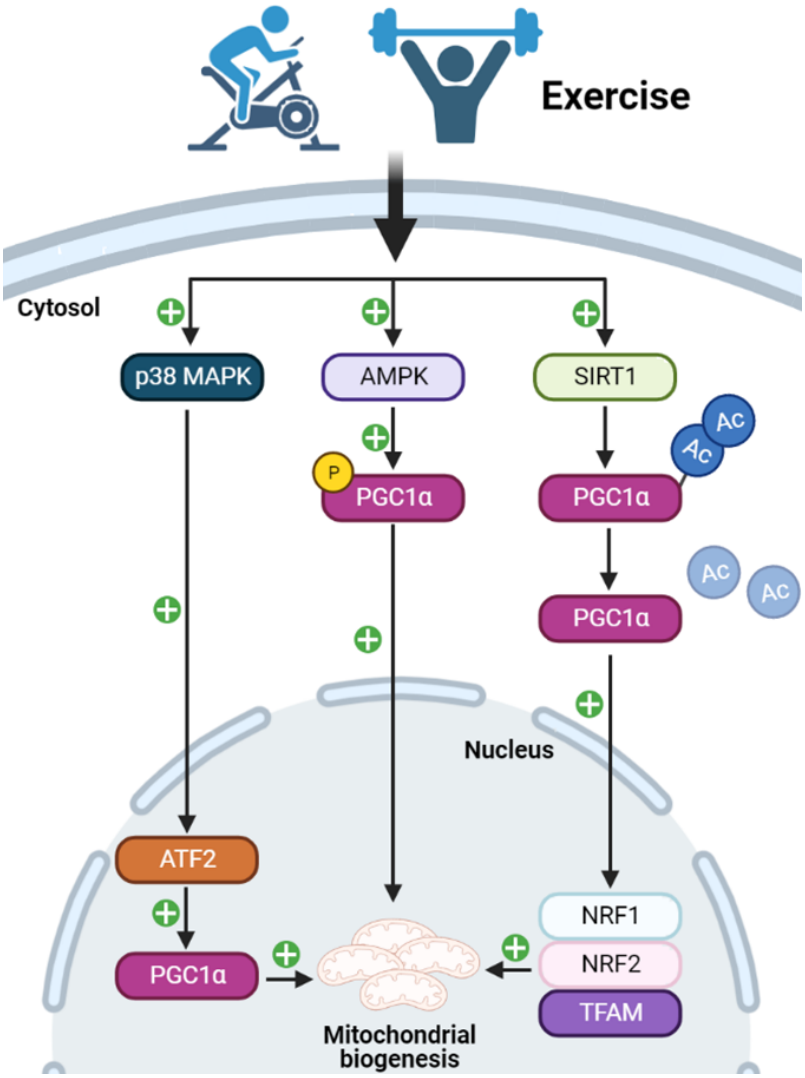

Figure 1.9. Mitochondrial adaptations by skeletal muscle in response to exercise
Modulation of mitochondria function is one of the major adaptations undertaken by skeletal muscle in response to exercise. Mechanistically, these changes occur primarily through induction of mtDNA genes and mitochondrial biogenesis for formation of new mitochondria via activation and upregulation of PGC1α, the master transcriptional regulator of mitochondria. PGC1α can be activated by 1) p38 MAPK-mediated phosphorylation of ATF2, 2) direct phosphorylation by AMPK or 3) deacetylation by SIRT1. Collectively, the augmented mitochondrial adaptations result in increased oxidative capacity of skeletal muscle and subsequently, basal metabolic rates.

1.2. NAD$^+$

1.2.1. History and discovery

Fundamental to all cells, NAD was initially identified as “cozymase” at the turn of the 20th century. This heat-stable factor was first identified within low molecular weight fractions of yeast elevating fermentation [88]. Subsequent success in isolation and characterization unravelled that it was composed of two mononucleotides: nicotinamide mononucleotide (NMN) and Adenosine monophosphate (AMP) [89] (Fig. 1.10). Significance of NAD$^+$ in metabolism was truly appreciated by the Pellagra epidemic in the 1900s, a condition that manifested in profound disease including characteristic dermatitis (photosensitive), diarrhoea, dementia and death. Subsequently, it was established that dietary absence of the essential amino acid tryptophan and vitamin B3 from dietary sources was the main cause of this condition [90].

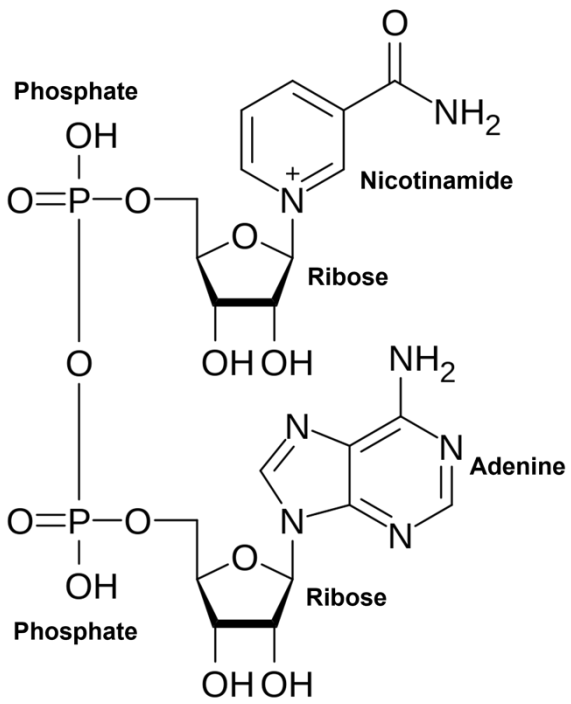

Figure 1.10. NAD$^+$
The molecular structure of NAD$^+$ is composed of phosphate groups that attach adenine to ribose to form an AMP group, as well as NAM to form an NMN group.

Further work detailed NAD as a cofactor contributing to REDOX reactions either via the donation or acceptance of electrons catalysed by oxidoreductases to entail the existence of 2 forms: oxidized as NAD^+, or reduced into NADH [89] (Fig. 1.11). The ratio between these species are critical for key metabolic processes including nutrient uptake, where both forms are utilized for the coupling of the TCA cycle and oxidative phosphorylation for energy generation [91], processes which have been discussed previously in *Section 1.1.5*.

Aside from the aforementioned NAD species, its phosphorylated form, nicotinamide adenine dinucleotide phosphate ($NADP^+$) can be produced in a reaction catalysed by NAD kinases using a phosphate group from ATP [89]. $NADP^+$ can also be reduced into NADPH as part of the pentose phosphate pathway, which subsequently acts a reducing agent in metabolic pathways including nucleic acid and lipid biosynthesis [92]. More importantly, NADPH plays dual roles in ROS balance and oxidative stress defence, where NADPH oxidases use NADPH to produce ROS [93], while also serving as the donor of reductive power for a plethora of ROS detoxifying enzymes [94].

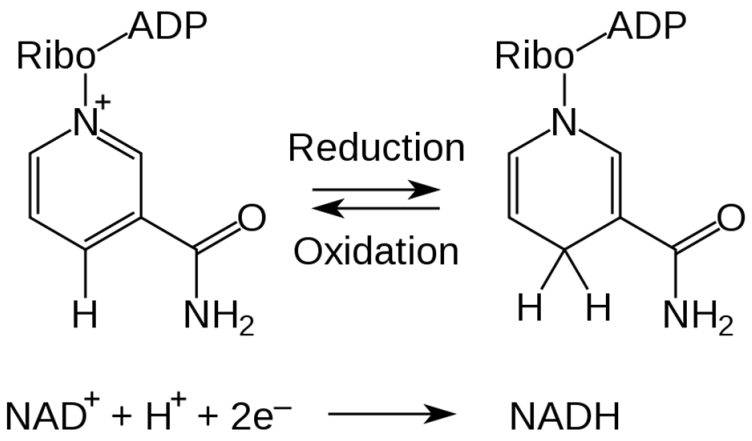

Figure 1.11. NAD is a cofactor in REDOX biology
As a molecule, NAD can be presented in two forms: NAD^+ or NADH. NAD^+ which accepts electrons from molecules is reduced to NADH, while NADH that donates electrons to target molecules becomes oxidized into NAD^+.

Supplementary to REDOX contributions, NAD^+ also acts as a rate-limiting co-substrate for a number of protein and Ribonucleic Acid (RNA) modifying enzymes – these include the Poly-(ADP-ribose) polymerases (PARPs), sirtuins (SIRTs), cyclic ADP-ribose (cADPR) synthases and the ecto-ADPR transferases (ARTCs). Through studies dating back more than a century, we now understand NAD^+ and its derivates to be critical in driving numerous biochemical reactions as a cofactor for energy metabolism and contributes towards cell and tissue homeostasis. Acquiring an understanding of its generation and breakdown has been fundamental in developing a greater understanding of metabolic processes and pathological disorders that are ascribed to NAD^+ imbalance.

1.2.2. The biosynthesis of NAD^+

Three pathways of NAD^+ biosynthesis within mammals have been identified: Salvage, *de novo*, and Preiss-handler (Fig. 1.12). The major pathway is the salvage pathway. This physiological pathway begins via recycling of the NAD^+ precursor nicotinamide (NAM) that is released as a by-product following NAD^+ utilization by consuming enzymes. NAM is subsequently converted into NMN in a reaction catalysed by NAM phosphoribosyltransferases (NAMPTs) through the consumption of ATP. NMN, in the final step, is then converted into NAD^+ by NMN adenylyl transferases (NMNATs), again requiring ATP [2,95]. In addition, Nicotinamide riboside (NR) (or referred to as vitamin B3) that is a precursor of NAD^+, can also be converted into NMN via phosphorylation as part of the NAM riboside kinase (NMRK) 1 and 2 pathways [2,96–98].

The beginning of the *de novo* and Preiss-handler pathways are dependent on dietary supplementation of vitamin B3 derived NAD^+ precursors (Fig. 1.12). For the former, which some might refer to as the kynurenine metabolic pathway, tryptophan is converted into quinolinic acid that is subsequently converted into Nicotinic Acid (NA) Mononucleotide (NAMN) by quinolinate phosphoribosyltransferases (QPRTs). NMNAT then catalyses the conversion of NAMN into Nicotinate adenine dinucleotide (NaAD) which is finally converted by NAD synthases (NADSs) into NAD^+ [95,99]. The Preiss-handler pathway on the other hand, utilizes NA, which is converted into NAMN by Nicotinate phosphoribosyltransferases (NAPRTs) [91,99]. This NAMN is subsequently converted into NAD^+ in the same manner as just described. In recent times, evidence has been presented that NAD^+ biosynthesis pathways can switch between [100], and compensate for one another [91,95,101].

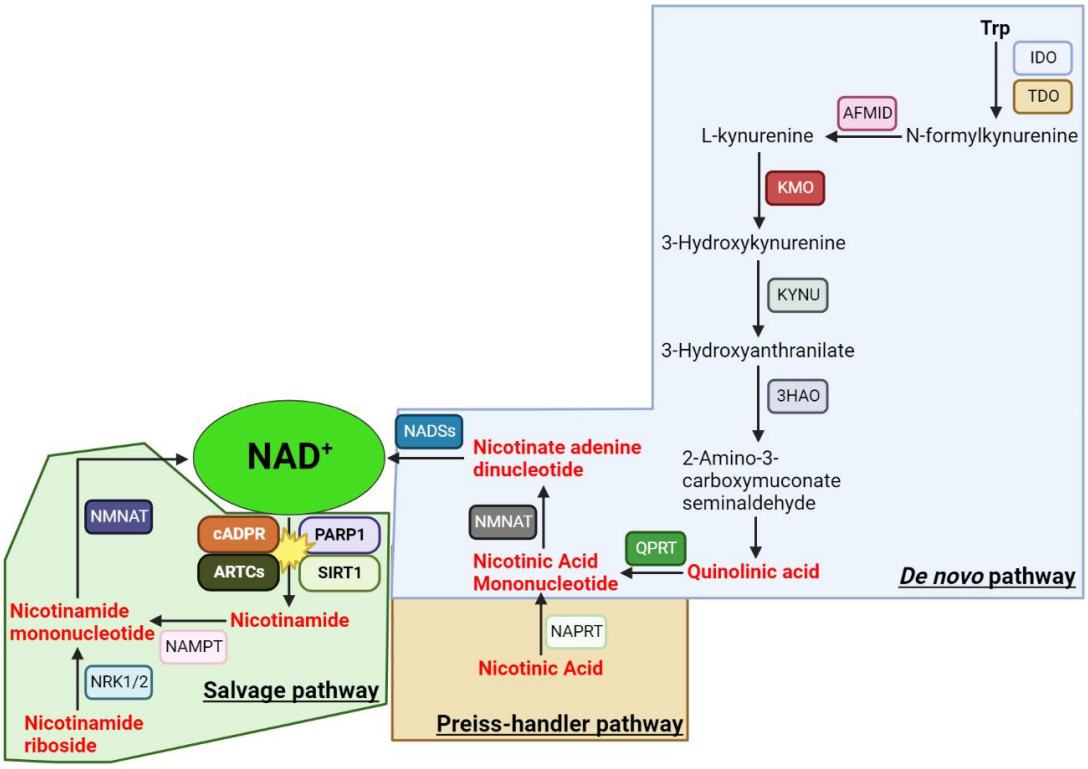

Figure 1.12. NAD^+ biosynthesis pathways

Three pathways exist for the biosynthesis of NAD^+. The salvage pathway is the major NAD^+ biosynthetic pathway, where NAD^+ cleavage by the by the major NAD^+ consuming enzymes PARPs, SIRTs, cADPR synthases or the ARTCs releases nicotinamide as a by-product that is subsequently recycled through the NAMPT and NMNAT enzymes to regenerate NAD^+. Supplementation with nicotinamide riboside can also feed into this pathway. The *de novo* pathway involves the use of tryptophan to generate NAM from quinolinic acid and subsequently NAD^+, while the Preiss-handler pathway involves the supplementation of nicotinic acid that is then converted into nicotinic acid mononucleotide and subsequently NAD^+ by the same group of enzymes in the final stages of the *de novo* pathway. Abbreviations: AFMID, Arylformamidase; 3HAO, 3-Hydroxy- anthranilate 3,4-dioxygenase; IDO: Indoleamine 2,3-dioxygenase; KMO, Kynurenine 3-monooxygenase; KYNU, Kynureninase; Trp, Tryptophan

1.2.3. NAD$^+$ compartmentalization

NAD$^+$ levels also exhibit subcellular compartmentalization. For example, the 3 isoforms of mammalian NMNATs are localized to different subcellular components, with NMNAT1 in the nucleus, NMNAT2 in the cytoplasm and Golgi apparatus, and NMNAT3 in the mitochondria [95,102,103]. Evidence of compartmentalization is further supported by the presence of comparable NAD$^+$ levels between cytosol and nuclear fractions [91,104]. Mitochondrial NAD$^+$ levels, on the other hand, are distinctively higher in comparison to those within nuclear and cytosol fractions [102,104], and cytosol NAD$^+$ production exerts influence over mitochondrial NAD$^+$ [104]. Factors that alter the subcellular distribution of NAD$^+$ include cell type, cellular state and growth conditions [105], exerting differential overall metabolic profiles. For example, higher mitochondrial NAD$^+$ levels have been ascribed to the ability of the mitochondria to uptake NAD$^+$ precursors [106–108] as well as NAD itself [108,109], indicating the existence of a mitochondria-based NAD$^+$ transporter. Indeed, a novel mammalian NAD$^+$ mitochondrial transporter, SLC25A51, has been identified to govern NAD$^+$ import into the mitochondria [108], corroborating previous observations of NAD$^+$ in the mitochondria. On the other hand, distinct compartmentalised pools allow effective sharing of NAD$^+$ between NAD$^+$ consuming enzymes such as PARP1 that are localized to different subcellular components, as well as maintaining metabolic balance of NAD$^+$/NADH within essential TCA cycle and oxidative phosphorylation processes.

1.2.4. NAD$^+$ boosting and precursor supplementation

Aberrant NAD$^+$ biosynthesis pathways result in accelerated poor aging and increased prevalence of metabolic disorders. It's well-established that NAD$^+$ levels decline in humans with age [2,110]. This is exacerbated by age-related gradual decline in overall skeletal muscle mass. The repercussions of skeletal muscle loss depletes body's capabilities for aerobic respiration and energy expenditure, processes detailed in *Section 1.1.4*. This is in contrast to the white adipose tissues that contain relatively few mitochondria, beginning to increase in mass to compensate for skeletal muscle loss [70,111]. Subsequently, the depletion of NAD$^+$ by consuming enzymes exceeds NAD$^+$ biosynthesis. In theory, declines in NAD$^+$ subsequently predispose aging individuals to debilitating conditions such as insulin resistance, obesity, Parkinson's disease and increased susceptibility to pathogenic infection, all of which have been documented [91,106,112–116] – this trend suggests that NAD$^+$ decline is a cause and consequence of age-related disorders.

While one strategy to counter age-related NAD$^+$ decline is via regular physical activity and incorporation of protein-rich diets for skeletal muscle preservation [69,70], boosting of NAD$^+$ has also emerged in recent years as a viable candidate for therapy. Such strategies include 1) direct supplementation of NAD$^+$ or its precursors [110,117], 2) inhibition of NAD$^+$ consuming enzymes [118–120], and 3) modulating activity of players within NAD$^+$ biosynthesis pathways [121–123]. Supplementation has been described in fruit flies, rodent, mouse and nematode models [91,106,107,124], and crucially, in humans as well without adverse effects [110,117,125,126]. However, it's worth noting that excess NAD$^+$ in the healthy phenotype seemingly does not significantly perturb central metabolic activity

[127,128]. More recently, a novel precursor based on a reduced form of NR, known as NRH, was developed and demonstrated significantly greater potency than NR in increasing NAD^+ levels, which could pave the future for oral intake of NAD^+ precursors for therapy [129,130].

The pharmacological and genetic inhibition of the major NAD^+ consuming enzymes (further discussed in *Section 1.3*) such as PARPs and cADPR synthases, have been largely useful in boosting NAD^+ – for the former, there is substantial consensus that PARP inhibition entails positive metabolic benefits and overall wellbeing [115,131–135], and is also implicated as a pioneer therapeutic for the treatment of cancers [135,136]. Currently, PARP inhibitors such as Olaparib and Rucaparib have been approved for therapeutic use in ovary, prostate and breast cancers [119,120]. Likewise, inhibition of the cADPR synthase CD38 has demonstrated comparable efficacy as with PARP inhibition [124,137,138] and inhibitors such as Isatuximab are undergoing phase 1/2 clinical trials for the treatment of multiple myeloma [139].

Similarly, the overexpression of NAMPT has been successful in increasing overall NAD^+ levels [140–142] and is metabolically beneficial [140,143]. However, its overexpression is also associated with increased cancer progression [144–146], making its inhibition a viable therapeutic target in this regard. Subsequently, pharmacological compounds such as P7C3 [122,123] and SBI-797812 [121] have been developed and demonstrated relatively high efficacy in elevating NAD^+ levels through enhanced activation of NAMPT. Similarly, NMNAT overexpression boosts NAD^+ levels in tandem with precursor administration [113,147], mediating metabolically beneficial effects [142,148–152].

1.3. NAD$^+$ consuming enzymes

As outlined in *Section 1.2.1*, NAD$^+$ also serves as a co-substrate for certain enzymes. Cleavage of NAD$^+$ by these enzymes releases NAM and ADP-ribose (ADPR) (Fig. 1.13) – NAM is subsequently recycled for regeneration of NAD$^+$ as outlined in *Section 1.2.2*, while ADPR is applied as in a site-specific manner as a form of post-transcriptional or post-translational modifications onto target substrates, altering their biological activities. Henceforth ADPR serves important functions as a signalling moiety.

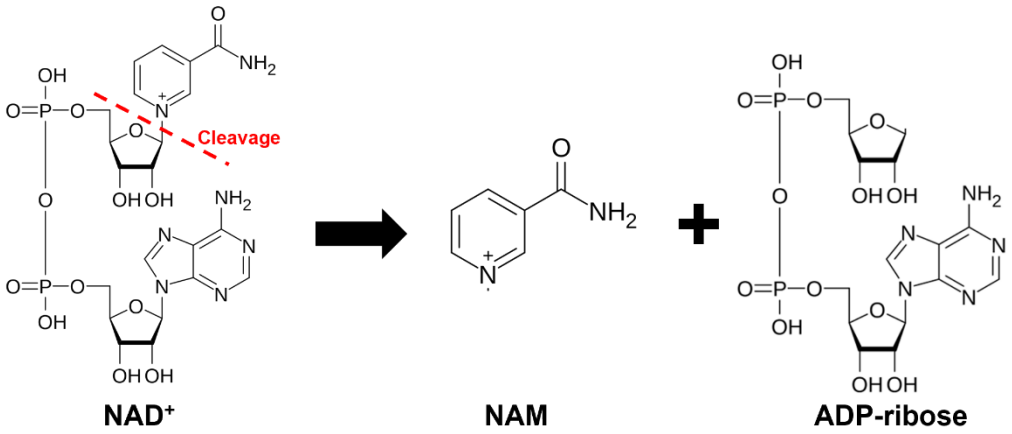

Figure 1.13. NAD$^+$ cleavage
Cleavage by the NAD$^+$ consuming enzymes occurs at the glycosidic bond as depicted in the red line. This releases NAM and ADP-ribose as by-products. NAM is subsequently recycled as part of the NAD$^+$ salvage pathway to regenerate NAD$^+$ while ADP-ribose is applied onto target substrates for modulation of downstream signalling pathways such as DNA damage repair, calcium signalling and metabolism.

Subsequently, decades of assiduous research have resulted in identification of families of enzymes that majorly consume NAD$^+$. These enzymes thus compete for the intracellular NAD$^+$ pool, necessitating further study towards understanding its competition between enzymes. Therefore, it should be considered that consumption of NAD$^+$ by a specific enzyme has an influence on the activity of other NAD$^+$ dependent enzymes.

1.3.1. PARPs – family and enzymology

Following the initial discovery of ADPR in the late 1960s [153–156], work was succeeded by the discovery of the multi-domained PARPs and their ability to apply ADPR onto target proteins as a form of post-translational modification through NAD^+ consumption [156–159]. New knowledge has unravelled specific sites in which ADPR monomeric units can be attached onto target substrates, and these include Thr, Glu, Asp, Lys, Arg, Cys or Ser residues [160]. Attachment of a single ADPR molecule, known as mono-ADP-ribosylation (MARylation), serves as the initiation step and can be succeeded by subsequent elongation and branching of Poly-ADPR (PAR) chains, known as Poly (ADP-ribosyl)ation (PARylation). PAR chains involve the formation of ribose-ribose linkages between MAR units, usually joined together by a 2″,1‴-glycosidic bond. PARylation is reversible and regulated through the rapid catalytic degradation of PAR chains by degrading enzymes such as PAR-glycohydrolase (PARG) and ADP-ribosylhydrolase 3 (ARH3) [161]. PAR chains can also be stabilized by macrodomain-containing proteins such as MacroH2A1.1 to prevent rapid degradation and subsequently preventing excess NAD^+ consumption [162] (Fig. 1.14), and PAR and PARylated substrates can be transferred to the cytosol [163].

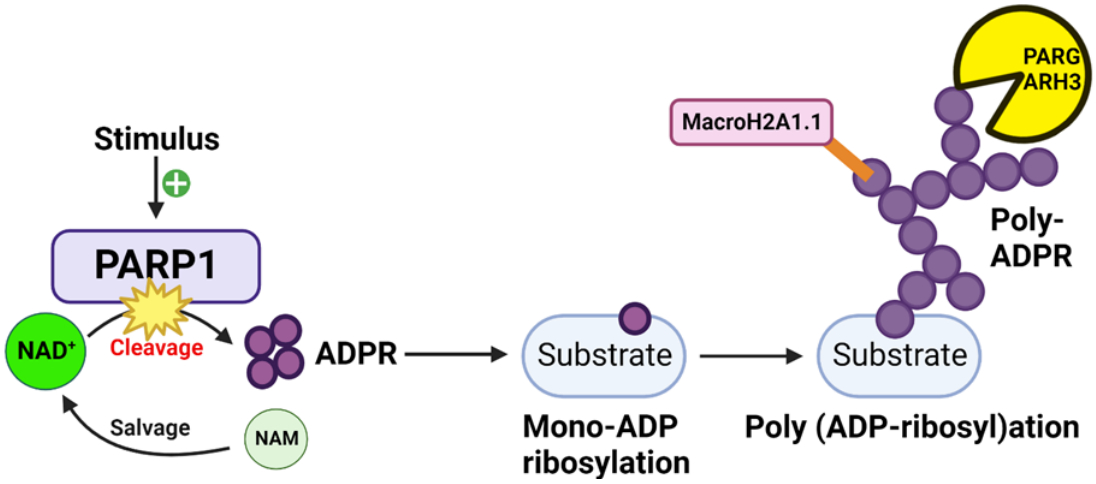

Figure 1.14. PARylation by PARP1
PARP1 enzymatically applies ADPR as a form of post-transcriptional or translational modification onto target substrates through the consumption of NAD^+. Attachment of a single ADPR monomer sequentially initiates the further addition of ADPR to yield Poly-ADPR (PAR) chains. These chains can subsequently elongate and branch out, in a process termed Poly (ADP-ribosyl)ation (PARylation). The extent of PARylation is a key determinant in the magnitude of signalling processes it regulates. Subsequently, PAR mediated signalling events are regulated by the PARG and ARH3 enzymes that catalyse the hydrolysis of PAR chains while the macrodomain containing proteins such as MacroH2A1.1 stabilizes the chains. Collectively, these regulatory events are fundamental for maintaining overall NAD^+ availability.

17 and 16 members comprise the PARP enzyme family in humans and mice respectively (Table 1.2). Interestingly, the majority of PARP activity, basal or stimulated, is exerted by either PARP1 (85 – 90%) or PARP2 (10 – 15%), most of which are localized to the nucleus, making these 2 members the most commonly studied forms. Cytoplasmic and mitochondrial PARP activity have also been presented [164–167], and NAD^+ levels within these subcellular compartments can mediate PARP activity in another subcellular compartment [168]. Thus far, only PARP1, PARP2, PARP5a (Tankyrase 1) and PARP5b/6 (Tankyrase 2) exhibit PARylating activity while remaining members exhibit MARylating activity except for PARP13, which is catalytically inactive [169]. Within the catalytic domain of PARylating members lies a characteristic and highly conserved NAD^+ binding pocket composed of a set of residues (H862, Y896 and E988) which form the His-Tyr-Glu (HYE) triad, a signature critical

for NAD^+ binding and PARylating activity [164,170]. Aside from PARylating target substrates, PARPs are capable of auto-PARylating themselves for regulation of intrinsic activity. The extent of PARylation is far-reaching in the modulation of cellular signalling pathways, with well documented roles in DNA repair, genome stability, inflammatory and immune response, and emerging roles in cellular differentiation programmes, glucose metabolism and skeletal muscle physiology [91,165].

PARP	Localization	Activity	Biological processes
PARP1	Nucleus	PARylation	Aging / Infection & Immunity / Differentiation / DNA repair / Chromosome structure / RNA metabolism / Metabolism / Transcription / Proteasome degradation / Cell cycle
PARP2	Nucleus	PARylation	DNA repair / Chromosome structure / Metabolism / Transcription / Cell cycle/ Inflammation
PARP3	Nucleus	PARylation	DNA repair / Cell cycle
PARP4	Nucleus / Exosomes / Cell membrane	MARylation	Cancer biology / Vault biology
PARP5a (Tankyrase 1)	Nucleus / Telomeres / Golgi / Cytoplasm	PARylation	Infection & Immunity / Cell cycle / Metabolism / Mitotic spindle formation / Telomere maintenance
PARP5b (Tankyrase 2)	Nucleus / Telomeres / Golgi / Cytoplasm	PARylation	Metabolism / Inflammation / Telomere maintenance?
PARP6	Cytoplasm*	MARylation	Cell proliferation
PARP7	Nucleus* / Cytoplasm*	MARylation	Infection & Immunity / Transcription
PARP8	Undefined	MARylation	Undefined
PARP9	Nucleus / Cell membrane / Cytoplasm*	MARylation	Cell migration / Tumour biology / Infection & Immunity
PARP10	Nucleus / Cytoplasm	MARylation	Cell proliferation / Infection & Immunity / Transcription
PARP11	Undefined	MARylation	Undefined
PARP12	Cytoplasm	MARylation	Infection & Immunity / RNA metabolism
PARP13	Cytoplasm	Inactive	Infection & Immunity / RNA metabolism
PARP14	Nucleus / Cell membrane	MARylation	Metabolism / Transcription / RNA metabolism / Tumour biology
PARP15	Cytoplasm	MARylation	RNA metabolism / Tumour biology
PARP16	Cell membrane / Endoplasmic reticulum	MARylation	Unfolded protein response

*potentially identified localization

Table 1.2. PARP family of enzymes [165,171]

1.3.2. PARP1 structure and function in genome maintenance

The founding PARP family member, PARP1 is an approximately 113 kDa protein comprised of 1014 amino acids [170]. It is a constitutive nuclear and mitochondria enzyme, and is composed of 7 major domains (Fig 1.15). Roles for PARP1 in DNA damage repair including pathways of base excision repair, the repair of single and double-strand breaks, as well as of stalled replication forks have been well-defined [172]. These primarily occur via the PARylation of substrates including DNA repair proteins, histones, chromatin remodelers, transcription factors and signal transduction elements [172]. Furthermore, PARP1 roles independent of PARylating activity have also been described through direct binding to nucleic acids [173–175] and transcription factors [176].

1.3.2.1. Zinc finger domains

A key domain of PARP1, the 3 Zinc Finger (ZF) domains making up the N-terminal domain (NTD) of PARP1 together govern the initiation of the DNA damage response pathway. ZF1 and ZF2 recognize, bind and self-assemble into damaged or nicked sites and this process is independent of ZF3 [170,177,178]. In contrast, ZF3 was discovered and characterized much later than ZF1 and ZF2, where ZF3 organizes DNA-damage dependent PARP1 binding and catalytic activity for allosteric activation of PARP1 [179,180]. Mutations in ZF domains results in the abolishment of DNA-damage dependent binding and activation of PARP1 [181,182]. Between ZF2 and ZF3 also lies a nuclear localization signal (NLS) and a caspase cleavage site [179], although the former is seemingly dispensable in the context of DNA-binding and catalytic activity [183]. The caspase cleavage site on the other hand is subjected to cleavage by caspases 3 and 7 during apoptosis into a DNA binding and catalytic fragment

for PARP1 auto-modification [184]. Consequently, caspase mediated PARP1 cleavage is ascribed to a range of neurological disorders including Parkinson's and Alzheimer's disease [115,185].

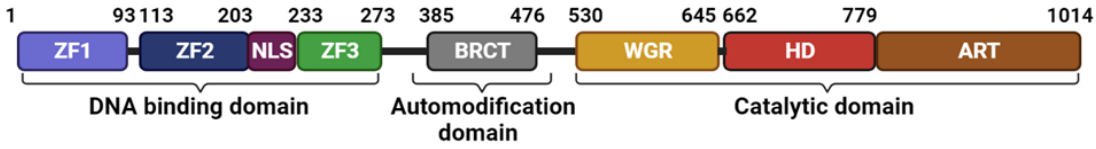

Figure 1.15. Domain structure of PARP1
The seven major domains of PARP1 collectively serve in the activation and auto-regulation of this enzyme. Zinc fingers (ZFs) 1, 2 and 3 form the DNA-binding domain for recognition and initiation of DNA damage repair pathways, and the enzyme's ability to self-assemble into damaged DNA sites is conferred by the nuclear localization signal (NLS). The BRCT domain is fundamental for DNA damage repair factor recruitment as well as the enzyme's auto-PARylation for intrinsic regulation of its activity, and is also a potential target for PARP1 inhibitory therapeutics. The WGR, HD and ART sub-domains collectively form the catalytic domain to facilitate NAD^+ binding and subsequent PARP1 activation and PAR chain generation.

1.3.2.2. Breast Cancer Associated 1 C-terminal domain

The Breast Cancer Associated 1 protein has been widely recognized as an important tumour suppressor protein. However, it was subsequently documented to possess a C-terminal domain (BRCT), and BRCT domains have been identified in other proteins to modify protein-protein interactions thereafter, specifically in those associated with DNA stability and repair [186]. In PARP1, the BRCT domain possesses auto-modification sites which entail PARP1 auto-PARylation and is predominantly the major site for this. This crucial process entails PARP1 mediated recruitment and interaction with DNA repair proteins such as X-ray Cross Complementing Group 1 (XRCC1) and 8-oxoguanine-DNA glycosylase (OGG1) that is PAR dependent for the activation and regulation of PARP1 [186–188]. While dispensable for global DNA damage repair [189,190], functional roles of this domain which extend beyond DNA repair have been documented, including protection from mutagenic effects arising from diversification of antibody genes in B-cells [190], DNA

mismatch repair [191], and BRCT domain targeting PARP1 inhibitors for improved selectivity [192].

1.3.2.3. Tryptophan-Glycine-Arginine domain

The Tryptophan (W)–Glycine (G)–Arginine (R) (WGR) rich domain of PARP1 spans approximately 90 amino acids. The WGR domain facilitates interdomain contact between PARP1 and damaged DNA for PARP1 binding and subsequent activation [170,193]. Specifically, the W589 residue is paramount for PARP1 dissociation from DNA breaks to facilitate PARP1 accumulation for efficient repair [194]. The pharmacological compound Salidroside acclaimed for neuroprotective and anti-inflammatory effects, exhibits its anti-oxidative stress effects through activation of PARP1 via the WGR domain in hematopoietic stem cells [195]. Interestingly, the WGR domain of PARP1 enables activation in a RNA-dependent manner [196], which explains PARP1's ability to regulate transcription amongst a plethora of its other functions in cellular homeostasis. Aside from this, the WGR domain is also implicated in other signalling cascades driving DNA damage repair, such as interaction with Homeodomain-interacting protein kinase 2 (HIPK2) and heat shock protein (HSP) 70 kDa (HSP70) [197].

1.3.2.4. Catalytic domain

The catalytic domain of PARP1 is further composed into 2 sub-domains – the Helical Subdomain (HD) and the ADP-ribosyltransferase (ART) domain. The HD is a helical structure that possesses auto-inhibitory properties. In its folded state, it selectively blocks the binding of NAD^+ to the NAD^+ pocket located within the ART domain [193,198], while unstimulated PARP1 exhibiting low basal activity can be ascribed to the HD providing access to low NAD^+ binding during DNA damage repair [198]. Recognition of damaged DNA sites induces a step-

wise reaction initiated by the ZF domains and interdomain contact between the WGR and damaged DNA that results in the destabilisation of the HD to expose the NAD^+ binding pocket, resulting in PARP1 activation and ART activity (Fig. 1.16). Complete deletion of HD from PARP1 results in activation in the absence of DNA damage [193]. While activity remains somewhat similar to wild-type (WT) PARP1 activated in the presence of DNA damage [193], it can be suggested that the repercussions from HD deletion translates into a rapid depletion of intracellular NAD^+ stores due to persistent activation.

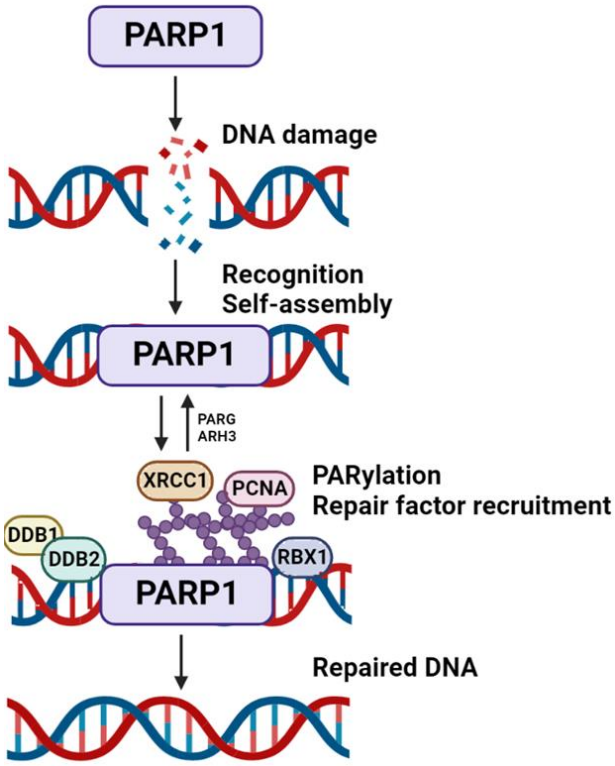

Figure 1.16. PARP1 mediated PARylation in the DNA damage repair response
PARP1 can facilitate base excision, nucleotide excision and double strand break repairs of DNA. The domains of PARP1 allow recognition and self-assembly into damaged DNA sites and initiate PARylation of substrates and itself to result in the recruitment of DNA damage repair factors such as XRCC1. Abbreviations: PCNA, proliferating cell nuclear antigen; DDB1, DNA damage-binding protein 1; DDB2, DNA damage-binding protein 2; RBX1, ring-box 1.

The ART domain of PARP1 is predominantly recognized as the catalytic core of the enzyme and highly conserved across PARP family members. It is composed of a donor site and acceptor loop, and within this donor site lies the HYE triad signature as detailed in *Section 1.3.1*. The H862 and Y896 residues are required for NAD^+ binding while the E988 residue mediates NAD^+ positioning and subsequent catalysis [199]. The significance of these residues have been underscored in mutation studies. H862 mutation results in catalytically inactive PARP1 [200], while E988 mutations abolishes PARP1's ability to elongate PAR chains [170,200]. More recently, a T910A mutation was identified in a patient exhibiting resistance to the therapeutic PARP1 inhibitor Olaparib [201], highlighting challenges and a remit for development of novel PARP1 inhibitors to target different regions of PARP1. The acceptor loop, on the other hand, contributes to PARP1 activity by serving to initiate, elongate and branch PAR chains by binding to the target proteins [160], and residues implicated in normal function include M890 and Y896 [202].

1.3.3. PARP1 roles in transcription regulation and RNA metabolism

Given PARP1 roles in genome maintenance as detailed in *Section 1.3.2*, emerging studies have implicated roles for transcriptional control by this enzyme that is mediated by, or independently of, its PARylating activity. For example, PARP1 can act as a nucleosome binding protein that maintains open regions of chromatin at promotor regions [203]. PARP1 can also facilitate the binding of the pioneer transcriptional factor SRY-box 2 (Sox2) to nucleosomes within intractable chromatin regions [204], and also coregulate transcriptional factors [175,176,205–210] (Fig. 1.17). Chromatin remodelling, a fundamental process that modulates chromatin conformational changes to permit accessibility for

DNA-binding factors as well as transcriptional factors, is regulated by PARP1. Specifically, PARP1 exerts its role in this regard through regulation of the histone proteins and chromatin remodelling complexes and enzymes. Notably, the H1 histone is a substrate of PARP1 mediated PARylation, an event that result its dissociation from chromatin, causing chromatin decondensation to promote immediate early gene expression [211–213]. Furthermore, the four core histone (H2A, H2B, H3 and H4) proteins have also been documented as targets of PARP1 mediated PARylation [212,214]. PARP1 also mediates the recruitment of the histone PARylation factor 1 (HPF1) complex by acting as a histone chaperone to promote chromatin reassembly as part of the DNA damage response [215,216]. More recently, HPF1 has been demonstrated to regulate the length of PAR chains generated by PARP1 and also converts PARP1 into a NAD^+ hydrolase to result in hydrolysis of ADPR [217]. PARylation by PARP1 also mediates recruitment of chromodomain-helicase-DNA-binding protein 1-like (CHD1L) to trigger chromatin relaxation [218,219]. These imply PARP1 mediated roles in modulation of chromatin structure and subsequently, transcriptional control and gene regulation.

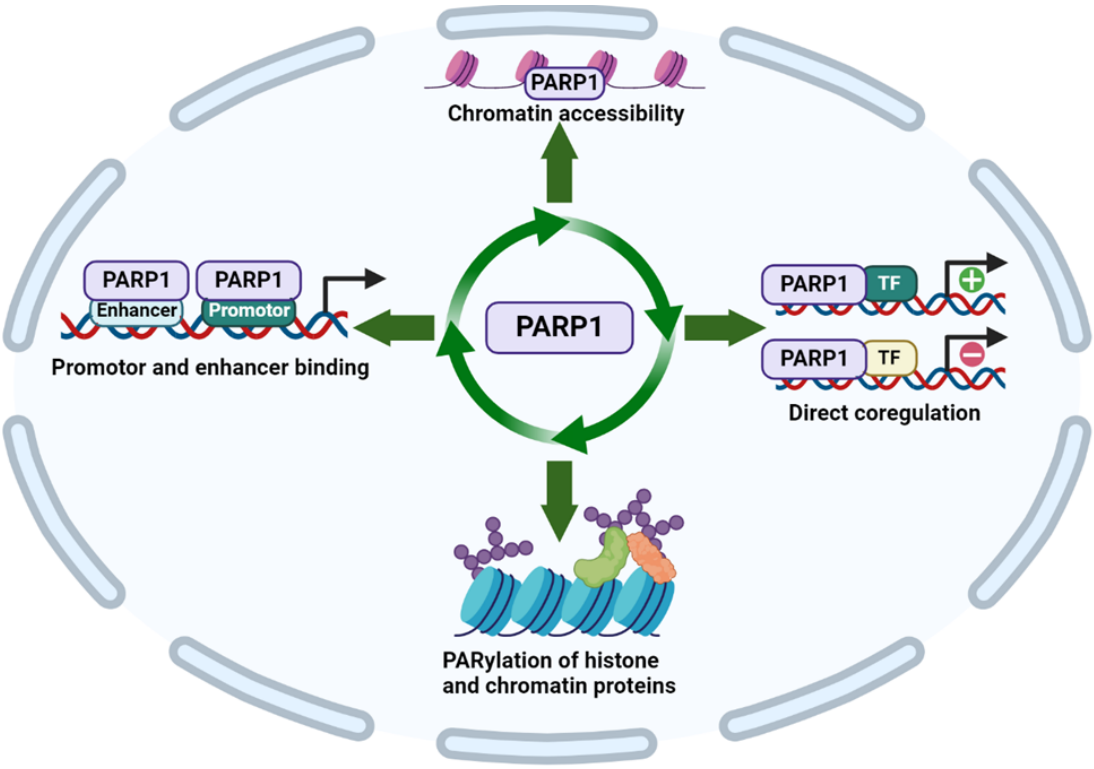

Figure 1.17. PARP1 roles in transcriptional regulation
Mechanisms of transcriptional regulation by PARP1. PARP1 can 1) modulate chromatin machinery and open chromatin regions for binding of DNA-binding factors, 2) bind directly to transcriptional factors, 3) PARylate histones and chromatin proteins to initiate chromatin remodelling and 4) bind directly to promotor and enhancer regions on DNA to modulate transcription. These mechanisms can occur independently of its catalytic activity.

Subsequently, PARP1 has been demonstrated to directly bind to RNA [220–222] and this is contributed by all PARP1 domains [223]. Further studies demonstrated that PARP1 utilizes a unique combination of domains for its binding to RNA, and domains that exert greater influence in PARP1's ability to bind RNA include its ZF3 and the C-terminal end [179,224]. PARP1 also plays fundamental roles in RNA metabolism, from biogenesis (transcription, splicing, and polyadenylation) to modifications, stability, export, and ribosome assembly. This regulation occurs either through its direct binding to its binding partners (DNA, RNA, protein) and/or through PARylation or PAR recognition by target molecules [225].

1.3.4. PARP1 in the mitochondria

PARP1 mediated PARylation also plays roles in the regulation of signalling networks controlling mitochondrial activity and health. While there is substantial consensus for PARP1 mediated PARylation in the nucleus and cytosol, mitochondrial roles for PARP1 and the PAR it deposits remain to be fully documented, but emerging. Recently, mitochondrial PARP1 presence and PARylating activity was corroborated and fundamental for mtDNA transcriptional regulation [167]. The hyperactivation of PARP1 due to oxidative stress and DNA damage is known to be antagonistic to overall mitochondria health, including distorted morphologies, increased mitochondrial ROS accumulation and subsequently reduced efficiencies of oxidative phosphorylation and ATP generation [226]. Excess PARP1 mitochondrial activity is also detrimental to mtDNA integrity [227]. The degradation of PAR chains have also been identified to trigger AMP-dependent mitochondrial energy failure [228]. Subsequently, depletion, pharmacological inhibition, or loss of function mutations of PARP1 promotes mitochondrial biogenesis and repair [132,229,230]. Additionally, PARP1 regulates transcriptional factors that themselves regulates the expression of mitochondrial complexes and proteins. For example, hypoxia-inducible factors (HIFs) are activated in response to hypoxia and oxidative stress, and activation of PARP1 serves to promote activity of HIFs [231]. Consequently, HIFs mediate the activation of transcriptional programmes to suppress glycolysis and subsequently, energy generation. Given PARP1 is a major consumer of NAD^+, and observations that NAD^+ is subcellularly compartmentalized (outlined in *Section 1.23*), recent studies have shown that mitochondrial NAD^+ exerts control over nuclear PARP1

mediated PARylation [168]. Furthermore, PARP1 activity impacts activity of other NAD^+ dependent enzymes in the mitochondria. This is evident with SIRT1, which is activated in response to elevated NAD^+ levels to subsequently deacetylate and activate transcriptional factors that drive mitochondrial biogenesis such as FOXO1 and PGC1α [106,131,132] and augment mitophagy [232]. This implies that mitochondrial dysfunction by PARP1 can occur as a cause and consequence of its activity.

1.3.5. Metabolic and aging implications of PARP1

PARP1 also exerts influence over metabolic regulation. Roles for PARP1 have been demonstrated in circadian rhythms through the PARylation of the heterodimer CLOCK-BMAL1, master genes in circadian regulation [233], and PARP1 null mice have increased activity and higher energy expenditures at night [131]. PARP1 activity also drives the translocation and transcription of Nuclear factor kappa B (NF-κB) [234,235], and this subsequently mediates expression of pro-inflammatory genes such as Tumour Necrosis Factor Alpha (TNFα) and Interleukin 6 (IL6) [236]. Direct regulation of pro-inflammatory genes such as Nuclear Factor of Activated T cell (NFAT) and Yin Yang 1 (YY1) by PARP1 have also been reported [237,238], whilst PARP1 null mice have exhibited inflammatory resistance [239]. Consequently, PARP1 itself can hold influence over severity of pathogenic infection and efficiency of immune system response [116].

The suppression of PARP1 activity and its expression, as well as NAD^+ precursor supplementation, are protective against age associated and high fat diet-induced obesity [106,131,240]. Administration of PARP inhibitors in mice improves glucose uptake, insulin sensitivity and exercise performance [132].

Furthermore, PARP1 null mice also have significant reductions in serum triglyceride and free fatty acid levels [241]. These studies further highlight PARP1 and SIRT1 NAD^+ dependent crosstalk, whereby increased SIRT1 activity is protective against the obesity phenotype [106,131,240]. In contrast, inhibition of SIRT1 activity results in exacerbated obesity phenotypes [242,243], implying PARP1 exerts negative metabolic impacts via SIRT1. PARP1 also has plausible roles in cholesterol metabolism in models of atherosclerosis although the mechanisms that underlie this remain elusive [244].

1.3.6. PARP1 in differentiation

Involvement of PARP1 in differentiation of various cellular models was initially described in bone-marrow derived cells such as monocyte/macrophages, neutrophils and erythroids [245–247]. Further studies have since demonstrated PARP1 as regulating differentiation of a broader spectrum of tissues including adipocytes, skeletal muscle, osteoclasts and oligodendrocytes [176,205,206,210,248]. These are mediated by PARP1's abilities to regulate gene expression, modulate chromatin structure and mitochondrial activity that themselves are events that occur during differentiation.

Adipogenesis, the differentiation of preadipocytes into mature adipocytes is dependent on the transcription of adipogenic genes such as PPARγ2 and C/EBPβ, which are targets of PARP1 mediated PARylation [209,249]. PAR deposition subsequently impedes adipogenesis in pre-adipocytes in a nuclear NAD^+ dependent manner [103,209], and PARP1 null 129/Sv mice presented hypersensitivity to diet-induced obesity and heightened insulin resistance [250]. Interestingly, PARP1 null C57BL/6J mice are leaner due to reduced white adipocyte mass, although high fat diets increased hepatic lipid accumulation

[241]. Similar results were observed in C57BL/6J mice treated with PARP inhibitors [131,240]. These strain-specific findings underscore the diversity the PARP1 plays in signalling pathways, and also further implies roles for PARP1 in adipocyte modelling within the context of adipogenesis and body fat accumulation.

During myogenesis, PARP1, independent of its catalytic activity, is able to bind to regulatory regions of the muscle genes p57 and myogenin, interfering with their targeted transcription by MyoD for initiation of myogenesis [176]. Following myogenesis, PARP1 levels are reduced in fully differentiated myotubes compared to undifferentiated myoblasts, and this is also important for conferment of oxidative stress resistance in the differentiated myotube [251]. It can therefore be inferred that the degradation of PARP1 is seemingly important with regards to driving the myogenic transcriptional programme. Recent work has also demonstrated that MyoD driven transdifferentiation of fibroblasts into myoblasts causes an increase in PARP1 mediated nuclear PAR deposition [207]. These emerging works suggest that PARP1 exerts impacts over myogenesis through the regulation of genes associated with myogenesis, which currently in this regard, is MyoD, and as a consequence, impacts on overall metabolism.

1.3.7. SIRTs

SIRTs derive their name from Silent Information Regulator 2 (SIR2), which was first identified in the late 1970s in *Saccharomyces cerevisiae* [252] with subsequent homologs later identified [253]. It was subsequently discovered that SIR2 was a NAD^+ consuming enzyme possessing ADP-ribosylation activity [254] and able to mediate deacetylation of histones [255]. Furthermore, SIR2 was able

to prolong lifespan in yeast [256], laying the foundation for its implications in whole body metabolism and wellbeing. To date, 7 mammalian SIRTs have been identified which are ubiquitously expressed and localized to different subcellular compartments (Table 1.3). All members possess a conserved catalytic domain entailing a NAD^+ binding pocket for activity [257].

SIRT	Localization	Activity	Alternate activity
SIRT1	Nucleus / Cytoplasm	Deacetylation	ADP-ribosylation
SIRT2	Cytoplasm	Deacetylation	Delipoylation
SIRT3	Nucleus / Mitochondria	Deacetylation	Undefined
SIRT4	Mitochondria	Deacetylation	Delipoylation / ADP-ribosylation
SIRT5	Mitochondria	Deacetylation	Desuccinylation / Demalonylation
SIRT6	Nucleus	Deacetylation	ADP-ribosylation/ Demyristoylation/ Depalmitoylation
SIRT7	Nucleolus	Deacetylation	Undefined

Table 1.3. SIRT family of enzymes

Generally, SIRTs catalyse target protein deacetylation at Lys residues through the hydrolysis of NAD^+ to yield O-Acetyl-ADPR (OAADPr) and NAM alongside the resulting deacetylated substrate (Fig 1.18). OAADPr can be subsequently hydrolysed by ARH3 into ADPR [258]. Like ADPR, OAADPr accumulation can also modulate homeostatic processes including chromatin and transcription regulation as well as Ca^{2+} signalling through interaction with binding partners such as transient receptor potential cation channel, subfamily M, member 2 (TRPM2) and MacroH2A1.1 [259].

Although predominantly protein deacetylases, some members of the SIRT family also possess alternate catalytic activities. Additionally, some SIRTs are

also able to translocate to different subcellular compartments. SIRT1 (nuclear and cytoplasmic), SIRT4 (mitochondria) and SIRT6 (nuclear) exhibit ADP-ribosylating activity [260,261]; SIRT3 (nuclear and mitochondria) exerts deacetylation activity only [261,262]; SIRT2 (cytoplasmic) and SIRT4 possess delipoylation activity [263]; SIRT5 (mitochondria) possesses desuccinylation and demalonylation activities [264]; SIRT6 also exerts demyristoylation and depalmitoylation activities [260,265]. Alternate activity for SIRT7 (nuclear) has yet to be ascertained, although its deacetylation activity is crucially involved in transcription during ribosomal biogenesis [266] (Table 1.3). Nevertheless, SIRTs are crucial in a plethora of whole body metabolic processes and beneficial aging [81,133,260].

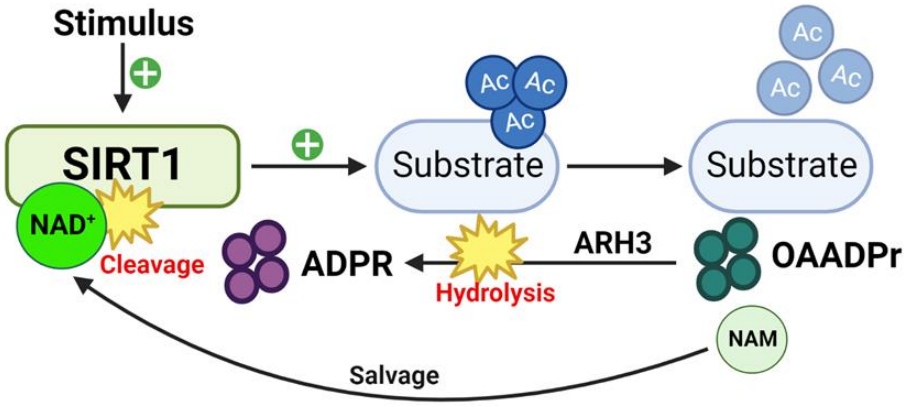

Figure 1.18. SIRT mediated consumption of NAD$^+$
Caloric restriction and pharmacological compounds can result in the activation of SIRTs such as SIRT1 to consume NAD$^+$ to deacetylate target substrates, releasing OAADPr and NAM in the process. OAADPr can be hydrolysed into ADPR in a reaction catalysed by ARH3, while NAM can be recycled via salvage pathways for NAD$^+$ regeneration. NAM can also act as an inhibitor of SIRT1 activity. SIRTs have documented roles in metabolic homeostasis including calcium signalling, mitochondrial function and glucose metabolism.

1.3.8. cADPR synthases

Beyond PARPs and SIRTs, another family of NAD$^+$ consumers are the cADPR synthases, also referred to as ADP-ribosyl cyclases. Upon stimulation, cADPR synthases catalyse synthesis of cADPR from NAD$^+$ to yield NAM as a by-

product that is subsequently recycled. cADPR is a crucial molecule in second messenger signalling for the regulation of Ca^{2+} signalling which is substantially pertinent and far reaching, controlling critical processes such as neurotransmitter release, immune response, muscle contraction and insulin release [267] (Fig. 1.19).

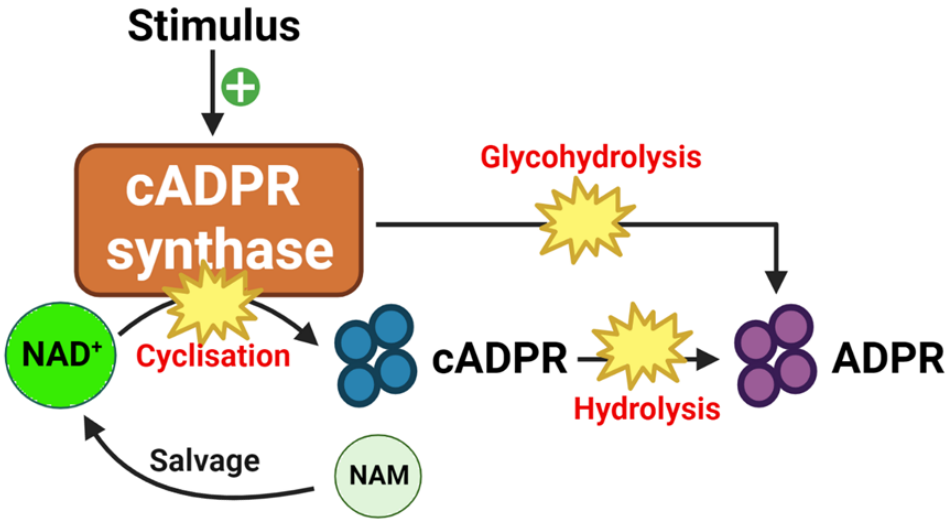

Figure 1.19. cADPR synthesis from NAD^+
Neurotransmitters such as acetylcholine and intracellular increases cause the activation of the cADPR synthase enzymes. These enzymes display multifaceted roles, where it can either 1) act as cyclases to generate cADPR directly from NAD^+, 2) catalyse the hydrolysis of cADPR into ADPR or 3) act as a NAD^+ glycohydrolase to directly produce ADPR from NAD^+. The type of activity exhibited is dependent on pH. Consequently, cADPR is crucial for Ca^{2+} signalling including muscle contraction and neurotransmission.

In mammals, CD38 are ubiquitously expressed transmembrane proteins that can function as receptors or enzymes. Its dominant expression on the surface of many immune cells such as natural killer and B cells [268,269], has rendered interest in its role in pathological studies and immunomodulation since its discovery. Studies have also reported CD38 diverse roles in cardiac injury, obstructive pulmonary disease and oxytocin response [137,270,271]. Like SIRTs, CD38 possesses multi-functional enzymatic activity, acting as a NAD^+ glycohydrolase (NADase), generating ADPR from NAD^+ or, hydrolyses cADPR into ADPR. In the presence of NA, CD38 can also mediate the

hydrolysis of NADP into NA-ADP in a reaction that is dependent on pH [268]. Interestingly, despite being the major contributor of cADPR activity in mammalian cells, only a minor amount of total product produced by CD38 following NAD^+ incubation is cADPR, whereas ADPR comprises the majority [271]. Consequently, its utilization of 100 NAD^+ molecules to generate a single cADPR molecule therefore renders CD38 a major NAD^+ consuming enzyme in mammals [102,117]. Notably, CD38 can mediate NR and NMN degradation before their entry into the cell and is upregulated in tissues of the aging phenotype [2]. Therefore, not only does CD38 impacts activities of other NAD^+ consuming enzymes and overall NAD^+ homeostasis, it further exacerbates age-related NAD^+ decline as well.

CD157, a homolog of CD38, is another member of cADPR synthases and also exhibits NADase activity. Unlike CD38, however, CD157 is: 1) significantly less efficient in cADPR synthesis [91,268], 2) predominantly expressed within tissues of the gut and lymphoid [110,272], and 3) unable to hydrolyse cADPR to ADPR [110]. Like CD38, CD157 is implicated in a plethora of immunomodulatory processes, notably the migration, adhesion and extravasation of leukocytes [272].

Sterile alpha and TIR motif-containing 1 (SARM1) is another recently discovered NAD^+ consuming enzyme, possessing a Toll/Interleukin 1 receptor (TIR) catalytic domain. Although SARM1 is mainly expressed in neurons, its TIR domain is able to partake in Toll-like receptor signalling for modulation of immune response [273]. The TIR domain utilises NAD^+ to produce ADPR and NAM, as well as cADPR. This process of NAD^+ utilization by SARM1 manifests into axon destruction during neuronal injury [274,275], and destruction is

attenuated by SARM1 deletion [124,275,276], supplementation of NR and NAMPT or NMNAT overexpression [142,150].

1.3.9. ARTCs

ARTCs degrade NAD^+ in a similar fashion as PARPs for the transfer of ADPR groups specifically, onto Arg residues of target proteins [277]. ARTC1 was the first mammalian ARTC identified within the rabbit skeletal muscle as a membrane-associated ARTC [278]. Subsequently, five mammalian ARTCs have been identified. Humans, however, possess a pseudo ARTC2 gene, thereby expressing only four of the ARTCs as a result, while murine ARTC2 exists in 2 allele variants, ARTC2.1 and ARTC2.2 [277]. ARTCs 1 – 4 are ecto-enzymes anchored via a glycosylphosphatidylinositol tail to the outer membrane, and ARTC5 is secreted to the extracellular space [277]. ARTCs 1, 2 and 5 possess a characteristic Arg (R)-Ser (S)-Glu (E) (RSE) triad signature which have been corroborated to exert NAD^+ binding and Arg-specific MARylation activity while ARTC3 and ARTC4 do not possess this triad, rendering them catalytically inactive [279,280].

Amongst the catalytically active ARTCs, ARTC1 and ARTC2 are the most well-studied. ARTC1 is predominantly expressed in airway cells as well as in skeletal and cardiac muscle [281–283]. In skeletal and cardiac muscles, ARTC1 basally MARylates Arg residues of a number of proteins on the cell surface and extracellular space associated with cell adhesion, muscle contraction, and regulation of signal transduction, and its functional significance was underscored with ARTC1 null mice exerting muscle weakness [283]. ARTC1 also has roles in endoplasmic reticulum stress response via the MARylation of glucose-regulated protein of 78 kDa/immunoglobulin heavy-chain-binding

protein (GRP78/BiP) [284]. Other substrates of ARTC1, including integrin α7, fibroblast growth factor 2 (FGF2) and platelet-derived growth factor-BB (PDGF-BB) have been identified [285–288].

In contrast, the murine ARTC2, initially identified as RT6 as an alloantigen, is expressed within T cells, natural killer cells and macrophages [289–291]. This, together with studies of ARTC1 in airway cells controlling inflammatory response, strongly imply roles for these catalytically active ARTCs in immunomodulatory response. To date, the functional characterisation of ARTC5 and its associated substrates remains relatively elusive. Nevertheless, the presented studies suggest that ARTCs also exert dynamic influence over different aspects of physiology.

1.4. Glucocorticoids

Glucocorticoids (or cortisol in humans, corticosterone in rats/mouse) are a major class of steroid hormones with pleiotropic physiological effects. They serve as ligands for the ubiquitously expressed glucocorticoid receptor (GR) to subsequently modulate cellular phenotypic and inflammatory status. Mineralocorticoid receptors (MR), while not as ubiquitously expressed as their GR counterparts, can also bind glucocorticoids with higher affinities. The pharmacological use of glucocorticoids have attracted tremendous interest in understanding the molecular mechanisms of GR mediated signalling and mammalian transcriptional regulation due to their anti-inflammatory effects and sensitivity within tissues. In humans, GR is encoded by the *NR3C1* gene and two main isoforms exist: GRα comprised of 777 amino acids and GRβ comprised of 742 amino acids [292]. GR is composed of 4 major domains: the

NTD, the DNA binding domain (DBD), the hinge region and the ligand binding domain (LBD) (Fig. 1.20).

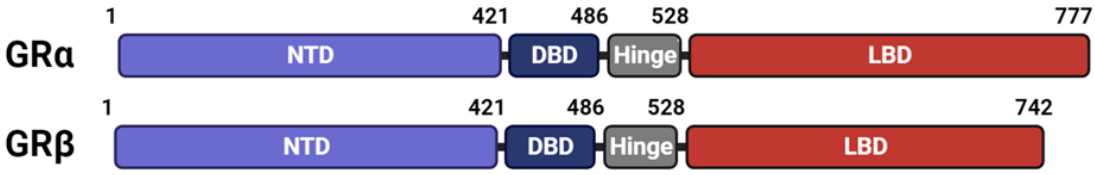

Figure 1.20. Domain structure of the two main glucocorticoid receptor isoforms in humans
Two GR isoforms exist from alternative splicing. Both isoforms possess four distinct domains: the N-terminal domain (NTD), DNA binding domain (DBD), hinge domain and the ligand binding domain (LBD). The NTD entails the recruitment of transcriptional coregulators and machinery. The DBD domain is highly conserved, and is comprised of two zinc finger motifs which also allow dimerization between other GR partners. The flexible hinge region possesses nuclear localization sequences, and the LBD fundamentally serves for glucocorticoid binding and activation of GR. GRβ possesses a shorter LBD and is consequently unable to bind glucocorticoids, rendering this isoform catalytically inactive, but still able to contribute to glucocorticoid actions.

Subsequently, GRα is perceived to be the main isoform in mediation of glucocorticoid effects due to 1) its major abundance amongst other isoforms and 2) GRβ possessing a shorter LBD, restricting its ability to bind glucocorticoids [293]. However, GRβ actions have been documented to influence GRα activity [294].

1.4.1. Mechanisms of GR activation by glucocorticoids

Glucocorticoids are typically produced and secreted in response to stress. Activation of the hypothalamus–pituitary–adrenal axis (HPA) following release of corticotropin-releasing hormone initiates the subsequent synthesis and release of adrenocorticotropic hormone to the adrenal glands where glucocorticoids are synthesised and secreted [295]. The paracrine and endocrine effects of glucocorticoids are mediated by the corticosteroid-binding globulins (CBG) which bind, transport and release glucocorticoids into cells. Glucocorticoid bioavailability is mediated by two enzymes: 11β-hydroxysteroid

dehydrogenase 1 (HSD11β1) and 2 (HSD11β2) (Fig. 1.21). The former activates, while the latter enzyme catalyses oxidation to consequently inactivate glucocorticoids [296].

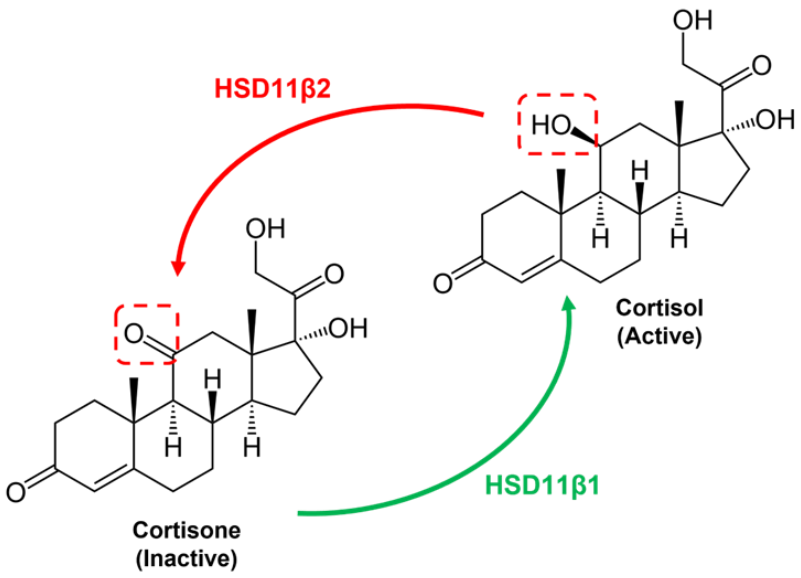

Figure 1.21. Regulation of glucocorticoid bioavailability
In humans, glucocorticoids can be metabolized into two forms. The inactive form, cortisone, is reduced and activated by HSD11β1 into the active form, cortisol. Conversely, active cortisol is oxidized by HSD11β2 back into inactive cortisone.

Basally, GR resides primarily in the cytoplasm, kept inactive by a complex of chaperone and HSPs as well as immunophilins [294,297]. Upon glucocorticoid binding, this complex dissociates from GR, permitting the receptor's activation and translocation from the cytoplasm into the nucleus via a nuclear pore [298]. Within the nucleus, GR recognizes specific glucocorticoid response elements (GRE) on DNA, and exerts genomic effects by 1) tethering itself to transcription factors, 2) recruitment of transcriptional coactivators or corepressors (Fig. 1.22). These genomic effects can be mediated by GR as a monomer, dimer or tetramer [299].

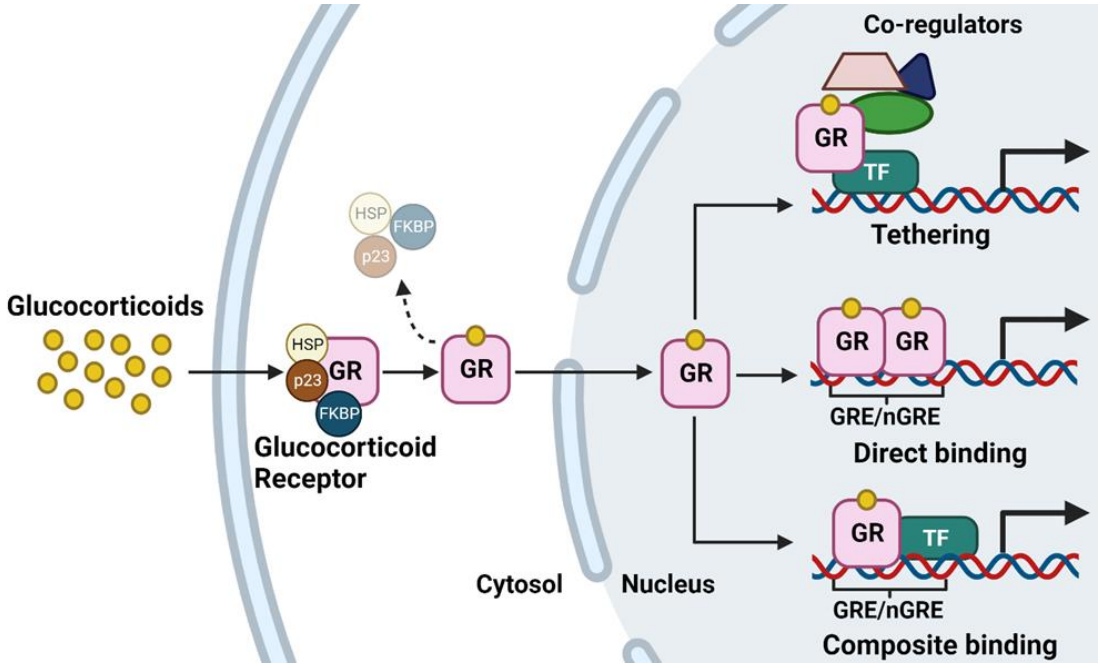

Figure 1.22. Mechanisms of classical GR activation
Inactive GR is predominantly localized within the cytosol that is held within an inactive multimeric complex with other proteins such as heat shock proteins. Upon glucocorticoid binding to the GR, this complex dissociates, permitting the translocation of activated GR into the nucleus to initiate genomic responses by 1) tethering with other transcriptional factors (TF) to result in the recruitment of transcriptional co-regulators, 2) directly binding to glucocorticoid response elements (GRE) or negative GRE (nGRE) and 3) exhibiting composite binding via binding to both GREs and transcriptional factors. GR can exert these genomic effects either as monomeric or tetrameric forms. GR can also exhibit nongenomic effects.

1.4.2. Nongenomic effects of GR activity

GR activation by glucocorticoids also exerts nongenomic effects, which occur independently of transcription. These can occur by three established mechanisms: 1) non-specific glucocorticoid interaction with cell membranes, 2) glucocorticoid interaction with cytosolic GR, and 3) glucocorticoid interaction with membrane-bound GR [300]. Some processes regulated by nongenomic GR effects include Ca^{2+} signalling [300–303] and immune cell response [304–307].

Notably, nongenomic GR effects have been observed in the mitochondria. First, presence of GR has been documented in the mitochondria [308].

Additionally, GR binding sites within mtDNA display homology to GRE, and induction of mitochondrial oxidative phosphorylation gene expression following GR activation has been documented [309]. These suggest that glucocorticoids themselves can directly regulate mtDNA, and consequently, mitochondrial homeostasis in a nongenomic fashion.

1.4.3. Metabolic repercussions of long-term glucocorticoid response

Largely documented side effects of long-term glucocorticoid administration are associated with metabolic dysfunction phenotypes collectively classified as Cushingoid features, some of which are abdominal obesity, dyslipidemia, cervical fat deposits, insulin resistance and hyperglycemia [310–313]. Notably, glucocorticoid deleterious effects disrupt glucose metabolism. Within the pancreas, chronic glucocorticoid exposure induces apoptotic mediated β cell death and subsequent failure of insulin secretion [314–318]. In adipose tissue, glucocorticoids promote lipodystrophies where visceral adipose tissue mass is increased concomitantly with a decline in subcutaneous fat [319,320]. Additionally, glucocorticoids also promote lipolysis and release of free fatty acids that are transported in circulation and deposited into other organs of metabolic importance such as the liver and skeletal muscle [319,320], as well as downregulate the glucose transporters GLUT1 and GLUT4, reducing glucose uptake [321] to exacerbate metabolic dysfunction. Within the liver, glucocorticoids can also induce insulin resistance through inhibition of the insulin receptor pathway whilst promoting activity of enzymes and pathways of gluconeogenesis which manifest in a hyperglycaemic phenotype [322,323]. Crucially, dexamethasone treatment compromised structural and functional integrity within hepatocyte mitochondria mediated by alterations in mtDNA,

increased ROS accumulation and dysfunctional pathways of energy generation [324]. While short-term glucocorticoid therapy might be effective, these studies necessitate a remit for further understanding and development of alternative forms of non-steroidal treatments for long-term therapy.

1.4.4. Impacts of glucocorticoids on skeletal muscle

Skeletal muscle is also a target of glucocorticoid mediated effects. The application of dexamethasone at the myoblast stage enhances subsequent myogenesis [325–327]. However, administration of glucocorticoids in fully differentiated myotubes results in an upregulation of skeletal muscle atrophy factors such as MuRF1, atrogin1 and myostatin to induce myopathy [326,328–331]. As detailed in *Section 1.4.3*, the deleterious impacts of chronic glucocorticoid exposure within skeletal muscle also pertain to glucose homeostasis via suppression of insulin-induced GLUT4 transporter translocation [332] and glycogen synthase to inhibit glycogenesis [333]. Clinically however, intermittent glucocorticoid treatments improve outcomes of skeletal muscle regeneration following injury [334]. These paradoxical effects on skeletal muscle further underscore the short-term beneficial effects of glucocorticoids, necessitating mechanistic study into fully utilizing the benefits of glucocorticoid therapy in this organ.

1.5. Thesis Rationale

PARP1 is well-established as an enzyme that facilitates DNA damage repair through its consumption of NAD^+ for PARylation and regulation of substrates. Significant advancements have also demonstrated roles for PARP1 independent of its catalytic activity in biological processes too, including myogenesis [176] and chromatin remodelling [203,204]. In tandem with its PARylating activity, this enables PARP1 to modulate biological outcomes in the regulation of tissue-specific gene expression, with documented roles in almost every organ of the human body (Fig. 1.23).

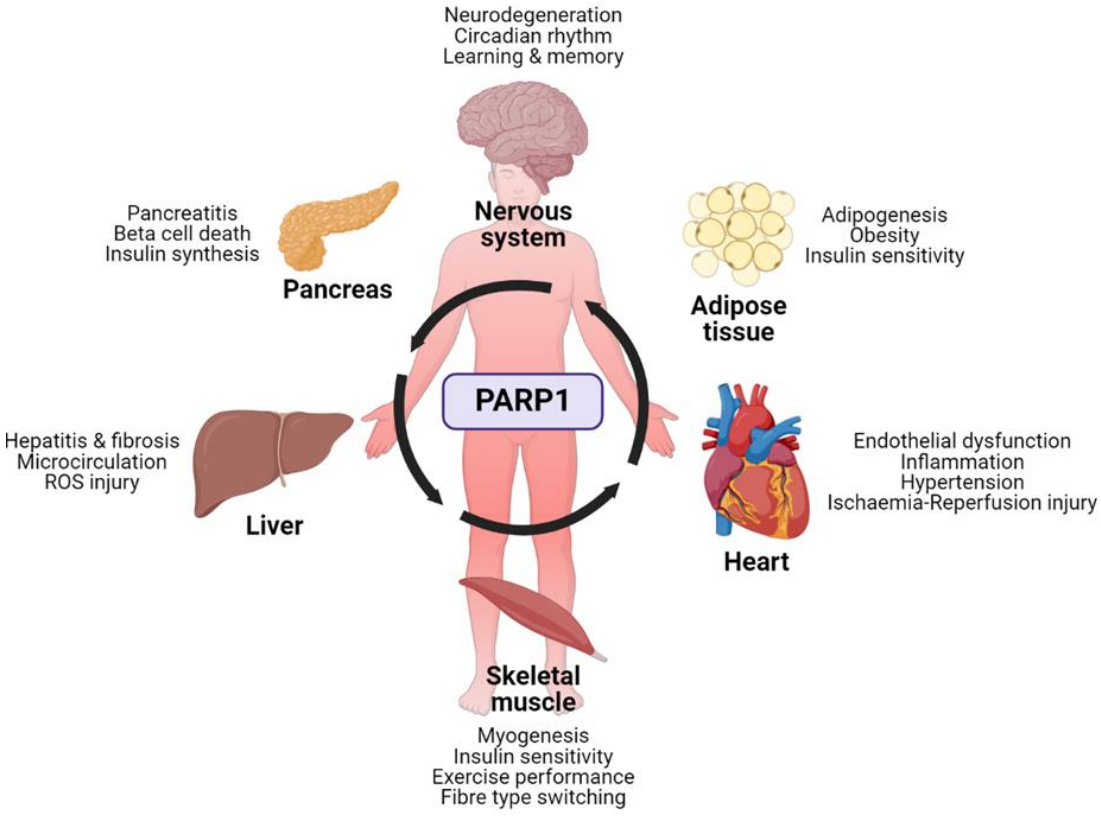

Figure 1.23. Documented roles for PARP1 in human organs
PARP1 actions have impacts on whole body metabolic homeostasis.

Mounting evidence is emerging for roles of PARP1 in the skeletal muscle. Studies employing strategies that downregulate PARP1 activity results in enhanced metabolic phenotypes and functional performance [131–133,251,335]. While roles for PARP1 mediated PARylation have already been described in differentiation programmes, detailed in *Section 1.3.6*, knowledge of this process in skeletal muscle myogenesis remain, undefined. Additionally, processes such as inflammation and transcriptional regulation are mutual between PARP1 and glucocorticoid actions.

This work seeks to deepen our understanding and appreciation of PARP1 mediated PARylation in skeletal muscle myogenesis, physiology and potential mechanisms delineating glucocorticoid response outcomes. In order to address this fundamental question, the work utilizes strategies to modulate PARP1 activity at the induction of myogenesis. This would be supplemented with further work exploring the proteome and transcriptome of skeletal muscle to give broader perspectives into the physiological impacts of PARP1 catalytic activity modulation. Understanding these impacts would serve to provide a basis for PARP1 inhibition as a potential form of therapy in maintenance of skeletal muscle mass during aging and disease.

1.6. Hypothesis

We postulate that skeletal muscle myogenesis and function are impacted by PARP1 mediated PARylating events. Further to this, we hypothesize that PARP1 has roles in governing glucocorticoid response within skeletal muscle and may mediate the effects of glucocorticoid exposure.

1.7. Aims

The work in this thesis seeks to address the following research questions.

1. Establish dynamics and impacts of PARP1-mediated PARylation in skeletal muscle myogenesis trajectory using protein analysis techniques and preliminary assessment of myotube development (Chapter 3).
2. Understand how inhibition of PARP1 activity at the induction of myogenesis affects subsequent muscle function by exploring the muscle proteome and transcriptome (Chapter 4).
3. Investigate mechanisms whereby the skeletal muscle response to glucocorticoids occurs via a PARP1-dependent mechanism (Chapter 4).
4. Characterise the dynamics of PARP1 and PAR deposition in mice subjected to metabolic challenge using high fat diet and knockout (KO) of genes associated with glucocorticoid and NAD^+ metabolism (Chapter 5).

Chapter 2

Materials and Methods

2.1. Tissue culture

2.1.1. C2C12 and LHCN-M2 cell lines

The murine myoblast cell line C2C12, an eminent cellular model for skeletal muscle research, was purchased from the American Type Culture Collection (VA, USA). This cell line was derived following serially passaged myoblasts from the thigh muscles of C3H/HeJ mice 70 hours after crush injury [336].

LHCN-M2 was purchased from Evercyte GmbH in Austria. This cell line was derived from satellite cells within the pectoralis major of a 41-year-old Caucasian heart transplant donor. These human myoblasts were subjected to immortalization via viral transduction of retroviruses expressing lox-hygro-hTERT (LH) and Cdk4-neo (CN) cloned into a pBABE vector backbone. Following characterisation, M2 was the designated clone number selected for further passaging due to its exemplary myotube formation amongst the other clones, giving rise to the cell line name LHCN-M2 [337].

2.1.1.1. Proliferation and cell line maintenance

Cell lines were grown and maintained in 75 cm^2, (or T75) tissue culture flasks in the growth media (GM). For the C2C12 cell line, this was composed of Dulbecco's Modified Eagle's Medium (DMEM) 25 mM glucose (Lonza, UK) supplemented with 10% (v/v) foetal bovine serum (FBS) (Thermo, UK) and 1% Penicillin/Streptomycin (P/S) (Thermo, UK). In contrast, the LHCN-M2 GM was composed of a 4:1 ratio of DMEM and Medium 199 (Sigma-Aldrich, UK) supplemented with 15% FBS, 200 mM HEPES (Thermo, UK), 0.03 µg/ml zinc sulfate (Sigma-Aldrich, UK), 1.4 µg/ml vitamin B12 (Sigma-Aldrich, UK), 0.055 µg/ml dexamethasone (Sigma-Aldrich, UK), 2.5 ng/ml hepatocyte growth factor (Proteintech, UK), 10 ng/ml basic fibroblast growth factor (Sigma-Aldrich,

UK) and 1% P/S. This composition was selected in accordance to established protocols [337].

Regular passaging of cells was performed when the confluency was approximately 70%. The cells were washed with 1x phosphate buffered saline (PBS) solution and trypsinized using TrypLE solution (Thermo, UK) for 5 minutes. GM was added to stop trypsinization and cells were pelleted by centrifugation at 1000 RPM for 5 minutes at room temperature (RT) and resuspended in fresh GM before being subsequently split into fresh flasks at the desired split ratios, or plated into culture plates for further experiments. Both cell lines were constantly maintained in a humidified incubator at 37°C supplied with 5% CO_2. Cells used for the experiments throughout this thesis were at a maximum passage number of 15, after which they were discarded.

2.1.1.2. Differentiation induction

Upon cells reaching 70 – 80% confluency, cells were differentiated by switching them from the GM into the differentiation medium (DM). For C2C12 myoblasts, the DM was composed of DMEM 25 mM glucose supplemented with 2% horse serum (HS) (Thermo, UK) and 1% P/S; for LHCN-M2 myoblasts, the DM was composed of a 4:1 ratio of DMEM and Medium 199 supplemented with 2% HS and 1% P/S. Subsequently, myoblasts were left to differentiate for a total of 6 days, sufficient for the development of mature myotubes (Fig. 2.1). Fresh DM changes were performed every other day.

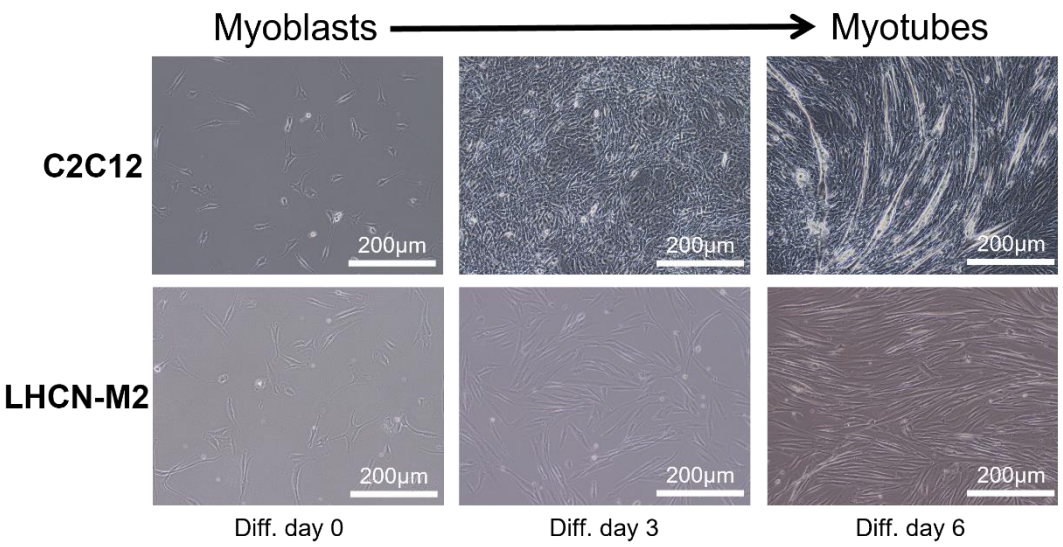

Figure 2.1. Myogenic differentiation of C2C12 and LHCN-M2 myoblasts
Myoblasts were seeded in growth media and differentiation was induced via replacement with the differentiation medium. Myoblasts were allowed to differentiate where they align and subsequently fuse together to form multi-nucleated myotubes within 6 days of differentiation.

2.1.1.3. Cryopreservation and thawing

Cryopreservation of cells were performed to ensure sufficient stocks. To do this, confluent cells were trypsinized in a similar fashion as per regular passaging as detailed in *Section 2.1.1.1*. Before centrifugation, cells were counted on a haemocytometer. Following centrifugation, cells were resuspended in the freezing media which was composed of their respective GM + 10% Dimethyl sulfoxide (DMSO), in a volume that yielded a concentration of approximately 500,000 cells/ml. 1 ml was distributed into each cryovial. Cryovials were then packed into a freezing container (commonly known as 'Mr Frosty') (Nalgene, UK) and stored at -80ºC. This freezing container, which also contains isopropanol, allows cells to be frozen at a steady state rate of 1ºC/min to prevent shock freezing and subsequently poor viability upon future use. Frozen cryovials were then transferred to liquid nitrogen until use.

For thawing of frozen cell stocks, frozen cryovials were placed into a 37ºC water bath. The thawed cells were quickly transferred into a tube containing

their respective GM pre-warmed to 37ºC and centrifuged at 1000 RPM for 5 minutes at RT, resuspended in fresh GM and transferred into a fresh T75 tissue culture flask. Cells were returned to the incubator and allowed to grow until approximately 70% confluency before being subjected to passaging as detailed in *Section 2.1.1.1*.

2.1.2. Cell treatments

Treatments detailed below were performed during differentiation induction, unless stated otherwise. Treatments were diluted in DM and left for 24 hours before washout and replaced with fresh DM and myoblasts were left to differentiate as detailed in *Section 2.1.1.2*.

2.1.2.1. PARP inhibitors

The PARP inhibitors BYK204165 (Tocris, UK) and PJ34 (MedChemExpress, NJ, USA) were reconstituted in DMSO. These compounds were diluted in DM to working concentrations of 10 µM. These concentrations were selected based on previous studies as the optimal concentration used to treat skeletal muscle cells with minimal impacts on cellular viability [251]. DMSO was used as the vehicle control.

2.1.2.2. Nicotinamide Riboside

NR (Chromadex, CA, USA) was dissolved in 1x PBS to create the stock solution which was filter sterilized. The working concentration used was 0.5 mM with 1x PBS used as the vehicle control. This concentration was selected based on previous studies as the minimal concentration required to induce the greatest elevation in NAD^+ levels in C2C12 myoblasts [106]. 1x PBS was used as the vehicle control.

2.1.2.3. FK866

FK866 is a NAMPT specific inhibitor that results in NAD^+ depletion. It was dissolved in DMSO to yield the stock solution of 100 mM, and a working concentration of 50 nM was used. This concentration was selected based on previous studies as the optimal concentration based on a dose-response curve without compromising cellular viability [338]. DMSO was used as the vehicle control.

2.1.2.4. Low glucose differentiation media

DMEM powder (Sigma-Aldrich, UK) was dissolved in water according to the manufacturer's instructions. 4 mM L-glutamine (Thermo, UK), Sodium bicarbonate (Sigma-Aldrich, UK) and 1% Sodium pyruvate (Thermo, UK), 2% HS and 1% P/S/G were added and the medium was filter sterilized. A stock of filter sterilized 1M D-(+)-Glucose (Sigma-Aldrich, UK) was added accordingly to the media to achieve the desired concentration to make up the low glucose DM which was replaced every other day of differentiation.

2.1.2.5. Dexamethasone

Dexamethasone is a synthetic glucocorticoid that exerts preferential binding to GR, and does not undergo conversion between active and inactive forms by HSD11β1 and HSD11β2 unlike endogenous glucocorticoids [339]. The stock solution was made by dissolving in ethanol, and a working concentration of 1 µM was used. This concentration was selected based on previous studies as the highest concentration that maintained cellular viability and proliferation rates in comparison to control groups [325].

2.1.3. Transfection of small interfering RNA

Small interfering RNA (siRNA) is a synthetic class of double stranded RNA that specifically targets a particular mRNA for degradation after transcription, subsequently inhibiting translation. The work in thesis utilised either Silencer™ Select Negative Control No. 1 scrambled siRNA (Thermo, UK) or a selection of siRNAs targeting *PARP1* (IDs: s62055, s62053, s62054) (Thermo, UK). For transfection, cells were seeded at approximately 100,000 cells/well in 6 well culture plates in GM and left into the incubator for at least 3 hours to allow cell adherence. For siRNA transfection, two separate tubes were set up – tube A was composed of 4 µl of the siRNA diluted to a concentration of 0.5 µg/µl and 246 µl of Opti-Mem serum and antibiotic free media (Thermo, UK). Tube B was composed of 4 µl of the transfecting reagent Lipofectamine 2000 (Thermo, UK) and 246 µl Opti-Mem serum free media. Both tubes were incubated separately for 5 minutes at RT before being mixed and incubated for a further 30 minutes at RT to allow siRNA complexes to form. Cells were first washed with 1x PBS and 1 ml of the transfection mix was added. Transfected cells were returned to the incubator for 24 hours, after which the transfection mix was replaced with fresh GM. Transfected cells were further incubated for 24 hours to enable optimal siRNA effects on translation.

2.2. Animal tissue collection

Animal tissues were kindly donated from the laboratory of Gareth Lavery at the Institute of Metabolism and Systems Research within the University of Birmingham, UK. Experimental animals were sacrificed by cervical dislocation at the end of *in vivo* experimental timepoints. Confirmation that circulation was fully ceased was made before initiation of tissue dissection and collection. The

muscle groups such as the soleus, quadriceps, tibialis anterior (TA) and gastrocnemius, as well as other tissues of metabolic importance such as the liver and heart were collected. All tissues were snapped frozen in liquid nitrogen and stored in -80 ºC until use.

2.3. Molecular Biology techniques

This section details the methodologies used to assess changes in gene expression.

2.3.1. RNA isolation

RNA was extracted using TRIzol Reagent (Life Technologies, UK). This reagent is the most effective and widely used in the initial cell harvesting process for RNA extraction due to its ability to maintain RNA integrity through inhibition of RNA degrading enzymes known as ribonucleases (RNases), dissolving cellular components and denaturing proteins to obtain optimal yield and RNA purity that is free from contaminants following isolation. For optimal RNA yields and quality, all surfaces and pipettes were wiped down with RNAase AWAY™ surface decontaminant (Thermo, UK) prior to initiation of harvesting and isolation. Filter tips were also used throughout the processes which will be detailed below.

In a 6 well plate, cells at the end of experimental timepoints were washed with 1x PBS. 1 ml of TRIzol reagent was added and the wells were rinsed by pipetting up and down to ensure maximal disruption and harvesting of cells. Harvested lysates can be used immediately for RNA isolation or can be stored in -80 ºC until use.

Subsequent RNA isolation was performed using the phenol-chloroform method. For each sample, 200 µl of chloroform per 1 ml of TRIzol lysate was added and mixed by vortex for 30 seconds which was incubated for 5 minutes at RT to enable phase separation. This was then centrifuged at 12,000 g for 10 minutes at 4°C, after which the upper aqueous phase was carefully collected with minimal disruptions to the other phases and transferred to a fresh microcentrifuge tube for further isolation. To this, 500 µl of ice-cold isopropanol was added and mixed by inverting the tube. This was then centrifuged at 12,000 g for 10 minutes at 4°C to form the RNA pellet. The supernatant was carefully discarded and the pellet was washed via resuspension in 75% ethanol before re-centrifugation at 7,500 g for 5 minutes at 4°C. The supernatant was carefully discarded and washing was repeated once more. After discarding the supernatant, tubes were left open to air dry the RNA pellet in a fume hood for 10 minutes. Finally, the RNA pellet was resuspended in 20 µl of nuclease free water (NFW). RNA was stored at -80 ºC until use.

2.3.2. RNA quantification

RNA quality and yield was measured using Nanodrop (Thermo, UK). 1 µl of the NFW used to resuspend the RNA pellet in *Section 2.3.1* was used as a blank to remove background interference during sample measurement. 1 µl each isolated RNA sample was then used to assess RNA quality and yield, with the measuring arms cleaned in between measurements. The resulting yield was presented in a concentration of ng/µl, and quality was presented on the absorbance ratios between wavelengths 260 and 280 nm – ratios between 1.80 to 2.00 was determined as of sufficient quality and integrity.

2.3.3. cDNA synthesis

2 µg of each quantified RNA sample was diluted to a final volume of 20 µl with NFW. This was then subjected to reverse transcription to obtain complementary DNA (cDNA), using a High-Capacity cDNA Reverse Transcription Kit (Thermo, UK) according to the manufacturer's instructions.

A master reverse transcription mix was first prepared. This was composed of 2 µl of reverse transcription buffer, 0.8 µl of deoxynucleotide triphosphates (dNTPs), 2 µl of random primers, 1 µl of reverse transcriptase enzyme and 4.2 µl of NFW to yield a final volume of 10 µl. This was added to 10 µl of the diluted RNA sample to yield a reaction volume of 20 µl. Reverse transcription was performed on a PCR thermal cycler (Applied Biosystems, UK), at the following settings: 25°C for 10 minutes, 37°C for 120 minutes, 85°C for 5 minutes and followed by an indefinite holding cycle at 4°C till collection. cDNA was stored at -20°C until use.

2.3.4. Quantitative Polymerase Chain Reaction (qPCR)

Real-time PCR, or commonly referred to as quantitative PCR (qPCR) is a powerful and highly sensitive molecular biology technique that assesses the transcriptional level of a gene of interest. Differential temperature cycles result in amplification of the gene of interest, during which three phases of amplification occurs – the first being the geometric phase whereby maximal amplification occurs cycle-to-cycle, followed by the linear phase where amplification efficiency begins to decline due to reduced reagent availability within the PCR mix and finally, the plateau phase where little to no amplification occurs.

The components used in a typical qPCR reaction mix entail the generation of a fluorescent signal that is detected and quantified, with the fluorescence intensity proportionate to the levels of the gene of interest amplified. Relative quantitative data of qPCR comes from the fluorescent signal that is emitted during the geometric phase. Typically, a threshold level would be set where the qPCR reaction reaches a fluorescent intensity value that is above background levels. Subsequently, the number of cycles required for a gene of interest to intersect this threshold level is reported as the threshold cycle (Ct) value. Ct values correlate to the amount of amplified gene of interest products, whereby lower Ct values indicate high levels of amplified product and higher Ct values indicate low levels of amplified product.

2.3.4.1. Chemistries of qPCR

Two well-known fluorescence-based chemistries are used in qPCR to detect amplified products. The first, the TaqMan sequence probes, which are composed of a fluorophore and quencher which are present on the 5’ and 3’ end respectively, binds complimentary to the gene of interest. Following denaturing of cDNA strands during the PCR process, the Taq polymerase enzyme within the qPCR mix initiates the primer hybridization process – presence of the gene of interest consequently causes the binding of the TaqMan sequence probes. Subsequent amplification by Taq polymerase cleaves the fluorophore from the quencher to then emit the fluorescence signal. The amount of signal emitted can be monitored in real time and is presented in the form of an amplification plot (Fig 2.2).

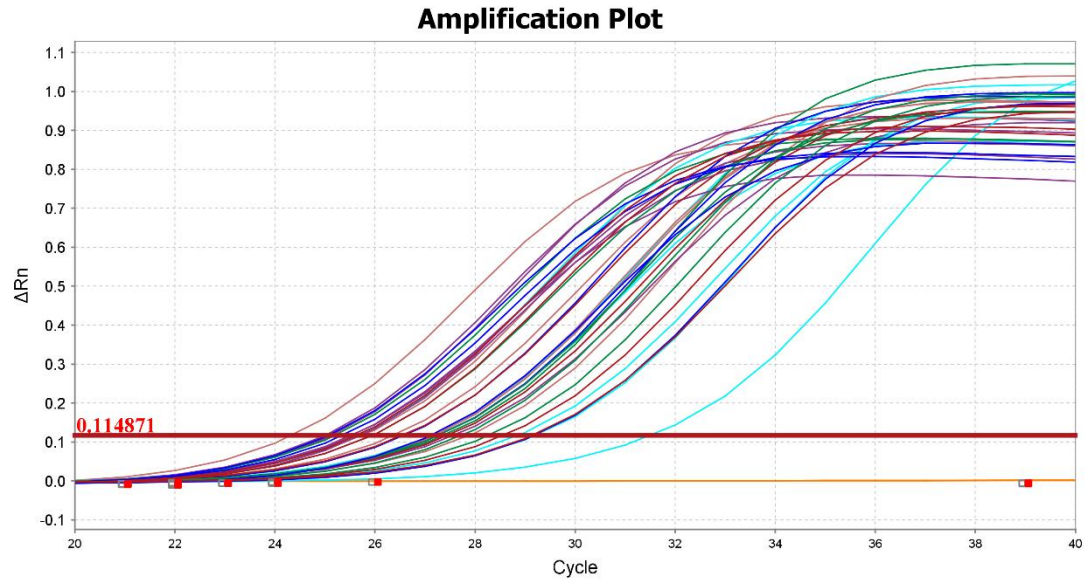

Figure 2.2. qPCR amplification plot
The amplification plot details the number of cycles needed for a gene of interest to be amplified to above a set threshold based on the fluorescent intensity value that is emitted by qPCR chemistries used, presented as the Ct value. The curve of the plot also provides an indication of assay quality, producing a linear curve of amplification that eventually plateaus off due to reduced amplification efficiencies.

SYBR green is another chemistry that can be used, which is a double stranded DNA (dsDNA) binding dye. As PCR progresses, forward and reverse primers specific for the gene of interest bind and the resulting amplified PCR product presents itself as a dsDNA that is rapidly detected and bound by SYBR green to produce the fluorescent signal. Like the TaqMan sequence probe chemistry, the increase in SYBR green mediated fluorescence signal can be monitored in real time and presented via the amplification plot (Fig 2.2).

Although simpler and cheaper in its application, SYBR green binds to any dsDNA that arise due to off-targeting of primer pairs used and contaminating DNA, increasing risk of false positive signals due to non-specific binding. These can be offset via a confirmatory step to determine if the PCR amplicon bound by SYBR green is indeed the gene of interest. At the end of the qPCR run, the temperature is cooled to permit SYBR green binding to amplified PCR

products, increasing fluorescence signal. This is succeeded by a rise in temperature where the fluorescence signal begins to decline due to SYBR green dissociation as the dsDNA PCR products denature, creating a peak of fluorescence intensity against temperature plotted as a melt curve (Fig. 2.3). Because only a single pair of primers for a single gene of interest is used for each qPCR reaction, it is therefore expected that only a single melt curve peak exists. Additional qPCR reaction controls such as a no cDNA or use of RNA that is not reversibly transcribed can also be set up to give confidence in cDNA purity and reaction component integrity. Presence of multiple melt curve peaks within a sample should warrant further investigation and mitigations such as reassessment of primer pair specificity, reagent and cDNA integrity should be considered.

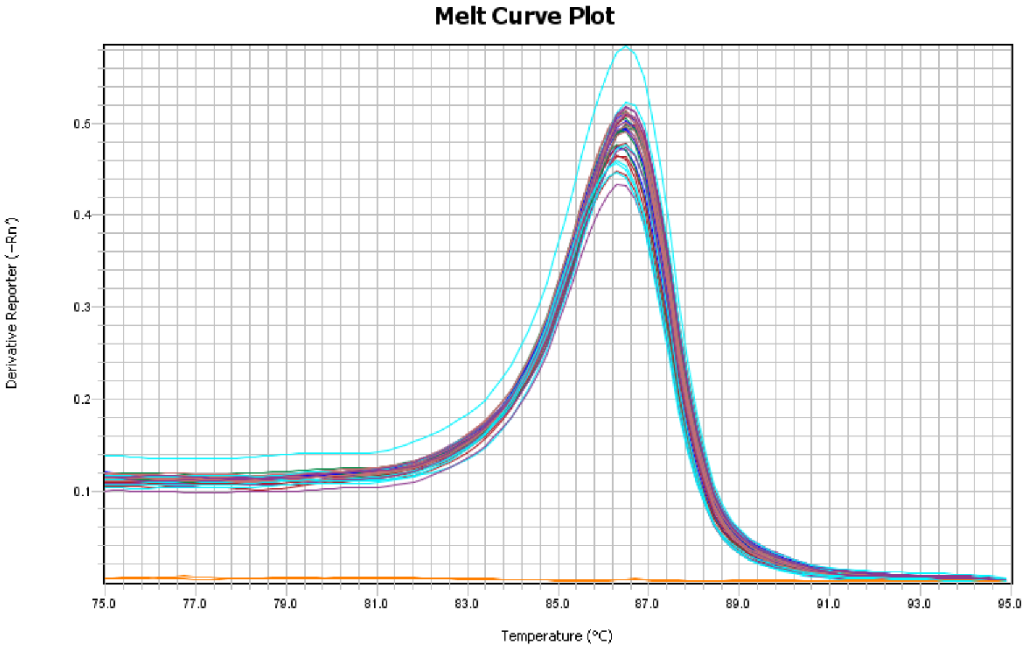

Figure 2.3. qPCR SYBR green melt curve
The melt curve provides an indication of the quality and specificity of primers used in SYBR green based qPCR. Only one peak should be presented, which delineates that the PCR amplicon is free from contaminants and is indeed amplified from the gene of interest.

2.3.4.2. Preparation of qPCR reactions and experimental procedures

cDNA from reverse transcription as detailed in *Section 2.3.3* was diluted 1:3 in NFW. qPCR reactions were set up on MicroAmp Optical 384 well or 96 well reaction plates (Thermo, UK). qPCR reaction mixes were dependent on the type of chemistry used. For TaqMan sequence probe chemistry, TaqMan™ Universal PCR Master Mix (Thermo, UK) was used according to the kit's instructions. 384-well plate assays utilised a qPCR TaqMan mix composed of 10 µl TaqMan™ master mix buffer, 1 µl TaqMan™ gene expression assay primers, 1 µl of the diluted cDNA and 8 µl of NFW to yield a reaction volume of 20 µl. For 96-well plate assays, a qPCR TaqMan mix was composed of 25 µl TaqMan™ master mix buffer, 2.5 µl TaqMan™ gene expression assay primers, 1 µl of the diluted cDNA and 21.5 µl of NFW to yield a reaction volume of 50 µl.

For SYBR green based qPCR, PowerUp™ SYBR™ Green Master Mix (Thermo, UK) was used according to the kit's instructions. For both 384 and 96 well plate assays, 20 µl qPCR reaction mixes were prepared, composed of 10 µl PowerUp™ SYBR™ Green Master Mix buffer, 2.5 µl forward primer, 2.5 µl reverse primer, 1 µl of the diluted cDNA and 4 µl NFW.

For both qPCR based chemistries, each sample for each gene of interest was prepared in duplicates or triplicates. Plates were sealed with Adhesive PCR plate seals (Thermo, UK) and run on QuantStudio™ 7 Flex Real-Time PCR System (Applied Biosystems, UK). 18S was used as the housekeeping gene throughout. Running cycles were set up according to the kit instructions of the chemistry used. List of gene probes and primer pairs used in the work for this thesis can be found in Appendix A.

2.3.4.3. Interpretation and analysis

To calculate relative fold change in gene expression following qPCR, $2^{-\Delta\Delta Ct}$ method was used. First, the Ct values across replicates for a gene of interest and the 18s housekeeping gene was averaged. The ΔCt value of a gene of interest was obtained as follows:

ΔCt = Ct (gene of interest) – Ct (18s housekeeping gene)

Subsequently, the ΔΔCt values were calculated for comparison of relative fold change of a gene of interest between different treatment groups. This is determined as follows:

$\Delta\Delta$Ct = ΔCt (treated sample gene of interest) – ΔCt (control sample gene of interest)

Application of the formula $2^{-\Delta\Delta Ct}$ subsequently yields the fold change in gene expression of the particular gene of interest.

2.3.5. Chromatin immunoprecipitation (ChIP)

Chromatin Immunoprecipitation (ChIP) is an experimental technique that aims to investigate protein-DNA interactions to reveal insights into delicate pathways of gene regulation and expression. These can include transcription factors, promotors, DNA binding sites, co-regulatory proteins, modified histones, polymerases and chromatin-modifying enzymes.

ChIP was performed using ChIP-IT High Sensitivity® kit (Active Motif, CA, USA) according to the kit's instructions. The typical ChIP process involves a multitude of steps (Fig. 2.4) – first, samples are fixed with a complete cell fixation buffer that contains formaldehyde, which maintains cross-links between DNA and associated proteins. Fixated cells are subsequently

harvested, washed with PBS before being lysed and homogenised in the chromatin preparative buffer to release the chromatin. Subsequently, chromatin is sheared into smaller fragments by sonication and eluted, which is incubated with an antibody specific for the DNA-binding protein of interest to form the chromatin immunocomplex. Subsequent incubation with Pierce™ ChIP-grade Protein A/G Magnetic Beads (Thermo, UK) with rotation results in the immunoprecipitation of this complex that is eluted to yield the ChIP DNA. Cross-links are then reversed and any remaining protein is digested, and DNA is purified a final time before analysis for gene of interest with qPCR as detailed in *Section 2.3.3*.

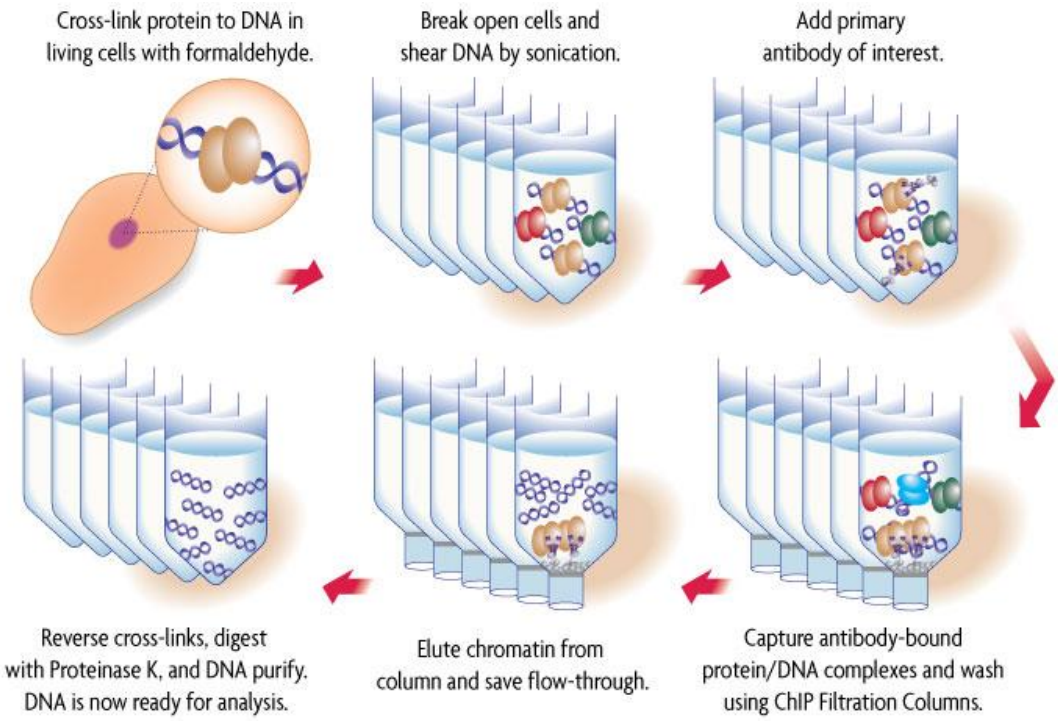

Figure 2.4. An overview of the chromatin immunoprecipitation process
Intact cells are first fixated in a formaldehyde buffer to cross-link and maintain DNA-protein interactions. DNA is sheared into smaller fragments following cell lysis and incubated with an antibody specific for the protein of interest to form the chromatin immunocomplex. This complex is subsequently immunoprecipitated using Protein A/G beads which are then washed. The cross-links are then reversed and the resulting ChIP DNA is cleaned to remove any proteins and other potential contaminants before being subjected to downstream analytical processes such as qPCR or whole genome analysis [408].

2.3.6. RNA sequencing (RNAseq)

RNA sequencing (RNAseq) is an indispensable transcriptome-wide analytical technique. It allows assessment for differential gene expression, splicing of mRNAs and post-transcriptional modifications, permitting comparative analysis between conditions (eg. gene KO, pharmacological treatments). This allows connection between the transcriptome and subsequent protein functionalities.

2.3.6.1. RNAseq sample preparation

RNA was first extracted as detailed in *Section 2.3.1* at the end of experimental timepoint. Following isolation, the RNA was subject to a further clean-up process by column purification using the RNA Clean & Concentrator Kit (Zymo Research, CA, USA) according to the kit's instructions. For assessment of RNA integrity, cleaned up RNA samples were analysed on a 2100 Bioanalyzer Instrument (Agilent Technologies, UK), with samples having achieved at least an RNA integrity number of > 9.5. At least 500 ng per sample was aliquoted and diluted to 20 µl with NFW for RNAseq sample preparation.

2.3.6.2. Sequencing and post-processing

Sample quality control, poly-A enrichment library preparation and sequencing at 20 million read pairs per sample were conducted by Novogene Inc in Cambridge, UK. Data was returned as FASTQ format files. All RNAseq data and downstream analysis was conducted by the bioinformatics team within Nottingham Trent University. Reads were first mapped using the kallisto RNA-seq quantification program, developed based on pseudoalignment of reads and fragments and utilising a combination of the transcriptome de Bruijn graph constructed with *k*-mers present in the transcriptome, allowing analysis of

unaligned pair-end RNA-seq reads with greater efficiency that other programs such as TopHat2 [340].

Further expression analysis was conducted using R in RStudio (MA, USA) using the Bioconductor package. Data was summarized to genes using tximport and normalized using edgeR. For accounting of variance, the limma package with its *voom* method was used [341], and differentially expressed genes were subsequently identified.

2.3.6.3. Gene set enrichment analysis

While RNAseq analysis itself is powerful in understanding differential transcriptional expression, these only give a superficial understanding into how these differential changes affect overall functionality of pathways. Gene set enrichment analysis provides a deeper insight into understanding a group of differentially expressed genes and the biological functions they exert over [342]. For the work in this thesis, g:Profiler was used. Differentially expressed genes identified from RNAseq were uploaded into g:GOSt, one of the tools available within g:Profiler. Subsequently, this maps the uploaded differentially expressed gene sets to known information sources such as Gene Ontology, Reactome and Esembl, which documents their functions and detects statistically significant enriched processes and pathways [343]. These findings can then be presented as a representative dot plot of pathway enrichment, or collectively as a Manhattan plot.

2.4. Protein analytical techniques

This section details the methodologies used to assess changes in protein expression.

2.4.1. Protein extraction

All protein extraction procedures were performed on ice to minimise protease activity which would otherwise reduce protein yields.

2.4.1.1. Cells

For whole cell lysis, cells grown in 6 well plates were first washed with 2 ml ice-cold 1x PBS. PBS was aspirated and 125 µl of RIPA lysis buffer (50 mM Tris pH 8.0, 150 mM sodium chloride (NaCl), 0.5% (w/v) sodium deoxycholate, 0.1% (w/v) SDS, 1% NP-40) supplemented with 1x Pierce™ EDTA-free protease inhibitor cocktail (Thermo, UK) was added and cells were scraped using cell scrapers, with the lysates collected into a clean microcentrifuge tube. Lysates were incubated on ice for 30 minutes to enable maximal lysis, and subsequently clarified through centrifugation at 12,000 RPM for 15 minutes at 4ºC. The resulting supernatant was transferred into a clean microcentrifuge tube. If not used immediately, lysates were stored at -80ºC.

2.4.1.2. Tissues

Protein extraction from tissues was performed via homogenisation using TissueLyser LT (Qiagen, Germany). Per tissue sample, a TissueLyser LT stainless steel bead was dispensed into a 2 ml microcentrifuge tube containing 300 – 400 µl of RIPA lysis buffer and approximately 30 mg of tissue. Tissues were homogenized at a setting of 50 Hz for 3 minutes in the first instance. If visible chunks were observed, additional lysis buffer was added and homogenization was repeated. Upon complete homogenization, lysates were

incubated on ice for 30 minutes. The stainless steel beads were removed and lysates were clarified through centrifugation at maximum speed for 30 minutes at 4ºC to permit maximal pelleting of debris. The resulting supernatant was then transferred into a clean microcentrifuge tube. If not used immediately, lysates were stored at -80ºC.

2.4.2. Protein quantification

Total protein concentration was quantified using the DC™ protein assay kit (Bio-Rad, UK). For this, 5 µl of protein standards, samples and a blank (lysis buffer only) were each added into a clear bottom 96 well plate, in triplicates. A working reagent A solution was prepared by mixing reagent A with reagent S in a 1:50 ratio. 25 µl of this working solution was added to each well, followed by 200 µl of the protein assay reagent B, which was incubated at RT for 15 minutes for colorimetric changes to develop. Plates were then read at a wavelength of 750 nm using the Infinite® 200 PRO plate reader (Tecan, Switzerland) to obtain the absorbance values.

Protein quantification is a colorimetric based assay, where the concentration of known protein standards such as Bovine serum albumin (BSA) is associated to its corresponding absorbance values emitted at a certain wavelength. These values are then used to plot a standard curve and the line of equation is used to determine the concentration of unknown samples in µg/µl based on the average of their corresponding absorbance values (Fig. 2.5).

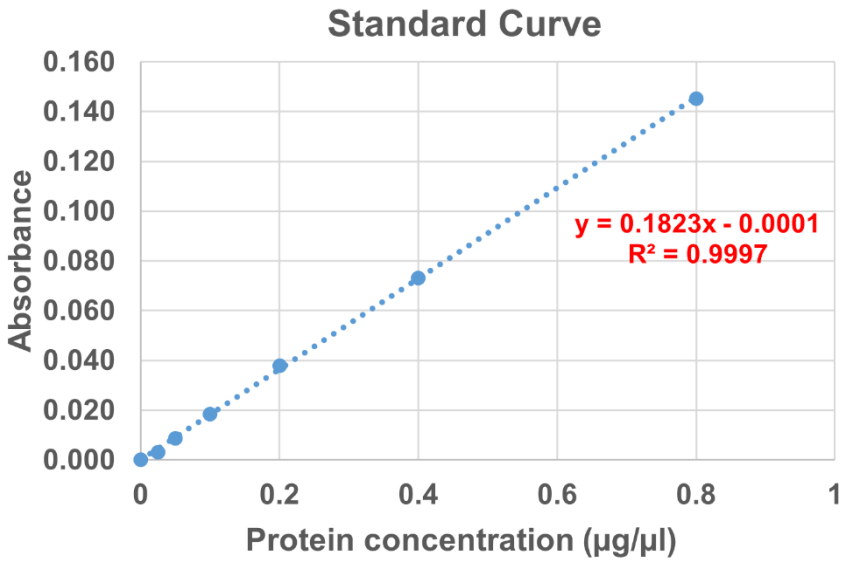

Figure 2.5. A typical protein assay standard curve
The curve is generated based on the absorbance values emitted by a set of protein standards (e.g. BSA) with known concentrations. These values are also used to create the equation of straight line based on the formula y = mx + c, which is then applied to solve for the unknown protein concentration of a sample based on the absorbance value it emits.

2.4.3. Western blotting

2.4.3.1. Sample preparation

At least 20 µg of protein per sample would be used for western blot. For one sample, 10 µl of 2x Laemmli sample buffer (0.125 mM Tris-HCl pH 6.8, 4% sodium dodecyl sulfate (SDS), 0.004% bromophenol blue, 10% 2-mercaptoethanol, 20% glycerol) was added to the amount of lysate in µl required for 20 µg and topped up to 20 µl with lysis buffer. These values can be multiplied or adjusted for higher protein load as required for an experiment to yield a sample master mix where every 20 µl yields 20 µg of protein. Prepared samples were then boiled at 96ºC for 15 minutes to allow protein denaturation. Thereafter, samples were loaded onto prepared gels immediately or stored in -20ºC until required.

2.4.3.2. Gel preparation

For the first phase of western blot, prepared protein samples would be first loaded onto SDS–polyacrylamide gel electrophoresis (SDS-PAGE) fixed percentage (v/v) acrylamide gels. SDS-PAGE is a process that serves to resolve and separate denatured proteins within the sample by their respective molecular weights. Components within the sample buffer enable this process: SDS is a detergent that confers upon proteins negative charges, allowing proteins to migrate and separate down the SDS-PAGE gel when an electrical field is applied, while bromophenol blue serves as a tracker dye to indicate the position of the protein samples whilst migrating down the gel.

A typical SDS-PAGE gel is composed of two layers, the stacking layer and the resolving layer. The stacking layer serves exclusively for loading of protein samples, while the resolving layer not only separates, but also influences the speed in which proteins of various molecular weights within a sample migrate and separate: heavier molecular weight proteins migrate slower down the gel compared to lighter molecular weight proteins, and they would be confined to the upper regions of the resolving layer. In contrast, the lighter molecular weight proteins migrate faster and would be confined to the lower regions or potentially run out of the gel altogether. The speed in which these proteins migrate and separate is dependent on the percentage of the acrylamide used to make the SDS-PAGE gel: lower molecular weight target proteins require a higher acrylamide percentage to impede their speed of migration and separation, preventing them from running out of the gel. Similarly, higher molecular proteins require a lower acrylamide percentage to facilitate their migration and separation.

All gels were made using ProtoGel reagents (National diagnostics, UK) and SDS-PAGE apparatus (Bio-Rad, UK). Table 2.1 outlines the composition of a typical SDS-PAGE fixed percentage (v/v) acrylamide gel. The resolving layer was first prepared and poured into the gel plates – ethanol was then added to remove any bubbles and straightens the resolving layer. Upon polymerisation of the resolving layer, ethanol was washed off with water and the stacking layer was prepared and poured. Either 10 or 15 well gel combs were inserted into the stacking layer and allowed to polymerize. Prepared gels were either used immediately or kept in distilled water at 4ºC until use for no more than a week.

	Resolving gel (%)			
Component	**8%**	**10%**	**12%**	**15%**
Acrylamide (30%)	2.67 ml	3.33 ml	4 ml	5 ml
Resolving Buffer (4x)	2.5 ml	2.5 ml	2.5 ml	2.5 ml
1.5% Ammonium persulfate	0.5 ml	0.5 ml	0.5 ml	0.5 ml
H_2O	4.33 ml	3.67 ml	3 ml	2 ml
TEMED	10 µl	10 µl	10 µl	10 µl
Component	**Stacking gel**			
Acrylamide (30%)	0.6 ml			
Stacking Buffer (4x)	1.25 ml			
1.5% Ammonium persulfate	0.2 ml			
H_2O	2.6 ml			
TEMED	15 µl			

Table 2.1. Fixed percentage acrylamide gel composition

2.4.3.3. Western blotting

Prepared gels were loaded onto SDS-PAGE gel tanks (Bio-Rad, UK). A 10x resolving buffer (250 mM Tris, 1.92 M Glycine, 1% (w/v)) was diluted to 1x and poured to completely fill the inner chamber, as well as the outer chamber up to the point that was demarked on the tank. Combs were carefully removed and samples were loaded alongside a Prestained Protein Ladder (Abcam, UK) for identification of protein molecular weights. The gel tank was connected to a power supply (Bio-Rad, UK) and gels were run at 90V until samples entered the resolving layer, where the voltage was then increased to 120V and migration was allowed to take place until the bromophenol blue tracker dye was diffused out of the gel.

Proteins were then transferred from the gel onto polyvinylidene fluoride (PVDF) membranes. Prior to use, PVDF membranes were quickly soaked and activated in methanol. Transfer was performed using a Trans-Blot Turbo Transfer System (Bio-Rad, UK) according to the manufacturer's instructions.

Transferred membranes were then subjected to the blocking step to prevent non-specific binding by antibodies. This was performed by incubating membranes in a blocking solution with rocking for at least 1 hour at RT. The blocking solution was composed of 5% (w/v) BSA diluted in 1x Tris-buffered saline with Tween 20 (TBST) (20 mM Tris, 150 mM NaCl, 0.2% Tween 20). The primary antibodies were then added directly into the blocking solution at the desired dilutions. A table of primary antibodies used are provided in Appendix B. Membranes were then incubated overnight on rocking at 4ºC. Membranes were washed with 1x TBST for 10 minutes with rocking at RT. 1x TBST was then discarded and replaced with fresh 1x TBST and washing was

repeated two more times for a total of three washes. Membranes were then incubated with either anti-rabbit or anti-mouse secondary antibodies conjugated to horseradish peroxidase (HRP) (Dako, Denmark) at a 1:10,000 dilution with rocking for 1 hour at RT and the washing steps were repeated.

For development of western blots, the enhanced chemiluminescence (ECL) based detection system was utilized, using the Pierce™ ECL Substrate kit (Thermo, UK). The ECL substrate was added onto the membrane and bands were visualized using the G:BOX Chemi XX6 system (Syngene, UK), with exposure times automatically determined by the system. For selected blots, quantification of bands were performed using ImageJ densitometry and normalized to those of the loading control protein.

2.4.4. Protein immunoprecipitation (IP)

Similar to ChIP (outlined in *Section 2.3.5*), protein immunoprecipitation (IP) is a fundamental assay for determining protein-protein interactions. First, protein extraction from cells or tissues and quantification was performed as outlined in *Section 2.4.1* and *2.4.2*. Per sample, 20 µl of Pierce™ ChIP-grade Protein A/G Magnetic Beads was dispensed with a cut pipette tip into a 1.5 ml microcentrifuge tube. 400 µl of RIPA lysis buffer was added and the beads were washed by gently inverting the tube until they returned into solution. The beads were then pelleted using a magnetic rack and the supernatant was removed. Washing was repeated once more.

The volume of lysate in µl that yielded between 500 µg to 1 mg of protein was calculated and added to the washed beads. If necessary, this was topped up with RIPA lysis buffer to at least 400 µl. This was then incubated on rotation

for 20 minutes at RT to pre-clear the lysates, which is fundamental to further minimise non-specific binding. Beads were then pelleted and the pre-cleared lysate was transferred to a fresh microcentrifuge tube. 5 µl of the antibody detecting the protein of interest was added and this was incubated overnight on rotation at 4ºC to form the immunocomplexes. 20 µl of washed magnetic beads were directly added and incubated on rotation for 20 minutes at RT to immunoprecipitate the immunocomplexes.

Immunoprecipitated beads were subsequently pelleted and the supernatant was discarded. Beads were washed for five times on ice and 20 µl of 1x Laemmli sample buffer was added directly to the beads. The tube was flicked to dislodge the beads into solution, briefly centrifuged and boiled at 96ºC for 15 minutes to denature the antibodies and release the protein of interest. Magnetic beads were pelleted and the supernatant was loaded for SDS-PAGE and western blotting as detailed in *Section 2.4.3*.

2.4.5. Unbiased proteomics

Like RNAseq, various proteomic analytical tools have been developed to give insights into proteome changes between different conditional groups in cells or tissues, further complementing transcriptome and genome wide analyses. Unbiased proteome profiling is predominantly performed using Liquid chromatography coupled with mass spectrometry (LC-MS). This subsequently identifies peptides that can be quantified to the overall abundance level of proteins.

For this procedure, cells were directly scraped on ice-cold 1x PBS at the end of experimental timepoints and pelleted through centrifugation at 1000 RPM

at 4ºC. The supernatant was discarded and the cell pellet was resuspended directly in ice-cold RIPA lysis buffer supplemented with 1x Pierce™ EDTA-free protease inhibitor cocktail and stored immediately at -80ºC.

Samples were sent to the Nottingham Trent University Biological Mass Spectrometry & Clinical Proteomics facility led by David Boocock and Clare Coveney. These were analysed on a TripleTOF® 6600+ System instrument (SCIEX, MA, USA) with samples analysed using both Sequential Window Acquisition of All Theoretical Mass Spectra (SWATH-MS) in data-independent acquisition mode and information-dependent acquisition (IDA) modes for quantitation and spectral library generation respectively. IDA data was searched together using ProteinPilot 5.0.2 to generate a spectral library and SWATH data was analysed using Sciex OneOmics software extracted against the locally generated library. Normalization, log fold change and *p*-value determination was performed on Microsoft Excel as outlined [344].

2.5. Histological analytical techniques

This section details the methodologies used to characterise changes in cellular morphology and localization of target proteins.

2.5.1. Immunofluorescence

Cells were grown in coverslips that were housed in 12 well cell culture plates. At the end of the experimental timepoint, coverslips were rinsed with 1x PBS, fixed with 4% paraformaldehyde (PFA) (Sigma-Aldrich, UK) and permeabilized with 0.1% Triton X-100 (Sigma-Aldrich, UK) and subjected to blocking for 1 hour at RT. The blocking solution was composed of 10% goat serum diluted in 1x PBS (Life Technologies, UK). Coverslips were then incubated in primary

antibodies diluted in blocking buffer overnight in darkness at 4ºC. Coverslips were rinsed in 1x PBS for three times before incubation with AlexaFluor® secondary antibodies and the DAPI nuclear dye (Thermo, UK) for 1 hour at RT. Coverslips were mounted with Aqua/Poly-Mount (Polysciences) on slides and allowed to set. Imaging was performed using the EVOS™ M7000 Imaging System (Thermo, UK).

2.5.2. Giemsa-Jenner staining of myotubes

Cells were grown and differentiated on 6 well plates as outlined in *Section 2.1.1*. The Giemsa-Jenner staining protocol for myotubes was employed as described [345]. Cells were washed with 2 ml 1x PBS that was aspirated before subjected to fixation with 1 ml methanol for 5 minutes. Methanol was subsequently aspirated and plates were left to air dry in a fume hood for 10 minutes, covered with their lids and stored until staining.

For the staining procedure, fixed cells were first stained with 1 ml Jenner staining solution (Alfa Aesar, UK) diluted 1:3 in 1 mM sodium phosphate pH 5.6 for 5 minutes at RT and washed with distilled water. Wells were then incubated with 1 ml Giemsa staining solution (Alfa Aesar, UK) diluted 1:20 in 1 mM sodium phosphate pH 5.6 for 10 minutes at RT and washed with distilled water and left to air dry. All wells belonging to the same experiment(s) were stained simultaneously with the same batch of diluted staining solutions. Cells were imaged using a camera attached to an inverted microscope (Olympus, Japan) in three randomly selected regions. Similarly, all wells for a single experiment were photographed simultaneously using the same microscope settings. Subsequently, protein-rich myotube fibres presented themselves as dark/deep purple while the nuclei stained shallow purple/pink (Fig. 2.6).

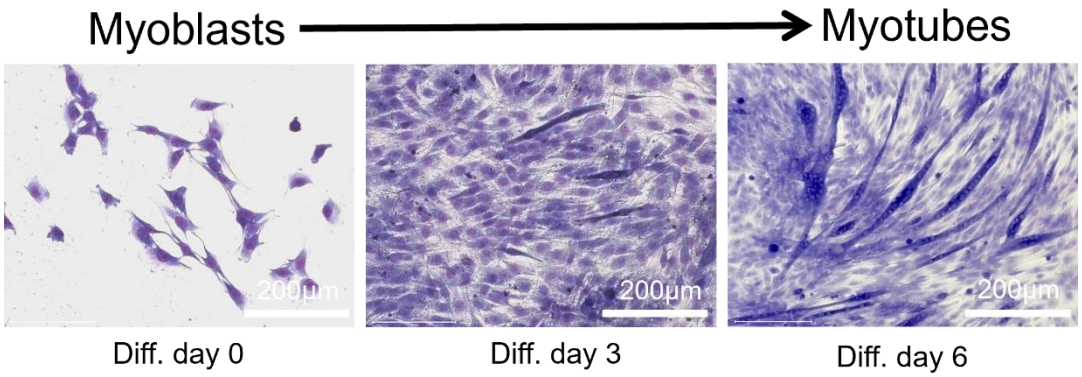

Figure 2.6. Giemsa-Jenner staining of C2C12 myotubes
The staining method is capable of revealing dark and denser myotube structures and the nuclei that resides within them. These denser structures start to manifest approximately 3 days following differentiation induction amongst the lightly stained myoblasts. Myotube size and numbers are also increased by day 6 of differentiation.

2.5.2.1. Myotube fusion index scoring

Captured images were processed in ImageJ. The number of nuclei within stained myotubes and the total number of nuclei in the entire field was manually scored using ImageJ's multipoint tool. Myotube fusion index was calculated as a percentage of myotube nuclei over total number of nuclei.

2.5.2.2. Myotube density

Images taken were at a resolution of 2048 x 1536 pixels in red-green-blue (RGB) format and converted to grayscale. The histogram function within ImageJ (windows ctrl + H) was used to determine the myotube density of a given image. The range of 255 gray tones was represented on the x-axis of the resulting generated histogram, while the y-axis presented the number of pixels attributed to each tone. Subsequently, the mean number of pixels attributed to tones 0 – 75 (darker tones) was calculated between replicates to obtain the myotube density. Images with dense myotubes naturally presented greater number of pixels attributed to the darker tones and henceforth, greater myotube densities.

2.6. NAD$^+$/NADH measurement assay

The NAD$^+$/NADH colorimetric assay was derived from the protocol as described [108,346]. Cells were grown in 12 well cell culture plates for this assay. At the end of experimental timepoints, cells were washed with 1x ice-cold PBS. For NAD$^+$ measurement, cells were lysed and scraped in 150 µl of 0.6 N perchloric acid; for NADH measurement, cells were lysed and scraped in 150 µl of 0.25 M potassium hydroxide (KOH) diluted in 50% ethanol. Lysates were clarified through centrifugation at 12,000 RPM for 15 minutes at 4ºC. The supernatant was transferred to a clean microcentrifuge tube. For subsequent protein quantification and normalization, pellets from NAD$^+$ lysates were stored at -80ºC.

For NAD$^+$ measurement, lysates were diluted 1:10 in ice-cold 100 mM sodium phosphate pH 8.0; for NADH measurement, lysates were diluted 1:5 in 100 mM sodium phosphate pH 8.0. For both measurements, 5 µl of each NAD standard, samples and a blank (1x PBS). The cycling mix was then prepared, composed of 8.4 ml H_2O, 1 ml 1M sodium phosphate pH 8.0, 20 µl BSA (50 mg/ml), 100 µl 1M NAM, 200 µl ethanol, 10 µl 10 mM flavin mononucleotide, 10 µl 20 mM resazurin, 110 µl alcohol dehydrogenase (10 mg/ml) and 110 µl diaphorase (1 mg/ml). 95 µl of the cycling mix was then added to the wells. Subsequently, plates were read using a plate reader at an excitation wavelength 544 nm and emission wavelength at 590 nm for 0 to 20 minutes at 5 minute intervals. During this process, the enzymes within the cycling mix utilize NAM to catalyse the rapid synthesis and resynthesis of cADPR from NAD$^+$ and NAD$^+$ from cADPR, during which each cycle produces a molecule of highly fluorescent resorufin (Fig. 2.7).

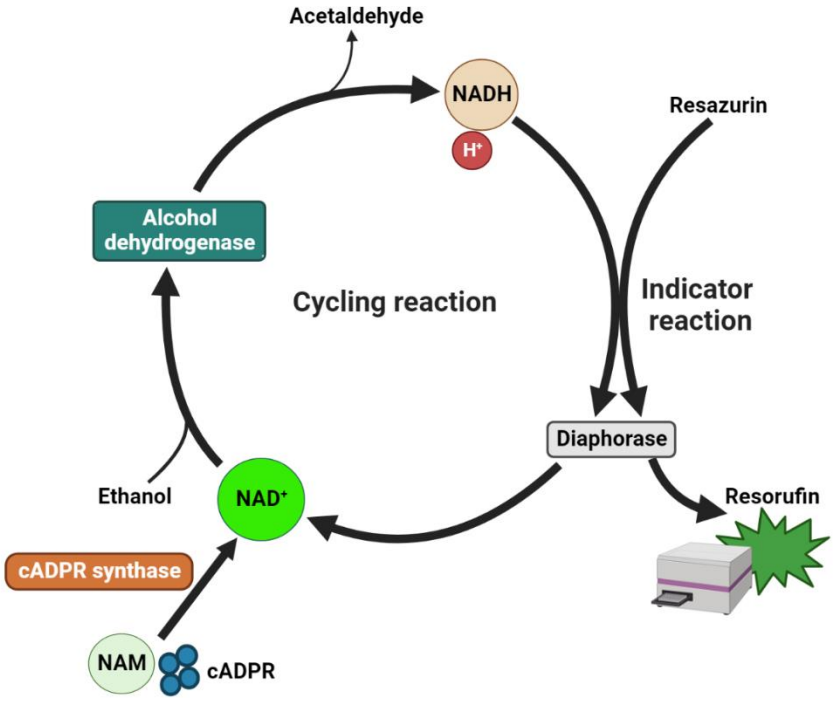

Figure 2.7. Cycling assay schematic for the NAD^+/NADH measurement assay
cADPR synthases mediate the conversion of cADPR into NAD^+ in the presence of high levels of NAM. NAD^+ is then directed into the into a coupled enzymic cycling reaction using a cycling mix where the presence of ethanol and alcohol dehydrogenase reduces NAD^+ into NADH. Concomitantly, the diaphorase enzyme utilises resazurin to cycle NADH back to NAD^+, releasing resorufin as a by-product that is fluorescent which can be measured in a plate reader.

The resulting absorbance values corresponded to resorufin accumulation. The average absorbance values per standard and sample obtained at 20 minutes was used to subtract values obtained at 0 minutes. These values were then used to plot a standard curve of known NAD concentrations, and the line of equation was used to determine NAD^+ and NADH concentrations of unknown samples. To further normalize for protein content, pellets collected from NAD^+ lysates were resuspended in 100 µl RIPA lysis buffer and protein quantification was performed as detailed in *Section 2.4.2*, and the pMol concentration of NAD^+ or NADH was divided by the total protein from the NAD^+ pellet to yield the NAD^+ and NADH concentrations in in pMol/µg.

2.7. Statistical analysis

All data obtained was compiled, copied into, and analysed using GraphPad Prism 9 software. Student's unpaired t-test was used for comparison between control and treatment groups. For multiple comparisons between 2 or more treatment groups to a common control, Ordinary one-way analysis of variance (ANOVA) with Dunnet's multiple comparisons test was used for determination of significance. ΔΔCt values from qPCR experimental procedures calculated as detailed in *Section 2.3.4.3* were used for statistical analysis. Statistical significance was demonstrated by * $p<0.05$, ** $p<0.01$, *** $p<0.001$, and data was presented as mean ± the standard error of mean (SEM).

Chapter 3

PARP1 mediated PARylation dynamics in skeletal muscle myogenesis

3.1. Introduction

Aside from locomotive functions, skeletal muscle has crucial implications in whole body metabolic homeostasis due to its contributions to nutrient storage, basal metabolic rate and thermogenesis [5]. Its importance is evident in aging individuals who experience natural decline in skeletal muscle mass that consequently pre-disposes them to metabolic disorders – this necessitates maintenance of healthy skeletal muscle mass for improved quality of life. During myogenesis, formation of individual myofibres is dependent on alignment and fusion of progenitor myoblasts that themselves, are products of muscle residing, self-renewing myogenic precursors called satellite cells, capable of re-entering proliferative cycles, entailing regenerative repair in response to skeletal muscle injury, disease or exercise [34]. Current understanding of the myogenic process and impacts of endocrine mediated signals, exogenous factors and underlying health status in influencing these processes remains to be ascertained [62,347,348]. Such gaps in knowledge are reflected in the lack of clinical interventions aimed at myopathy. There are no current tools available to prevent or reverse the decline in muscle functional traits manifested in conditions including cachexia, sarcopenia and obesity related muscle loss.

The role of NAD^+ within skeletal muscle has expanded over recent years with the discovery of NAD^+ consuming enzymes that are involved in various cellular functions from DNA repair to calcium signalling. PARP1 is one of the major NAD^+ consuming enzymes that catalyses the formation of ADPR from NAD^+, which is subsequently covalently attached onto target proteins. This is succeeded by subsequent elongation and branching of PAR chains in a

process termed PARylation. PARP1 mediated PARylation has well-established roles in DNA damage repair response – this has seen PARP inhibition successfully applied to a range of cancers in the context of synthetic lethality. In parallel, studies have identified the potential roles for PARP1 over skeletal muscle metabolism and differentiation [131,132,176,251]. Notably, PARP1 is downregulated during differentiation, a process shown to enhance resistance to oxidative stress in myotubes [251]. Recent work has demonstrated PARP1 to transcriptionally influence expression of the archetypal skeletal muscle MRF *MyoD*, negatively regulating its ability to bind to target genes such as *myogenin* and *KvDMR1* [176].

PARP1 inhibitors have been applied for alleviation of inflammation in non-communicable chronic diseases including myopathy. This necessitates further understanding of PARP1 activity modulation in myogenic trajectory and subsequent impacts on preservation of skeletal muscle mass and function.

In this chapter, we used the murine and human muscle myoblast cell lines C2C12 and LHCN-M2, capable of differentiating into multinucleated myotubes, to better understand the dynamics of PARP1 mediated PARylation and NAD^+ balance during myogenesis. We also sought to investigate the impacts of PARP1 inhibition on overall myogenic trajectory.

3.2. Materials and Methods

3.2.1. Cell culture and treatments

All work was carried out in C2C12 and LHCN-M2 cell lines. Cell culture protocols are detailed in *Section 2.1.1*.

3.2.1.1. Cell plating

C2C12 or LHCN-M2 myoblasts were seeded into 6 well plates in GM at a seeding density of approximately 150,000 cells/well. The cells were cultured in DM for 5 days with the media changed every other day.

3.2.1.2. Pharmacological treatments

The PARP inhibitors BYK204165 and PJ34 were treated at working concentrations of 10 µM. NR was diluted to a working concentration of 0.5 mM. FK866 was diluted to a working concentration of 50 nM. All treatments were performed concomitantly with differentiation induction of myoblasts.

3.2.1.3. C2C12 Low glucose differentiation medium

Glucose-free DMEM powder was dissolved according to the manufacturer's instructions and subsequently filter sterilized. 2% HS, antibiotics and filter sterilized glucose were added to make up differentiation medium with glucose concentrations of 6.25, 12.5 and 25 mM.

3.2.2. Protein analysis

Western blot analysis was conducted on protein lysates harvested in RIPA lysis buffer supplemented with 1x Pierce™ EDTA-free protease inhibitor cocktail. Proteins were loaded onto 10 or 12 % acrylamide gels run at 90 V (stacking) and at 120 V (resolving). Separated proteins were transferred to PVDF membranes and blocked with 5% BSA for 1 hour at room temperature, after which incubation with primary antibodies: PAR, PARP1, MyoD, Myogenin,

TNNT1, α-tubulin and GAPDH antibodies was performed overnight at 4°C. Anti-rabbit or mouse secondaries were used before visualisation using ECL. Detailed methodologies are delineated in *Section 2.4.3* and primary antibody details can be found in Appendix B. Selected western blots which were further analysed was performed via densitometry using ImageJ software's gel analyser feature, with measurements normalised to loading control intensities.

3.2.3. Immunofluorescence

At the end of the experimental timepoint, cells initially seeded on coverslips were rinsed with 1x PBS, fixed with 4% PFA, permeabilized with 0.1% Triton X-100 and blocked with 10% goat serum for 1 hour at room temperature. Cells were then incubated in primary antibodies: PAR and MyoD, diluted in blocking buffer overnight at 4ºC. Secondary antibodies and DAPI nuclear dye were incubated for 1 hour at RT. Coverslips were mounted with Aqua/Poly-Mount on slides and allowed to set prior to imaging.

3.2.4. NAD^+/NADH measurement assay

NAD^+ was measured in lysates extracted in 0.6 N perchloric acid as described [349]. Briefly, standards or samples in phosphate buffer were combined with the cycling mixture composed of 2% ethanol, 100 µg/ml alcohol dehydrogenase, 10 µg/ml diaphorase, 20 µM resazurin, 10 µM flavin mononucleotide, 10 mM nicotinamide and 0.1% BSA, in 100 mM phosphate buffer pH 8.0. Resorufin accumulation was evaluated by reading excitation at 544 nm and emission at 590 nm using the Infinite® 200 PRO plate reader. Detailed methodologies for this assay can be found in *Section 2.6*.

3.2.5. Giemsa-Jenner staining

Differentiated myotubes were subject to Giemsa and Jenner staining as described [345]. Briefly, cells were washed with 1x PBS and fixed in 100% methanol for 5 minutes. Jenner staining solution diluted in 1 mM sodium phosphate was added for 5 minutes, washed out in distilled water, and incubated for 10 minutes in Giemsa staining solution diluted in 1 mM sodium phosphate and washed out. Stained myotubes were visualised using an inverted microscope with a digital camera attachment, and 3 randomly selected regions of a 6 well plate were imaged. Myotube fibres were identified by deep purple colours while nuclei appeared shallow purple/pink. Myotube fusion index was scored as a percentage of nuclei incorporated into myotubes over the total number of nuclei counted using ImageJ software. Images taken were at a resolution of 2048 x 1536 pixels in RGB format and converted to grayscale before application of ImageJ's histogram analysis, and the mean number of pixels attributed to tones 0 – 75 (darker tones) was calculated between replicates to obtain the myotube density.

3.2.6. Statistical analysis

Students t-test or ANOVA statistical comparisons were used with the Graphpad Software Inc. Prism version 9. Data are presented as mean ± SEM with statistical significance determined as *. $P< 0.05$, **. $P<0.01$, ***. $P<0.001$. Differences between two groups were determined using unpaired t-test compared treatments or genotypes. For multiple comparisons between 2 or more treatment groups to a common control, Ordinary one-way analysis of variance (ANOVA) with Dunnet's multiple comparisons test was used for determination of significance.

3.3. Results

3.3.1. PARP1 and PARylation dynamics during myoblast to myotube differentiation

PARP1 mediated PARylation during myogenesis has been reported to exert influence on phenotypic characteristics such oxidative stress resistance in fully differentiated myotubes [176,251]. This would suggest that the modulation of PARP1 mediated PARylation during myogenesis has profound effects on both the process and phenotypic outcomes following differentiation. Knowledge in this regard remains limited and this would serve to better understand its implications in development and maintenance of skeletal muscle mass. To investigate whether PARP1 mediated PARylation is connected to myogenic transition, we first sought to ascertain the dynamics of PARP1 and PAR during the differentiation of the murine myoblast cell line C2C12 over 6 consecutive days (Fig. 3.1A). To do this, whole cell lysates of C2C12 myoblasts prior to differentiation induction in reduced serum media (Day 0) and daily from the induction of differentiation (Days 1 – 6) were harvested and subjected to immunoblotting analysis. Basally (Day 0), myoblasts express total PARP1 and PAR at a detectable level. Subsequently, we observed that total protein levels of PAR were dynamic, reaching zenith within day 1 and nadir by day 5 of myogenesis. Levels of PARP1 were also significantly reduced in differentiated myotubes, in line with observations from previous studies [176,251]. These data suggest that PARP1 mediated PARylation is associated with the initiation of myogenesis and indicates elevation in NAD^+ driven PARP1 PARylating activity. Total levels of MyoD and Myogenin, the MRF family members of proteins driving skeletal muscle differentiation, also decreased and increased

respectively over days of myogenesis, implying the establishment of myogenic commitment in myoblasts (Fig. 3.1A). These observed trends were also observed in the human myoblast cell line LHCN-M2 (Fig. 3.1B). Subsequent quantification reveal the significant increase in total PAR levels on Day 1 post differentiation induction (Fig. 3.1C).

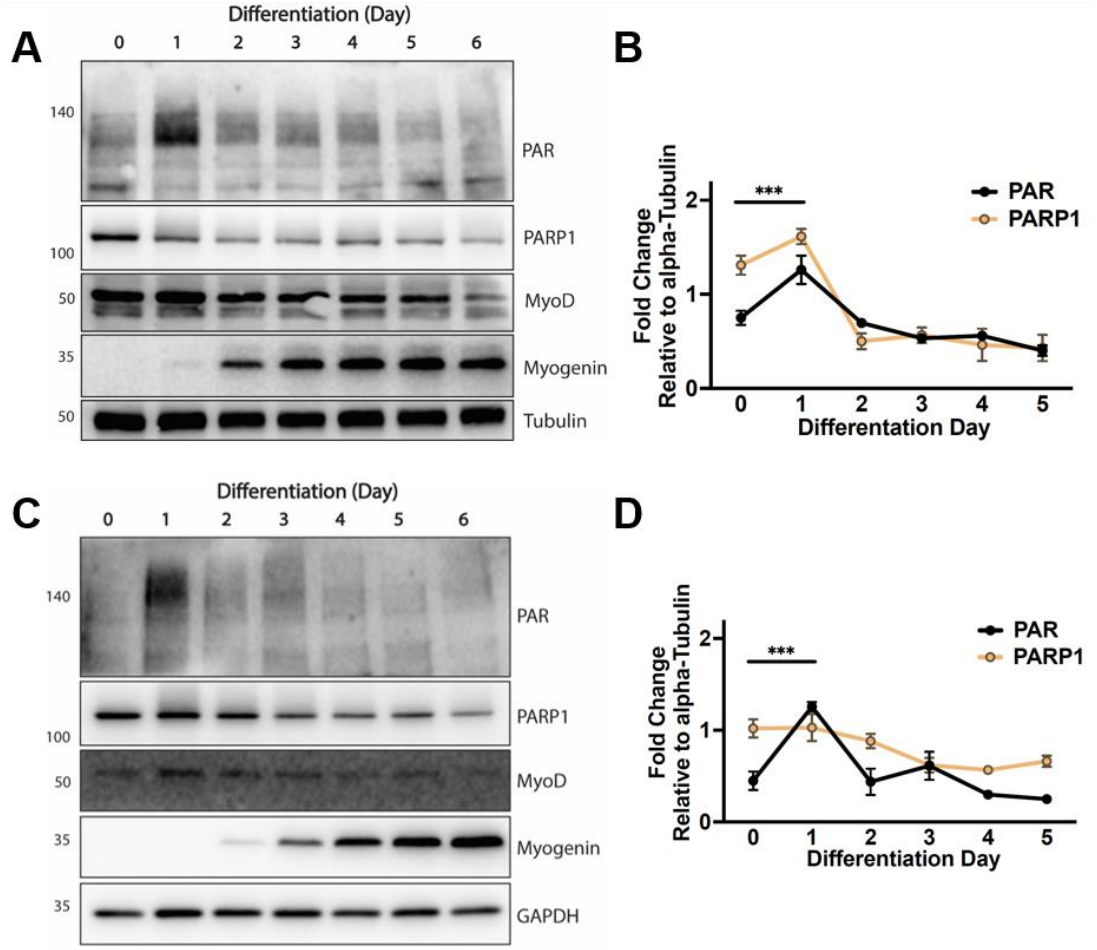

Figure 3.1. Analysis of PARP1 and PARylation dynamics during myogenesis
Western blot analysis shows levels of PARP1 and total PAR in differentiating **(A)** C2C12s **(B)** Quantification of Western blots shown in **(A)** for PAR and PARP1 throughout days of myogenesis. Western blot analysis of differentiating **(C)** LHCN-M2s **(D)** Quantification of Western blots shown in **(C)** for PAR and PARP1 throughout days of myogenesis
All data are normalised to loading control protein and are the mean ± SEM
C2C12s *n=3*, LHCN-M2s *n=3*

3.3.2. Modulation of PARP1 mediated PARylation during myogenesis

The PAR dynamics in differentiating myoblasts prompted us to further investigate the catalytic role of PARP1 during this process by utilising experimental approaches to modulate PARP1 activity (Fig. 3.2). To that end, C2C12s during myogenic induction were pharmacologically treated with the PARP1 inhibitors PJ34 or BYK204165. PJ34 is a broad spectrum PARP inhibitor that targets other members of the PARP family of enzymes, as well as the PARylating Tankyrases, albeit to a lesser extent [350]; BYK204165 is a highly specific and selective inhibitor for PARP1 [351].

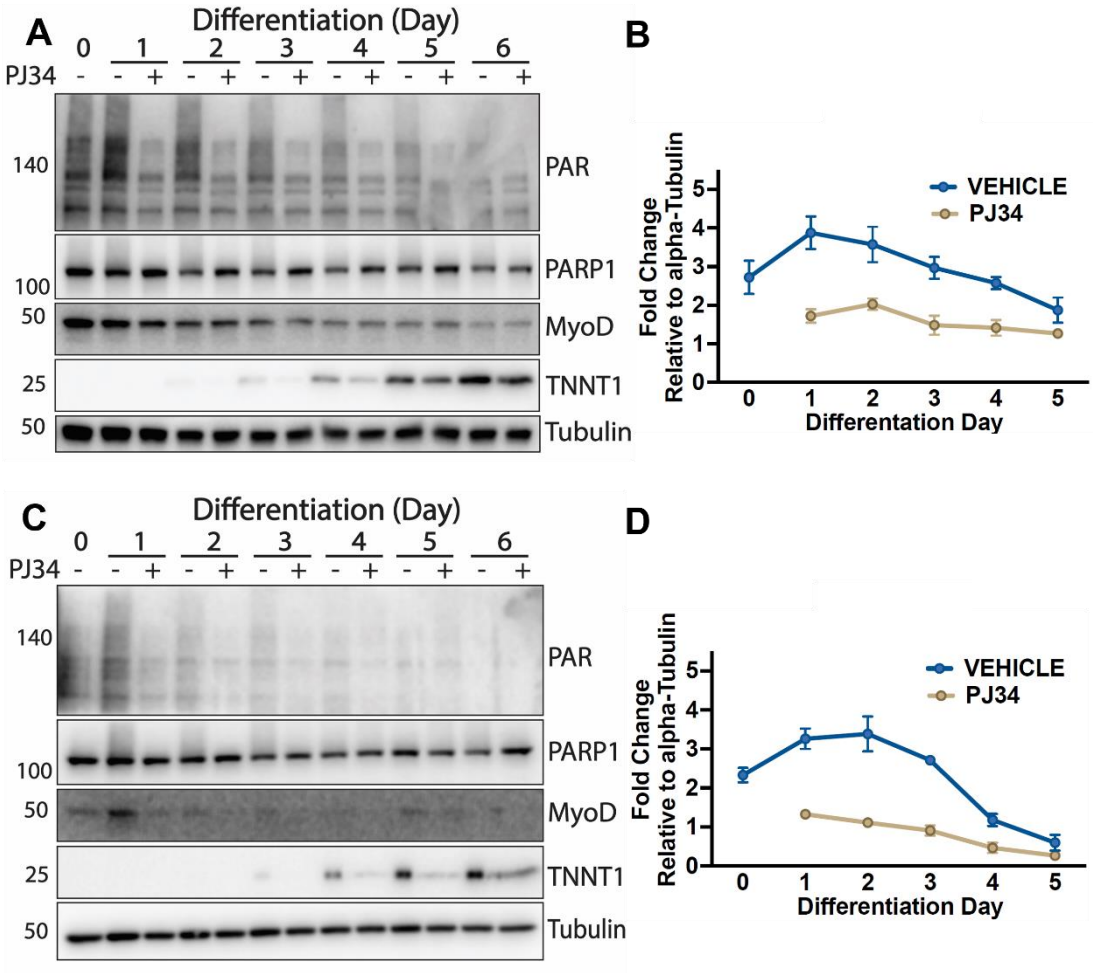

Figure 3.2. Modulation of PARP1 activity using PJ34 in differentiating myoblasts
Western blot analysis shows levels of PARP1 and total PAR in early-stage differentiation PJ34 treated **(A)** C2C12s **(B)** Quantification of western blots shown for PAR. Western blot analysis in PJ34 treated **(C)** LHCN-M2s **(D)** Quantification of western blots probed for PAR
All data are normalised to loading control protein and are the mean ± SEM, C2C12s *n=3*, LHCN-M2s *n=3*

We assessed PAR levels as well as subsequent impacts on differentiation trajectory. As shown, ablation in total PAR protein levels in PJ34 (Fig. 3.2) and BYK204165 (Fig. 3.3) treated groups corroborates each of the compound's specificity and efficacy. Notably, PJ34 treated groups across days of differentiation exhibited slightly elevated PARP1 expression (Fig. 3.2A, C), suggesting compensatory mechanisms in differentiating myoblasts and underscoring significance of PARylation during the myogenic process – this could be ascribed to accumulation of PARP1 as a response to its inhibition and auto-PARylation which remains to be elucidated. Notably, MyoD levels are consistent with an indication of myogenic commitment following PARP inhibition – however, levels of the muscle specific protein TNNT1 and the MRF Myogenin were seemingly downregulated by the end of the myogenic timepoint. Accordingly, these trends were also observed in differentiating LHCN-M2 myoblasts (Fig. 3.2C, D & Fig. 3.3B). These trends indicate that PARylation by PARP1 exerts influence over proteins that are known to be differentially expressed during myogenesis. Furthermore, suppression of PAR levels is further supported in immunofluorescence experiments in day 1 differentiating C2C12s treated with PJ34, where nuclear localization of PAR was observed, giving merit for PARylation in driving the myogenic transcriptional programme (Fig. 3.4).

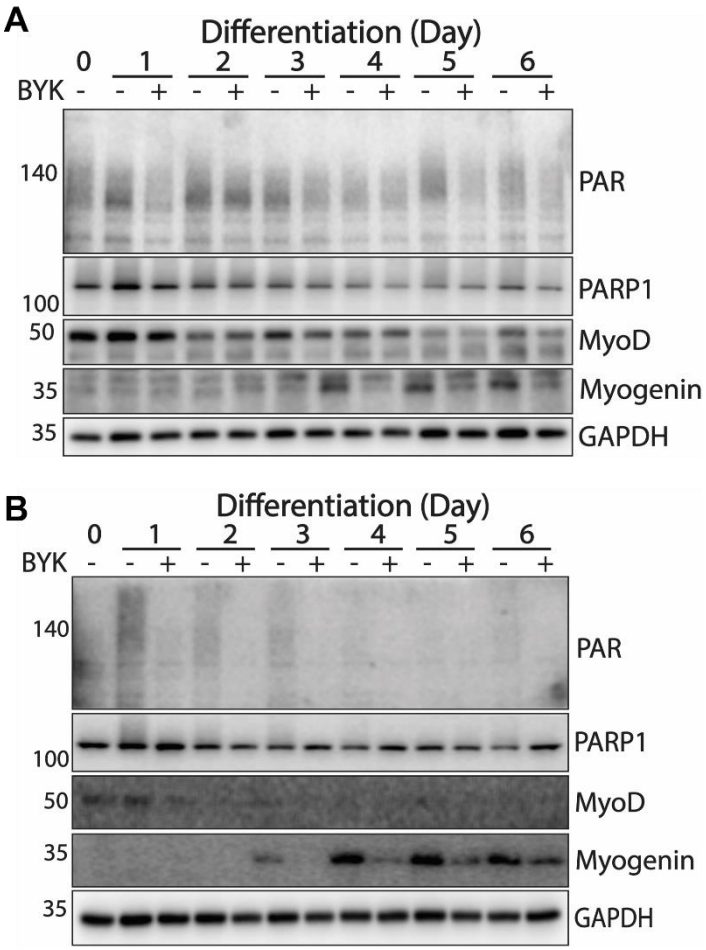

Figure 3.3. Modulation of PARP1 activity using BYK204165 in differentiating myoblasts
Western blot analysis shows levels of PARP1 and total PAR in early-stage differentiation BYK204165 treated **(A)** C2C12s and **(B)** LHCNM2s
C2C12s *n=3*, LHCN-M2s *n=3*

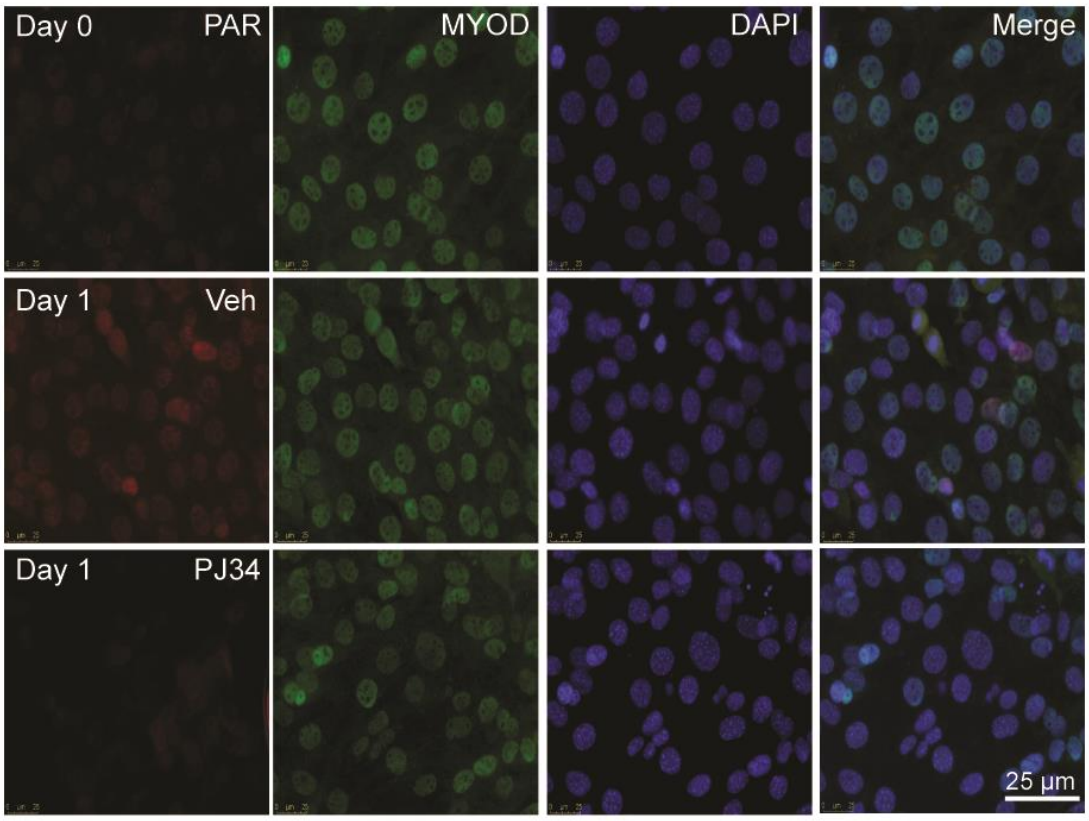

Figure 3.4. Immunofluorescence of PJ34 treated C2C12 myoblasts
Immunofluorescence analysis shows levels of PAR in day 1 differentiating C2C12 myoblasts treated with PJ34.
C2C12s *n=3*

We next sought to modulate energy availability in differentiating C2C12s to better understand implications for PAR and subsequent effects on myogenic trajectory. Given NAD^+ serves as the rate-limiting substrate for PARP1 PARylating activity, C2C12s were either supplemented with NR, the precursor substrate for NAD^+ synthesis or FK866, a highly specific non-competitive inhibitor of the NAMPT enzyme which partakes in NAD^+ biosynthesis pathways. While no significant changes were observed in the extent of PARylation following NR supplementation (Fig. 3.5A), PAR levels in FK866 treated differentiating C2C12s were suppressed in similar fashion to PARP1

pharmacologically inhibited differentiating C2C12s (Fig. 3.5B). These further support NAD^+ driven PARP1 PARylating activity during myogenesis.

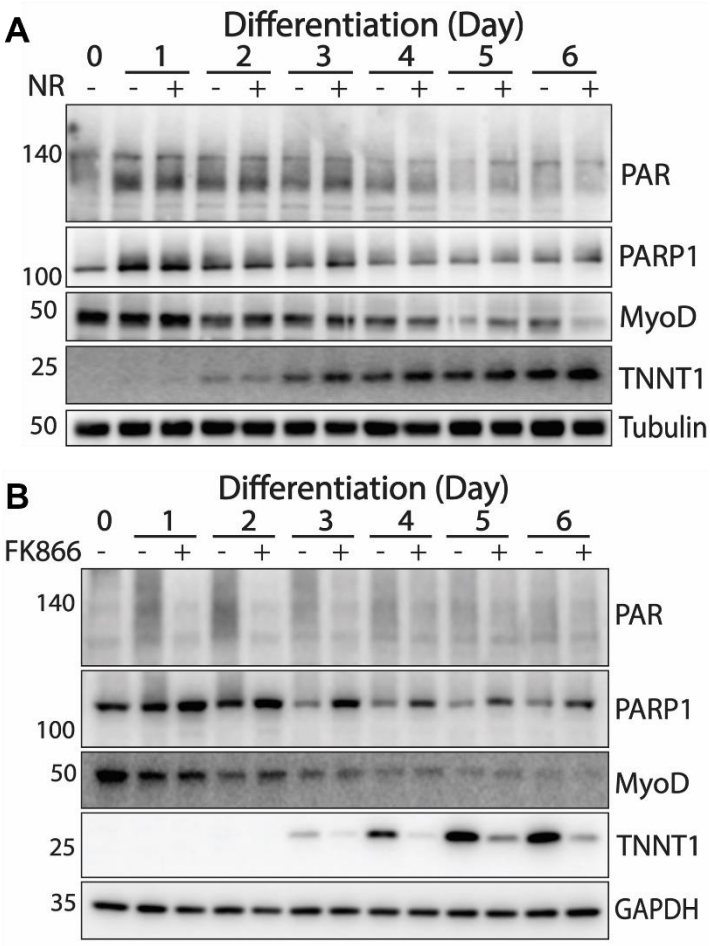

Figure 3.5. Effects of NAD^+ modulation on PARP1 and PAR dynamics during C2C12 myogenesis
C2C12s during differentiation induction were treated with **(A)** NR and **(B)** FK866,
All data are normalised to loading control protein and are the mean ± SEM
C2C12s *n=3*

To further establish the impact of energy status during myogenesis, C2C12s were also differentiated in differentiating media of varying glucose concentrations – intriguingly, we observed plasticity in PAR levels in this regard, with significantly increased levels observed in glucose deprived conditions up to Day 3 of myogenesis (Fig. 3.5C), after which notable cell death was observed in lower glucose concentrations. Collectively, these data

suggest that PARP1 mediated PARylation is dynamic and exerts plasticity in response to cellular energetic status during myogenesis.

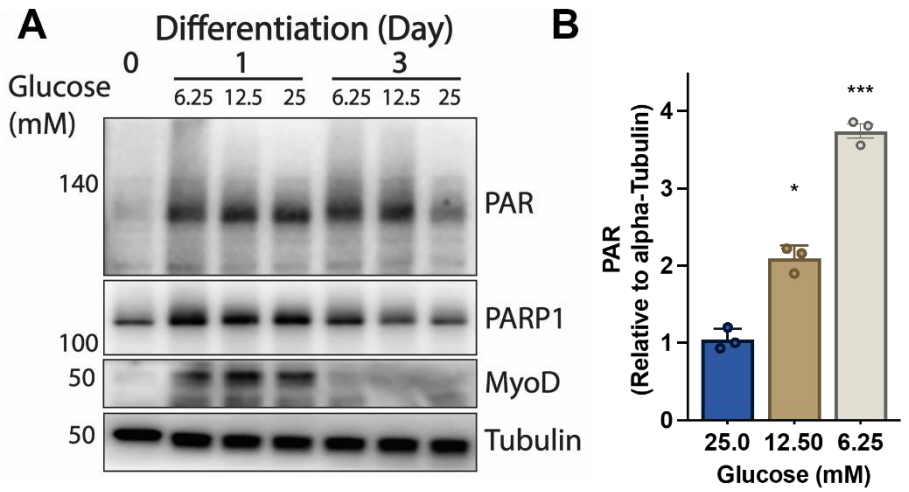

Figure 3.6. Impacts on PARP1 and PAR dynamics during C2C12 myogenesis in glucose deprived environments
C2C12s during differentiation induction were subjected to **(A)** varying concentrations of glucose within differentiation media **(B)** Quantification of western blots probed for PAR as presented in **(A)**.
All data are normalised to loading control protein and are the mean ± SEM
C2C12s *n=3*

3.3.3. NAD$^+$ dynamics during myogenesis

Given that total PAR protein levels diminish over the days of myogenesis, we postulated that this was due to NAD$^+$ depletion that consequently results in low NAD$^+$ availability for PARP1 to utilise for PAR generation. C2C12s were treated with PJ34 during differentiation induction. Extracts for NAD$^+$ and NADH measurement were collected daily for each day of differentiation and subjected to a fluorometric assay based measurement [346]. Both vehicle and PJ34 treated C2C12s exhibited a linear trend whereby NAD$^+$ and NADH levels increased throughout days of differentiation (Fig. 3.7). Intriguingly however, PJ34 treated groups exhibited lower levels of NAD$^+$ (Fig. 3.7A), suggesting compensatory mechanisms of NAD$^+$ buffering in response to excess bioavailability following PARP inhibition. Collectively, these give merit that myogenesis is an

energetically expensive process in initiation, maintenance, and proper myotube development, and the diminishment of PARP1 is rather, as a consequence of its subsequent degradation by the end of myogenesis rather than depletion of NAD^+ due to PARylating activity.

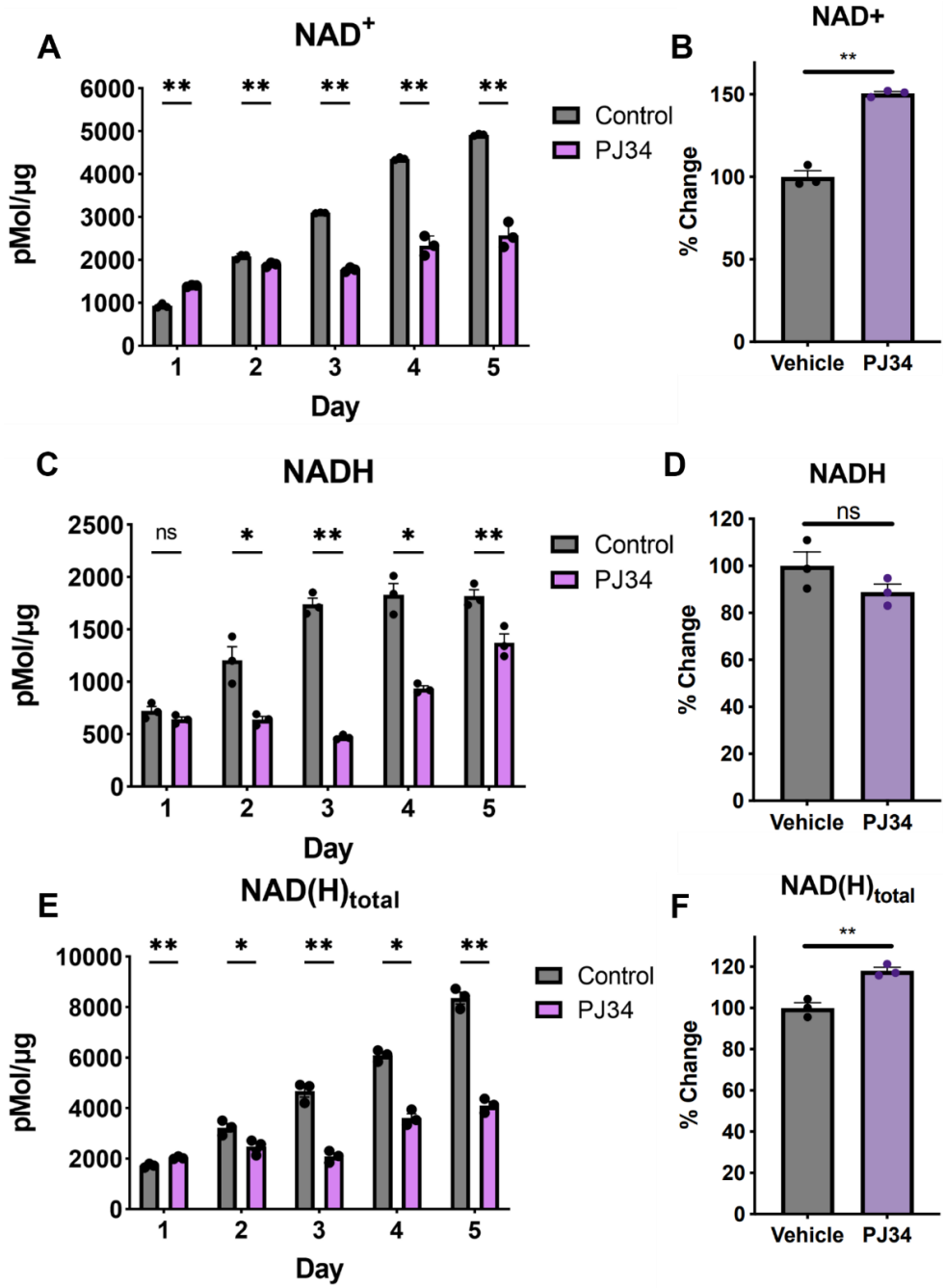

Figure 3.7. NAD dynamics during myogenesis
C2C12s were treated with PJ34 during differentiation induction and measured for **(A)** NAD+ throughout days 1 to 5 of myogenesis, **(B)** on day 6 of myogenesis, **(C)** NADH throughout days 1 to 5 of myogenesis, **(D)** on day 6 of myogenesis, **(E)** total NAD(H) throughout days 1 to 5 of myogenesis and **(F)** on day 6 of myogenesis
All data are normalised to total protein levels and are the mean ± SEM
C2C12s *n=3*

3.3.4. Early-stage PARP1 inhibition does not affect myogenic trajectory

Next, we sought to investigate if the inhibition of PARP1 PARylating activity exerted impacts over myogenesis in C2C12s. To do this, C2C12s were treated with either BYK204165, PJ34 or FK866 during differentiation induction. Cells were fixed on days 0, 1, 3 and 6 of differentiation, and subsequently subjected to a duo staining method of Giemsa-Jenner as described [345]. Visually, formation of myotubes was observed to be not impaired regardless of treatments (Fig. 3.7A). However, upon further assessment of myotube features, including the fusion index and myotube density, the inhibition of PARP1 does exert influence – while fusion index and myotube densities exhibited a linear trend whereby both increased across all treatments throughout myogenesis, further comparison with vehicle treated groups delineated decreases in both features in day 6 myotubes (Fig. 3.7B, C). These data suggest that while PARP1 is not the sole mediator of myogenesis, where myotube fusion and development can still occur during its inhibition, it does however suggest that the reduction in the aforementioned features could associate PARP1 activity during myogenesis to influence the phenotype of the developed myotube.

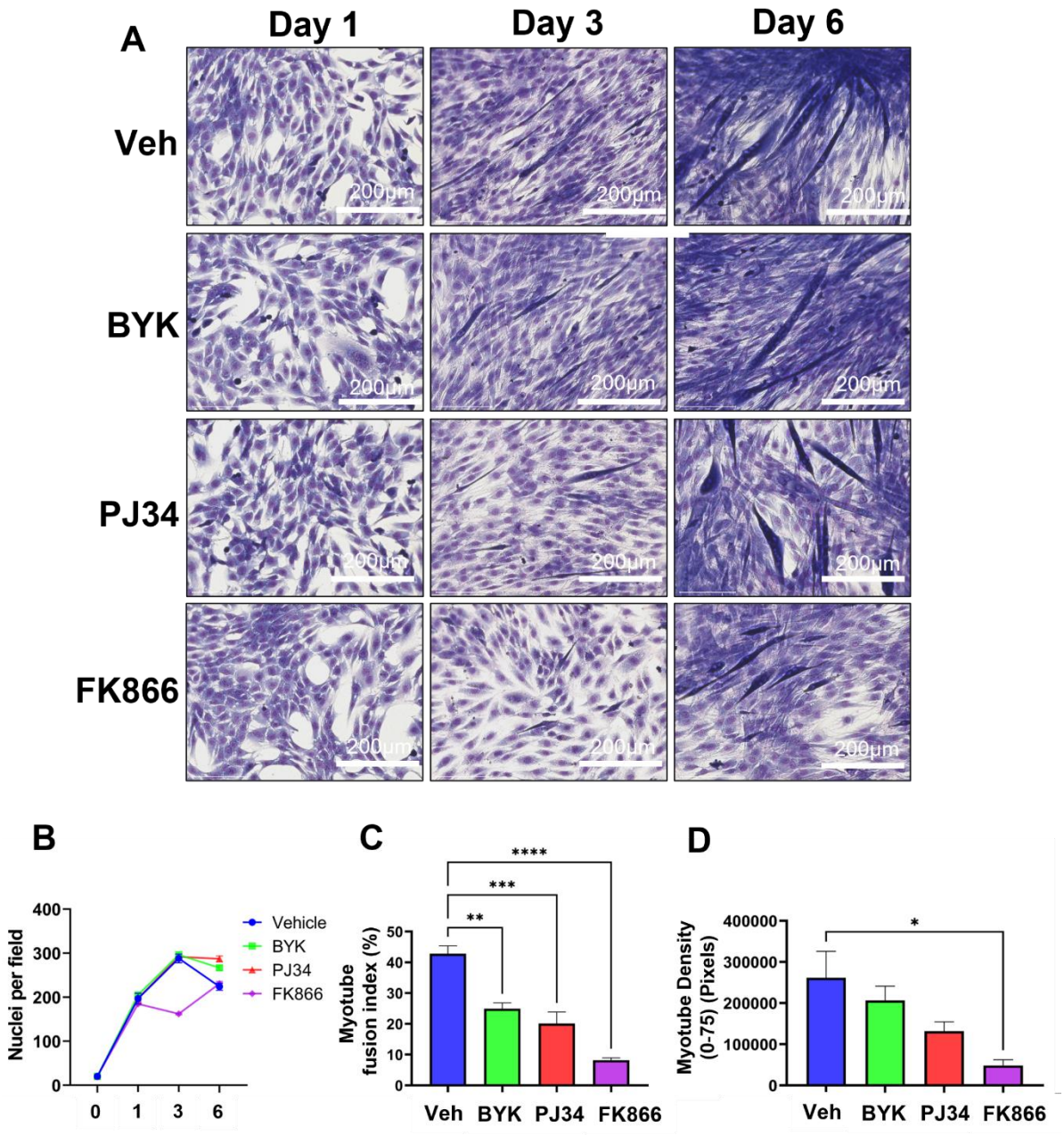

Figure 3.8. Giemsa-Jenner staining of myotubes

C2C12s during differentiation induction were treated with either **(A)** BYK204165, PJ34 or FK866 and stained **(B)** ImageJ quantification and ordinary one-way ANOVA with Dunnet's multiple comparisons analysis was performed for total nuclei **(C)** myotube fusion index and **(D)** myotube density

All data are presented as mean ± SEM

C2C12s *n=3*

3.4. Discussion

The aim of this work was to identify the influence of PARP1 mediated PARylation over the trajectory of skeletal muscle myogenesis. To achieve this, we utilized PARP1 activity modulation strategies including broad spectrum and highly specific PARP1 inhibitors as well as energy availability modulation to ascertain the dynamics of PARP1 and PAR. PARP1 is the cell's dominant source of PAR and has been shown as a transcriptional regulator of key MRFs including *MyoD* and *KvDMR1* [176].

Mounting evidence have suggested an association between PARP1 and skeletal muscle physiology – particularly, the inhibition of PARP1 entails a plethora of positive metabolic benefits, including enhanced exercise performance, increased energy expenditure, enhanced mitochondrial function and resistance to oxidative stress [131–133,251,335]. However, the dynamics of PAR applied by PARP1 remain to be elucidated, particularly within the remits of myogenesis. In line with published studies, we first demonstrate that PARP1 expression is reduced in the differentiated myotube following myogenesis [251]. We also observe a fluctuation in PAR dynamics, with an initial surge in total PAR within Day 1 which gradually diminishes over the myogenic timepoint. Given that PAR functions as a post-translational modification implicated in transcriptional regulation and cellular signalling, combined with the nature of the myogenic process that is dependent on the simultaneous downregulation and upregulation of myogenic-specific proteins including the MRFs, and input from other signalling pathways such as Notch [352,353], we hypothesized that modulation of PAR levels through modulation of PARP1 within the cell would impact the myogenic trajectory. However, the PARP1 modulation paradigms

utilised in this chapter on a whole did not affect myoblast to myotube formation despite considerable suppression of total PAR levels. These observations were unsurprising, given the emergence of studies suggesting the physical presence of PARP1 rather than its catalytic PARylating activity holds greater exertion over the myogenic trajectory [176]. Fundamentally, our findings explored that the process of development and myotube fusion is not entirely dependent on PARP1 mediated PARylating activity.

Interestingly, our data also demonstrate PARP1 accumulation in differentiating myoblasts treated with PARP1 inhibitors during myogenic induction. These findings suggest that PARP1 is indeed the major determinant of total PAR levels during myogenic induction and its upregulation following pharmacological inhibition implies compensatory mechanisms in myogenesis that remain to be unravelled. Low levels of PARP1 in fully differentiated myotubes are associated with conferment of oxidative stress resistance [251] and driving the myogenic transcriptional programme [176], underlying the importance of this trend. However, the mechanisms which underlie PARP1 degradation throughout myogenesis remain elusive. Auto-PARylation of PARP1, as well as the degradation of PAR chains by PAR-binding proteins, has been well-defined for regulation of PARylating activity [170]. Subsequently, PARP1 degradation has been documented in a ubiquitin-proteasome dependent manner [354,355], although this has yet to be elucidated in skeletal muscle, further obfuscating knowledge in this regard. Thus far, muscle biopsies of aging individuals have increased basal PARP1 expression that is attenuated with exercise [335], and its deletion is associated with isotype switching to type I fibers, subsequently improving insulin tolerance and

endurance [131]. These studies suggest the presence of undefined mechanisms that regulate PARP1 expression within skeletal muscle.

Our data also reflect the fluctuating levels of NAD^+/NADH during myogenesis, and increased NAD^+ availability following PARP1 inhibition exerts little consequence on the myogenic trajectory. Given that SIRT1, another NAD^+ consuming enzyme, has been shown to antagonize skeletal muscle myogenesis [356,357], our observations suggest mechanisms that repress SIRT1 activity during myogenic events with increased NAD^+ availability in early-stage PJ34 treated differentiating myoblasts.

It's been demonstrated that adipogenesis, the process where pre-adipocytes differentiate into mature adipocytes, is regulated by PARP1. Nuclear PARP1 activity results in PARylation of pro-adipogenic transcriptional genes to inhibit adipogenesis, and is dependent on competition between the cytoplasm and nucleus for NAD^+ availability mediated by increased glucose uptake during differentiation [103,209], with low glucose levels inhibiting the process altogether [103]. Similarly, low glucose levels inhibit myogenesis [356], as well as excessive levels (> 60 mM) [358]. Subsequently, studies utilising global PARP1 null mouse model paradigms have implied PARP1 mediated NAD^+ consumption exerts influence over the metabolic plasticity of cells and consequently, mitochondrial function [131–133,335]. We show that PARP1 mediated PARylation displays plasticity in response to glucose availability during myogenesis, with low glucose levels increasing PAR accumulation. This suggests a rather delicate balance for glucose metabolism in response to initiating and sustaining myogenesis through a PARylation dependent mechanism. Indeed, Hexokinase II, which catalyses the first step of glucose metabolism for

glucose-6-phosphate production has been demonstrated to possess PAR binding properties to result in inhibition of glycolysis [359,360]. Based on our data, the increased PARylation in myogenesis at lower glucose levels support the hypothesis that both PARP1 and PAR hold important influence as metabolic sensing and nutrient responsive processes crucial for sustaining myogenesis.

In summary, this work shows the full extent of PARP1 and the PAR it applies during myogenesis. While the modulation of PARP1 activity to suppress PAR accumulation during myogenesis is not fundamental for successful myotube development, we demonstrate that the PAR applied by PARP1 during myogenesis is metabolically sensitive and has potential implications in the outcome of the developed myotube phenotype.

Chapter 4

PARP1 impacts the skeletal muscle phenotype and glucocorticoid receptor transcriptional response

4.1. Introduction

Clinical interventions to alleviate age associated skeletal muscle decline usually involve a dual paradigm of lifestyle changes including incorporation of dietary and exercise routines to promote protein metabolism and muscle function. However, loss can be exacerbated by multi-factorial conditions such as sarcopenia. Consequently, loss and dysfunction of skeletal muscle are associated causes and consequence of metabolic dysfunction. While clinical strategies aid to impede rate of skeletal muscle decline, no current therapies exist to completely ameliorate this.

PARP1, the enzyme that catalyses PARylation, has demonstrated roles in skeletal muscle physiology. In aging individuals, PARP1 expression is increased across tissues including skeletal muscle [335], which is subsequently associated with increased risk of metabolic dysfunction due to depleted NAD^+ balance. Differential regulation of PARP1 and PARylation in skeletal muscle of varying exercise training status has been observed – basal PAR and PARP1 levels are elevated in aged muscle that decreases with exercise supplementation; on the other hand, young untrained muscle exhibited increased PAR and PARP1 levels following exercise in comparison to young trained muscle groups [335], suggesting exercise modulates chronically stressed events governed by PARP1 in the aging phenotype. While mechanisms underpinning these trends remain unclear, these provide insights into potential avenues for PARP1 as a target in age-associated muscle decline. Prudently, studies have shown PARP1 inhibition or its deletion bolsters skeletal muscle function, including exercise performance, protection against diet-induced obesity, and enhancement of mitochondrial metabolism [131,132]. More

importantly, these studies demonstrate mechanisms of a NAD^+/PARP1/SIRT1 crosstalk axis, where PARP1 inhibition increases NAD^+ bioavailability to increase SIRT1 activity. Activated SIRT1 consequently drives the activation of pro-oxidative metabolic genes such as PGC1α by deacetylating them [81,82,131]. SIRT1 has also been shown to deacetylate and further reduce PARP1 activity [133,361]. This knowledge has translated into development of SIRT1 activators such as Quercetin and Resveratrol, as well as NR, as forms of therapy to drive SIRT1 activation [106,362].

GRs are ubiquitously expressed receptors that bind the steroid hormones glucocorticoids secreted in response to stress to consequently modulate cellular phenotypic and inflammatory status. While prescribed as forms of therapy, chronic exposure of glucocorticoids induces dysfunctions in tissues of metabolic importance such as liver and adipose tissue [294]. In skeletal muscle, documented deleterious effects include the inhibition of both glucose uptake through the downregulation of GLUT transporters and impairment of insulin signalling pathways, as well as glycogen synthesis via inhibition of the glycogen synthase enzymes to exacerbate a hyperglycaemia phenotype [332,333]. Within the remits of skeletal muscle development, conflicting studies on effects of glucocorticoid exposure exist – GR agonists such as dexamethasone promote protein catabolism and muscle atrophy [326,330340,341]. On the other hand, *in vitro* application of dexamethasone to myoblasts promotes their differentiation [325–327]. Glucocorticoids are also prescribed intermittently for skeletal muscle injury recovery and performance enhancement [360,363]. This, as a result, impedes efforts to delineate clear mechanisms of GR signalling impacts in skeletal muscle physiology.

While studies on GR in inflammation are well-established, PARP1 also has demonstrated roles in inflammation, albeit to a lesser extent. Inhibition of PARP1 has been shown to repress the induction of pro-inflammatory genes such as NF-κB [234], and has also been used for alleviation of inflammation in non-communicable chronic diseases including myopathy. In relation to GR signalling, PARP1 null mice exhibit elevated serum cortisol [364], as well as part of the *Top2β* complex, regulates GR mediated transcription of target genes in adrenal cells [365].

In the previous chapter, we have demonstrated that the depletion of PARP1 mediated PARylation exerts minimal impacts on proper myotube development. In this chapter, we seek to better understand the implications of PARP1 mediated PARylation in skeletal muscle, specifically, the phenotype impacts of myotubes initially differentiated in the presence of PARP1 inhibition. Concomitantly, we also aim to establish PARP1 influence in GR transcriptional response within skeletal muscle and impacts on regulation of skeletal muscle mass and physiology.

4.2. Materials and Methods

4.2.1. Cell culture and treatments

All work in this chapter was carried out in the C2C12 myoblast cell line. Cell culture protocols are detailed in *Section 2.1.1*.

4.2.1.1. Cell plating

C2C12 myoblasts were seeded into 6 well plates in GM at a seeding density of approximately 100,000 cells/well. The cells were cultured in DM for 5 days with the media changed every other day.

4.2.1.2. Pharmacological treatments

Myoblasts were treated with either vehicle controls or the PARP inhibitors BYK204165 (Tocris) and PJ34 (MedChemExpress) at working concentrations of 10 µM. Dexamethasone (Sigma-Aldrich) treatment was performed at 1 µM. All treatments were performed in the DM during differentiation induction, after which treatments were washed out after 1 day. Fresh differentiation medium was then added and myoblasts were allowed to differentiate for the time desired.

4.2.1.3. Transfection of siRNA

C2C12s were seeded at a density of 100,000 cells/well in 6 well cell culture plates and incubated for at least 3 hours to allow adherence. The siRNA transfection mix was composed of Lipofectamine 2000 (Thermo Fisher) and 0.5 µg/ul of siRNA PARP1 sequence or scrambled siRNA control sequence (Thermo Fisher). Transfection was conducted in Opti-Mem (Thermo Fisher) serum and antibiotic free media and incubated for 24 hours, after which the transfection mix was replaced with fresh medium and incubated for a further 24 hours.

4.2.2. Protein analysis

Western blot analysis was conducted on protein lysates harvested in RIPA lysis buffer supplemented with 1x Pierce™ EDTA-free protease inhibitor cocktail. Proteins were loaded onto fixed percentage acrylamide gels run at 90 V (stacking) and at 120 V (resolving). Separated proteins were transferred to PVDF membranes and blocked with 5% BSA for 1 hour at room temperature, after which incubation with primary antibodies: PAR, PARP1, MyoD, Myogenin, GR, α-tubulin, β-actin or GAPDH antibodies was performed overnight at 4°C. Anti-rabbit or mouse secondaries were used before visualisation using ECL detection method. Detailed background and methodologies can be found in *Section 2.4.3*, and primary antibody details can be found in Appendix B. Selected western blots which were further analysed was performed via densitometry using ImageJ software's gel analyser feature, with measurements normalised to intensities of the housekeeping protein blotted.

4.2.2.1. Immunoprecipitation (IP)

Harvested protein lysates were subjected to IP assay. A detailed outline of this is presented in *Section 2.4.4*. Briefly, lysates were first pre-cleared in A/G magnetic beads. At least 1 mg of pre-cleared protein lysate per sample was incubated with 5 µl of GR or IgG antibody controls overnight on rotation at 4°C to form immunocomplexes. This immunocomplex was then incubated with A/G magnetic beads for 20 minutes on rotation at room temperature for immunoprecipitation, washed in RIPA lysis buffer and eluted by boiling at 95°C in 1x Laemmli sample buffer. Elutions were then subjected to western blot analysis as described.

4.2.3. RNA analysis

RNA was harvested using Trizol and extracted using chloroform and isopropanol precipitation. Gene expression data was subsequently analysed using qPCR, with a detailed outline in *Section 2.3.4*. Gene probes used were *PARP1*, *PARP2*, *SIRT1*, *PARG* and *NAMPT*, and the primer pairs can be found in Appendix A. All genes were referenced to 18S as the housekeeping gene during analysis.

Samples designated for RNAseq were further assessed for quality using the Agilent bioanalyzer with all samples having a RNA integrity number of > 9.5. RNAseq library preparation and sequencing were conducted by Novogene Inc., UK.

4.2.4. Chromatin immunoprecipitation

ChIP assay of PARP1 or IgG antibodies was performed on harvested cells using the ChIP-IT high sensitivity kit (Active Motif, CA, USA) according to the manufacturer's instructions.

4.2.5. Unbiased proteomics

Unbiased mass spectrometry was carried out at Nottingham Trent University's core proteomic facility, on a SCIEX TripleTOF 6600 instrument with samples analysed in both SWATH (Data Independent Acquisition) and IDA (Information Dependent Acquisition) modes for quantitation and spectral library generation respectively. Briefly, cells were directly scraped on ice-cold 1x PBS and pelleted through centrifugation at 1000 RPM at 4ºC. Cell pellets were resuspended directly in ice-cold RIPA lysis buffer supplemented with 1x

Pierce™ EDTA-free protease inhibitor cocktail and stored immediately at -80ºC until analysis.

4.2.6. Data analysis

4.2.6.1. RNAseq data processing

RNAseq data processing and downstream mapping were conducted by the bioinformatics team at Nottingham Trent University. Reads were mapped using the kallisto RNAseq quantification program [336]. Analyses were carried out using R in RStudio and Bioconductor. Briefly, transcript quantification data was summarized to genes by tximport and normalized using edgeR. Normalized and filtered data were variance stabilized with voom function from limma and differentially expressed genes were identified with limma.

4.2.6.2. Gene set enrichment analysis

Gene set enrichment and pathway analysis of differential expressed genes and proteins was conducted using g:Profiler for identification of functionally enriched and over-represented pathways [366]. Detailed methodology on this can be found in *Section 2.3.6.3*.

4.2.6.3. SWATH-MS data analysis

IDA data was searched together using ProteinPilot 5.0.2 to generate a spectral library and SWATH data was analysed using Sciex OneOmics software extracted against the locally generated library as described previously. Log fold change and P-values were calculated as described [344]. Further details can be found in *Section 2.4.5*.

4.2.6.4. Statistical analysis

All statistics were carried out using the GraphPad Prism 6 software. Students T-test or ANOVA statistical comparisons were used with the Graphpad

Software Inc. Prism version 9. Unpaired t-Test compared treatments or genotypes. ΔΔCt values from qPCR experimental procedures calculated as detailed in *Section 2.3.4.3* were used for statistical analysis. Data are presented as mean ± SEM with statistical significance determined as *. P<0.05, **. P<0.01, ***. P<0.001.

4.3. Results

4.3.1. Early stage PARP1 inhibition shifts the resulting myotube proteome

In the previous chapter, we revealed that suppression of PARP1 mediated PARylation during myogenesis does not impact myotube development. Based on the findings that myotube features such as fusion index and density were decreased following early-stage PARP1 inhibition, we decided to investigate the full description of early-stage PARP1 inhibition during differentiation over the muscle proteome. To that end, we first subjected daily harvested lysates of day 1 to day 6 differentiating C2C12 myoblasts treated with PJ34 during differentiation induction to unbiased SWATH-MS analysis. This subsequently recovered peptides which were aligned to 2911 identified proteins differentially expressed from day 1 to day 6 of myogenesis in PJ34 treated differentiating C2C12 myoblasts (Fig. 4.1A). Further examination of day 1 PJ34 treated lysates revealed differentially expressed proteins to be functionally associated with documented roles of PARP1 in chromosome biology – these downregulated proteins (> 1.5 fold change) included PTMA (-2.14 fold change; p = 1.1), CBX6 (-1.59 fold change; p = 5.1), STIM2 (-2.37 fold change; p = 8.1) and HDAC6 (-1.90 fold change; p = 2.8) (Fig. 4.1B). These observations corroborate PARP1 dictating chromatin features, a canonical feature in

initiation of differentiation transcriptional programmes across tissues. Subsequently, the downregulated proteins from day 2 differentiating myoblasts treated with PJ34 shifted towards functions associated with skeletal muscle including MYMK (p = 2.6), TNNT1 (-1.60 fold change; p = 2.7), SCD2 (p = 3.3) and GYS1 (p = 2.8) – these were consistently observed across day 3 to day 6 lysates treated with PJ34 (Fig. 4.1B). Additionally, notable proteins fundamental to acquisition of skeletal muscle phenotype and contractility were reduced in PJ34 treated differentiating lysates, including TNNT3, TNNT2, MYMK, MYL1, MYL4.

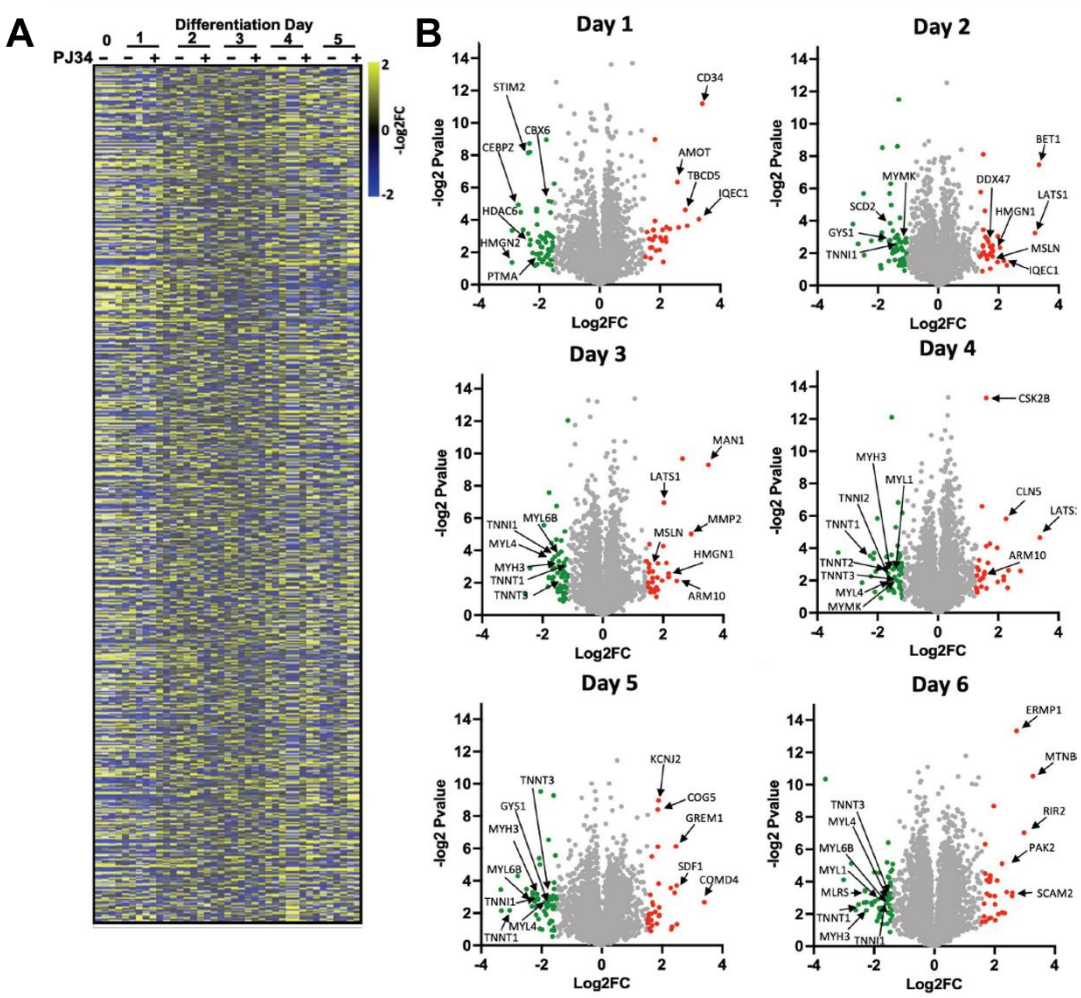

Figure 4.1. PARP1 regulates the proteome on each day of myogenesis
C2C12s during differentiation induction were treated with PJ34 **(A)** Heatmap showing 2,911 detected proteins in muscle samples ± PJ34 over days of differentiation **(B)** Volcano plots showing differentially abundant proteins in presence of PJ34 on each day of the 6 days of differentiation. Downregulated proteins are green (>-1.5 fold change), upregulated are red (>1.5 fold change). Arrows highlighting named proteins**.**
C2C12s *n=3*

To further corroborate our results presented in the previous chapter that demonstrate an increase in PAR levels within 24 hours of myogenesis, we sought to corroborate if this event has impacts over the differentiated myotube phenotype and the extent of PARP1 catalytic activity involvement. To do this, C2C12 myoblasts were treated with BYK204165 during differentiation induction which was washed out after day 1 and replaced with fresh DM. Lysates were harvested after 6 days of differentiation and subjected to

unbiased proteomic analysis. This subsequently detected 2921 proteins, of which 180 were differentially expressed in BYK204165 treated differentiating lysates (Fig. 4.2A, B). Of the downregulated proteins, these again included muscle contractile proteins including TNNT1 (-1.31 fold change) MYL4 (-1.86 fold change), TNNT3 (-1.53 fold change) MYL1 (-1.81 fold change) and MYH3 (-1.83 fold change) (Fig. 4.2B). These proteome induced changes were consistent with our unbiased proteomic analysis of PJ34 treated differentiating lysates (Fig. 4.1). Further gene set enrichment analysis of these differentially expressed proteins revealed functional pathways over-represented to biological processes governing actin binding, cytoskeletal protein binding, cytoskeletal motor binding, troponin binding, actin filament binding and structural constituent of muscle (Fig. 4.2C).

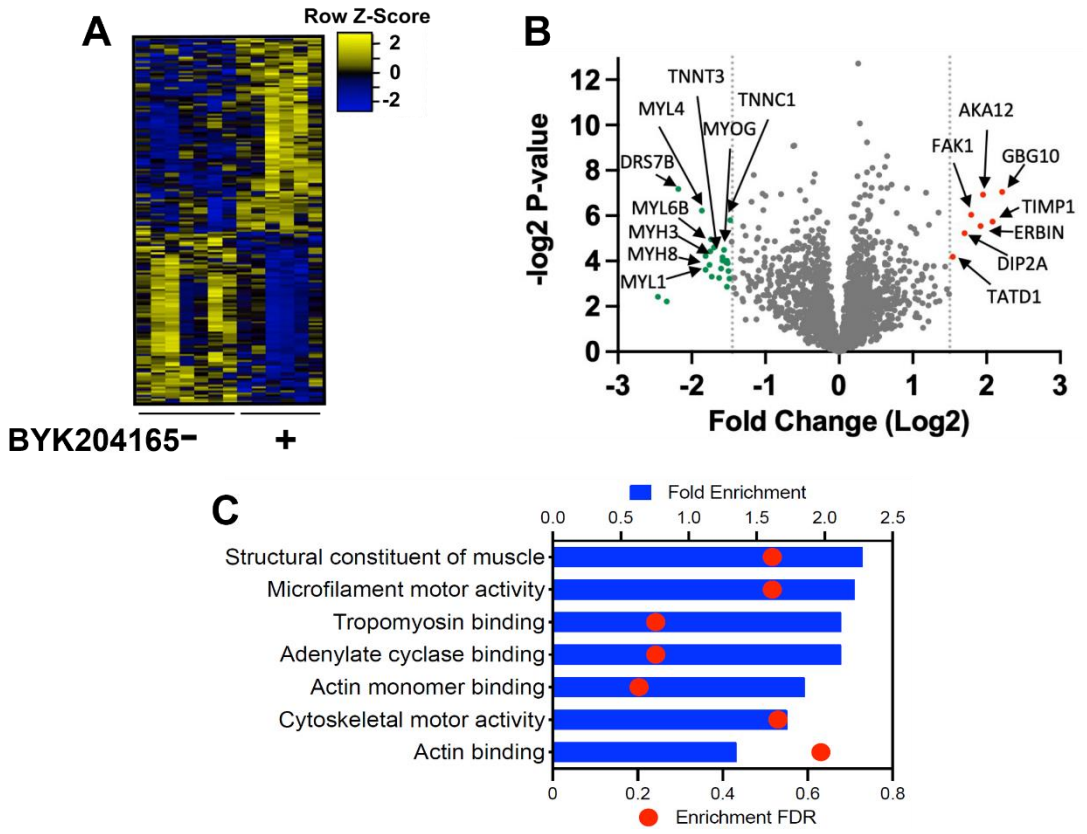

Figure 4.2. Specific PARP1 inhibition during early-stage differentiation induces shifts in resulting C2C12 myotube proteome
C2C12s during differentiation induction were treated with BYK204165 and allowed to differentiate for 6 days before lysate harvest **(A)** Heatmap representing differential abundance of proteins ± BYK204165 **(B)** Volcano plot of differential protein expression shown with downregulated proteins marked green and upregulated proteins marked red **(C)** g:GOSt gene set enrichment analysis of differentially expressed proteins identified in myotube lysates ± BYK204165.
C2C12s *n=3*

4.3.2. PARP1 holds influence over the myoblast transcriptome

To further complement the presented proteomic data in differentiating C2C12 myoblasts, we sought to unravel *PARP1* impacts on the C2C12 transcriptome. To that end, we conducted RNAseq on undifferentiated C2C12s that were subjected to siRNA transient knockdown of *PARP1* (*siPARP1*) (Fig. 4.3A). Because PARP1 is a major NAD^+ consuming enzyme, accounting for up to 90% of cellular NAD^+ driven PARylation, we also investigated impacts on NAD^+ homeostasis in *siPARP1* C2C12 myoblasts based on the expression profiles

of *PARP2*, *PARG*, *NAMPT* and *SIRT1*, which are key players in NAD^+ homeostasis and subsequently, NAD^+ dependent PARylation (Fig. 4.3B). Conversely, no changes were observed in the expression of these genes, implying *siPARP1* exerted minimal impacts on the subsequent expression of these players.

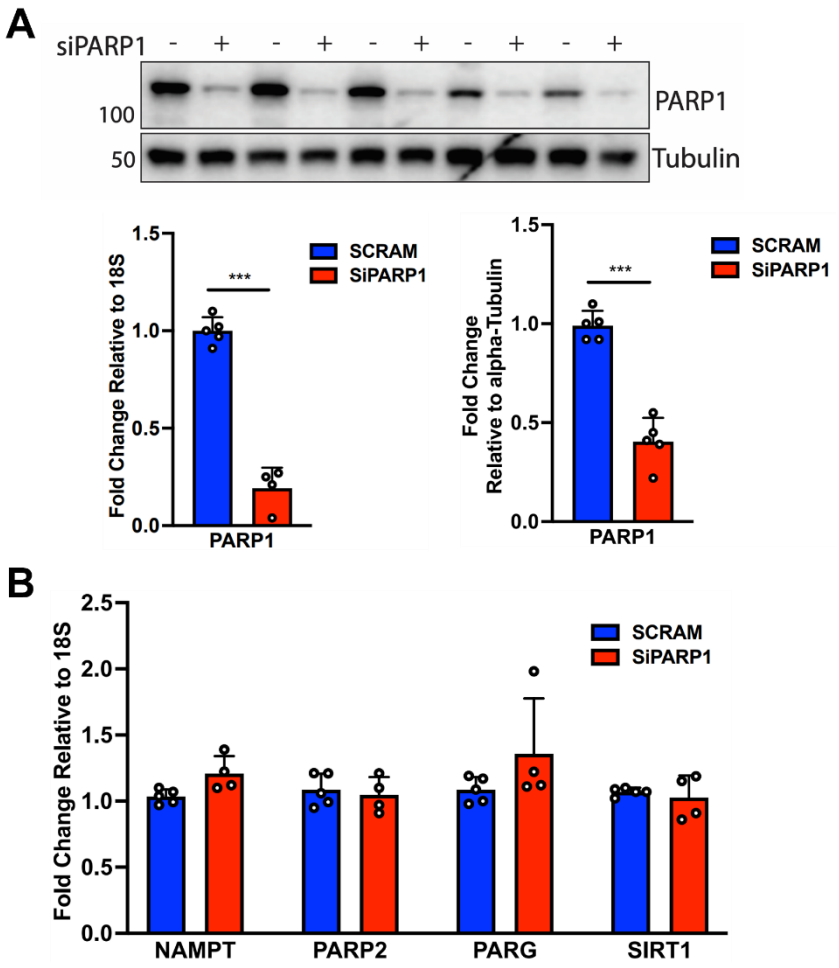

Figure 4.3. siRNA mediated knockdown of PARP1 does not impact expression of key NAD^+ metabolism players

C2C12s were seeded and subjected to knockdown of PARP1 **(A)** qPCR and western blot comparative analysis of PARP1 in samples transfected with Scrambled or PARP1 siRNA (*siPARP1*) **(B)** qPCR analysis of key players within NAD^+ biosynthesis pathways as well as NAD^+ consuming enzymes.
All data are normalised to loading controls and are the mean ± SEM
C2C12s *n=5*

When compared to scrambled siRNA sequence controls following RNAseq, *siPARP1* presented 123 uniquely expressed gene transcripts (FPKM > 0.5) in comparison to 51 in scrambled controls (Fig. 4.4A). These changes imply that *PARP1* already exerts transcriptional influence in the myoblast, consistent with observations observed in gene regulatory programmes specific to different cell types [210]. Furthermore, we also identified the *NR3C2* gene, which codes for the glucocorticoid binding MR as being downregulated.

Further to these initial findings, gene set enrichment analysis of these differentially expressed genes revealed overrepresentation of pathways pertaining to metal ion binding and endopeptidase activity which are fundamental for excitation-contraction coupling and protein catabolism respectively – these molecular functions were observed to be upregulated in *siPARP1*. (Fig. 4.4B). There was further enrichment into pathways governing muscle structure differentiation and metabolism, including molecular pathways regulating NAD^+ binding events, actin binding events, cytoskeletal structural organization and phosphatase activity, all of which collectively serve as integral determinants of cellular identity. A selection of these genes are presented (Fig. 4.4C).

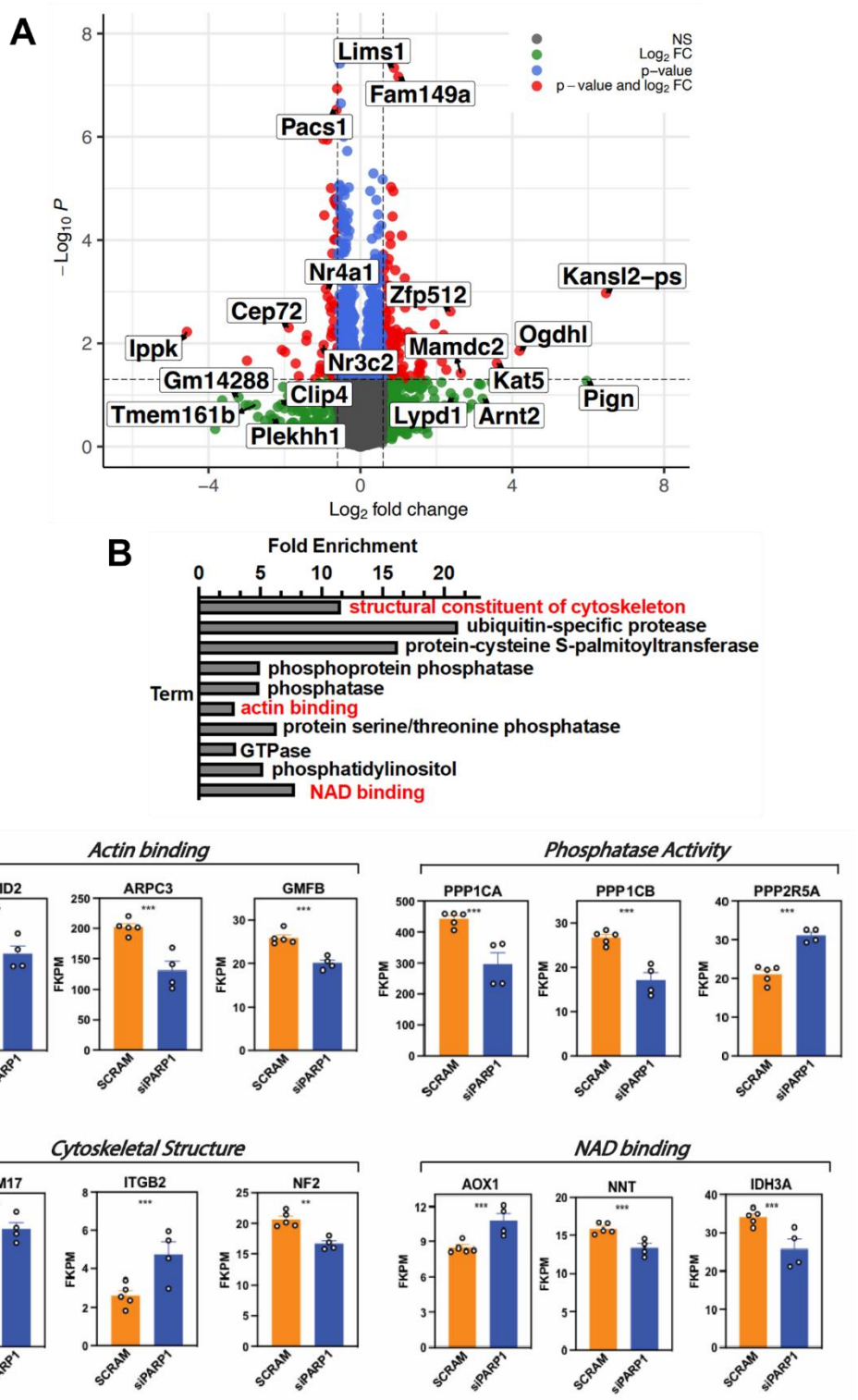

Figure 4.4. siRNA mediated knockdown of PARP1 is sufficient to induce shifts in the transcriptome of undifferentiated C2C12s

C2C12s were seeded and subjected to knockdown of PARP1 and harvested for RNAseq **(A)** Representative volcano plot showing differential gene expression from scrambled and *siPARP1* samples **(B)** Gene set enrichment analysis of differentially expressed genes identifies enrichment in processes associated to skeletal muscle cellular identity and architecture **(C)** Representative gene expression levels identified from RNAseq governing functionally enriched processes – transcript levels expressed in fragments per kilobase of transcript per million reads mapped (FPKM).

C2C12s *n=3*

However, also suppressed were pathways and metabolic processes regulating fundamental metabolism including pantothenate metabolism, palmitoylation and mitochondrial import; in contrast, upregulated processes by *siPARP1* were associated with immune cell adhesion, autophagosome, cell adhesion and REDOX regulation (Fig. 4.5A). Further gene set enrichment analysis reported shifts in major pathways of hypoxia regulation (NES 1.5, P Value 0.001, myogenesis (NES 1.3, $p = 0.052$) and TNFα via NF-κB (NES -1.3, $p = 0.039$) (Fig. 4.5B). PARP1 regulation of hypoxia, as is interaction with the NF-κB immune signalling cascades, have been documented [234,367]. Moreover, these features are also commonly reported as being regulated by glucocorticoid signalling [294].

To further identify the major transcriptional processes governed by PARP1 and PAR inhibition during day 1 of differentiation, we conducted RNAseq on PJ34 treated 24 hour differentiating myoblasts compared to vehicle controls (Fig. 4.5C). Gene set enrichment analysis revealed suppression of pathways regulating assembly of the skeletal muscle myofibrils and muscle stretch. Additionally, suppression of the phosphorylation of RNA polymerase C-terminal may suggest global shifts in transcriptional rates as a consequence of reduced PARP1 activity within the genome. These data confirm the dynamic nature of PAR in skeletal muscle and a background of transcriptional coordination in this tissue is influenced by PARP1. Put together, our data show that *PARP1*, independent of its catalytic PARylating activities, exert influence over the myoblast transcriptome.

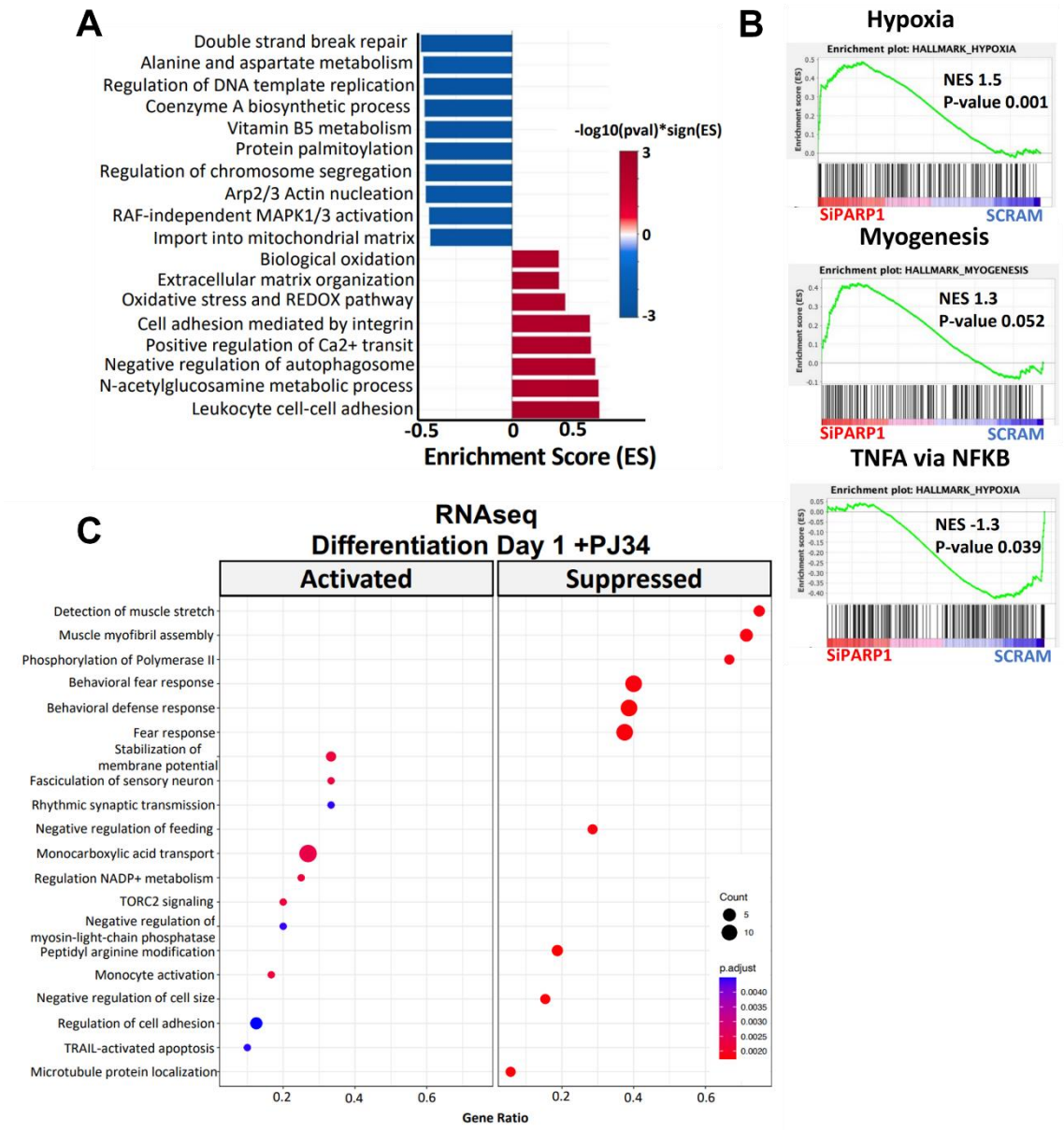

Figure 4.5. Gene set enrichment analysis of *siPARP1*

C2C12s were seeded and subjected to knockdown of *PARP1* and harvested for RNAseq, and differentially expressed genes were identified and subjected to gene set enrichment analysis **(A)** Enriched processes in *siPARP1* samples following gene set enrichment analysis for global metabolism processes **(B)** Enrichment plots of gene set enrichment analysis in *siPARP1* samples for hypoxia, myogenesis and TNFα via NF-κB **(C)** Reactome dot plots demonstrating differences in pathway enrichment of early-stage PJ34 treatment of C2C12s differentiating for 1 day.
C2C12s *n=3*

4.3.3. PARP1 and glucocorticoid receptor interactions in differentiating C2C12s

We observed the *NR3C2* gene which codes for the glucocorticoid binding MR, to be downregulated in *siPARP1* C2C12 myoblasts. Studies on PARP1 and GR activity over the years have demonstrated their mutual roles over homeostatic processes including inflammation and glucose metabolism. GR activity, as mentioned in the introduction to this chapter, also holds influence over skeletal muscle physiology and there is emerging evidence pertaining to PARP1 regulating GR mediated transcription [364,365]. Together with our proteomic and transcriptomic findings in *siPARP1* C2C12 myoblasts, we postulated that PARP1 has potential roles in glucocorticoid response in skeletal muscle. We first assessed interactions between PARP1 and GR – C2C12s were treated with dexamethasone during differentiation induction and lysates were harvested on each day of myogenesis for 5 days. Intriguingly, we observed a reduction in total PAR levels (Fig 4.6A, B) in a similar fashion to our previously presented findings where C2C12s were treated with PARP inhibitors during differentiation induction (Fig. 3.2 and Fig. 3.3).

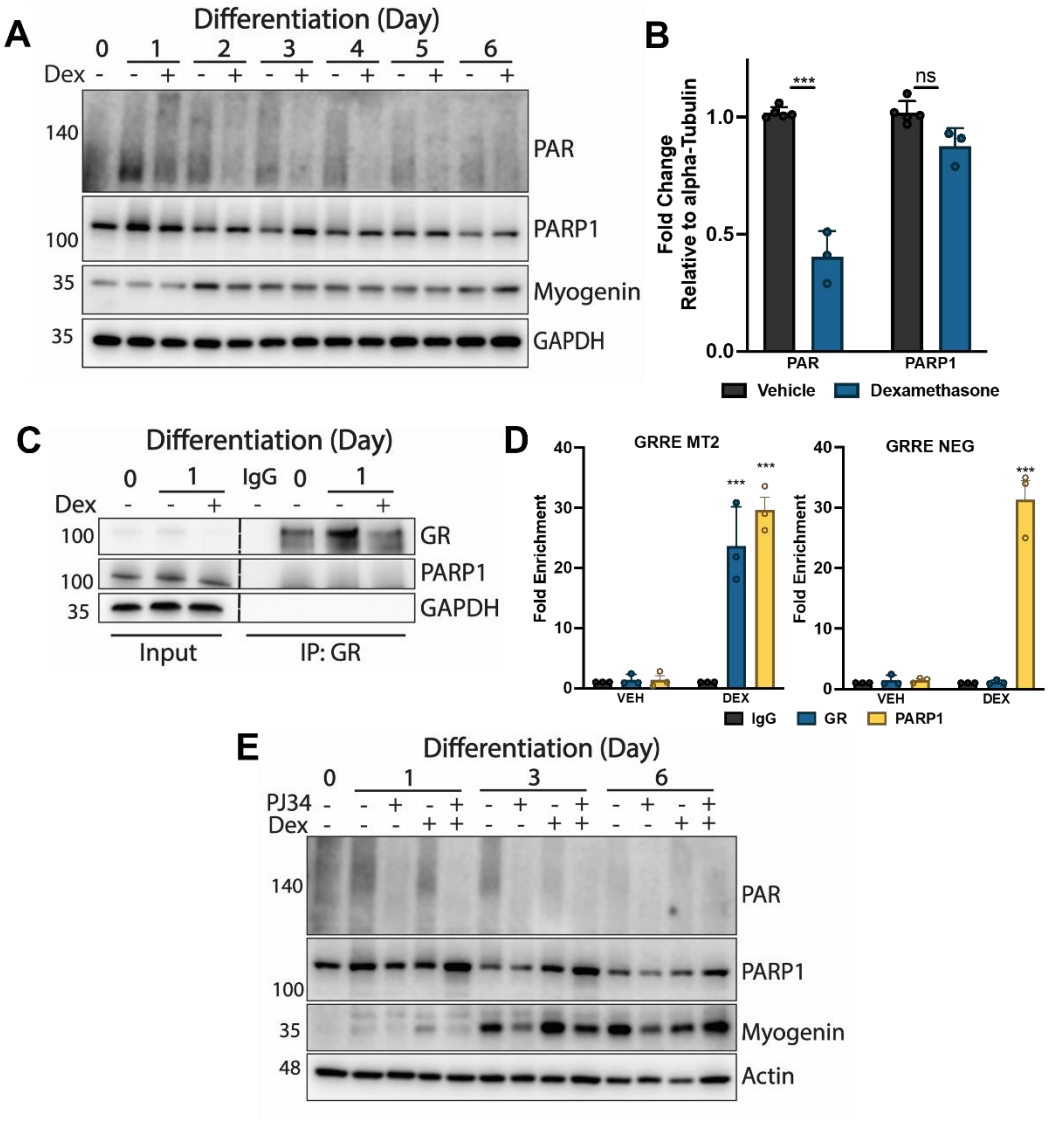

Figure 4.6. Characterisation of PARP1, PAR and glucocorticoids

C2C12s were seeded and treated with 1 µM dexamethasone during differentiation induction **(A)** Western blot analysis of lysates collected on each day of differentiation **(B)** Quantification of western blots for PAR and PARP1 between treated groups **(C)** Protein immunoprecipitation assay of dexamethasone treated 24 hour differentiating C2C12s **(D)** Chromatin immunoprecipitation assay of dexamethasone treated 24 hour differentiating C2C12s **(E)** Western blot analysis of C2C12s treated with either dexamethasone, PJ34 or a combination of both during differentiation induction over days 1, 3 and 6 of differentiation.

All data are normalised to loading controls and are the mean ± SEM

C2C12s *n=3*

To corroborate potential interactions, we performed IP assay in lysates of 24 hour differentiating C2C12 myoblasts treated with dexamethasone. This subsequently revealed however, no physical interaction between PARP1 and GR (Fig 4.6C). Given both PARP1 and GR roles in transcriptional control, we also conducted ChIP of these lysates – this consequently revealed a 30-fold enrichment in *PARP1* binding (± 3.2 SEM) to GREs on the *MT2* promoter region in response to dexamethasone treatment (Fig. 4.6D). The absence of *PARP1* binding to nGREs suggests that the recruitment of *PARP1* is occurring independent of GR activity, leading us to infer a transcriptional basis for GR-PARP1 interaction in governing skeletal muscle phenotype and the glucocorticoid transcriptional response. Furthermore, we also demonstrate a synergistic relationship between both the inhibition of PARP1 activity and dexamethasone treatment upon PAR levels during myogenesis (Fig. 4.6E) – here, in accordance with our initial proteomic analyses, we also show that PJ34 treated differentiating myoblasts display downregulation in muscle specific proteins including myogenin. Consequently, a dual treatment of PARP1 inhibition with PJ34 and dexamethasone rescues this downregulation. This finding, at least based on myogenin levels, is in agreement, with previous studies that demonstrate dexamethasone treatment enhances myogenesis [326,327] and further underscores the potential for glucocorticoid treatment impacts during myogenesis to manifest via a PARP1 mechanism.

4.3.4. PARP1 partially governs the glucocorticoid transcriptional response

To gain better insights into GR-PARP1 transcriptional paradigms, RNAseq was conducted on *siPARP1* C2C12 myoblasts subjected to 24 hour dexamethasone treatment. Respectively, this yielded 4791 differentially expressed genes (Fig 4.7A). These differentially expressed genes were associated with mediators of glucocorticoid signalling as we expected (Fig. 4.7B, C) – specifically, we identified activation of canonical glucocorticoid genes including *SerpinA3N* (9.50 fold change; $5.22x^{-08}$ FDR), *HIF3A* (7.40 fold change; $4.29x^{-10}$ FDR) and *Mt2* (3.97 fold change; $9.07x^{-24}$ FDR). A selection of genes is presented (Fig. 4.7D). This initial finding suggests that *PARP1* impacts chromatin level organisation and contractile protein expression during differentiation, but is dispensable for the archetypal glucocorticoid activated transcriptional response.

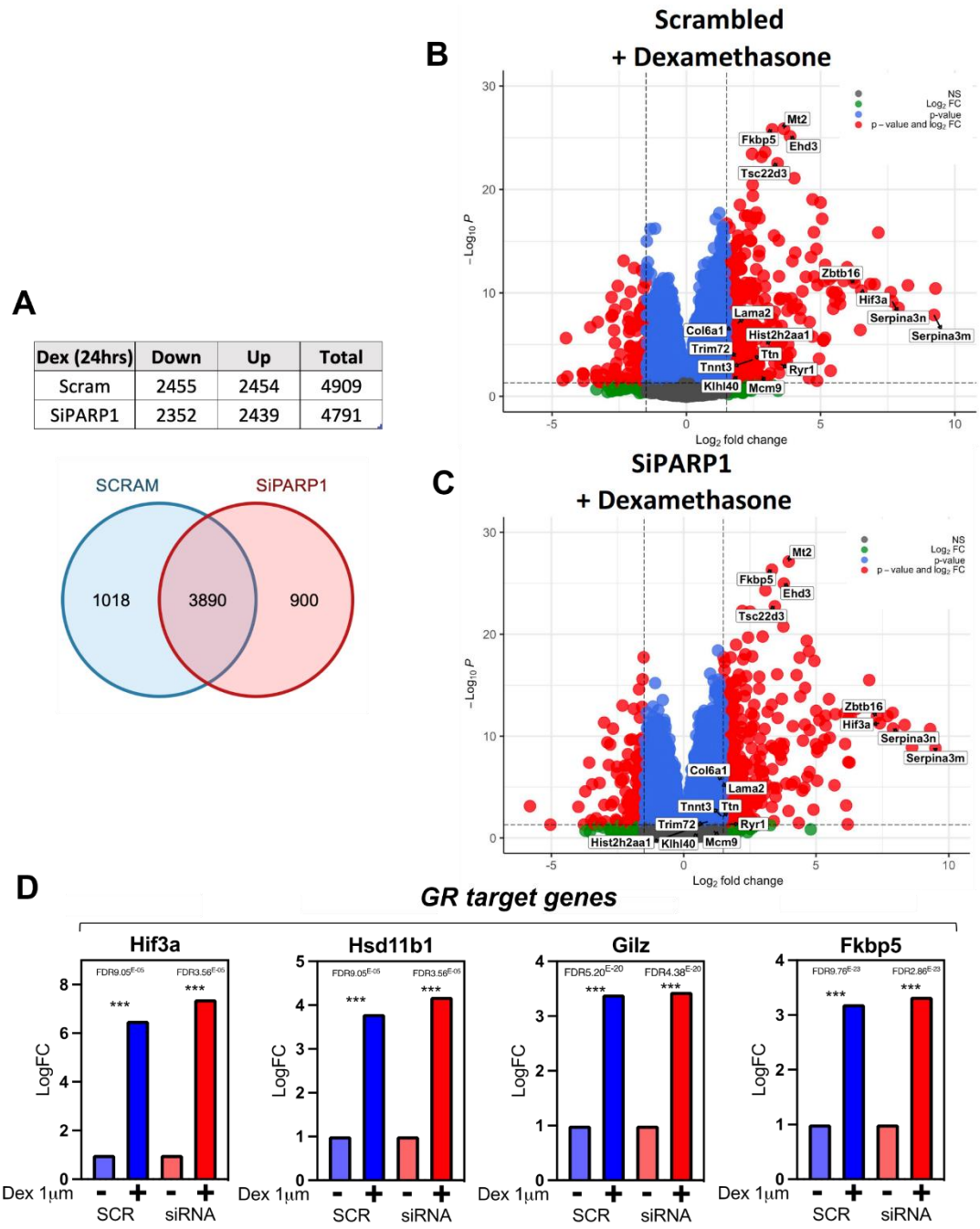

Dex (24hrs)	Down	Up	Total
Scram	2455	2454	4909
SiPARP1	2352	2439	4791

Figure 4.7. Differentially expressed genes in *siPARP1* C2C12s following dexamethasone treatment

C2C12s were seeded, transfected with scrambled or *siPARP1* siRNA, then treated with 1 μM dexamethasone and harvested for RNAseq **(A)** Representative table and Venn diagram of differentially expressed genes between scrambled and *siPARP1* C2C12s treated with dexamethasone **(B)** Volcano plot of differentially expressed genes in scrambled siRNA transfected C2C12s treated with dexamethasone **(C)** Volcano plot of differentially expressed genes in *siPARP1* C2C12s treated with dexamethasone **(D)** Representative gene expression levels of canonical GR signalling players identified from RNAseq analysis – transcript levels expressed in Log fold change and false discovery rate (FDR)

All data are presented as the mean ± SEM

C2C12s *n=6*

Glucocorticoid actions and response are determined by activated GR binding to GREs that entail recruitment of transcriptional co-activators and co-repressors to regulate transcription or directly binding to other transcriptional factors in a tethering mechanism. Subsequently, genes targeted by GR activation entails them as mediators of glucocorticoid response. Crucially, we identified 86 differentially expressed genes that were not induced following dexamethasone treatment in the *siPARP1* myoblasts compared to their scrambled controls (Fig. 4.8A), with a selection of these genes presented (Fig. 4.8B). These 86 genes were subjected to g:GOSt functional profiling within the g:Profiler program, revealing enrichment for gene ontological processes and functions associated to skeletal muscle physiology including calcium release (*Padj*. $1.49x10^{-2}$), as well as biological processes including striated muscle differentiation (*Padj*. $1.03x10^{-8}$) and cellular development (*Padj*. $3.34x10^{-6}$). Furthermore, enrichment of the cellular compartment forming the thin filament of the myofibril was recorded (I band (FDR $5.06x10^{-6}$) and Z disc (FDR $5.59x10^{-5}$)). Further mapping for these 86 genes for transcription factor motifs generated enrichment for key regulatory factors of muscle including *Pax4*, a regulator of muscle protein turnover (*Padj*. $4.67x10^{-3}$), *LKLF* (*Padj*. $5.72x10^{-3}$), *PTF1* (*Padj*. $8.84x10^{-3}$) and *myogenin* (*Padj*. $8.98x10^{-3}$). Finally, human phenotype mapping identifies this gene cohort as being characteristic of skeletal muscle dysfunctions including proximal muscle weakness, muscular dystrophy and Gowers sign (childhood muscle weakness) (Fig. 4.8C) [368]. Subsequent application of these genes to transcriptional profiling using the ARCHS4 database reveals further MRFs including *MyoD* and *MYF6*, while ENCODE gene set enrichment identifies *MyoD* (Fig. 4.8D). These data

indicate there are a subset of genes regulated by glucocorticoids in skeletal muscle which are also regulated by *PARP1*, that contribute towards muscle homeostasis.

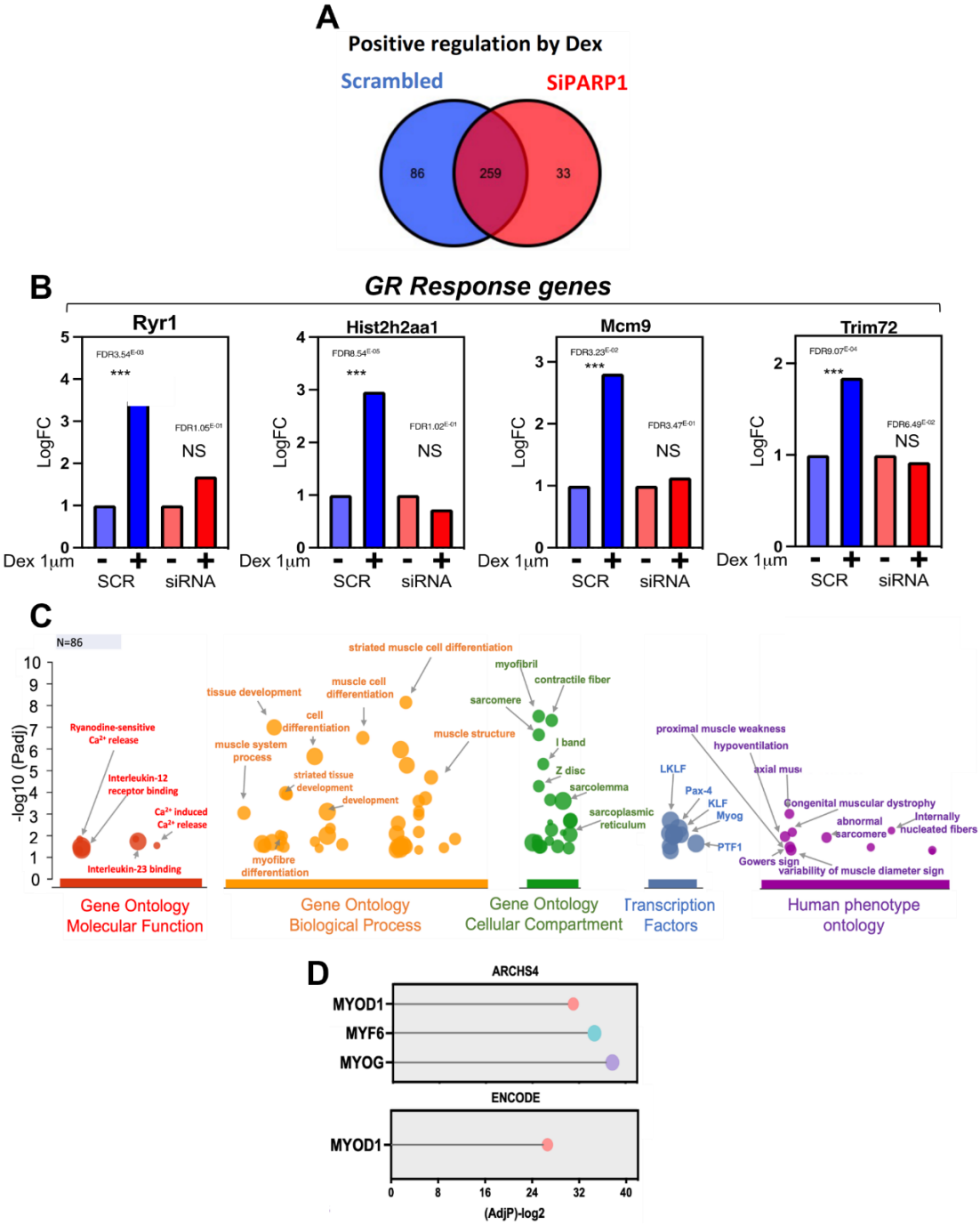

Figure 4.8. *siPARP1* causes loss of expression in glucocorticoid response genes associated to skeletal muscle physiology

C2C12s were seeded, transfected with scrambled or *siPARP1* siRNA, then treated with 1 µM dexamethasone and harvested for RNAseq **(A)** Venn diagram of genes positively regulated by glucocorticoids in scrambled and *siPARP1* C2C12s **(B)** Representative gene expression levels of GR response mediating genes identified from RNAseq analysis – transcript levels expressed in log fold change and FDR **(C)** Manhattan plot using g:GOSt produced using the 86 genes whose response to dexamethasone is lost in *siPARP1* myoblasts. Plot shows overrepresented processes by molecular function (red), biological process (orange), cellular compartment (green), transcription factors (blue) and human phenotype (purple) **(D)** Application of transcriptional profiling of MRFs differentially expressed in dexamethasone treated *siPARP1* cells using ARCHS4 and ENCODE database.

All data are presented as the mean ± SEM

C2C12s *n=6*

Finally, to examine broader functional impacts in *siPARP1* following glucocorticoid exposure in skeletal muscle, the wider cohort of differentially expressed genes from our RNAseq data were subjected to functional enrichment analysis. This gave us further insight into the GR associated biological and molecular processes that were either retained or modulated. Additionally, to gain a better insight into impacts in *siPARP1* myoblasts following short-term glucocorticoid exposure, we also conducted RNAseq on C2C12 myoblasts treated with dexamethasone for 2 hours. Here, we observed an enrichment of processes central to initiation of glucocorticoid signalling as well as other cellular pathways activated by glucocorticoid stimulus, all of which remained unchanged in *siPARP1* (Fig. 4.9A). This supported earlier findings presented that suggested no significant impacts on the induction of canonical GR target genes (Fig. 4.7D). In contrast, we also observed enrichment of glucocorticoid mediated responses that were subsequently lost – these were associated with skeletal muscle function and development, as well as structural organisation (Fig. 4.9B). Subsequently, we observed enrichment of processes associated with GR mediated signalling which were increased in *siPARP1* (Fig. 4.9C).

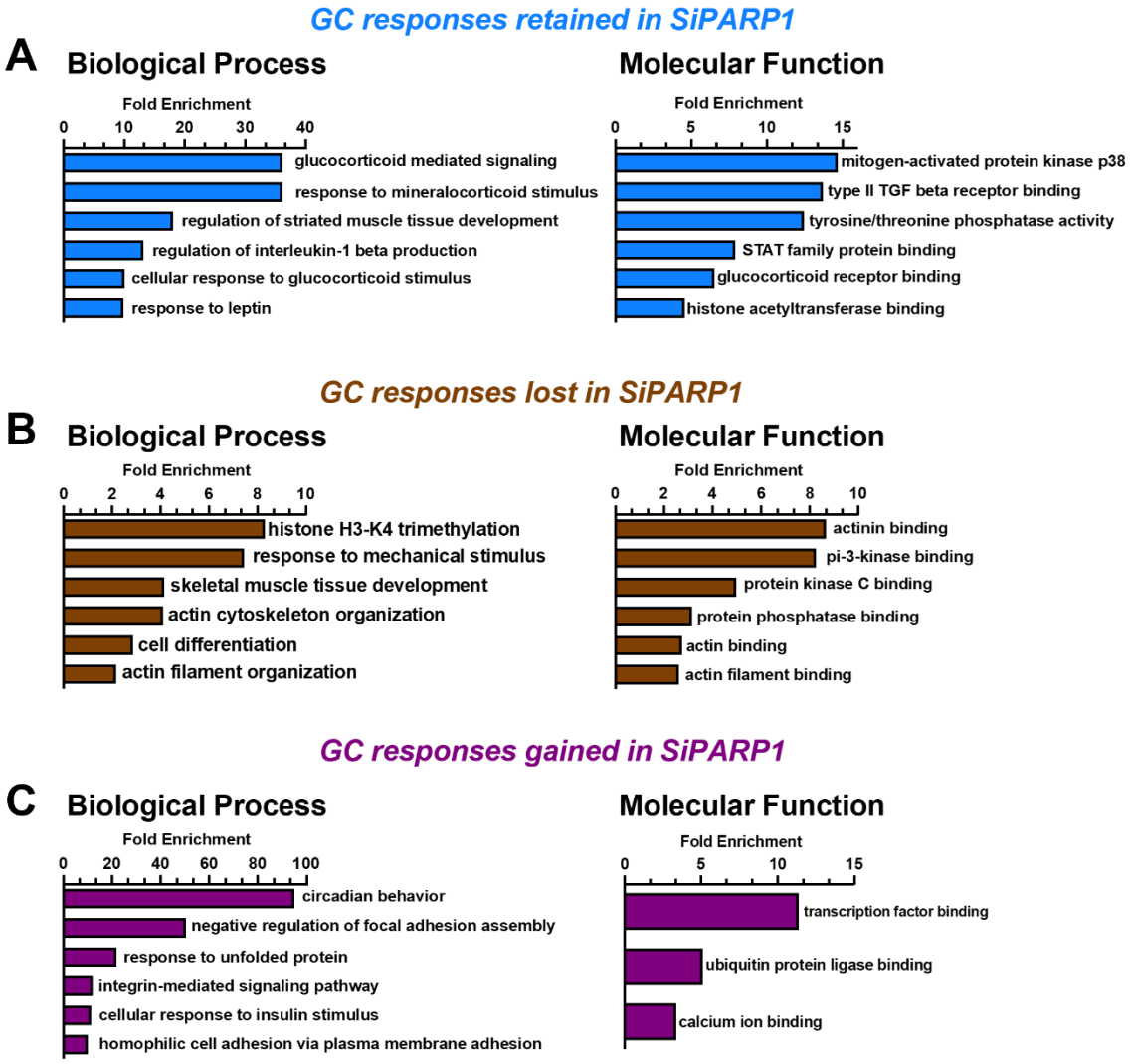

Figure 4.9. Functional profiling of the wider cohort of differentially expressed genes in *siPARP1* C2C12 myoblasts treated with dexamethasone for 2 hours
C2C12s were seeded, transfected with scrambled or *siPARP1* siRNA, treated with 1 µM dexamethasone and harvested for RNAseq. Identified differentially expressed genes were subjected to gene set enrichment analysis for functionally enriched processes that were **(A)** Retained **(B)** Downregulated and **(C)** Upregulated
C2C12s *n=6*

On the other hand, the cohort of differentially expressed genes following 24 hours dexamethasone treatment in *siPARP1* C2C12 myoblasts revealed shifts from enrichment in pathways ascribed to skeletal muscle development to pathways governing phenotype, including cell division, mitochondrial metabolism and genome stability (Fig. 4.10 A, B). Fundamentally, an enrichment in proteasome-mediated ubiquitin dependent catabolism, the

classical pathway in glucocorticoid induced muscle atrophy, was observed to be decreased in *siPARP1* and implies a role for *PARP1* in the outcome of glucocorticoid mediated side effects in skeletal muscle. We also observed an enrichment of pathways associated with NF-kB signalling, NAD^+ kinase activity and viral infection, which were increased in *siPARP1* (Fig. 4.9C). Given that PARP1 has roles in infection and immunity [116], this suggests that the prescription of glucocorticoid based therapy could potentially predispose individuals to greater risk and morbidity in pathogen induced myositis via a PARP1 dependent mechanism. Collectively, our data reveal that initiation of canonical GR signalling following glucocorticoid binding occurs independently of PARP1. However, the subsequent mediation of glucocorticoid response, based on GR response gene expression profiles and functional profiling, is dependent upon PARP1. As the use of glucocorticoids in skeletal muscle therapy continue to remain contentious, it is reasonable to suggest that the outcome of glucocorticoid treatments occur via a PARP1 mechanism that certainly necessitates further investigation.

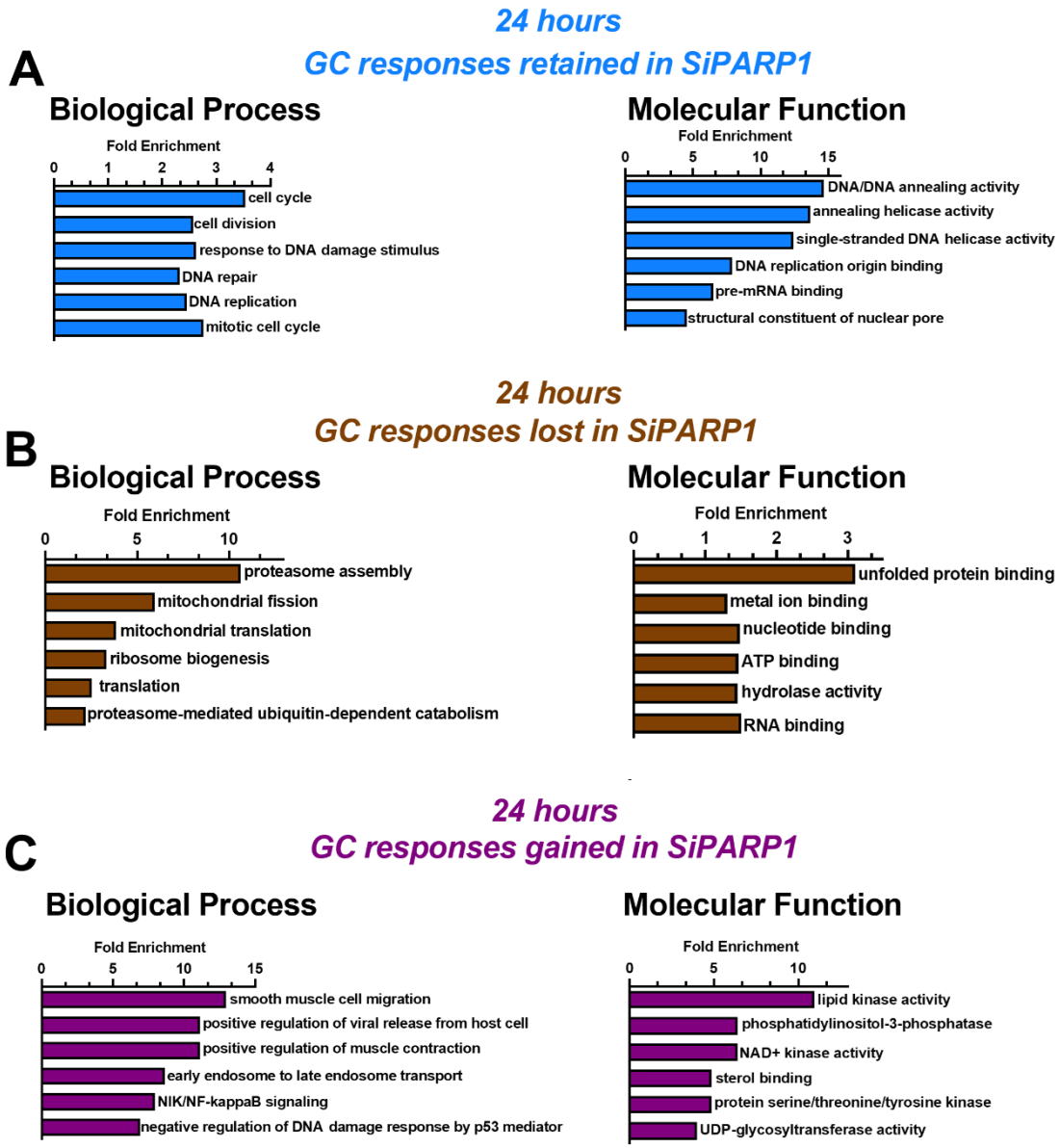

Figure 4.10. Functional profiling of the wider cohort of differentially expressed genes in *siPARP1* C2C12 myoblasts treated with dexamethasone for 24 hours

C2C12s were seeded, transfected with scrambled or *siPARP1* siRNA, treated with 1 µM dexamethasone and harvested for RNAseq. Identified differentially expressed genes were subjected to gene set enrichment analysis for functionally enriched processes that were **(A)** retained **(B)** downregulated and **(C)** upregulated
C2C12s *n=6*

4.4. Discussion

PARP1 mediated PARylation events have been demonstrated to exert greater and direct influence on the differentiation of other tissues, including adipocytes [103,209,240], oligodendrocytes [248] and osteoclasts [206,369]. Knowledge on these events in skeletal muscle differentiation remains hitherto limited. However it seems the presence of PARP1, rather than its catalytic activity, influences skeletal muscle differentiation to a greater extent [176]. At the transcriptional level, *PARP1* associates with the regulatory regions of genes to subsequently interfere with their targeting by the MRF *MyoD* to inhibit transcription and induction of myogenic genes associated with the differentiation programme [176]. This led us to postulate roles for PARP1 mediated PARylation events during early-stage differentiation in subsequent determination of developed myotube phenotype. Using proteomic and transcriptomic approaches, we demonstrate that PARP1 exerts influence over the transcriptional regulation and protein abundance of genes associated with overall skeletal muscle phenotype in C2C12 myoblasts, and also further demonstrate that changes also occur as a consequence of early-stage PARP1 activity modulation during differentiation. Specifically, changes in expression of genes and proteins in subsequent developed myotubes are associated with skeletal muscle function, including glucose metabolism, muscle contraction and structural organization. Consequently, we also observe differential expression of genes mediating overall glucocorticoid response in skeletal muscle, which implies roles for a PARP1-GR paradigm in the effects of chronic glucocorticoid exposure in skeletal muscle including conditions of myopathy and steroid-induced diabetes. Put together, our proteomic, transcriptomic and biochemical studies

demonstrate interplay between PARP1 mediated PARylation, skeletal muscle phenotype and glucocorticoid response. This suggests any potential role for PARP modulation as a tool for sustaining muscle function must be carefully considered in relation to the ability of the tissue to repair and replace muscle fibres.

4.4.1. Developed myotube phenotype is determined by early stage PARP1 mediated PARylation events during myogenesis

Suppression of PARP1 elicits beneficial metabolic effects which include enhanced exercise performance, increased energy expenditure, enhanced mitochondrial function and resistance to oxidative stress [131–133,251]. Additionally, PAR and PARP1 levels are dynamically and differentially regulated during exercise between aged untrained and aged trained muscle [335] – crucially, knowledge of these trends with regards to skeletal muscle development remains limited. Thus far, a previous study demonstrated the ability of *PARP1* to block the MRF *MyoD* mediated transcription of myogenic genes during myogenesis by physically binding to the regulatory regions of these genes, indicating that PARP1 PARylating activity is not essential for proper myotube development [176]. To that end, we postulated that the PARP1 mediated PAR accumulation occurring in day 1 of myogenesis exerts a greater consequence on the developed myotube than on its development. In this regard, we observed in C2C12 myoblasts treated with PARP inhibition during myogenic induction, differentially expressed genes and proteins that were predominantly associated with skeletal muscle functions including glucose metabolism and contractility. Through use of the broad spectrum PARP inhibitor PJ34 and the PARP1 specific inhibitor BYK204165, which both yielded similar trends, we

showed that these expression profile changes are indeed related to PARP1 mediated PARylation that occurs within the first day of myogenesis. We also found that downregulation of *PARP1* alone in undifferentiated C2C12 myoblasts is sufficient to cause shifts in the skeletal muscle transcriptome, and subsequent functional profiling revealed biological and molecular processes that were enriched were similar to those of early-stage PARP1 inhibition during myogenesis. Further insight into which substrates are PARylated within the first day of myogenesis where PAR levels are at its highest will be useful in unravelling downstream signalling pathways that determine myotube phenotype which are regulated by PARylation. However, existing evidence suggests that MyoD could be a potential target – a recent study by Bisceglie et al. presented an increase in nuclear PARP1 mediated PARylation activities in the myoblast following successful MyoD driven transdifferentiation from fibroblasts [207]. Our data also show that the expression of MRFs such as myogenin and muscle-specific proteins including the troponins are governed by PARP1 inhibition – it is therefore probable that PARP1, through direct interaction or enzymatic application of PAR chains, coregulates their mRNA transcription. Incidentally, impacts over troponin expression by PARP1 may be relevant in cardiac muscle [370], and our data show reduced levels of myogenin in C2C12 myoblasts treated with PJ34 during differentiation induction (Fig. 4.6E). Taken together with our results, these suggest that both PARP1 itself and its PARylating activity hold influence over the skeletal muscle phenotype, and further underscores PARP1's role as a multifaceted protein being able to bind to nucleic acids as well catalysing the PARylation of target substrates [173–175].

4.4.2. PARP1 partially governs glucocorticoid transcriptional response in skeletal muscle

Evidence for PARP1 in the regulation of GR mediated transcriptional response has been presented in other cells [365]. Furthermore, cortisol levels in PARP1 null mice are increased [364]. Our transcriptomic analysis of *siPARP1* C2C12 myoblasts reveals changes in expression of the *NR3C2* gene which codes for MR (Fig. 4.4A) – while not as ubiquitously and predominantly expressed as its GR counterpart, MR can also bind glucocorticoids with higher affinities [294]. Furthermore, we demonstrated pathways commonly classified as glucocorticoid controlled including hypoxia, myogenesis and TNF response through *NF-κB* were shifted in the *siPARP1* myoblasts (Fig. 4.5B). In this regard, since *PARP1* has perceived roles in the *NF-κB* mediated inflammatory response [234], and the anti-inflammatory effects of glucocorticoids manifest through the suppression of *NF-κB*, this suggests that glucocorticoid mediated effects occur via PARP1. In this regard, the *NF-κB* pathway has been implicated in differentiation programmes of other tissues, including myogenesis [206,371,372] – notably, PARP1 and its PARylating activity are key determinants in osteoclast differentiation and bone modelling via a *NF-κB* dependent transcription of *IL1β* [206] and glucocorticoid induced osteoporosis is a consequence of the inhibition of IL1 production [373]. Put together with our findings, these certainly provide plausibility for PARP1 exertions over glucocorticoid mediated outcomes in skeletal muscle turnover via regulation of NF-κB which warrants further investigation.

Given roles for glucocorticoids in skeletal muscle myogenesis and myopathy, as well as shared roles with *PARP1* in other cellular processes such as

inflammation and transcriptional regulation, we further explored the potential for glucocorticoids and PARP1 in skeletal muscle myogenesis. Interestingly, we first showed that addition of dexamethasone, a synthetic GR activator during C2C12 myogenic induction, suppresses the PARP1 mediated PAR accumulation in day 1 of myogenesis, implying that this event is also sensitive to endogenous signal hormones (Fig. 4.6A). However, glucocorticoid use in skeletal muscle has remained albeit ambiguous – chronic glucocorticoid exposure has been demonstrated to induce skeletal muscle myopathy [326,330], while the *in vitro* application of dexamethasone to myoblasts promotes their differentiation [325–327]. However, this has been obfuscated by other studies that posited factors including cell confluency as well as the type of glucocorticoid receptor agonist applied can impact glucocorticoid mediated outcomes in differentiation [374]. In our presented data at least, we show, through the expression of myogenin, that dexamethasone application is capable of reversing the downregulation of this MRF protein following PARP inhibition (Fig. 4.6E), supporting the notion that dexamethasone enhances myogenesis.

By examining the transcriptomic changes in 24 hour dexamethasone treated *siPARP1* C2C12 myoblasts, we observe that the expression of GR canonical target genes such as *FKBP5* that dissociates from ligand bound GR to allow its translocation into the nucleus, remained intact (Fig. 4.7D). This suggests that genes directly regulated by GR actions are not dependent on *PARP1*. Further g:GOSt analysis shows that the 86 genes in *siPARP1* that fail to induce following dexamethasone treatment are ascribed to skeletal muscle physiology with diverse molecular functions (Fig. 4.8). Of particular note, these included two players involved in muscle remodelling – *RYR1* possesses *MyoD*

regulatory elements and governs calcium signalling critical for excitation-contraction coupling, and its mutations are associated with a plethora of congenital myopathies [375], and *TRIM72*, an E3 ligase within the ubiquitin-proteasome system, has been demonstrated to antagonise myogenesis of C2C12s [376], and is a target for PARP1 mediated MARylation in myocardial injury [377]. These suggest that *PARP1* exerts influence over outcomes of glucocorticoid response genes in skeletal muscle; furthermore, *PARP1* has demonstrated involvement in myopathy [208], and so does chronic glucocorticoid exposure [326,330]. These could imply mechanisms for PARP1 in the transcriptional pathways that result in glucocorticoid induced myopathy, warranting broader studies in this regard. Already, studies have presented *PARP1* influence over glucocorticoid responsiveness of Gonadotropin-releasing hormone receptors [378], and our current study illustrates that glucocorticoid mediated impacts on skeletal muscle occur through PARP1 and its PARylating activity.

In summary, this work further underscores that PARP1 holds influence over skeletal muscle phenotype, with regards to the outcome of differential expression of genes and proteins in developed myotubes subject to early-stage inhibition of PARP1 mediated PARylation activity during differentiation induction. We also demonstrate PARP1's role as a transcription factor given that its reduction is sufficient to induce changes in the myoblast transcriptome. We also reveal that as a consequence of its activity inhibition or downregulation in expression, PARP1 also partially governs skeletal muscle glucocorticoid transcriptional response. This provides further basis for PARP1-GR transcriptional interactions in skeletal muscle physiology, and potentially,

avenues for therapeutic strategies for ameliorating glucocorticoid induced side effects. While PARP1 inhibition mediates beneficial effects in fully developed muscle tissue due to increased NAD^+ availability, potential negative impacts over myogenic mechanisms and efficacy of glucocorticoid therapies implies that using PARP inhibitors as therapy should be assessed on risk:benefit ratio.

Chapter 5

Preliminary *in vivo* characterisation of PARP1 mediated PAR and glucocorticoid receptor dynamics

5.1. Introduction

ADPR and PAR are signalling moieties that are generated through the consumption of NAD^+ that then serves as post-translational and transcriptional modification molecules onto target substrates and key signalling players in whole body processes including DNA repair and cellular death and differentiation pathways. Combined with the importance of NAD^+ as a cofactor in a plethora of biochemical reactions, metabolic regulation of ADPR and PAR generation and stability is associated with conditions including diabetes, inflammation, glucocorticoid sensitivity, pathogenic infection, differentiation and exercise performance [116,131,132,165,189,335].

NAD^+ is synthesized through three main pathways: salvage, *de novo* and preiss-handler. The type of pathway utilized is dependent on the substrate and each pathway involves intricate steps catalysed by a series of enzymes. For example, external supplementation of NR is catalysed by the NRK enzymes into NMN that undergoes further conversion to yield NAD^+. The importance of these enzymes have been detailed in KO studies within skeletal muscle, demonstrating absence of NR metabolism into NAD^+, implying that specific enzymes are required for metabolism of external precursor supplements [96]. Similarly, the overall balance of NAD in its different forms are mediated by enzymes that directly catalyse its reduction, oxidation or phosphorylation, or released as by-products of metabolic processes – for example the hexose-6-phosphate dehydrogenase (H6PD) mediates the oxidation of glucose-6-phosphate during glycolysis and releases NADPH in the process to consequently modulate $NADP^+$/NADPH balance [379]. Fundamentally, *H6PD* deletion results in perturbation of glucocorticoid homeostasis – deletion and

resulting NADPH decrease has been demonstrated to switch HSD11β1 activity to oxidative, resulting in inactivation of glucocorticoids in a condition known as apparent cortisone reductase deficiency [380,381], causing hyperactivation of the HPA axis [379] and glucocorticoid insensitivity to impair glucose and lipid metabolism within the liver and adipose tissue [382,383]. In the skeletal muscle, *H6PD* deletion is ascribed to skeletal muscle myopathies – effects which are independent of the enzyme's role in glucocorticoid metabolism [384].

Given the nature of ADPR and PAR generation from the consumption of NAD^+, it is therefore evident that both molecules also exert far reaching and potentially indirect effects on pathways it might not necessarily exert influence over through alterations of NAD balance. The work in this final chapter seeks to culminate and bridge findings from the previous chapters. Specifically, we attempt to characterise impacts on PARP1, its mediated PARylation and GR expression within tissues of metabolic importance harvested from mice subjected to metabolic perturbations such as high fat diet and gene KO. These findings collectively serve to give a holistic understanding and potential future directions of studies pertaining to PARP1 and GR interactions in governing skeletal muscle as well as whole body metabolism.

5.2. Materials and Methods

5.2.1. Mouse models

C57/BL6J mouse models with age ranges from to 12 to 52 weeks used for work in this chapter were from the laboratory of Gareth Lavery at the Institute of Metabolism and Systems Research within the University of Birmingham, UK. Work was approved by and performed under British Home Office Guidance Act 1986. Mouse were housed in standard cages according to gender in 22°C and 12:12 hour light/dark cycle environments. Mice were fed *ad libitum* with standard chow.

5.2.1.1. NRK2 transgenic mice

Skeletal muscle specific NRK2 overexpressing mice, also known as NRK2 transgenic (NRK2.Tg), were generated by utilization of the Cre-Lox recombination system. NRK2 is encoded by the *NMRK2* gene. The transgenic *NMRK2* allele within NRK2.Tg mice is spliced into the ROSA26 locus on chromosome 6 within the mouse genome. Subsequently, a LoxP flanked stop codon is present to inhibit transcription of the transgene – however, the presence of the Cre recombinase results in deletion of the stop codon, allowing constitutive transcriptional activation and protein production of NRK2.

5.2.1.2. NRK2 knockout mice

NMRK2 KO mice obtained from the Jackson Laboratory in Maine, USA. These were generated using the Knockout Mouse Phenotyping Program (KOMP2) and the ZEN-UB1 Velocigene cassette. Homologous recombination was performed to insert the cassette into the coding exons of the *NMRK2* gene to impair its transcription. This construct was transfected into embryonic stem

cells which were injected into blastocysts and implanted into mice and bred. Genotyping was performed to corroborate heterozygous deletion of *NMRK2*.

5.2.1.3. HSD11β1 knockout mice

HSD11β1 KO mice were generated via the Cre-Lox recombination system using a vector targeting the catalytic domain of *HSD11β1* that was cloned into pBluescript SK(+) containing a thymidine kinase cassette. Constructs were electroporated into mouse embryonic stem cells, screened and expanded before injection into blastocysts and implanted into mice and bred. Genotyping was performed to corroborate deletion of *HSD11β1* [384].

5.2.1.4. H6PD knockout mice

H6PD KO mice were obtained from the European Conditional Mouse Mutagenesis Program in Munich, Germany. These mice were generated using a splice acceptor-β-galactosidase/neomycin phosphotransferase fusion gene-bovine growth hormone polyadenylation sequence (SA-βgeo-pA) reporter cassette system in tandem by a flippase recognition target sequence. These were subsequently subjected to Flp and Cre recombinase expression systems to generate Acta1-Cre transgenic mice to generate skeletal muscle specific *H6PD* KO mice. Genotyping was performed to corroborate successful deletion of *H6PD* [385].

5.2.2. Mouse model treatments

5.2.2.1. Oral NR supplementation

Mice were orally supplemented with NR via drinking water, to which nicotinamide riboside chloride was added at a concentration of 5 g/L and regularly replaced.

5.2.2.2. High fat diet

Mice were fed with a High fat chow diet that composed of 42% or 60% of total daily caloric intake for 16 weeks. Mice were periodically weighed for linear weight gained over the course of the diet.

5.2.3. Animal tissue collection

At the end of experimental timepoints, tissue dissection of muscle groups and metabolic importance was performed after animal sacrifice. Muscle groups included the soleus, quadriceps, hamstrings, TA and gastrocnemius, while other metabolically pertinent tissues included the heart, liver, kidney and lungs. Tissues collected were immediately snap frozen in liquid nitrogen and stored in -80 ºC until use.

5.2.4. Protein extraction from tissues

Protein extraction from tissues was performed via homogenisation using TissueLyser LT (Qiagen, Germany). The protocol is further detailed in *Section 2.4.1.2*. Briefly, 30 mg of tissue was cut and transferred to a microcentrifuge tube containing RIPA lysis buffer supplemented with 1x Pierce™ EDTA-free protease inhibitor cocktail and a TissueLyser LT stainless steel bead. Tissues were homogenized until no visible chunks were observed. Lysates were incubated on ice for 30 minutes and centrifuged at maximum speed for 30 minutes at 4ºC. The supernatant was transferred into a clean microcentrifuge tube and stored at -80ºC until use.

5.2.5. Protein analysis

Western blot analysis was conducted on protein lysates harvested in RIPA lysis buffer supplemented with 1x Pierce™ EDTA-free protease inhibitor cocktail. Proteins were loaded onto fixed percentage acrylamide gels run at

90V (stacking) and at 120V (resolving). Separated proteins were transferred to PVDF membranes and blocked with 5% BSA for 1 hour at room temperature, after which incubation with primary antibodies: PAR, PARP1, GR or GAPDH antibodies was performed overnight at 4°C. Anti-rabbit or mouse secondaries were used before visualisation using ECL detection method. Detailed background and methodologies are delineated in *Section 2.4.3*, and primary antibody details can be found in Appendix B.

5.2.5.1. Immunoprecipitation (IP)

Homogenized tissue lysates were subjected to IP assay. A detailed outline of this is presented in *Section 2.4.4*. Briefly, lysates were first pre-cleared in A/G magnetic beads. At least 1 mg of pre-cleared protein lysate per sample was incubated with 5 µl of PAR or IgG antibody controls overnight on rotation at 4°C to form immunocomplexes. This immunocomplex was then incubated with A/G magnetic beads for 20 minutes on rotation at room temperature for IP, washed in RIPA buffer and eluted by boiling at 95°C in 1x Laemmli sample buffer. Elutions were then subjected to western blot analysis as described.

5.3. Results

5.3.1. Validation of PAR immunoprecipitation assay

PAR and PARP1 has been well characterized to be expressed at low levels basally and induced only under stimuli conditions such as DNA damage. To that end, we performed an IP assay using PAR antibodies to identify basal PAR levels within the quadricep muscles of mice subjected to 42% and 60% high fat diets. We corroborated in whole cell tissue lysates that PAR levels exhibit low detection – subsequently, application of a IP assay for PAR in these lysates was successful and specific for PAR detection, supported by

an IgG negative control (Fig. 5.1). We also find that within these tissues, no significant change in PAR dynamics between chow and both high fat diets within the quadriceps.

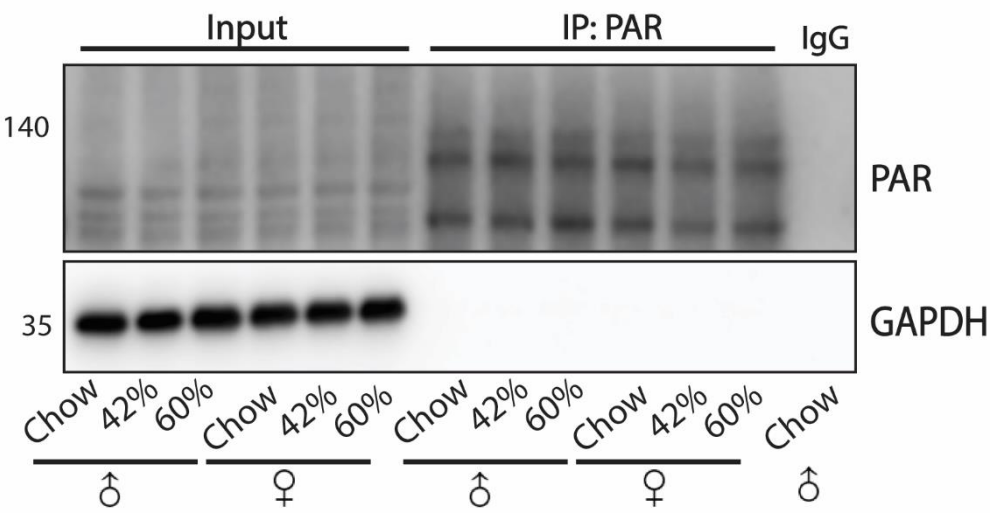

Figure 5.1. Characterisation of a PAR IP assay
Mice subjected to various percentage high fat diets were sacrificed and the quadricep muscles were dissected and homogenized into protein lysates. 1 mg of lysate input was used for the PAR IP assay, and all of the resulting elutions were used for protein analysis. *n=2*

5.3.2. NRK2.Tg mice exhibit increased levels of PAR

We next assessed PAR and PARP1 dynamics within the NRK2.Tg mice. The TA muscle group within WT and NRK2.Tg mice were dissected at 4 hour intervals for 24 hours that were housed in 12:12 hour light/dark cycle environments. Given NMRK2's role in NAD^+ biosynthesis, we postulated that its deletion would deplete NAD^+ bioavailability for PAR synthesis by PARP1. Consequently, IP assay revealed that PAR levels were slightly elevated in NRK2.Tg groups – furthermore, total PARP1 levels were seemingly elevated in transgenic groups during conditions of light and diminished in conditions of darkness, and this trend was also observed with regards to cleaved PARP1 levels (Fig. 5.2). This finding suggests mechanisms for circadian based cleavage of PARP1. In comparison with our earlier findings within the

quadricep muscle groups, these suggest that PAR might be differentially regulated amongst different tissue groups.

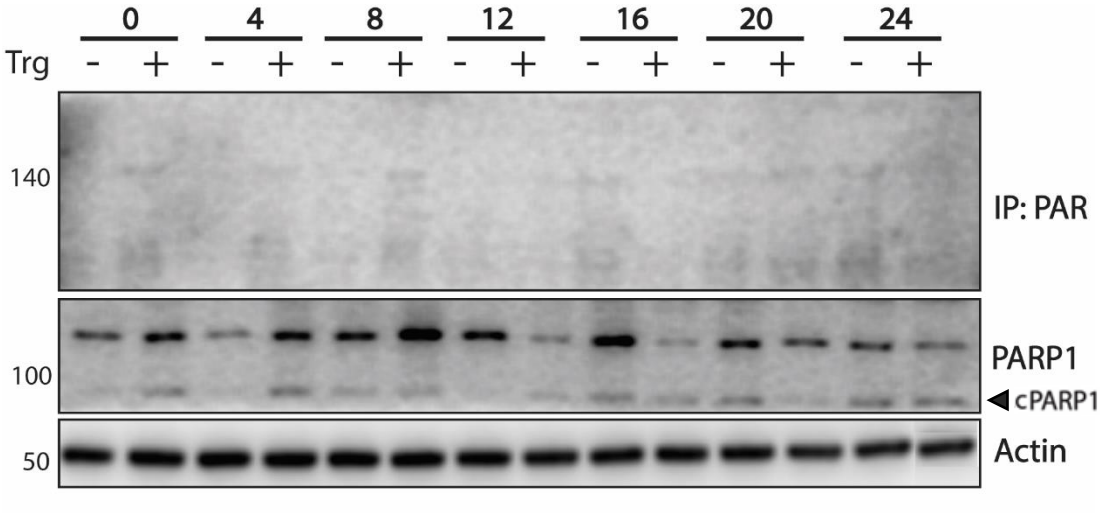

Figure 5.2. PAR IP in the TA muscle group of NRK2.Tg mice
NRK.Tg and WT mice were sacrificed every at 4 hour intervals and the TA muscle group was dissected and homogenized into protein lysates. 1 mg of lysate input was used for the PAR co-IP assay, and all of the resulting elutions were used for protein analysis. Abbreviations: cPARP1, cleaved PARP1; Trg, Transgenic
n=2

5.3.3. NMRK2 KO high fat diet challenged mice

To assess impacts of NMRK2 KO on high fat diet, muscle and metabolic tissues were dissected from WT and NMRK2 KO mice fed with 60% high fat diet and subjected to PAR IP assay. As with previous trends, we find that only the quadricep muscle groups exhibit detectable PAR following immunoprecipitation amongst the other tissues (Fig. 5.3). Furthermore, we identify WT high fat diet fed mice induced PAR accumulation that was diminished in NMRK2 KO mice fed with high fat diet. These suggest that diminished NAD^+ bioavailability by NRMK2 KO did exert impacts on PAR synthesis – furthermore, we also observed increased cleaved forms of PARP1 within the quadriceps and soleus muscle groups, as well as the heart and kidney – given that cleaved PARP1 forms serve as an indication of apoptotic

pathway activation [115,184,185], this finding gives merit that metabolic dysfunction as a repercussion of high fat diet driven apoptosis highly likely occurs through PARP1. We also find that GR expression within the tissues in both WT and NMRK2 KO mice remained relatively unchanged following high fat diet challenge, and similar to PAR trends, its expression is dynamic across tissues, with significant expression within the liver and minimal expression within the kidney. Notably, we also observed dynamic trends of PARP1 cleavage in association with GR expression profiles across tissues, where increased GR expression within the liver exhibited lower levels of cleaved PARP1, while low GR expression within the heart exhibited higher levels of cleaved PARP1. This indicates potential GR involvement in PARP1 cleavage during PARP1 driven apoptotic signalling events that like PAR, is dynamic across tissues.

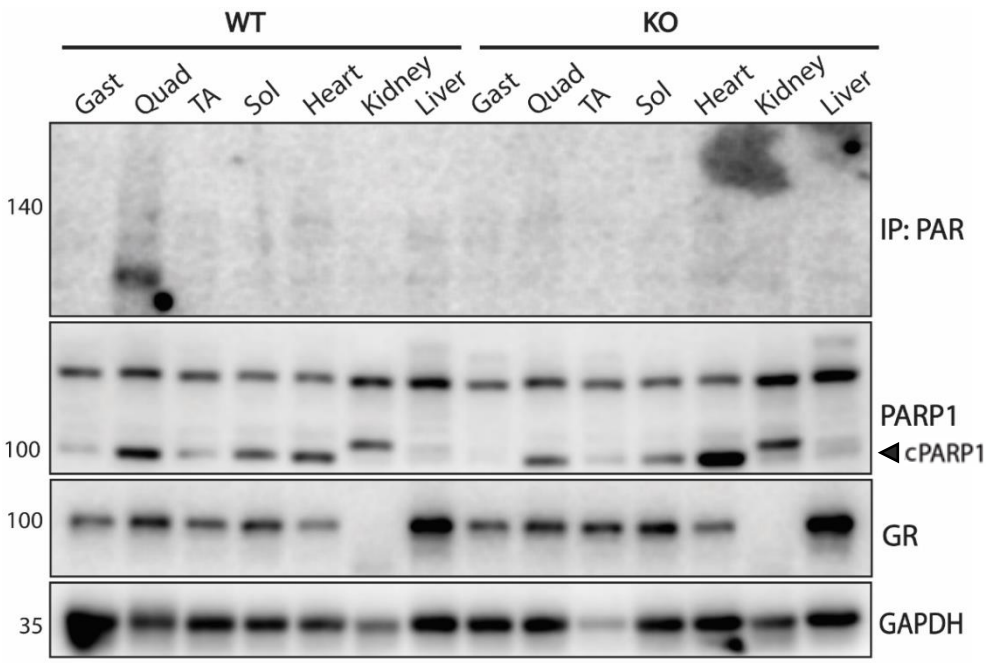

Figure 5.3. PAR levels are induced by high fat diet mice through NMRK2 dependent NAD^+ generation

WT and NMRK2 KO mice were subjected to high fat diet for 16 weeks were sacrificed and tissues were dissected and homogenized into protein lysates. 1 mg of lysate input was used for the PAR IP assay, and all of the resulting elutions were used for protein analysis. Abbreviations: cPARP1, cleaved PARP1; Gast, Gastrocnemius; Sol, Soleus; TA, Tibialis Anterior

n=2

5.3.4. PAR levels are potentially influenced by HSD11β1 mediated glucocorticoid regulation

We next sought to assess how glucocorticoid bioavailability can impact on PAR and PARP1 dynamics. Tissues from HSD11β1 KO mice were subjected to PAR IP. Remaining consistent with our previous observations, the quadricep muscles exhibited discernible PAR levels in WT mice that was diminished following HSD11β1 KO, suggesting a plausible relationship between glucocorticoids and PAR synthesis. Additionally, we find that PARP1 levels are seemingly elevated in HSD11β1 KO across tissues, while GR expression trends remained relatively unchanged between both groups (Fig. 5.4). These collectively support our findings from the previous result chapters pertaining to PARP1 and GR interactions as potential determinants of overall glucocorticoid transcriptional response and PARP1 does not directly impact GR expression. Given HSD11β1's roles in GR biology, it further suggests a relationship between GR and PARP1 and the PAR it deposits.

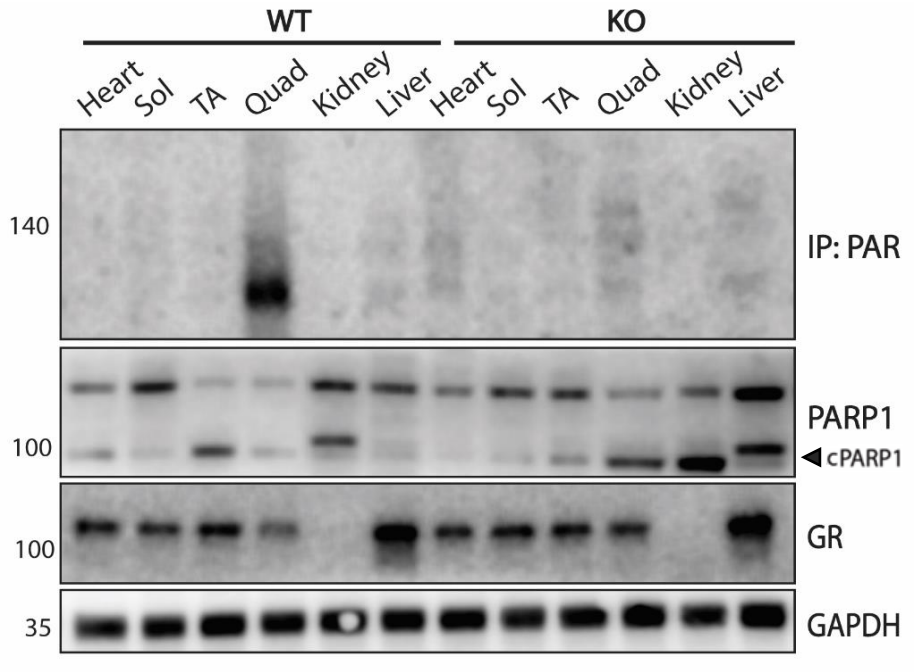

Figure 5.4. PAR levels are potentially influenced by HSD11β1 mediated control of glucocorticoid availability
52 week old WT and HSD11β1 KO mice were sacrificed and tissues were dissected and homogenized into protein lysates. 1 mg of lysate input was used for the PAR IP assay, and all of the resulting elutions were used for protein analysis. Abbreviations: cPARP1, cleaved PARP1; Quad, Quadriceps; Sol, Soleus; TA, Tibialis Anterior
n=2

5.3.5. H6PD has no discernible impact on PAR and GR dynamics

Given H6PD roles in glucocorticoid and NADP homeostasis, we finally sought to characterise the impacts of H6PD deletion on PAR and PARP1 dynamics. Tissues of H6PD KO mice fed with NR were dissected and subjected to PAR IP. Consequently, the differing PAR dynamics across different tissues presented challenges in identification of specific trends (Fig. 5.5). However, we observed that the deletion of H6PD increased levels of cleaved PARP1 within the heart, implying plausible roles for H6PD mediated regulation of PARP1 driven apoptosis, most likely due to increased NAD availability from NR supplementation. Like the deletion of HSD11β1, we did not observe significant impacts on overall GR expression within the tissues examined,

further implying that PARP1 plays potential roles in glucocorticoid response through the regulation of response genes rather than regulation of GR expression.

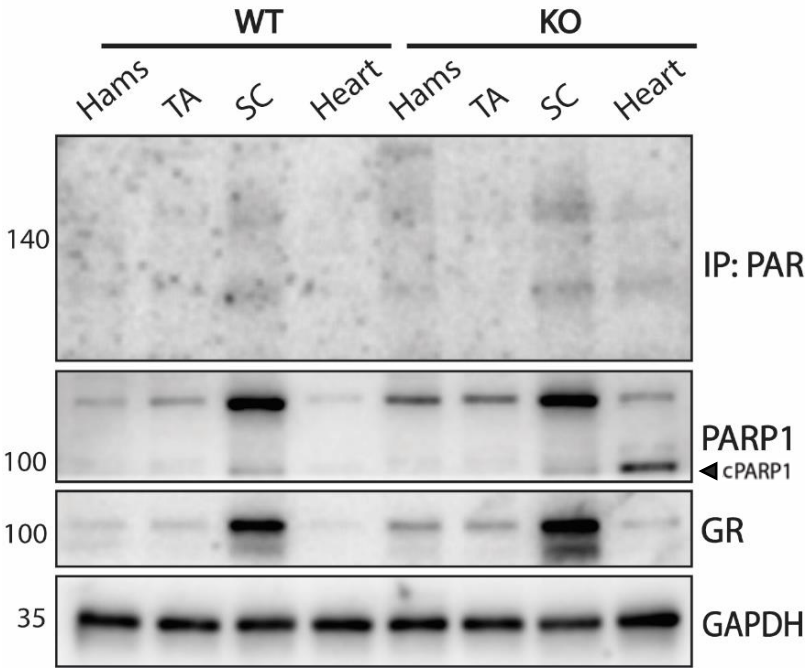

Figure 5.5. H6PD deletion does not impact PAR dynamics
52 week old WT and H6PD KO mice supplemented with NR were sacrificed and tissues were dissected and homogenized into protein lysates. 1 mg of lysate input was used for the PAR IP assay, and all of the resulting elutions were used for protein analysis. Abbreviations: cPARP1, cleaved PARP1; Hams, Hamstring; SC, Subcutaneous fat; TA, Tibialis Anterior
n=2

5.4. Discussion

Emerging evidence has been presented of PARP1 and GR interactions. While PARP1 has been linked to regulation of GR mediated transcriptional signalling events [365], the mechanisms behind this remain to be unravelled, particularly in an *in vivo* setting. Specifically, whether PARP1 regulates glucocorticoid levels and GR expression either through direct binding or via PARylating catalytic activity have yet to be defined. Unravelling these trends would further underscore PARP1 roles in metabolism. In addition with previous studies and the results presented in the previous chapter of this thesis, this would further understanding on the mechanistic impacts of glucocorticoids on regulation of

skeletal muscle metabolism and mass. Therefore, the focus of this chapter was to provide preliminary insights into the plasticity of PAR and PARP1 expression dynamics and how these impact GR expression in mice exposed to various metabolic stimuli changes and challenges.

NMRK2 is a fundamental NAD^+ generating enzyme through utilisation of external NAD^+ precursor supplementation. While studies have shown that it is dispensable for overall NAD^+ homeostasis in skeletal muscle [96], it does present roles for itself in auxiliary NAD^+ generation during conditions of metabolic stress [97]. Additionally, its upregulation has been ascribed to myopathy models [97] and response to muscle injury [386]. To this end, we first demonstrate within the TA muscle group of NRK2.Tg mice which have constitutive activation and expression of NMRK2 to exhibit fluctuations in PARP1 expression levels in a circadian dependent manner (Fig. 5.2). While roles for PARP1 in circadian biology have been identified in fed and fasted states, PARP1 expression levels remained minimally impacted in light/dark cycles – in contrast however, PAR accumulation was seemingly regulated by light/dark cycle, implying PARP1 PARylating activity to be circadian [233]. This observation presents potential impacts on NAD^+ balance and subsequent metabolic processes that utilizes NAD^+ throughout the day [387,388]. Furthermore, NRK2.Tg mice exhibited increased NAD^+ within the TA and soleus muscle groups during active hours [389]. To better understand how constitutively induced NMRK2 affects PARP1 mediated PAR accumulation, we utilized a verified and optimized PAR IP protocol that was performed within the quadricep muscle group of mice subjected to high fat diet (Fig. 5.1). Consequently, we show that the TA muscle group of NRK2.Tg mice exhibits

minimally detectable PAR – while it is well-known that PAR at basal levels are relatively low in the absence of stimuli such as DNA damage and feeding [172,233,354], this observation suggests that PAR levels are not only dynamic across subcellular components, but also tissues. To further corroborate this, we analysed tissues from mice subjected to NRMK2 deletion and high fat diet and demonstrate that PAR levels are dynamic and maximally detected within the quadricep muscle group (Fig. 5.3). While PARylation has been most certainly reported within other tissues, our findings in this context suggest, at least through observations within the quadricep muscle group, that NMRK2 deletion does reduce PARP1 mediated PAR accumulation during conditions of high fat diet. However, given that NMRK1 has been shown to compensate for NMRK2 reduction with regards to NAD^+ salvage [96], the degree of influence the NMRK kinases have on the extent of PARP1 mediated PAR accumulation remains to be ascertained.

Currently, the influence of PARP1 on glucocorticoid bioavailability and vice versa remains to be established. Assessment of tissues within HSD11β1 KO mice revealed within the quadricep muscle group, a reduction of PAR levels. Given that PARP1 and GR have mutual roles in inflammatory regulation [136,236,294], and evidence that PARP1 regulates activities of a plethora of nuclear receptors including GR within endocrine sensitive tissues [365,390], one could speculate a paradigm whereby PARP1 and GR activity act antagonistically of one another. However, this is unlikely to be the sole cause for these observations, as we found that GR expression levels were minimally impacted throughout the findings in this study in tissues with reduced PAR levels following gene knockout or metabolic perturbation. Additionally, while PARP1

mediated PARylating activity has been shown to influence proteasome mediated degradation of the substrates it targets [391,392], and GR being subjected to proteasomal targeting [393], delineating GR as a target of PARylation would be a fundamental first step towards testing this theory as well as its regulation. Exploring insights into PARP1 null mice subjected to cortisol supplementation would also be a viable strategy. Subsequently, the deletion of H6PD exhibited no significant impacts on PAR trends across tissues, although this could be well ascribed to challenges presented in the IP assay in the extrapolation of unstimulated PAR levels across tissues. Alternative approaches to supplement IP analysis of basal PAR levels such as autoradiography and *in vivo* reporter based systems which have been successfully applied [233,394], could prove useful in clarifying these trends. Given roles for H6PD in both NADP and glucocorticoid metabolism, our results suggest that potential direct PARP1 and GR interactions do not occur through H6PD – rather, our results show that H6PD deletion has potential impact on PARP1 driven apoptotic pathways within the heart through the observation of increased cleaved PARP1 (Fig. 5.5). In line with this, mechanistic studies of PARP inhibitors have shown that reduction of H6PD levels induces apoptosis and further sensitizes cancer cells to PARP inhibitor treatment [395]. Within the skeletal muscle, H6PD deletion also causes an upregulation NMRK1 to compensate for NAD^+ depletion [96], and this could possibly elevate PARP1 activity and activation of apoptotic pathways. Consequently, the overall consequence of NAD^+ bioavailability on the activities of other NAD^+ consuming enzymes including SIRT1 that antagonizes PARP1 activity warrants further investigation. Collectively, the preliminary findings in this chapter reveal that

PAR levels are dynamic across different tissues, and suggest that PARP1 plays roles in glucocorticoid response through modulation of GR target genes rather than directly regulating GR expression and glucocorticoid metabolism. These provide potential avenues and strategies worth exploring for understanding PARP1 roles in GR physiology.

Chapter 6

Final Discussion

Integrity of cellular homeostasis is dependent on the function of cellular signalling pathways. Post-translational modifications such as ADP-ribosylation and PARylation as presented throughout this thesis are critical events implicated in DNA damage repair and the control of differentiation programmes including myogenesis as well as subsequent metabolic function in paracrine tissues. Application of post-translational modifications often require substrates that are utilized by the catalysing enzyme. In this regard, PARP1 is a major NAD^+ consuming enzyme that catalyses the PARylation of target substrates, and NAD^+ itself is a critical biochemical molecule vital for cellular metabolism where it is utilized in REDOX reactions including glycolysis and the mitochondrial electron transport chain. Given the diversity of NAD^+ consuming enzymes, research has been invested into understanding not only how NAD^+ is synthesised but also how it is consumed by these enzymes [116,173,269,283].

The PARP family of enzymes have been extensively studied in this regard. Specifically, research into these enzymes is generally motivated by addressing 2 key research questions – first, the role of PARPs in whole body homeostasis and second, the extent of their activities on NAD^+ bioavailability and crosstalk with other NAD^+ consuming enzymes such as SIRTs and how this impacts overall metabolic integrity. The work in this thesis seeks to bridge and address these research questions to build up on existing knowledge on PARP1 within the skeletal muscle, an organ serving as a major determinant of overall metabolic integrity.

Previous work has delineated that PARP1 physical presence independent of its PARylating activity plays a greater role in the regulation of skeletal muscle myogenesis [176]. The work in this thesis corroborates the involvement of PARP1 mediated PARylating activity in myogenesis – first, we elucidate PARP1 PARylating activity, where the early-stage PAR accumulation that occurs within 24 hours of myogenic induction, is dynamic and metabolically sensitive. This observation is further supported by transiently elevated NAD levels during myogenesis, suggesting mechanisms to meet energy demands from both myogenesis and elevated PARP1 PARylating activity. The findings also support recent reports of PARP1 mediated PARylation in the transdifferentiation of fibroblasts into myoblasts [207]. Future work into unravelling substrates that are PARylated during the onset and progression of myogenesis would serve to appreciate the functional significance of these PAR dynamics.

Consistent with previous observations that PARP1 PARylating activity does not impact myotube development in C2C12s, we demonstrate that critical processes during myogenesis such as myotube fusion can still occur, but these events are reduced. This was further supported through observations that expression of the MRF Myogenin was reduced in myotubes subjected to PARP1 inhibition during myogenic induction. Depletion of NAD^+ for reduced PARP1 mediated PAR accumulation consequently exerted the greatest impact on myotube fusion events – however, this could be also attributed to the repercussions of broad NAD^+ depletion rather than impacts on PARylation in myogenesis.

Subsequently, we find via proteomic and transcriptomic analysis that modulation of PARP1 PARylating activity during the onset of myogenesis induces changes in the expression of genes and proteins associated with skeletal muscle function in the developed myotube – these include glucose metabolism, muscle contraction and structural organization. Further work demonstrated that the overexpression of PARP1 hinders myogenesis altogether [176,251] – complementary to these, our work further implies that PARP1 mediated PARylating activity is dispensable for successful myogenesis but rather exerts impact on developed myotube phenotype. This is further evident in two contexts: first, *in vivo* PARP1 deletion alone is not embryonically lethal [131] and second, adult PARP1 null mice are healthy under basal conditions, and have increased metabolic capacities, energy expenditure and exercise performance [131,132].

Consistent with our observations of reduced PARP1 in differentiated myotubes, studies have ascribed this phenomenon to be required for oxidative stress resistance [251] and also, driving the MyoD mediated activation of the myogenic transcriptional programme [176]. PARP1 reduction is also implicated in the differentiation programmes of other tissues such as adipogenesis and osteoclastogenesis [206,209]. However, mice with PARP1 deletion are more sensitive to ionizing radiation [396], highlighting the multifaceted role PARP1 as an important enzyme in cellular integrity. Hitherto, the mechanisms underpinning degradation of PARP1 throughout myogenesis remain to be elucidated. However, emerging studies have documented PARP1 degradation being mediated by the ubiquitin-proteasome system to facilitate biological processes including cardiac remodelling [397], ameliorating oxidative stress in

umbilical cells [398] and also, for DNA damage response [354]. E3 ligase enzymes, which catalyze the final transfer of ubiquitin molecules onto target substrates, exist in skeletal muscle, and these include MuRF1 and MAFbx which are associated with muscle atrophy [329,331]. Additionally, absence of proteasomal activity impairs skeletal muscle differentiation of C2C12 myoblasts [399]. This collectively gives merit for PARP1 being degraded in this manner during myogenesis (Fig. 6.1A). The inhibition of the proteasome in undifferentiating C2C12 myoblasts causes accumulation of PARP1 (Fig. 6.1B), and conversely, proteasome inhibition at various myogenesis timepoints induced a dedifferentiation based on lower myogenin expression levels, corroborating previous observations [399] (Fig. 6.1C). However, given that PARP1 was capable of undergoing degradation, it could be speculated that serum levels which differ between proliferating and differentiating paradigms could possibly act as a 'switch' for PARP1-targetted ubiquitination, a phenomenon that has been recently presented for PARP2 [400]. Put together, mechanistic investigation into pathways of PARP1 degradation in maintenance of skeletal muscle mass and myogenesis are avenues warranting further study.

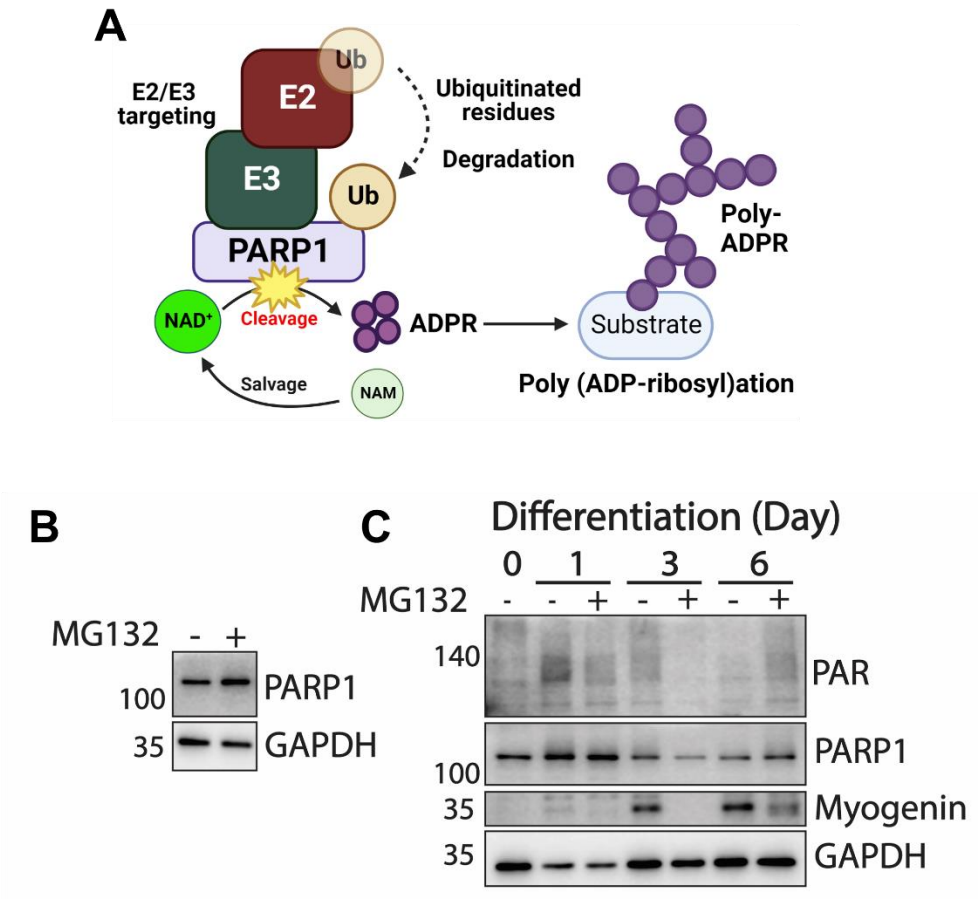

Figure 6.1. PARP1 is ubiquitinated in undifferentiating but not differentiating myoblasts
Understanding mechanisms of PARP1 degradation within C2C12 myoblasts **(A)** Schematic paradigm of the ubiquitination of PARP1 for subsequent proteasome degradation **(B)** Western blot analysis of undifferentiated C2C12s treated for 2 hours with the proteasome inhibitor compound MG132 and **(C)** differentiating C2C12s treated with MG132 for 6 hours at various days of myogenesis
C2C12s n=3

PARP1 has roles in poor ageing, and one of the hallmarks includes age-associated skeletal muscle decline exacerbated by sarcopenia. In contrast, chronic glucocorticoid exposure in skeletal muscle also induces conditions of metabolic dysfunction, including myopathies [326,328–331]. Information on PARP1 and GR interactions are relatively elusive – however, elevated circulatory cortisol levels are observed in mice with PARP1 deletion [364] and further *in vitro* work reveals PARP1 playing regulatory roles in GR mediated transcriptional signalling [365]. Given that both PARP1 and GR also play mutual roles in the inflammatory response, this prompted us to investigate a basis for PARP1-GR

interactions in skeletal muscle. We established that *PARP1*, at a transcriptional level, is recruited to GREs in a similar fashion to canonical initiation of GR transcriptional signalling following dexamethasone treatment during onset of myogenesis. Furthermore, dexamethasone treatment in combination with PARP1 inhibition during early-onset myogenesis revealed a rescue of myogenin expression in differentiated myotubes, supporting observations that dexamethasone application enhances subsequent myogenesis [325–327].

Further RNAseq analysis of undifferentiated *siPARP1* C2C12s subjected to dexamethasone treatment was sufficient to induce transcriptomic shifts in the myoblast transcriptome, of which, canonical genes of GR signalling remained unchanged. Through further utilization of gene set enrichment analysis, the work within this thesis also revealed for the first time that the differentially expressed gene sets underpinning the aforementioned transcriptome shifts were enriched in processes associated with mediators of glucocorticoid response and skeletal muscle function, and these were further aligned to a plethora of processes in skeletal muscle physiology that spanned across molecular and biological processes as well as muscle architecture and structure. An alignment with muscular dystrophy phenotypes was also observed with these differentially expressed gene sets, and given how chronic glucocorticoid exposure is associated with these dysfunctions, our results collectively show for the first time that within the skeletal muscle, PARP1 and its PARylating activity does influence the outcome and effects of glucocorticoid exposure through the regulation of downstream response genes of GR signalling in pathways of muscular atrophy. This supports reported work for

PARP1 involvement in the regulation of glucocorticoid responses within Gonadotropin-releasing hormone receptors [378], as well as muscular myopathy [208].

A key limitation within this thesis is that the work was mostly carried out in *in vitro* systems. While *in vitro* work is fundamental in ascertaining specific cell-type responses and pathways, as well as the ease of application in research methodologies, the aim of the work presented in this thesis was to further knowledge on human health and disease, as well as improving and pioneering treatment strategies and outcomes. In this regard, we attempted to circumvent and supplement our *in vitro* findings through tissues kindly donated by the laboratory of Gareth Lavery at the University of Birmingham. Our preliminary findings from these tissues corroborated our findings that PARP1 and its mediated PARylation was indeed dynamic across different tissues. Consequently, we also demonstrate that basal PARylation was minimally detected which required use of IP assays – in agreement with previous studies which reported higher PAR detection within larger muscle groups [106,131], we demonstrate that our IP PAR assay was specific. However, this itself still presented challenges in ascertaining PAR dynamics in tissues that displayed low levels of PAR, which were observed in smaller muscle groups including the TA and the soleus during our study. It is therefore vital to gain a holistic view over different muscle groups to strengthen findings presented throughout this thesis. However, the rapid turnover and tight regulation of PAR physiology *in vivo* presents further complexities and this has been evidently present [401]. Given that measurement of PAR levels are a more accurate representation of PARP1 activity rather than expression levels of the enzyme alone, *in vivo*

approaches have been developed to provide clarity in PAR dynamics [233,394]. Utilization of mouse models expressing such systems for PAR tracking and detection would prove useful in strengthening translatability of findings within the work in this thesis and appreciate the roles of PARP1 PARylating activity within the skeletal muscle.

Put together, the work in this thesis is summarized in Figure 6.2. Through employment of proteomic, transcriptomic and biochemical approaches, we demonstrate novel roles for PARP1 mediated PARylation in skeletal muscle, ascertaining that PARylation exerts less influence over the trajectory of myogenesis, but rather, greater influence on overall developed myotube phenotype, one of which includes glucocorticoid response. This suggests any potential role for PARP modulation as a tool for sustaining muscle function must be carefully considered in relation to the ability of the tissue to repair and replace muscle fibres.

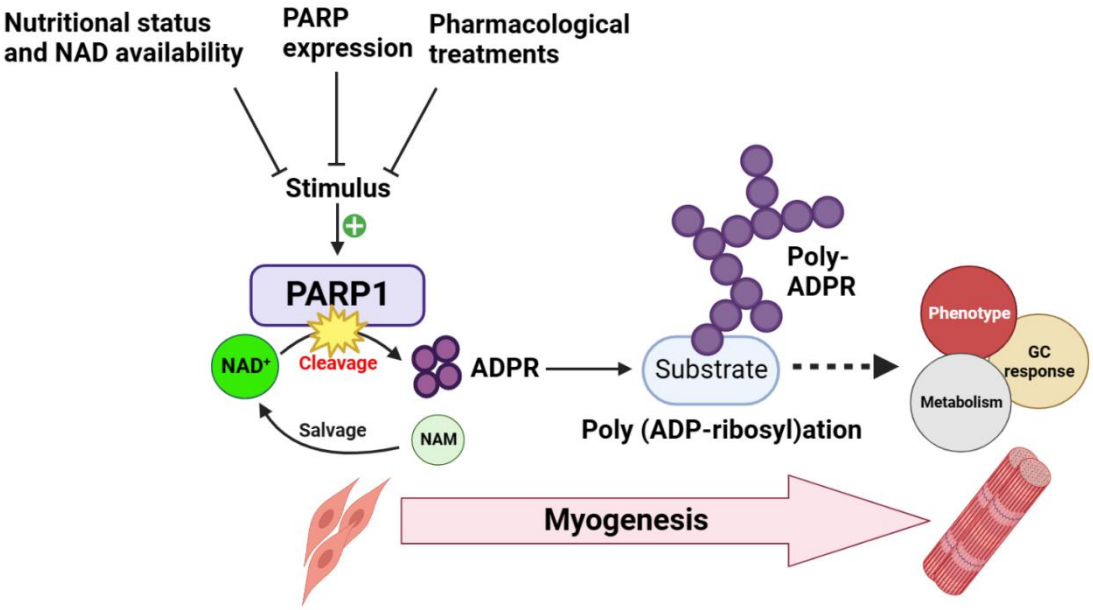

Figure 6.2. Dynamics of PARP1 and PARylation in skeletal muscle physiology
The work and models used within this thesis identified that PARP1 driven PARylation of substrates is increased during the onset of skeletal muscle myogenesis. Modulation strategies used to diminish this PAR accumulation revealed greater impacts on subsequently developed myotube phenotype rather than myogenic progression itself. Phenotypic characteristics that were affected included genes and proteins enriched to processes including glucocorticoid response, metabolic and biological processes such as glucose metabolism and calcium signalling. These genes and proteins were also aligned to human muscular dysfunction phenotypes, suggesting that PARP1 mediated PARylation during myogenesis has downstream impacts on developed skeletal muscle health and physiology.

Appendix

Appendix A – qPCR gene probes and primer pairs

Gene	qPCR chemistry	Probe number (TaqMan) / Primer sequence (SYBR)
NAMPT	TaqMan	Mm00451938_m1
PARG	SYBR	Forward: GTGCCAGTTTCGATCCGTAGA Reverse: GGCCAGCATCGTGTAGATGA
PARP1	SYBR	Forward: CCTGAACAACGCAGACAGC Reverse: CGTTGTGCGTGGTAGCATGA
PARP2	SYBR	Forward: GGAAGGCGAGTGCTAAATGAA Reverse: GGAAGGCGAGTGCTAAATGAA
SIRT1	SYBR	Forward: GGCTACCGAGACAACCTCCTG Reverse: AGTCCAGTCACTAGAGCTGGCG

Appendix B – Primary antibodies

Antibody	Source	Catalogue number	Host	Dilution
β-actin	CST	4967	Rabbit	1:1000
GAPDH	Abcam	ab9485	Rabbit	1:1000
GR	CST	3660	Rabbit	1:1000
MyoD	Santa Cruz Biotechnology	sc-377460	Mouse	1:1000
Myogenin	Abcam	ab1835	Mouse	1:5000
PAR	Merck-Millipore	MABE1031	Rabbit	1:1000
PARP1	Actif Motif	39559	Rabbit	1:1000
TNNT1	Abcam	ab155028	Rabbit	1:5000
α-tubulin	Santa Cruz Biotechnology	sc-5286	Mouse	1:1000

Appendix C – Associated Manuscript

CDDpress

www.nature.com/cddiscovery

ARTICLE OPEN

Check for updates

PARP1 mediated PARylation contributes to myogenic progression and glucocorticoid transcriptional response

Arnold Tan[1], Awais Z. Younis[1], Alexander Evans[1], Jade V. Creighton[1], Clare Coveny[2], David J. Boocock[2], Craig Sale[3], Gareth G. Lavery[1], Amanda S. Coutts[1] and Craig L. Doig[1]✉

© The Author(s) 2023

The ADP-ribosyltransferase, PARP1 enzymatically generates and applies the post-translational modification, ADP-Ribose (ADPR). PARP1 roles in genome maintenance are well described, but recent work highlights roles in many fundamental processes including cellular identity and energy homeostasis. Herein, we show in both mouse and human skeletal muscle cells that PARP1-mediated PARylation is a regulator of the myogenic program and the muscle transcriptional response to steroid hormones. Chemical PARP1 modulation impacts the expression of major myocellular proteins, including troponins, key in dictating muscle contractile force. Whilst PARP1 in absence of DNA damage is often assumed to be basally inactive, we show PARylation to be acutely sensitive to extracellular glucose concentrations and the steroid hormone class, glucocorticoids which exert considerable authority over muscle tissue mass. Specifically, we find during myogenesis, a transient and significant rise in PAR. This early-stage differentiation event, if blocked with PARP1 inhibition, reduced the abundance of important muscle proteins in the fully differentiated myotubes. This suggests that PAR targets during early-stage differentiation are central to the proper development of the muscle contractile unit. We also show that reduced PARP1 in myoblasts impacts a variety of metabolic pathways in line with the recorded actions of glucocorticoids. Currently, as both regulators of myogenesis and muscle mass loss, glucocorticoids represent a clinical conundrum. Our work goes on to identify that PARP1 influences transcriptional activation by glucocorticoids of a subset of genes critical to human skeletal muscle pathology. These genes may therefore signify a regulatory battery of targets through which selective glucocorticoid modulation could be achieved. Collectively, our data provide clear links between PARP1-mediated PARylation and skeletal muscle homeostatic mechanisms crucial to tissue mass maintenance and endocrine response.

Cell Death Discovery (2023)9:133 ; https://doi.org/10.1038/s41420-023-01420-2

INTRODUCTION

PARP1 irreversibly cleaves NAD^+, producing nicotinamide for re-salvage and monomeric ADP-Ribose (ADPR) units. ADPR functions as a signaling moiety through site-specific attachment to target molecules, altering their biological activity. ADPR units can be mono- or poly-elongated: the latter produces poly-ADPR (PAR) chains, in a process termed PARylation [1]. To date, PARP1, alongside PARP2 and the tankyrases, are capable of performing PARylation. Recent studies of PARylation have revealed roles ancillary to the well-characterized genome repair. For example, PARP1 activity has been shown to govern fundamental processes including adipogenesis, RNA stability, and transdifferentiation [2–6].

The conserved and constitutive nature of PARP1 and PARylation underlies the variety of documented actions. Emerging studies implicate PARP1 within skeletal muscle metabolism and myogenesis [4, 7–9]. For example, in myogenic progression, down-regulation of PARP1 in fully formed myotubes is required for oxidative stress resistance [9]. More recent work has demonstrated *PARP1* binding to regulatory regions of the *MYOD* target muscle genes *p57* and *myogenin* [4]. These works demonstrate PARP1 also exerts myogenic influence independent of its PARylating activity, however, the impacts of PARylation in skeletal muscle remain poorly characterized. Despite this incomplete understanding, PARP inhibitors have been suggested for alleviation of inflammation in non-communicable chronic diseases including myopathy.

Herein, we used transcriptomic and proteomic analyses to explore PARP1-mediated PARylation during myogenic progression. We show PARP1 and the PAR it applies during myogenesis are dynamic, and sensitive to both hormonal status and metabolic demand. Early-stage muscle cell differentiation sees a transient rise in PARylation that holds influence over the fully developed myotube. This indicates that the molecular targets of PARP1 during early-stage differentiation are pivotal in determining the functional quality of the muscle fiber. We also demonstrate that PARP1 holds impacts over the skeletal muscle transcriptional response to glucocorticoids, steroid hormones with governance over muscle protein synthesis and metabolic rate. We identify a subset of genes that are critical to muscle mass and contractile function that are co-regulated by PARP1. These results reveal whilst PARP1 inhibition mediates beneficial effects in fully developed muscle tissue, the potential for negative impacts exists for muscle differentiation and steroid hormone activation. Therefore, the use of clinically available PARP inhibition should be

[1]School of Science and Technology, Department of Biosciences, Nottingham Trent University, Nottingham NG11 8NS, UK. [2]John van Geest Cancer Research Centre, Nottingham Trent University, Nottingham NG11 8NS, UK. [3]Institute of Sport, Manchester Metropolitan University, Manchester M1 7EL, UK. ✉email: craig.doig@ntu.ac.uk

Received: 11 November 2022 Revised: 22 March 2023 Accepted: 29 March 2023
Published online: 22 April 2023

Official journal of CDDpress

SPRINGER NATURE
CDDpress

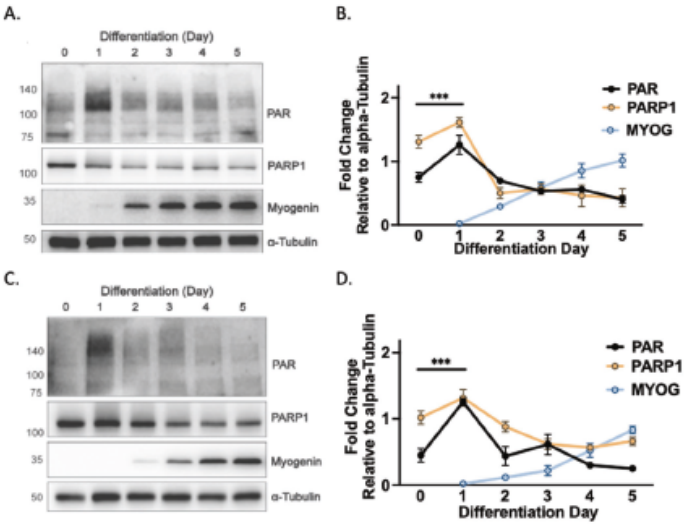

Fig. 1 PARP1 and PARylation are dynamic during myogenesis. A Western immunoblotting of differentiating C2C12 myoblasts probed for PARylation (PAR), PARP1, Myogenin, and Alpha-Tubulin (representative of $n = 4$). **B** Quantification of MYOG, PAR, and PARP1 present over differentiation. Each bar represents means ± S.D ($n = 4$) ***$P < 0.001$. **C** Western immunoblotting of differentiating LHCN-M2 human myoblasts probed for MYOG, PAR, PARP1, Myogenin, and Alpha-Tubulin (representative of $n = 4$). **D** Quantification of PAR and PARP1 present over differentiation. Each bar represents means ± S.D ($n = 4$) ***$P < 0.001$.

subject to greater consideration for impacts on the whole-body muscle mass.

RESULTS

PARP1-mediated PARylation is dynamic during skeletal muscle differentiation

Molecular assessment of PARP1 and PAR during myogenesis remains limited. Given PARP1 non-enzymatically regulates the myogenic regulatory factor *MYOD* [4], we hypothesized that enzymatically driven PARylation also contributes to myogenic transition. To address this, C2C12 myoblasts were differentiated and interrogated for PAR and PARP1 levels on each day of differentiation. We report that levels of PAR were dynamic during myoblast alignment and fusion, reaching peak within day 1 and nadir by day 5 of differentiation (Fig. 1A, B). Identical dynamic regulation of PAR and PARP1 abundance was recorded in the human muscle cell line LHCN-M2 (Fig. 1C, D). Total levels of myogenin also increased, demonstrating the establishment of myogenic commitment in these myoblasts (Fig. 1A, C). Together, these data indicate, at least in mammals, a conserved process of PAR regulation driven by PARP1 that is associated with the initiation of the myogenic program.

PARylation in skeletal muscle myogenesis is metabolically sensitive

Conventionally, PARP1 is regarded as inactive in the absence of genotoxic stress. However, several studies have demonstrated that both PARP1 and PARylation are fundamental to a variety of biological processes [1]. As such, we explored the response of PARP1 and PAR to conditions of NAD^+ excess or deficit during myogenesis. The NAD^+ precursor nicotinamide riboside (NR) is bioavailable to human skeletal muscle and can directly generate NAD^+ [10]. However, we find that NR supplementation of myoblasts during differentiation induction did not alter the levels of day 1 PAR accumulation (Fig. 2A, B). In contrast, we find NAD^+ depletion through specific NAMPT inhibition with FK866 reduced day 1 PAR levels and myogenin expression, supporting an association of the enzymatic product of PARP1 with myogenic progression (Fig. 2C, D). We also found PAR during myogenesis to be regulated by the external cellular environment, with a dose-dependent increase in PAR in response to glucose deprivation (Fig. 2G, H) and is sensitive to steroid hormone levels following exposure to the glucocorticoid receptor (GR) agonist dexamethasone (Fig. 2E, F). Collectively, these data show that PARP1-mediated PARylation is active in differentiating myoblasts and exerts plasticity. Moreover, we find a synergistic interaction of both the inhibition of PARP1 with the inhibitor PJ34 and dexamethasone treatment during differentiation induction upon subsequent PAR abundance (Fig. 2I, J). Together, these data show PARP1 and PAR in skeletal muscle to be basally detected and responsive to the changing cellular environment. This implies PAR in skeletal muscle is a signaling motif with potential roles to play in the variety of pathways governing muscle homeostasis.

Modulation of PARylation during early-stage myogenesis

To modulate PAR generation, we applied the broad-spectrum PARP inhibitor PJ34 during differentiation induction and demonstrate significant reduction of early-stage PAR accumulation in both murine and human skeletal muscle cells (Fig. 3A–D). PJ34 treatment also significantly increased cellular NAD^+ (Supplementary Fig. 1A). To further investigate if the transient day 1 PAR accumulation is a determinant of developed myotube functional quality, we also assessed levels of Troponin T1 (TNNT1), a subunit of the sarcomere. This was reduced in myotubes exposed to PJ34 during early-stage differentiation and suggests PARylation is required for proper thin filament assembly (Fig. 3A, C). These PAR trends were also replicated using Rucaparib (Supplementary Fig. 2A, B). Inhibition of PARP1 with PJ34 is also shown by immunofluorescence, with the day 1 PAR accumulation impaired in the PJ34-treated differentiating myoblasts (Fig. 3E). To identify the major transcriptional processes governed by PARP1 inhibition,

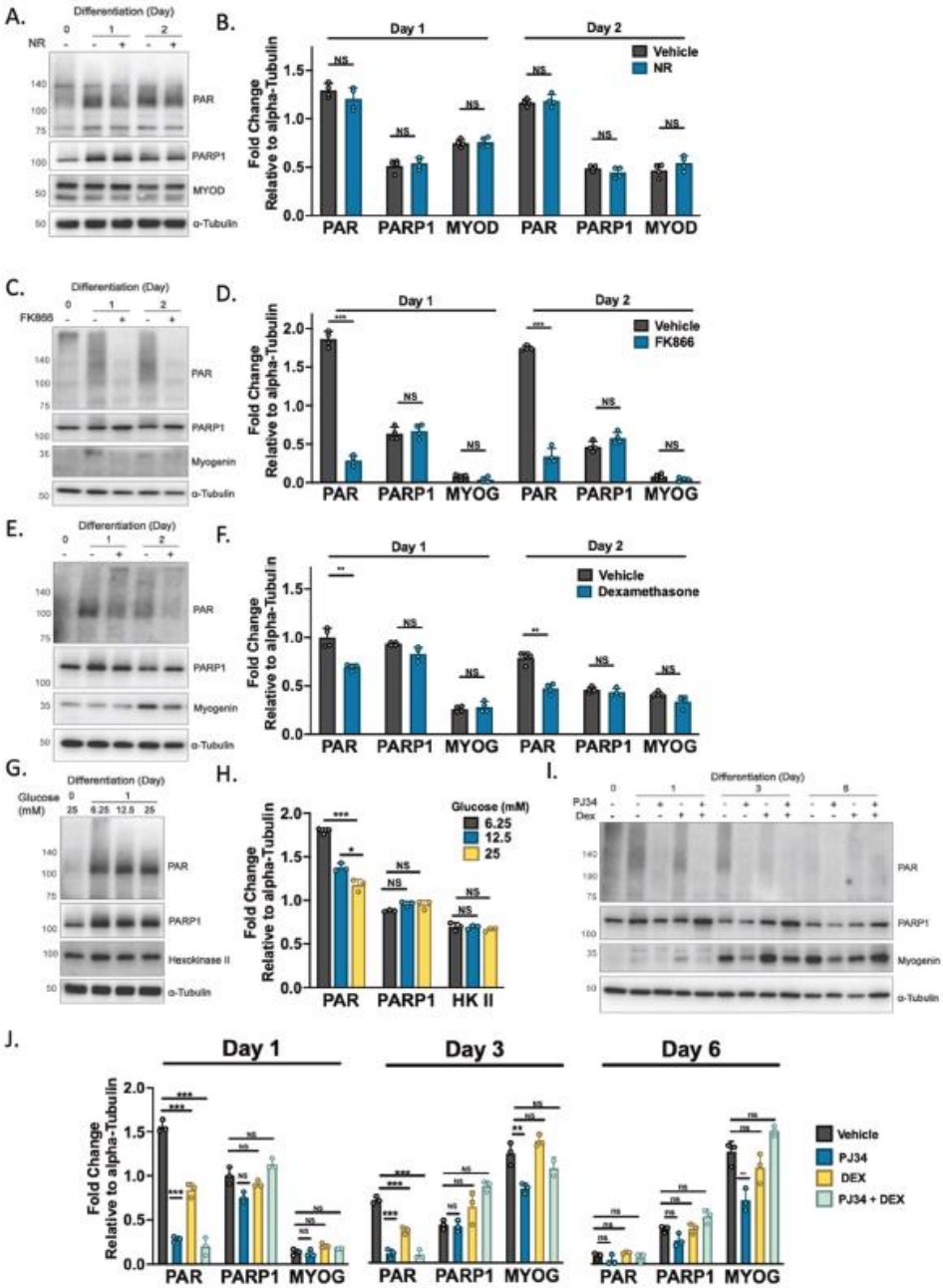

we conducted RNAseq on PJ34 treated early-stage differentiating C2C12 myoblasts compared to vehicle controls (Fig. 3F). Gene Ontology analysis revealed suppression of pathways regulating assembly of the skeletal muscle myofibrils and detection of muscle stretch, a table of differentially expressed genes is provided (Supplementary Table S1). Additionally, in line with documented actions of PARP1 in transcriptional regulation [11] suppression of the phosphorylation of RNA polymerase II suggests

Fig. 2 PARP1 and PARylation in differentiating myoblasts are sensitive to changes in metabolism. A, B Western immunoblotting of differentiating myoblasts differentiated in ±nicotinamide riboside (NR) (0.5 mM) (representative of $n = 4$) probed for PAR, PARP1, MYOD, and Alpha-Tubulin. **C, D** Western immunoblotting of differentiating myoblasts differentiated in ± NAMPT specific inhibitor FK866 (50 nM) (representative of $n = 4$) probed for PAR, PARP1, Myogenin, and Alpha-Tubulin, $^{***}P < 0.001$. **E, F** Western immunoblotting of differentiating myoblasts differentiated in ±dexamethasone (1 μM) probed for PAR, PARP1, MYOD and Alpha-Tubulin (representative of $n = 4$, $^{**}P < 0.01$). **G, H** C2C12 myoblasts differentiated in differentiation medium containing different glucose concentrations before lysate harvest and immunoblotted for PAR, PARP1, Hexokinase II, and Alpha-Tubulin (representative of $n = 3$, $^{*}P < 0.05$). **I, J** Western immunoblotting of differentiating myoblasts differentiated in ±dexamethasone (1 μM), PARP inhibitor PJ34 (10 μM) or both in combination (representative of $n = 3$, $^{*}P < 0.05$, $^{**}P < 0.01$).

global shifts in transcriptional rate as a result of reduced PARP1 activity. Collectively, these data confirm the dynamic nature of PAR in skeletal muscle and a background of transcriptional coordination during early-stage differentiation.

Differentiating skeletal muscle and impacts of PARP1 upon the proteome

To gain insight into proteomic changes during differentiation regulated by PARP1-generated PAR, we subjected lysates of differentiating myoblasts treated with PJ34 (Fig. 3A) to unbiased SWATH-MS analysis. These recovered peptides aligned with 2911 identified proteins expressed from day 0 to day 6 of differentiation ±PJ34 (Fig. 4A). Examination of PJ34 treated day 1 differentiating lysates revealed differentially abundant proteins associated with documented roles of PARP1 in chromosome biology, and down-regulated proteins (>1.5 fold change) included CEBPZ (−2.70 fold change, Pvalue 0.04), CBX6 (−1.59 fold change Pvalue 0.05), STIM2 (−2.37 fold change, Pvalue 0.004) and CDN1B (−2.09 fold change Pvalue 0.03) (Fig. 4B). These data describe muscle PARP1 as dictating chromatin features, consistent with regulation of transcriptional programs across tissues [12]. Subsequently, down-regulated proteins from PJ34 treated day 3 differentiating lysates shifted towards association with skeletal muscle functions including MYL4 (−1.68 fold change Pvalue 0.10), and TNNI1 (−1.60 fold change Pvalue 0.11) (Fig. 4B). Proteins fundamental to skeletal muscle phenotype and contractility also shift in PJ34 treated day 5 differentiating lysates, including TNNT1 (−3.35 fold change, Pvalue 0.05), INSR (-4.36 fold change *P* value 0.04). A tabular list of differentially abundant proteins is provided (Supplementary Table S2).

Proper myoblast differentiation requires PARP1 activity

PJ34 is a broad PARP inhibitor that can target other members of the PARP family of enzymes, including the ADP-ribosylating tankyrases [13]. Given this, we sought to explore the observed proteomic changes and challenge the extent of day 1 PARP1 mediated PARylation over myogenesis. To do this, we also treated C2C12 myoblasts with the highly specific PARP1 inhibitor BYK204165 [14] during differentiation induction. We assessed levels of PAR as well as subsequent impacts on differentiation trajectory and observed ablation in total PAR protein levels in BYK204165 treated groups (Supplementary Fig. S1B). Myoblasts were treated on day 1 with BYK204165 for 24 h before washout and subsequently left to differentiate for 6 days with media changed every 48 h (Fig. 5A). Lysates were harvested and subjected to unbiased SWATH-MS analysis. This detected 2921 proteins, of which 180 were significantly differentially expressed in BYK204165-treated differentiating lysates (Fig. 5B and Supplementary Table S3). Of the downregulated proteins, these again included muscle contractile proteins including TNNT1 (−1.31 fold change), MYL4 (−1.86 fold change), TNNT3 (−1.53 fold change), MYL1 (−1.81 fold change) and MYH3 (−1.83 fold change) (Fig. 5C). Pathway overrepresentation analysis of these samples reveals these proteins associated to biological processes governing actin binding, cytoskeletal protein binding, cytoskeletal motor binding, troponin binding, actin filament binding and structural constituent of muscle (Supplementary Fig. S1C). These observations reflect our SWATH-MS analysis of PJ34-treated differentiating lysates (Fig. 4B) and highlight the importance of PARP1-mediated PARylation events that take place on day 1 of differentiation. To better understand how PARylation during early-stage differentiation influences the fully differentiated myotube, we employed Giemsa-Jenner staining of C2C12 myoblasts treated with either PJ34 or BYK204165 during differentiation induction. Cells were fixed on day 6 of differentiation and subjected to an unbiased method of quantification of myogenic differentiation [15]. This analysis revealed subsequently reduced fusion index of myotubes treated with PJ34 (20.15 ± 6.41 S.D) and BYK204165 (24.94 ± 3.21 S.D) (Fig. 5D). These suggest PAR elevation at early-stage differentiation impacts myocyte fusion and PARylation targets during early-stage differentiation are critical to the proper formation of the muscle sarcomere, impacting the overall number of contractile units per fiber.

Reduction of PARP1 impacts the myoblast transcriptome

The muscle differentiation program is transcriptionally regulated by myogenic regulatory factors, some of which have been shown to be influenced by PARP1 [4]. However, the broader elements of PARP1 roles in the muscle transcriptome remain elusive. To provide insight, we conducted RNAseq on undifferentiated C2C12 myoblasts transfected with siRNA-mediated knockdown of *PARP1* (*siPARP1*) (Fig. 6A–C). As PARP1 is a major NAD^+ consuming enzyme, accounting for up to 90% of cellular PARylation [16], we examined by qPCR, impacts of *siPARP1* on the expression of *PARP2*, *PARG*, *NAMPT*, and *SIRT1*, genes involved in NAD^+ dependent homeostasis (Fig. 6D). No significant changes were observed in the expression of these genes. Additionally, RNAseq of *siPARP1* myoblasts showed the glucocorticoid binding partner *NR3C2* gene which codes for the mineralocorticoid receptor (MR), as being significantly downregulated (Fig. 6E and Supplementary Table S4). Gene Set Enrichment Analysis of the *siPARP1* differentially expressed genes revealed that consistent with PARP1 established DNA damage repair response functions, the double-strand break repair process was the major deregulated process (Fig. 6E, F). Also suppressed, were pathways and metabolic processes regulating fundamental metabolism including pantothenate metabolism, palmitoylation, and mitochondrial import. Gene Set Enrichment Analysis also reported shifts in major pathways of hypoxia regulation (Normalized Enrichment Score (NES) 1.5, Pvalue 0.001), myogenesis (NES 1.3, *P* value 0.052), and TNF-α via NF-κB (NES −1.3, *P* value 0.039). *PARP1* regulation of hypoxia, as is interaction with the *NF-κB* immune signaling cascades, has been documented [17, 18]. Moreover, these features are reported as being regulated by glucocorticoid signaling [19].

Reduced PARP1 impacts the glucocorticoid transcriptional response

Finally, as we show PARylation as being a glucocorticoid-sensitive post-translational modification (Fig. 2D, E), as well as *NR3C2* (MR) being downregulated in *siPARP1* C2C12 myoblasts (Fig. 6E), and glucocorticoid signaling being a determinant of muscle turnover [19–22], we set out to test if *PARP1* influences the glucocorticoid

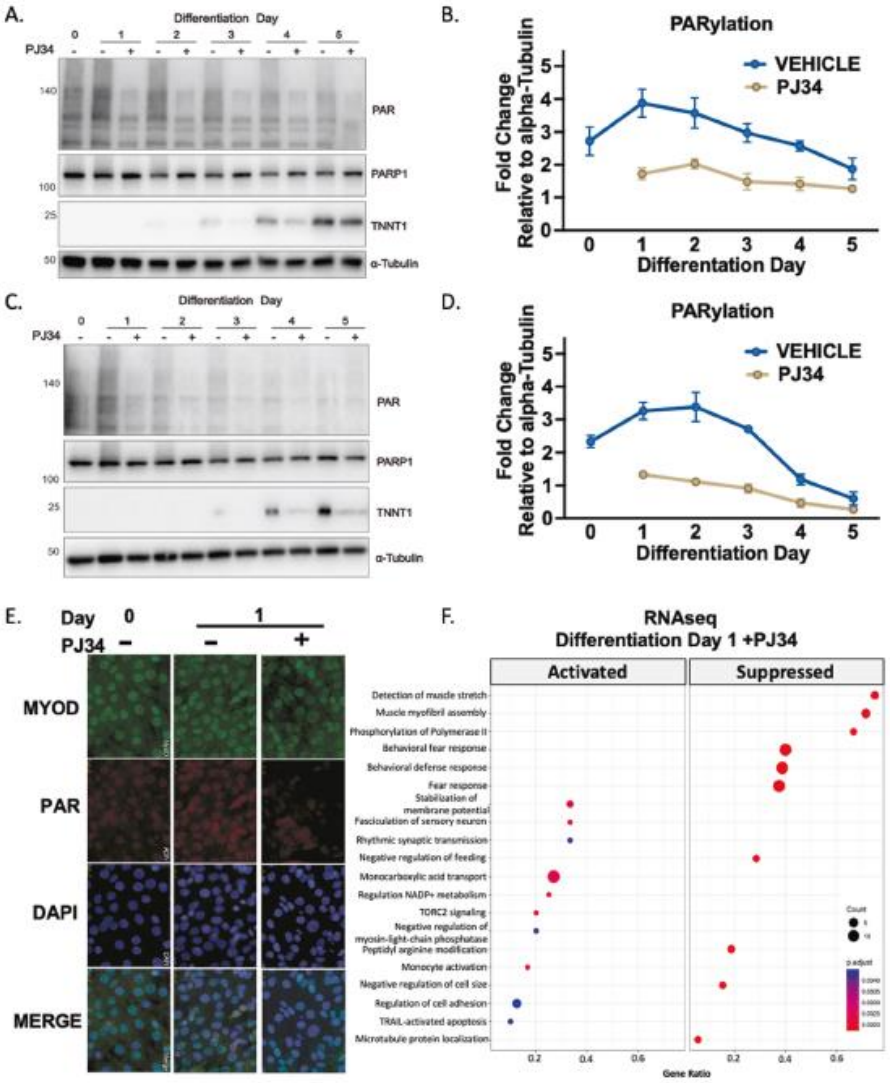

Fig. 3 Modulation of PARylation during myogenesis. A Western immunoblotting of differentiating C2C12 myoblasts differentiated in ±PARP inhibitor PJ34 (10 µM) probed for PAR, PARP1, Troponin 1 (TNNT1), and Alpha-Tubulin (representative of $n = 4$). **B** Quantification of PAR and PARP1 during differentiation. Each bar represents means ± S.D (representative of $n = 4$). **C** Western immunoblotting of differentiating LHCN-M2 myoblasts differentiated in ±PARP inhibitor PJ34 (10 µM) probed for PAR, PARP1, TNNT1, and Alpha-Tubulin ($n = 4$) $^{*}P < 0.05$, $^{**}P < 0.01$, and $^{***}P < 0.001$. **D** Quantification of PAR and PARP1 in human myoblasts during differentiation. Each bar represents means ± S.D (representative of n = 4). **E** Immunostaining of PAR (red), DAPI (purple), and MYOD (green) in differentiating C2C12 myoblasts ($n = 4$). **F** Dot plot of gene ontology (GO) overrepresentation analysis of C2C12 myoblasts differentiated in ±PARP inhibitor PJ34 (10 µM) ($n = 3$) on day 1 of differentiation. The *x* axis shows the gene ratio which represents the percentage of genes enriched in a term. The *y* axis represents the enriched pathways: size of the node represents the number of enriched genes in the term.

activated transcriptional program. To do this, we treated *siPARP1* and scrambled transfected C2C12 myoblasts with dexamethasone for 24 hours. RNA was collected and sequenced for differential gene expression. We found that *siPARP1* myoblasts retained the ability to upregulate genes in response to dexamethasone, sharing activation of typical glucocorticoid-regulated genes including *SerpinA3N* (9.50 fold change; 5.22×10^{-08} False Discovery Rate (FDR), *Hif3α* (7.40 fold change; 4.29×10^{-10} FDR) and *Mt2* (3.97 fold change; 9.07×10^{-24} FDR). However, we observed that the expression of 86 glucocorticoid-induced genes was lost in dexamethasone-treated *siPARP1* myoblasts (Fig. 7A, B and Supplementary Table S5). A tabular selection of these is presented

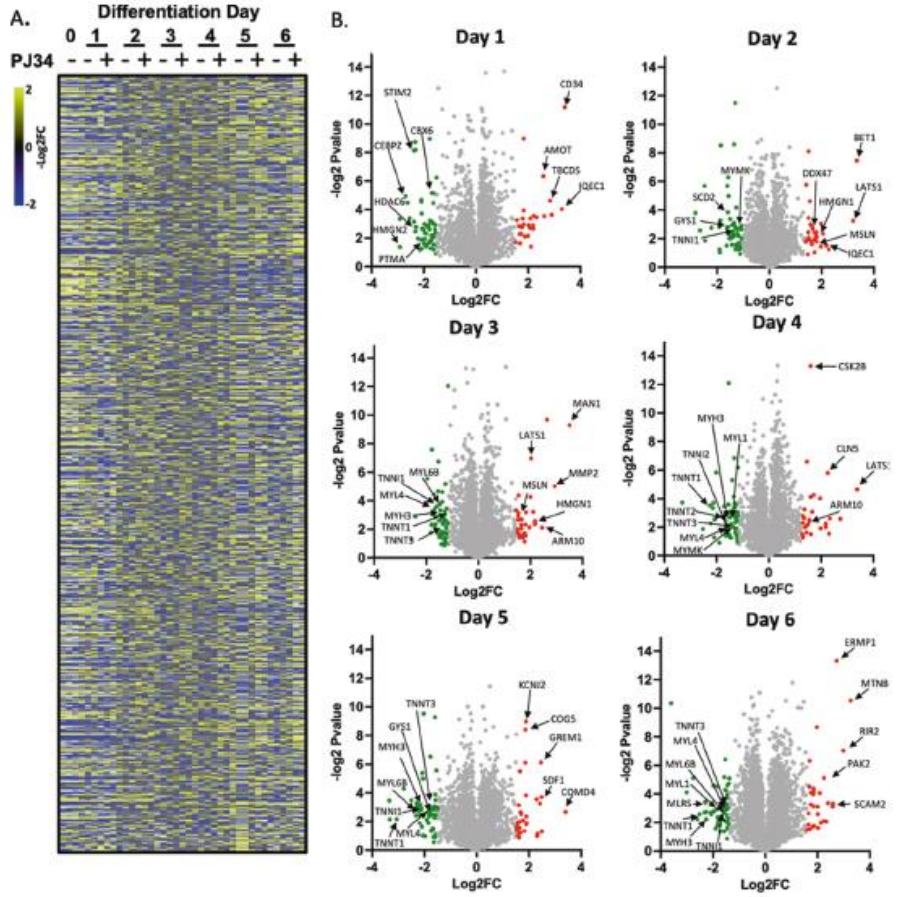

Fig. 4 The PARP1-regulated proteome in differentiating skeletal muscle. A Heatmap showing 2911 detected proteins in differentiating C2C12 myoblasts differentiated in ± PARP inhibitor PJ34 (10 µM) over days 0, 1, 2, 3, 4, 5, and 6 of differentiation ($n = 3$ per condition). **B** Volcano plots showing differentially abundant proteins in presence of PJ34 on each day of the 6 days of differentiation. Downregulated proteins are green (>−1.5 fold change), upregulated are red (>1.5 fold change). Arrows denote named proteins.

for scrambled and *siPARP1* myoblasts alongside classically glucocorticoid-activated genes (Fig. 7B), and the full list is provided (Supplementary Table S5). This cohort of genes, differentially regulated by dexamethasone in scrambled controls but not *siPARP1* myoblasts, were subjected to functional profiling using g:Profiler [23]. This revealed enrichment for gene ontological processes and functions of significance to skeletal muscle physiology including calcium release (Padj. 1.49×10^{-2}), as well as biological processes including straited muscle differentiation (Padj. 1.03×10^{-8}) and cellular development (Padj. 3.34×10^{-6}) (Fig. 7C). Furthermore, enrichment of the cellular compartment forming the thin filament of the myofibril was recorded (I band (FDR 5.06×10^{-6}); Z disc (FDR 5.59×10^{-5})). Mapping of these 86 genes for transcription factor motifs generated enrichment for key regulatory factors of muscle including *Pax4*, a regulator of muscle protein turnover [24] (Padj. 4.67×10^{-3}), *LKLF* (Padj. 5.72×10^{-3}), *PTF1* (Padj. 8.84×10^{-3}) and *myogenin* (Padj. 8.98×10^{-3}). Finally, human phenotype mapping identifies this gene cohort as being characteristic of skeletal muscle pathology including proximal muscle weakness, muscular dystrophy and Gower's sign [25]. These data indicate there are a subset of genes regulated by glucocorticoids in skeletal muscle which are also dependent on *PARP1*.

DISCUSSION

Herein, we demonstrate PARP1 and PARylation as being dynamically regulated during murine and human skeletal muscle differentiation. Specifically, we detail a conserved early-stage PAR accumulation that occurs within 24 h of myogenic induction that is both active and metabolically sensitive. We also show PARP1 may have roles in the cellular response to glucocorticoids, via regulation of a cohort of genes required for functional skeletal muscle.

PARP1 and PARylation are dynamic during skeletal muscle myogenesis

Suppression of PARP1 elicits beneficial metabolic effects which include enhanced exercise performance, increased energy expenditure, enhanced mitochondrial function, and resistance to

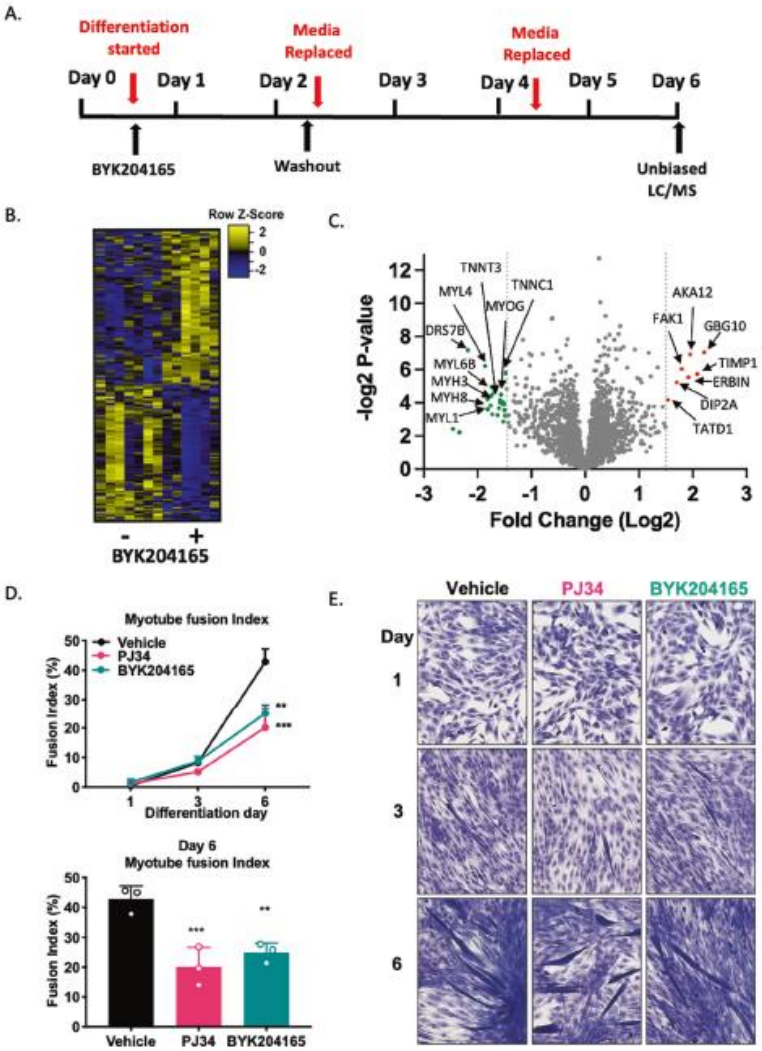

Fig. 5 PARP1-mediated PAR events on Day 1 impact the myogenic trajectory. A Schematic representation of the PARP inhibitor treatment protocol during C2C12 myoblast differentiation. **B** Heatmap representing differential abundance of proteins within samples differentiated in ±PARP1 specific inhibitor BYK204165 (10 µM) (Vehicle $n = 7$, BYK204165 $n = 6$). **C** Volcano plot of SWATH-LCMS lysates recovered from day 6 differentiated C2C12 myoblasts differentiated in ± PARP inhibitor PJ34 (10 µM). Differential protein abundance shown with downregulated proteins marked green and upregulated proteins marked red. **D** Myotube fusion index of differentiating myoblasts differentiated in ±PARP inhibitor PJ34 (10 µM) or ±PARP1 specific inhibitor BYK204165 (10 µM) ($n = 3$). Cells were fixed on days 1, 3, and 6 of differentiation. Upper panel shows days 1, 3, and 6 fusion index, lower panel shows day 6 fusion index. Each bar represents means ± S.D ($n = 3$) ***$P < 0.001$, **$P < 0.01$. **E** Representative photographs of Jenner-Giemsa stained differentiating myoblasts over days 1, 3, and 6 of differentiation ($n = 3$).

oxidative stress [7–9, 26]. Additionally, PARP1 and PAR levels are dynamically and differentially regulated in response to exercise between aged untrained and aged trained muscle [27]. Our results establish PAR deposition by PARP1 as well as its auto-PARylation occurring within the first 24 h of myogenesis, supporting recent work showing PARP1-mediated PAR deposition following MYOD-driven transdifferentiation of fibroblasts into myoblasts [28]. This increased PAR accumulation could be ascribed to metabolic pathway shifts from glycolysis to oxidative phosphorylation as the major energy source during myogenesis, which has been reported in embryonic stem cells and induced pluripotent stem cells [29, 30]. Initiation of myogenesis upregulates the muscle-restricted gene NMRK2, and this switch increases NAD^+ biosynthesis to drive PARP1 activity [31]. While the molecular recipients of the differentiating day 1 PAR accumulation are yet to be identified, existing evidence indicates MYOD is a likely target. Our data also show that this PAR accumulation is sensitive to changes in metabolism. Notably, we observed higher PAR levels in glucose-

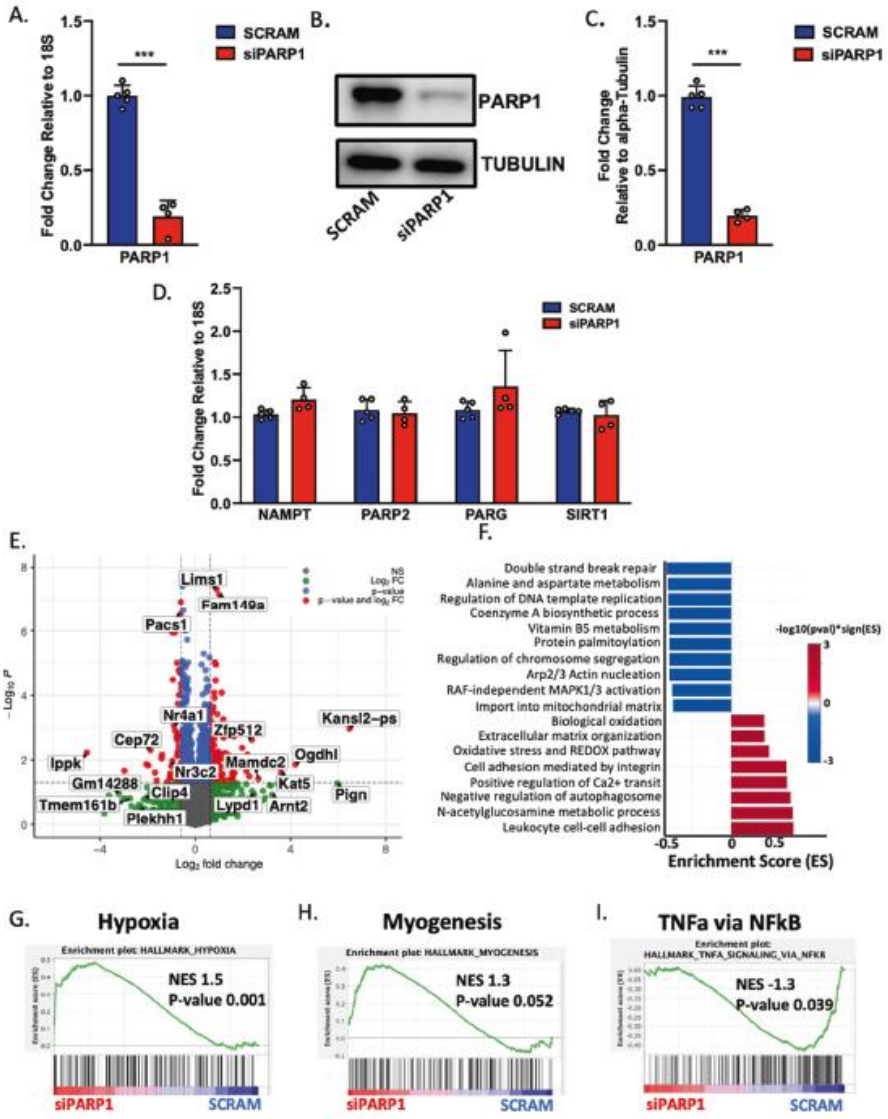

Fig. 6 PARP1 transcriptome in myoblasts. A qPCR of PARP1 in scrambled sequence controls ($n = 5$) and siRNA PARP1 transfected (*siPARP1*) C2C12 myoblasts ($n = 4$) ***$P < 0.001$. **B** Western immunoblotting of protein lysates collected from scrambled and *siPARP1* C2C12 myoblasts ($n = 5$). **C** Quantification of scrambled and *siPARP1* transfections by western blotting ($n = 5$). **D** qPCR of Scrambled control and *siPARP1* cDNA for PARP1, PARP2/PARP2, PARG, NAMPT, and SIRT1 transcripts. Scrambled ($n = 5$) and *siPARP1* ($n = 4$). **E** Representative volcano plot of differential gene expression following RNAseq of scrambled and *siPARP1* C2C12 myoblasts. **F** Gene set enrichment analysis (GSEA) of pathways over and under-represented in RNAseq data of *siPARP1* C2C12 myoblasts. **G** Enrichment plots of GSEA in *siPARP1* C2C12 myoblasts for hypoxia, **H** myogenesis and, **I** TNFα via NF-κB.

deprived conditions during myogenesis. However, PAR levels are induced in conditions of high glucose levels and fed states [7, 32]. These energetic requirements of day 1 differentiating myoblasts are likely specific to this point of myogenesis. This similarly has been found with autophagy and mitochondrial biogenesis which also upregulate PAR on day 1 [33, 34]. We also demonstrate that within myogenesis, that the troponins are also governed by PARP1 inhibition. It is therefore probable that PARP1, either through the direct or enzymatic application of PAR chains, coregulates their mRNA transcription. Incidentally, impacts over troponin expression by PARP1 hold relevance for cardiac muscle [35]. Given the nature of PARP1 PARylating activity, we also showed NAD^+

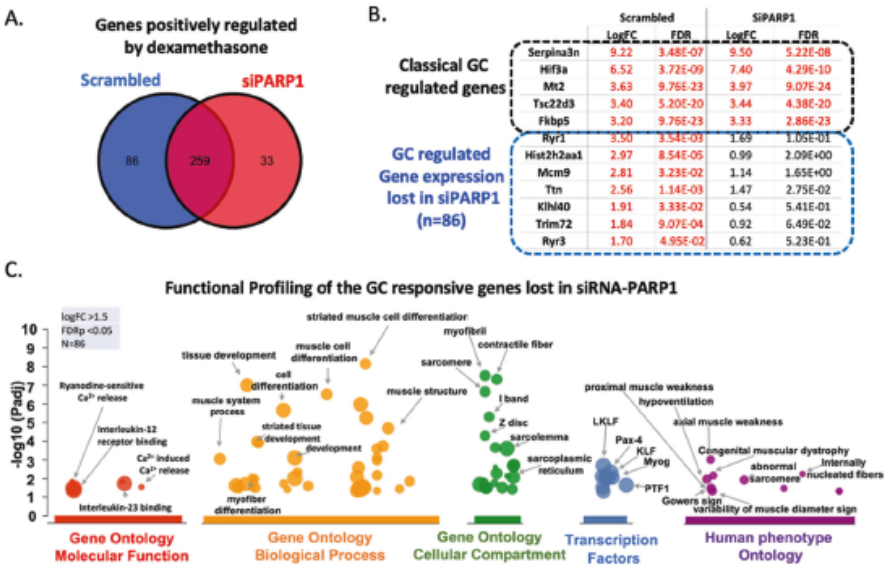

Fig. 7 PARP1 partially governs glucocorticoid-mediated transcriptional response. A Venn diagram of genes positively regulated by glucocorticoids in Scrambled and *siPARP1* C2C12 myoblasts (>1.5 Fold Change, <0.05 FDR) ($n = 5$ per treatment). **B** Selected list of genes responsive to dexamethasone and gene expression lost in *siPARP1* C2C12 myoblasts. **C** Manhattan plot produced following g:GOSt analysis using the 86 genes whose response to dexamethasone is lost in *siPARP1* C2C12 myoblasts. The plot shows overrepresented processes by Molecular function (red), Biological process (orange), Cellular compartment (green), Transcription factors (blue), and Human phenotype (purple).

precursor supplementation did not significantly impact PAR dynamics. This is possibly due to buffering mechanisms in response to NAD^+ availability [36], the specific inhibition of PARP1 was successful in reducing PAR supported via observed increases in NAD^+ (Supplementary Fig. 1A).

PARP1-mediated PARylation contributes to myogenesis

We postulated that PARP1-mediated PAR accumulation occurring on day 1 of myogenesis is to an extent, not dependent on myotube formation, but rather exerts consequences for the developed myotube. Using the broad-spectrum PARP inhibitor PJ34 and the PARP1-specific inhibitor BYK204165, we show that the expression profile changes are indeed related to PARP1-mediated PARylation on the first day of myogenesis. We also found downregulation of *PARP1* alone in undifferentiated C2C12 myoblasts was sufficient to cause shifts in the muscle transcriptome, and subsequent biological processes comparable to those of early-stage PARP1 inhibition during myogenesis. Further insight into which substrates are PARylated within the first day of myogenesis where PAR disposition is at its highest will be useful in defining downstream signaling. In this regard, nuclear PARP1-mediated PARylating activities are increased in the myoblast following successful transdifferentiation from fibroblasts, providing merit for this [28]. It is, however, likely that site-specific PARylation of key myogenic regulators occurs, although this remains to be tested, once performed, it would reveal specific amino acid sequences serving to impact the myogenic protein activity and the continual process of muscle turnover. With regards to skeletal muscle, the myogenic transcriptional regulator Yin Yang1 (*YY1*) has been directly shown to be both a recipient of PARylation by PARP1 [37], and regulated by the immunomodulatory NF-kB pathway during myogenesis [38]. Crosstalk between PARP1 and NF-kB has been reported in several cell and tissue types [17, 39, 40]. Therefore, it is probable that a greater level of coordination between the NF-kB pathway and PARylation exists and remains to be explored in skeletal muscle. Another direct recipient of PARylation and regulator of myogenic progression is the transcription factor CCAAT/enhancer binding protein beta (C/EBPb), which has been demonstrated to be PARylated during adipogenesis [2, 3]. Given C/EBPb roles in satellite cells, the myocyte, and its interactions with MYOD [41–43], there is potential for C/EBPb PARylation in muscle tissue. Additional mechanisms of both PARP1 and catalytic PAR control are also not discounted and exert influence over 3D chromatin organization [44, 45]. However, it should be noted that PARP2 which also contributes to PAR accumulation, has demonstrated roles in myogenesis and skeletal muscle structure [46]. Collectively, our presented results suggest that both PARP1 and its PARylating activity hold influence over the skeletal muscle phenotype, and further underscores PARP1's role as a multifaceted protein being able to bind to nucleic acids as well catalyzing the PARylation of target substrates [1, 47, 48].

PARP1 exerts influence over skeletal muscle glucocorticoid transcriptional response

Evidence for PARP1 in regulation of GR-mediated transcriptional response has been presented in other cells [49]. Furthermore, *PARP1* null mice have increased cortisol levels [50]. Our transcriptomic analysis of *siPARP1* C2C12 myoblasts reveals differentially expressed changes in the *N3RC2* gene coding for MR, and while not as ubiquitous as its GR counterpart, MR can also bind glucocorticoids with higher affinities [19]. Moreover, we demonstrate pathways commonly classified as glucocorticoid controlled, including hypoxia, myogenesis, and TNF-α response through NF-κB, being shifted in *siPARP1* myoblasts (Fig. 6g, h, i). Because PARP1 has documented roles in the NF-κB pathway for control of inflammatory response [17] and the mechanism of anti-inflammatory effects of glucocorticoids involves the repression of

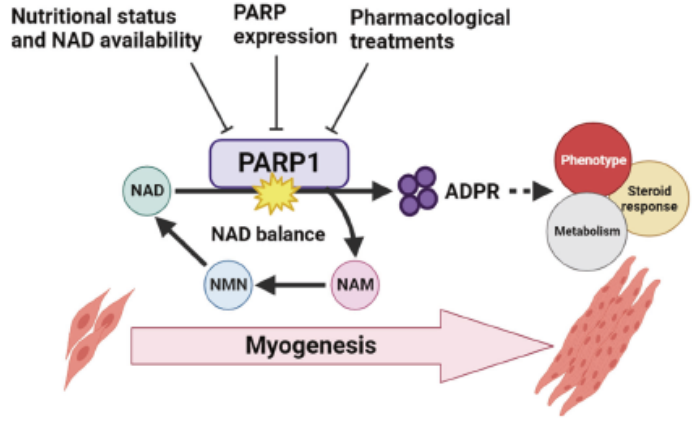

Fig. 8 PARP1-driven PARylation targets during early-stage differentiation and is central to proper development of the contractile unit. PARP1 in myoblasts also influences transcriptional regulation of glucocorticoids. These actions highlight the importance of NAD+ availability and PARylation to skeletal muscle.

NF-κB, it is plausible that this glucocorticoid-mediated effect occurs via PARP1. Furthermore, NF-κB has also been implicated in differentiation programs of other tissues, including myogenesis [38, 39, 51]. In this regard, PARP1 and its PARylating activity exert influence over osteoclast differentiation and bone remodeling via *NF-κB* dependent transcription of *IL-1β* [39], and glucocorticoid-induced osteoporosis is a consequence of the inhibition of IL-1 production [52]. Furthermore, as with PARP1, the suppression of NF-κB is fundamental for driving myogenesis [38, 51], while dexamethasone treatment at the myoblast stage enhances myogenesis [20–22]. Concurrently, we demonstrate that application of dexamethasone during differentiation induction of myoblasts reduces PAR levels (Fig. 2D) indicating glucocorticoids have impacts on PARP1-mediated PARylating activity. Recent studies have demonstrated that the tumor susceptibility gene TSG101 binds to and enhances GR transcriptional activity [53] and similarly, PARP1 drives enzymatic activity for DNA damage-induced IKK-NF-κB activation [54]. Therefore, we speculate a similar paradigm in which glucocorticoids can regulate PARP1-mediated PARylation within the skeletal muscle via PARP1 interacting partners. Together with our findings, there is suggested the potential for PARP1 and GR interactions for influencing glucocorticoid-mediated outcomes and muscle turnover.

By examining the transcriptomic changes in *siPARP1* C2C12 myoblasts treated with dexamethasone, we observe that the expression of glucocorticoid canonical target genes such as *FKBP5* remained intact (Fig. 7B). We observed differential expression in a cohort of genes whose response following dexamethasone treatment was lost in *siPARP1* myoblasts. These imply that PARP1 exerts influence over glucocorticoid transcriptional response in skeletal muscle. Furthermore, PARP1 has demonstrated involvement in myopathy [55], as does chronic glucocorticoid exposure [21, 56]. These indicate potential for PARP1 roles in the transcriptional pathways manifesting glucocorticoid-induced myopathy, necessitating broader studies. PARP1 mediates the glucocorticoid responsiveness of Gonadotropin-Releasing Hormone receptors [57], and here our findings demonstrate aspects of glucocorticoid-mediated impacts on skeletal muscle may occur through PARP1. However, it should also be appreciated that differential expression of glucocorticoid response genes could potentially be regulated by downstream events who themselves are impacted by *siPARP1*. Further investigation into direct GR and PARP1 interactions within the skeletal muscle would therefore establish clearer links into the extent PARP1 holds over overall glucocorticoid response.

Collectively, our studies demonstrate further potential for PARylation actions in skeletal muscle physiology and response to glucocorticoids (Fig. 8). While this might provide novel avenues for PARP inhibition in amelioration of chronic glucocorticoid-induced side effects, potential negative impacts over skeletal muscle turnover and repair should be considered.

MATERIALS AND METHODS

Cell culture

The murine muscle myoblast cell line C2C12 was purchased (ATCC, VA, USA) and maintained in proliferation media, composed of Dulbecco's Modified Eagle's Medium (DMEM) 25 mM glucose (Lonza, UK) supplemented with 10% (v/v) fetal bovine serum (FBS) (Thermo, UK) and 1% Penicillin/Streptomycin (P/S) (Thermo, UK). Upon cells reaching 70–80% confluence, the differentiation medium, composed of DMEM 25 mM glucose supplemented with 2% horse serum (HS) (Thermo, UK) and 1% P/S, was added to induce differentiation. The myoblasts were allowed to differentiate for 6 days with fresh differentiation medium added every other day, sufficient for the successful development of mature myotubes. The human muscle myoblast cell line LHCN-M2 (Evercyte, Germany) was grown in proliferation media as described [58], composed of a 4:1 ratio of DMEM and Medium 199 (Sigma-Aldrich, UK) supplemented with 15% FBS, 200 mM HEPES (Thermo, UK), 0.03 µg/ml zinc sulfate (Sigma-Aldrich, UK), 1.4 µg/ml vitamin B12 (Sigma-Aldrich, UK), 0.055 µg/ml dexamethasone (Sigma-Aldrich, UK), 2.5 ng/ml hepatocyte growth factor (Proteintech, UK), 10 ng/ml basic fibroblast growth factor (Sigma-Aldrich, UK) and 1% P/S. The differentiation media of LHCN-M2 was composed of a 4:1 ratio of DMEM and Medium 199 supplemented with 2% HS and 1% P/S. LHCN-M2 differentiation was performed similarly to C2C12 myoblasts.

Cell treatments

Myoblasts were treated with either vehicle controls or the PARP inhibitors BYK204165 (Tocris, UK) and PJ34 (MedChemExpress, NJ, USA) at working concentrations of 10 µM, as well as Rucaparib (Selleck Chemical) treatment at a working concentration of 1 µM. Treatments with nicotinamide riboside (NR) (Chromadex, CA, USA) were performed at 0.5 mM, FK866 (Sigma-Aldrich, UK) at 50 nM, and dexamethasone at 1 µM. All treatments were diluted in the differentiation medium and performed during differentiation induction of myoblasts, after which treatments were washed out after 1 day (24 h) of differentiation and replaced with fresh differentiation medium, and myoblasts were left to differentiate as described.

Transfection of silencing RNA
Cells were seeded at an approximate density of 100,000 cells/well in six-well cell culture plates and incubated for at least 3 h to allow adherence. The siRNA transfection mix was composed of Lipofectamine 2000 (Thermo, UK) and 0.5 µg/µl of siRNA PARP1 predesigned from three pooled siRNA PARP1 sequences (Merck, UK) or scrambled siRNA control sequence (Merck, UK). Transfection was conducted in Opti-Mem serum and antibiotic-free media (Thermo, UK) and incubated for 24 h, after which the transfection mix was replaced with fresh medium.

RNA extraction and quantitative PCR
Cells were washed with 1x PBS and harvested in TRIzol Reagent (Life Technologies, UK). Total RNA was isolated using chloroform extraction and isopropanol precipitation. RNA clean-up and purification were conducted using a column purification kit (Zymo, Germany) according to instructions and quantity was measured by Nanodrop. Samples designated for RNAseq were further assessed for quality using the 2100 Bioanalyzer Instrument (Agilent Technologies, UK) with all samples having at least an RNA integrity number of >9.5.

For quantitative PCR (qPCR), reverse transcription was performed on extracted RNA using a High-Capacity cDNA Reverse Transcription Kit (Thermo, UK) according to the manufacturer's instructions. cDNA was added to TaqMan™ Universal PCR Master Mix (Thermo, UK) with the appropriate primer pairs as follows: *PARP1* forward: CCTGAACAACGCAGACAGC, *PARP1* reverse: CGTTGTGCGTGGTAGCATGA, *PARP2* forward: GGAAGGCGAGTGCTAAATGAA, *PARP2* reverse: GGAAGGCGAGTGCTAAATGAA, *NAMPT* forward: CGCCATCTCCTTGAATGA, *NAMPT* reverse: GCACCACTAATCATCAGACC, *PARG* forward: GTGCCAGTTTCGATCCGTAGA, *PARG* reverse GGCCAGCATCGTGTAGATGA, *SIRT1* forward: GGCTACCGAGACAACCTCCTG, *SIRT1* reverse: AGTCCAGTCACTAGAGCTGGCG. Reactions were performed in 384 well plates and conducted using QuantStudio™ 7 Flex Real-Time PCR System (Applied Biosystems, UK) in single-plex format. All reactions were normalized to 18S rRNA (VIC™) (Applied Biosystems, UK). Data were collected as Ct values and used to obtain ΔΔCt values, and subsequently expressed as fold change ± standard error of the mean (S.D).

RNAseq
Library preparation and sequencing were conducted by Novogene Inc., UK, original fastq files can be found on EBI Array Express E-MTAB-12343. Reads were mapped using the kallisto RNAseq quantification program [59]. Analyses were carried out using R in RStudio and Bioconductor. Briefly, transcript quantification data were summarized to genes by tximport and normalized using edgeR. Normalized and filtered data were variance stabilized with voom function from limma and differentially expressed genes were identified with limma. Functional enrichment of differential expressed genes was conducted using g:Profiler [60].

Cell lysis and western blotting
For whole-cell lysis, cells were first washed in ice-cold 1x PBS and subsequently scraped in RIPA buffer (50 mM Tris pH 8.0, 150 mM NaCl, 0.5% (w/v) sodium deoxycholate, 0.1% (w/v) SDS, 1% NP-40) supplemented with 1× Pierce™ EDTA-free protease inhibitor cocktail (Thermo, UK) and incubated on ice for 30 min. Lysates were clarified by centrifugation at 12,000 rpm for 15 min at 4°C. The supernatant was recovered and stored at -80°C until use. Total protein concentration was determined by detergent-compatible protein assay (Bio-Rad, UK) according to the kit's instructions.

Total proteins were loaded and resolved on fixed percentage acrylamide SDS-PAGE gels and subsequently transferred onto PVDF membranes using Trans-Blot Turbo Transfer System (Bio-Rad, UK). Membranes were blocked with 5% bovine serum albumin (BSA) diluted in 1x TBS-T and incubated with primary antibodies overnight at 4°C: PARP1 (39559, Active-Motif, Belgium), PAR (MABE1031, Merck Millipore, UK), MYOD (sc-377460, Santa Cruz Biotechnology, Inc., USA), Hexokinase II (ab227198, Abcam, UK), Myogenin (ab1835, Abcam, UK), NF-kB (8242, Cell Signalling Technology, UK), α-Tubulin (sc-5286, Santa Cruz Biotechnology, Inc, USA), and subsequently with HRP-conjugated anti-mouse or anti-rabbit secondary antibodies (Dako, Denmark) for 1 h at room temperature. Blots were developed with Pierce™ ECL Western Blotting Substrate (Thermo, UK) and visualized using the G:BOX Chemi XX6 system (Syngene, UK). Bands were measured using Image J densitometry and normalized to those of loading controls.

Immunofluorescence
Cells grown on coverslips were rinsed with 1× PBS and fixed with 4% PFA (Thermo, UK). Permeabilization was performed with 0.1% Triton X-100 (Sigma-Aldrich, UK) and blocked with 10% goat serum (Life Technologies, UK). Coverslips were incubated with primary antibodies overnight at 4°C, before incubation with secondary antibodies and DAPI nuclear dye (Thermo, UK) for 1 h at room temperature. Coverslips were mounted on slides and allowed to set prior to imaging.

Unbiased proteomics
Unbiased mass spectrometry was carried out on a SCIEX TripleTOF 6600 instrument with samples analyzed in both SWATH (Data Independent Acquisition) and IDA (Information Dependent Acquisition) modes for quantitation and spectral library generation respectively. IDA data were searched together using ProteinPilot 5.0.2 to generate a spectral library and SWATH data was analyzed using Sciex OneOmics software extracted against the locally generated library. Log fold change and statistical analysis were calculated as described [60].

NAD^+ measurement
NAD^+ was measured in lysates extracted in 0.6 N perchloric acid as described [61]. Briefly, standards or samples in phosphate buffer were combined with the cycling mixture composed of 2% ethanol, 100 µg/ml alcohol dehydrogenase, 10 µg/ml diaphorase, 20 µM resazurin, 10 µM flavin mononucleotide, 10 mM nicotinamide and 0.1% BSA, in 100 mM phosphate buffer pH 8.0. Resorufin accumulation was evaluated by reading excitation at 544 nm and emission at 590 nm.

Giemsa–Jenner staining of myotubes
Cells stained during differentiation time points were performed as described [15]. Briefly, cells were fixed in methanol and stained with Jenner (Alfa Aesar, UK) diluted in 1 mM sodium phosphate pH 5.6, followed by Giemsa (Alfa Aesar, UK) diluted in 1 mM sodium phosphate pH 5.6. Cells were imaged using a camera attached to an inverted microscope. Protein-rich myotube fibers presented themselves as dark/deep purple while nuclei-stained shallow purple/pink. Total number of nuclei per image was manually scored and the number of nuclei inside myotubes was expressed as a percentage of total nuclei to obtain the fusion index.

Statistical analysis
Students *t* test or ANOVA statistical comparisons were used with the Graphpad Software Inc. Prism version 9. Western blots were quantified by densitometry using imageJ. Data are presented as mean ± S.D with statistical significance determined as $*P < 0.05$, $**P < 0.01$, $***P < 0.001$. Differences between two groups were determined using unpaired t-test compared treatments or genotypes. Statistical analysis derived from qPCR data was determined using ΔΔCt values throughout.

DATA AVAILABILITY
The datasets generated for this study are available on request to the corresponding author. RNAseq files are available at Array Express.

CODE AVAILABILITY
Code generated using RStudio version 4.2 and is available upon request.

REFERENCES
1. Gibson BA, Kraus WL. New insights into the molecular and cellular functions of poly(ADP-ribose) and PARPs. Nat Rev Mol Cell Biol. 2012;13:411–24.
2. Luo X, Ryu KW, Kim DS, Nandu T, Medina CJ, Gupte R, et al. PARP-1 controls the adipogenic transcriptional program by PARylating C/EBPβ and modulating its transcriptional activity. Mol Cell [Internet] 2017;65:260–71. https://pubmed.ncbi.nlm.nih.gov/28107648/. Accessed 1 Jul 2022.
3. Ryu KW, Nandu T, Kim J, Challa S, DeBerardinis RJ, Lee, et al. Metabolic regulation of transcription through compartmentalized NAD+ biosynthesis. Science 2018;360:eaan5780.
4. Matteini F, Andresini O, Petrai S, Battistelli C, Rossi MN, Maione R. Poly(ADP-ribose) Polymerase 1 (PARP1) restrains MyoD-dependent gene expression during muscle differentiation. Sci Rep. [Internet]. 2020;10:15086. Accessed 29 Jun 2022.

5. Wang Y, Zhang Y, Zhang S, Kim B, Hull VL, Xu J, et al. PARP1-mediated PARylation activity is essential for oligodendroglial differentiation and CNS myelination. Cell Rep. 2021;37:109695.
6. Jones A, Kraus WL. Multiomics analysis of the NAD +-PARP1 axis reveals a role for site-specific ADP-ribosylation in splicing in embryonic stem cells. Genes Dev. 2022;36:601–17.
7. Bai P, Cantó C, Oudart H, Brunyánszki A, Cen Y, Thomas C, et al. PARP-1 inhibition increases mitochondrial metabolism through SIRT1 activation. Cell Metab. 2011;13:461–8.
8. Pirinen E, Cantó C, Jo YS, Morato L, Zhang H, Menzies KJ, et al. Pharmacological Inhibition of poly(ADP-ribose) polymerases improves fitness and mitochondrial function in skeletal muscle. Cell Metab. 2014;19:1034–41.
9. Oláh G, Szczesny B, Brunyánszki A, Lopez-García IA, Gerö D, Radák Z, et al. Differentiation-associated downregulation of poly(ADP-Ribose) polymerase-1 expression in myoblasts serves to increase their resistance to oxidative stress. PLoS One [Internet] 2015;10:e0134227. https://journals.plos.org/plosone/article?id=10.1371/journal.pone.0134227. Accessed 29 Jun 2022.
10. Elhassan YS, Kluckova K, Fletcher RS, Schmidt MS, Garten A, Doig CL, et al. Nicotinamide riboside augments the aged human skeletal muscle NAD+ metabolome and induces transcriptomic and anti-inflammatory signatures. Cell Rep. 2019;28:1717–28.e6.
11. Eleazer R, Fondufe-Mittendorf YN. The multifaceted role of PARP1 in RNA biogenesis. Wiley Interdiscip Rev RNA [Internet]. 2021;12:e1617. https://pubmed.ncbi.nlm.nih.gov/32656996/. Accessed 11 Nov 2022.
12. Jubin T, Kadam A, Gani AR, Singh M, Dwivedi M, Begum R. Poly ADP-ribose polymerase-1: beyond transcription and towards differentiation. Semin Cell Dev Biol [Internet]. 2017;63:167–79. https://pubmed.ncbi.nlm.nih.gov/27476447/. Accessed 30 Sep 2022.
13. Wahlberg E, Karlberg T, Kouznetsova E, Markova N, Macchiarulo A, Thorsell AG, et al. Family-wide chemical profiling and structural analysis of PARP and tankyrase inhibitors. Nat Biotechnol [Internet]. 2012;30:283–8. https://pubmed.ncbi.nlm.nih.gov/22343925/. Accessed 29 Jun 2022.
14. Eltze T, Boer R, Wagner T, Weinbrenner S, McDonald MC, Thiemermann C, et al. Imidazoquinolinone, imidazopyridine, and isoquinolindione derivatives as novel and potent inhibitors of the poly(ADP-ribose) polymerase (PARP): a comparison with standard PARP inhibitors. Mol Pharm [Internet]. 2008;74:1587–98. https://pubmed.ncbi.nlm.nih.gov/18809672/. Accessed 29 Jun 2022.
15. Veliça P, Bunce CM. A quick, simple and unbiased method to quantify C2C12 myogenic differentiation. Muscle Nerve [Internet]. 2011;44:366–70. https://onlinelibrary.wiley.com/doi/full/10.1002/mus.22056. Accessed 25 Oct 2022.
16. Kamaletdinova T, Fanaei-Kahrani Z, Wang ZQ. The enigmatic function of PARP1: from PARylation activity to PAR readers. Cells [Internet]. 2019;8:1625. Accessed 5 Oct 2022.
17. Oliver FJ, Ménissier-de Murcia J, Nacci C, Decker P, Andriantsitohaina R, Muller S, et al. Resistance to endotoxic shock as a consequence of defective NF-κB activation in poly (ADP-ribose) polymerase-1 deficient mice. EMBO J. 1999;18:4446–54.
18. Martí JM, Garcia-Diaz A, Delgado-Bellido D, O'Valle F, González-Flores A, Carlevaris O, et al. Selective modulation by PARP-1 of HIF-1α-recruitment to chromatin during hypoxia is required for tumor adaptation to hypoxic conditions. Redox Biol. 2021;41:101885.
19. Vettorazzi S, Nalbantoglu D, Gebhardt JCM, Tuckermann J. A guide to changing paradigms of glucocorticoid receptor function—a model system for genome regulation and physiology. FEBS J [Internet]. 2022;289:5718–43. https://onlinelibrary.wiley.com/doi/full/10.1111/febs.16100. Accessed 30 Sept 2022.
20. Guerriero V, Florini JR. Dexamethasone effects on myoblast proliferation and differentiation. Endocrinol [Internet]. 1980;106:1198–202. https://pubmed.ncbi.nlm.nih.gov/7188899/. Accessed 29 Jun 2022.
21. Han DS, Yang WS, Kao TW. Dexamethasone treatment at the myoblast stage enhanced C2C12 myocyte differentiation. Int J Med Sci [Internet]. 2017;14:434–43. https://pubmed.ncbi.nlm.nih.gov/28539819/. Accessed 29 Jun 2022.
22. Lin JW, Huang YM, Chen YQ, Chuang TY, Lan TY, Liu YW. et al. Dexamethasone accelerates muscle regeneration by modulating kinesin-1-mediated focal adhesion signals. Cell Death Discov. 2021;7:1–16. Accessed 29 Jun 2022.
23. Raudvere U, Kolberg L, Kuzmin I, Arak T, Adler P, Peterson H, et al. g:Profiler: a web server for functional enrichment analysis and conversions of gene lists (2019 update). Nucleic Acids Res [Internet]. 2019;47:W191–8. https://academic.oup.com/nar/article/47/W1/W191/5486750. Accessed 28 Oct 2022.
24. Volodin A, Kosti I, Goldberg AL, Cohen S. Myofibril breakdown during atrophy is a delayed response requiring the transcription factor PAX4 and desmin depolymerization. Proc Natl Acad Sci USA [Internet]. 2017;114:E1375–84. https://www.pnas.org/doi/abs/10.1073/pnas.1612988114. Accessed 7 Oct 2022.
25. Caria F, Cescon M, Gualandi F, Pichiecchio A, Rossi R, Rimessi P, et al. Autosomal recessive Bethlem myopathy: a clinical, genetic and functional study. Neuromuscul Disord [Internet]. 2019;29:657–63. https://pubmed.ncbi.nlm.nih.gov/31471117/. Accessed 7 Oct 2022.
26. Mohamed JS, Wilson JC, Myers MJ, Sisson KJ, Alway SE. Dysregulation of SIRT-1 in aging mice increases skeletal muscle fatigue by a PARP-1-dependent mechanism. Aging [Internet]. 2014;6:820–34. https://pubmed.ncbi.nlm.nih.gov/25361036/. Accessed 17 Sept 2021.
27. Cobley JN, Sakellariou GK, Murray S, Waldron S, Gregson W, Burniston JG, et al. Lifelong endurance training attenuates age-related genotoxic stress in human skeletal muscle. Longev Healthspan [Internet]. 2013;2:11 https://pubmed.ncbi.nlm.nih.gov/24472304/. Accessed 17 Sept 2021.
28. Bisceglie L, Hopp AK, Gunasekera K, Wright RH, le Dily F, Vidal E, et al. MyoD induces ARTD1 and nucleoplasmic poly-ADP-ribosylation during fibroblast to myoblast transdifferentiation. iScience. 2021;24:102432.
29. Chung S, Dzeja PP, Faustino RS, Perez-Terzic C, Behfar A, Terzic A. Mitochondrial oxidative metabolism is required for the cardiac differentiation of stem cells. Nat Clin Pract Cardiovasc Med [Internet]. 2007;4:S60–7. https://pubmed.ncbi.nlm.nih.gov/17230217/. Accessed 6 Jan 2023.
30. Folmes CDL, Nelson TJ, Martinez-Fernandez A, Arrell DK, Lindor JZ, Dzeja PP, et al. Somatic oxidative bioenergetics transitions into pluripotency-dependent glycolysis to facilitate nuclear reprogramming. Cell Metab [Internet]. 2011;14:264–71. https://pubmed.ncbi.nlm.nih.gov/21803296/. Accessed 6 Jan 2023.
31. Fletcher RS, Ratajczak J, Doig CL, Oakey LA, Callingham R, da Silva Xavier G, et al. Nicotinamide riboside kinases display redundancy in mediating nicotinamide mononucleotide and nicotinamide riboside metabolism in skeletal muscle cells. Mol Metab. 2017;6:819–32.
32. Garcia Soriano F, Virág L, Jagtap P, Szabó É, Mabley JG, Liaudet L, et al. Diabetic endothelial dysfunction: the role of poly(ADP-ribose) polymerase activation. Nat Med [Internet]. 2001;7:108–13. https://pubmed.ncbi.nlm.nih.gov/11135624/. Accessed 5 Jan 2023.
33. Rodríguez-Vargas JM, Oliver-Pozo FJ, Dantzer F. PARP1 and poly(ADP-ribosyl)ation signaling during autophagy in response to nutrient deprivation. Oxid Med Cell Longev [Internet]. 2019;2019:2641712. https://pubmed.ncbi.nlm.nih.gov/31281570/. Accessed 15 Feb 2023.
34. Sin J, Andres AM, Taylo RDJR, Weston T, Hiraumi Y, Stotland A, et al. Mitophagy is required for mitochondrial biogenesis and myogenic differentiation of C2C12 myoblasts. Autophagy [Internet]. 2016;12:369–80. https://pubmed.ncbi.nlm.nih.gov/26566717/. Accessed 15 Feb 2023.
35. Zhang D, Hu X, Li J, Liu J, Baks-te Bulte L, Wiersma M, et al. DNA damage-induced PARP1 activation confers cardiomyocyte dysfunction through NAD+ depletion in experimental atrial fibrillation. Nat Commun [Internet]. 2019;10. https://pubmed.ncbi.nlm.nih.gov/30898999/. Accessed 7 Oct 2022.
36. Oakey LA, Fletcher RS, Elhassan YS, Cartwright DM, Doig CL, Garten A, et al. Metabolic tracing reveals novel adaptations to skeletal muscle cell energy production pathways in response to NAD + depletion. Wellcome Open Res. 2019;3:147.
37. Oei SL, Shi Y. Poly(ADP-Ribosyl)ation of transcription factor Yin Yang 1 under conditions of DNA damage. Biochem Biophys Res Commun. 2001;285:27–31.
38. Wang H, Hertlein E, Bakkar N, Sun H, Acharyya S, Wang J, et al. NF-kappaB regulation of YY1 inhibits skeletal myogenesis through transcriptional silencing of myofibrillar genes. Mol Cell Biol [Internet] 2007;27:4374–87. https://pubmed.ncbi.nlm.nih.gov/17438126/. Accessed 7 Oct 2022.
39. Robaszkiewicz A, Qu C, Wisnik E, Ploszaj T, Mirsaidi A, Kunze FA, et al. ARTD1 regulates osteoclastogenesis and bone homeostasis by dampening NF-κB-dependent transcription of IL-1β. Sci Rep [Internet]. 2016;6. Accessed 29 Jun 2022.
40. Ke B, Li A, Fu H, Kong C, Liu T, Zhu Q, et al. PARP-1 inhibitors enhance the chemosensitivity of leukemia cells by attenuating NF-κB pathway activity and DNA damage response induced by Idarubicin. Acta Biochim Biophys Sin [Internet]. 2022;54:91–8. https://pubmed.ncbi.nlm.nih.gov/35130631/. Accessed 7 Oct 2022.
41. Marchildon F, Fu D, Lala-Tabbert N, Wiper-Bergeron N. CCAAT/enhancer binding protein beta protects muscle satellite cells from apoptosis after injury and in cancer cachexia. Cell Death Dis 2016 7:2 [Internet]. 2016;7:e2109. https://www.nature.com/articles/cddis20164. Accessed 7 Oct 2022.
42. Marchildon F, Lala N, Li G, St-Louis C, Lamothe D, Keller C, et al. CCAAT/enhancer binding protein beta is expressed in satellite cells and controls myogenesis. Stem Cells [Internet]. 2012;30:2619–30. https://academic.oup.com/stmcls/article/30/12/2619/6404629. Accessed 7 Oct 2022.
43. Lala-Tabbert N, AlSudais H, Marchildon F, Fu D, Wiper-Bergeron N. CCAAT/enhancer binding protein β is required for satellite cell self-renewal. Skelet Muscle [Internet]. 2016;6:1–11. https://skeletalmusclejournal.biomedcentral.com/articles/10.1186/s13395-016-0112-8. Accessed 7 Oct 2022.
44. Muthurajan UM, Hepler MRD, Hieb AR, Clark NJ, Kramer M, Yao T, et al. Automodification switches PARP-1 function from chromatin architectural protein to histone chaperone. Proc Natl Acad Sci USA [Internet]. 2014;111:12752–7. Accessed 7 Oct 2022.

45. Posavec Marjanović M, Crawford K, Ahel I. PARP, transcription and chromatin modeling. Semin Cell Dev Biol. 2017;63:102–13.
46. Jankó L, Sári Z, Kovács T, Kis G, Szántó M, Antal M, et al. Silencing of PARP2 blocks autophagic degradation. cells [Internet]. 2020;9. https://pubmed.ncbi.nlm.nih.gov/32046043/. Accessed 5 Jan 2023.
47. Gupte R, Liu Z, Kraus WL. PARPs and ADP-ribosylation: recent advances linking molecular functions to biological outcomes. Genes Dev. 2017;31:101–26.
48. Kim DS, Challa S, Jones A, Kraus WL. PARPs and ADP-ribosylation in RNA biology: from RNA expression and processing to protein translation and proteostasis. Genes Dev. 2020;34:302–20.
49. Trotter KW, King HA, Archer TK. Glucocorticoid receptor transcriptional activation via the BRG1-dependent recruitment of TOP2β and Ku70/86. Mol Cell Biol. 2015;35:2799–817.
50. Drazen DL, Bilu D, Edwards N, Nelson RJ. Disruption of poly(ADP-ribose) polymerase (PARP) protects against stress-evoked immunocompromise. Mol Med. 2001;7:761–6.
51. Guttridge DC, Albanese C, Reuther JY, Pestell RG, Baldwin AS Jr. NF-κB controls cell growth and differentiation through transcriptional regulation of cyclin D1. Mol Cell Biol [Internet]. 1999;19:5785. Accessed 7 Oct 2022.
52. Ilias I, Milionis C, Zoumakis E. An overview of glucocorticoid-induced osteoporosis. J Clin Rheumatol [Internet]. 2022;5. https://www.ncbi.nlm.nih.gov/books/NBK278968/. Accessed 7 Oct 2022.
53. White JT, Rives J, Tharp ME, Wrabl JO, Thompson EB, Hilser VJ. Tumor susceptibility gene 101 regulates the glucocorticoid receptor through disorder-mediated allostery. Biochem [Internet]. 2021;60:1647–57. https://pubmed.ncbi.nlm.nih.gov/34009973/. Accessed 6 Jan 2023.
54. Tufan AB, Lazarow K, Kolesnichenko M, Sporbert A, von Kries JP, Scheidereit C. TSG101 associates with PARP1 and is essential for PARylation and DNA damage-induced NF-κB activation. EMBO J [Internet]. 2022;41:e110372. https://onlinelibrary.wiley.com/doi/full/10.15252/embj.2021110372. Accessed 6 Jan 2023.
55. Sharma V, Nand Pandey S, Khawaja H, Brown JK, Hathout Y, Chen YW. PARP1 differentially interacts with promoter region of DUX4 Gene in FSHD myoblasts. J Genet Syndr Gene Ther. 2016;7:303.
56. Schakman O, Kalista S, Barbé C, Loumaye A, Thissen JP. Glucocorticoid-induced skeletal muscle atrophy. Int J Biochem Cell Biol [Internet]. 2013;45:2163–72. https://pubmed.ncbi.nlm.nih.gov/23806868/. Accessed 29 Jun 2022.
57. Lee C, Cederberg RA, White BR. Poly [ADP-Ribose] polymerase-1 (PARP-1) confers glucocorticoid responsiveness of the porcine GnRH receptor (GnRHR) Gene. Biol Reprod. 2011;85Suppl_1:2–4.
58. Zhu CH, Mouly V, Cooper RN, Mamchaoui K, Bigot A, Shay JW, et al. Cellular senescence in human myoblasts is overcome by human telomerase reverse transcriptase and cyclin-dependent kinase 4: consequences in aging muscle and therapeutic strategies for muscular dystrophies. Aging Cell. 2007;6:515–23.
59. Bray NL, Pimentel H, Melsted P, Pachter L. Near-optimal probabilistic RNA-seq quantification. Nat Biotechnol. 2016;34:525–7. https://www.nature.com/articles/nbt.3519. Accessed 5 Oct 2022.
60. Aguilan JT, Kulej K, Sidoli S. Guide for protein fold change and p-value calculation for non-experts in proteomics. Mol Omics. 2020;16:573–82.
61. Luongo TS, Eller JM, Lu MJ, Niere M, Raith F, Perry C, et al. SLC25A51 is a mammalian mitochondrial NAD+ transporter. Nat [Internet]. 2020;588:174. Accessed 18 Oct 2022.

ACKNOWLEDGEMENTS

We would like to thank Prof. Mark Christian of Nottingham Trent University for helpful insight. We would also like to thank Chromadex for the supply of nicotinamide riboside.

AUTHOR CONTRIBUTIONS

AT and CLD performed study concept and design; AT, AE, JC, CLD, AC, DB, and CC performed experimental work. AT and CLD performed development of methodology and writing, edits and revision of the paper; CLD, DB, CC and AT provided acquisition, analysis and interpretation of data, and statistical analysis; GGL and CS provided technical and material support. All authors read and approved the final paper.

FUNDING

This work was part funded by The Physiological Society Research grant and Bioscientifica COVID-19 relief fund awarded to CLD. CLD is also funded by a Quality research award from Nottingham Trent University.

COMPETING INTERESTS

The authors declare no competing interests.

ADDITIONAL INFORMATION

Supplementary information The online version contains supplementary material available at https://doi.org/10.1038/s41420-023-01420-2.

Correspondence and requests for materials should be addressed to Craig L. Doig.

Reprints and permission information is available at http://www.nature.com/reprints

Publisher's note Springer Nature remains neutral with regard to jurisdictional claims in published maps and institutional affiliations.

Open Access This article is licensed under a Creative Commons Attribution 4.0 International License, which permits use, sharing, adaptation, distribution and reproduction in any medium or format, as long as you give appropriate credit to the original author(s) and the source, provide a link to the Creative Commons license, and indicate if changes were made. The images or other third party material in this article are included in the article's Creative Commons license, unless indicated otherwise in a credit line to the material. If material is not included in the article's Creative Commons license and your intended use is not permitted by statutory regulation or exceeds the permitted use, you will need to obtain permission directly from the copyright holder. To view a copy of this license, visit http://creativecommons.org/licenses/by/4.0/.

© The Author(s) 2023

References

1. White AT, Schenk S. Intracellular Signal for Skeletal Muscle Adaptation: NAD+/NADH and skeletal muscle mitochondrial adaptations to exercise. *Am J Physiol Endocrinol Metab*. 2012;303(3):E308. doi:10.1152/AJPENDO.00054.2012

2. Johnson S, Imai S ichiro. NAD + biosynthesis, aging, and disease. *F1000Res*. 2018;7. doi:10.12688/F1000RESEARCH.12120.1

3. Muiras ML, Müller M, Schächter F, Bürkle A. Increased poly(ADP-ribose) polymerase activity in lymphoblastoid cell lines from centenarians. *Journal of Molecular Medicine 1998 76:5*. 1998;76(5):346-354. doi:10.1007/S001090050226

4. Frontera WR, Ochala J. Skeletal muscle: a brief review of structure and function. *Calcif Tissue Int*. 2015;96(3):183-195. doi:10.1007/S00223-014-9915-Y

5. Zurlo F, Larson K, Bogardus C, Ravussin E. Skeletal muscle metabolism is a major determinant of resting energy expenditure. *J Clin Invest*. 1990;86(5):1423-1427. doi:10.1172/JCI114857

6. Larsson L, Degens H, Li M, et al. Sarcopenia: Aging-Related Loss of Muscle Mass and Function. *Physiol Rev*. 2019;99(1):427-511. doi:10.1152/PHYSREV.00061.2017

7. Wehrwein EA, Orer HS, Barman SM. Overview of the Anatomy, Physiology, and Pharmacology of the Autonomic Nervous System. *Compr Physiol*. 2016;6(3):1239-1278. doi:10.1002/CPHY.C150037

8. Light N, Champion AE. Characterization of muscle epimysium, perimysium and endomysium collagens. *Biochemical Journal*. 1984;219(3):1017. doi:10.1042/BJ2191017

9. Farah CS, Reinach FC. The troponin complex and regulation of muscle contraction. *The FASEB Journal*. 1995;9(9):755-767. doi:10.1096/FASEBJ.9.9.7601340

10. Squire JM. Architecture and function in the muscle sarcomere. *Curr Opin Struct Biol*. 1997;7(2):247-257. doi:10.1016/S0959-440X(97)80033-4

11. Rossi AE, Dirksen RT. Sarcoplasmic reticulum: The dynamic calcium governor of muscle. *Muscle Nerve*. 2006;33(6):715-731. doi:10.1002/MUS.20512

12. Calderón JC, Bolaños P, Caputo C. The excitation–contraction coupling mechanism in skeletal muscle. *Biophys Rev*. 2014;6(1):133. doi:10.1007/S12551-013-0135-X

13. Wingertzahn MA, Ochs RS. Control of calcium in skeletal muscle excitation-contraction coupling: implications for malignant hyperthermia. *Mol Genet Metab*. 1998;65(2):113-120. doi:10.1006/MGME.1998.2746

14. Huxley HE. The mechanism of muscular contraction. *Science*. 1969;164(3886):1356-1366. doi:10.1126/SCIENCE.164.3886.1356

15. Huxley H, Hanson J. Changes in the Cross-Striations of Muscle during Contraction and Stretch and their Structural Interpretation. *Nature 1954 173:4412*. 1954;173(4412):973-976. doi:10.1038/173973a0

16. Huxley AF, Niedergerke R. Structural changes in muscle during contraction; interference microscopy of living muscle fibres. *Nature*. 1954;173(4412):971-973. doi:10.1038/173971A0

17. Ciciliot S, Rossi AC, Dyar KA, Blaauw B, Schiaffino S. Muscle type and fiber type specificity in muscle wasting. *Int J Biochem Cell Biol*. 2013;45(10):2191-2199. doi:10.1016/J.BIOCEL.2013.05.016

18. Talbot J, Maves L. Skeletal muscle fiber type: using insights from muscle developmental biology to dissect targets for susceptibility and resistance to muscle disease. *Wiley Interdiscip Rev Dev Biol*. 2016;5(4):518-534. doi:10.1002/WDEV.230

19. Schiaffino S, Reggiani C. Fiber types in mammalian skeletal muscles. *Physiol Rev*. 2011;91(4):1447-1531. doi:10.1152/PHYSREV.00031.2010

20. Thorstensson A, Karlsson J. Fatiguability and fibre composition of human skeletal muscle. *Acta Physiol Scand*. 1976;98(3):318-322. doi:10.1111/J.1748-1716.1976.TB10316.X

21. Szent-Györgyi AG. The early history of the biochemistry of muscle contraction. *J Gen Physiol*. 2004;123(6):631-641. doi:10.1085/JGP.200409091

22. Liu G, mac Gabhann F, Popel AS. Effects of fiber type and size on the heterogeneity of oxygen distribution in exercising skeletal muscle. *PLoS One*. 2012;7(9). doi:10.1371/JOURNAL.PONE.0044375

23. Hilber K, Galler S, Pette D. Functional differences of myosin heavy-chain isoforms in skeletal muscle. *Naturwissenschaften*. 1997;84(5):201-204. doi:10.1007/S001140050378

24. Julien IB, Sephton CF, Dutchak PA. Metabolic Networks Influencing Skeletal Muscle Fiber Composition. *Front Cell Dev Biol*. 2018;6(SEP):125. doi:10.3389/FCELL.2018.00125

25. Röckl KSC, Hirshman MF, Brandauer J, Fujii N, Witters LA, Goodyear LJ. Skeletal muscle adaptation to exercise training: AMP-activated protein kinase mediates muscle fiber type shift. *Diabetes*. 2007;56(8):2062-2069. doi:10.2337/DB07-0255

26. Gannon J, Doran P, Kirwan A, Ohlendieck K. Drastic increase of myosin light chain MLC-2 in senescent skeletal muscle indicates fast-to-slow fibre transition in sarcopenia of old age. *Eur J Cell Biol*. 2009;88(11):685-700. doi:10.1016/J.EJCB.2009.06.004

27. Pette D, Staront RS. Mammalian skeletal muscle fiber type transitions. *Int Rev Cytol*. 1997;170:143-223. doi:10.1016/S0074-7696(08)61622-8

28. Lin J, Wu H, Tarr PT, et al. Transcriptional co-activator PGC-1α drives the formation of slow-twitch muscle fibres. *Nature 2002 418:6899*. 2002;418(6899):797-801. doi:10.1038/nature00904

29. Chal J, Pourquié O. Making muscle: skeletal myogenesis in vivo and in vitro. *Development*. 2017;144(12):2104-2122. doi:10.1242/DEV.151035

30. Christ B, Ordahl CP. Early stages of chick somite development. *Anat Embryol (Berl)*. 1995;191(5):381-396. doi:10.1007/BF00304424

31. Bentzinger CF, Wang YX, Rudnicki MA. Building Muscle: Molecular Regulation of Myogenesis. *Cold Spring Harb Perspect Biol*. 2012;4(2). doi:10.1101/CSHPERSPECT.A008342

32. Buas MF, Kadesch T. Regulation of skeletal myogenesis by Notch. *Exp Cell Res*. 2010;316(18):3028. doi:10.1016/J.YEXCR.2010.05.002

33. Wang Y, Jaenisch R. Myogenin can substitute for Myf5 in promoting myogenesis but less efficiently. *Development*. 1997;124(13):2507-2513. doi:10.1242/DEV.124.13.2507

34. MAURO A. Satellite cell of skeletal muscle fibers. *J Biophys Biochem Cytol*. 1961;9(2):493-495. doi:10.1083/JCB.9.2.493

35. Buckingham M, Relaix F. The role of Pax genes in the development of tissues and organs: Pax3 and Pax7 regulate muscle progenitor cell functions. *Annu Rev Cell Dev Biol*. 2007;23:645-673. doi:10.1146/ANNUREV.CELLBIO.23.090506.123438

36. Schmalbruch H, Lewis DM. DYNAMICS OF NUCLEI OF MUSCLE FIBERS AND CONNECTIVE TISSUE CELLS IN NORMAL AND DENERVATED RAT MUSCLES. Published online 2000. doi:10.1002/(SICI)1097-4598(200004)23:4

37. Cornelison DDW, Wold BJ. Single-cell analysis of regulatory gene expression in quiescent and activated mouse skeletal muscle satellite cells. *Dev Biol*. 1997;191(2):270-283. doi:10.1006/DBIO.1997.8721

38. Wozniak AC, Kong J, Bock E, Pilipowicz O, Anderson JE. Signaling satellite-cell activation in skeletal muscle: markers, models, stretch, and potential alternate pathways. *Muscle Nerve*. 2005;31(3):283-300. doi:10.1002/MUS.20263

39. Egan B, Zierath JR. Exercise metabolism and the molecular regulation of skeletal muscle adaptation. *Cell Metab*. 2013;17(2):162-184. doi:10.1016/J.CMET.2012.12.012

40. Seene T, Kaasik P. Biological Characteristics of Structural and Functional Remodelling in Skeletal Muscle: Effect of Exercise. *Adv Stud Biol*. 2013;5(6):251-278. doi:10.12988/asb.2013.327

41. White AT, Schenk S. NAD(+)/NADH and skeletal muscle mitochondrial adaptations to exercise. *Am J Physiol Endocrinol Metab*. 2012;303(3). doi:10.1152/AJPENDO.00054.2012

42. Jensen J, Rustad PI, Kolnes AJ, Lai YC. The Role of Skeletal Muscle Glycogen Breakdown for Regulation of Insulin Sensitivity by Exercise. *Front Physiol*. 2011;2. doi:10.3389/FPHYS.2011.00112

43. Goodpaster BH, Sparks LM. Metabolic Flexibility in Health and Disease. *Cell Metab*. 2017;25(5):1027-1036. doi:10.1016/J.CMET.2017.04.015

44. Jensen MD. Fate of fatty acids at rest and during exercise: regulatory mechanisms. *Acta Physiol Scand*. 2003;178(4):385-390. doi:10.1046/J.1365-201X.2003.01167.X

45. Lundsgaard AM, Fritzen AM, Kiens B. Molecular Regulation of Fatty Acid Oxidation in Skeletal Muscle during Aerobic Exercise. *Trends Endocrinol Metab*. 2018;29(1):18-30. doi:10.1016/J.TEM.2017.10.011

46. Galgani J, Ravussin E. Energy metabolism, fuel selection and body weight regulation. *Int J Obes (Lond)*. 2008;32 Suppl 7(Suppl 7). doi:10.1038/IJO.2008.246

47. Abbott WGH, Howard B v., Christin L, et al. Short-term energy balance: relationship with protein, carbohydrate, and fat balances. *Am J Physiol*. 1988;255(3 Pt 1). doi:10.1152/AJPENDO.1988.255.3.E332

48. Hettling H, van Beek JHGM. Analyzing the functional properties of the creatine kinase system with multiscale “sloppy” modeling. *PLoS Comput Biol*. 2011;7(8). doi:10.1371/JOURNAL.PCBI.1002130

49. Ponticos M, Lu QL, Morgan JE, Hardie DG, Partridge TA, Carling D. Dual regulation of the AMP-activated protein kinase provides a novel mechanism for the control of creatine kinase in skeletal muscle. *EMBO J*. 1998;17(6):1688. doi:10.1093/EMBOJ/17.6.1688

50. Baird MF, Graham SM, Baker JS, Bickerstaff GF. Creatine-Kinase- and Exercise-Related Muscle Damage Implications for Muscle Performance and Recovery. *J Nutr Metab*. 2012;2012:13. doi:10.1155/2012/960363

51. Vollestad NK, Blom PCS. Effect of varying exercise intensity on glycogen depletion in human muscle fibres. *Acta Physiol Scand*. 1985;125(3):395-405. doi:10.1111/J.1748-1716.1985.TB07735.X

52. Huckabee WE. RELATIONSHIPS OF PYRUVATE AND LACTATE DURING ANAEROBIC METABOLISM. I. EFFECTS OF INFUSION OF PYRUVATE OR GLUCOSE AND OF HYPERVENTILATION. *Journal of Clinical Investigation*. 1958;37(2):244. doi:10.1172/JCI103603

53. Felig P, Pozefsk T, Marlis E, Cahill GF. Alanine: key role in gluconeogenesis. *Science*. 1970;167(3920):1003-1004. doi:10.1126/SCIENCE.167.3920.1003

54. McCommis KS, Finck BN. Mitochondrial pyruvate transport: a historical perspective and future research directions. *Biochemical Journal*. 2015;466(3):443-454. doi:10.1042/BJ20141171

55. Utter MF, Keech DB. Formation of Oxaloacetate from Pyruvate and CO2. *Journal of Biological Chemistry*. 1960;235(5):PC17-PC18. doi:10.1016/S0021-9258(18)69442-6

56. Mitchell P, Moyle J. Chemiosmotic hypothesis of oxidative phosphorylation. *Nature*. 1967;213(5072):137-139. doi:10.1038/213137a0

57. Sacchetti M, Saltin B, Osada T, van Hall G. Intramuscular fatty acid metabolism in contracting and non-contracting human skeletal muscle. *J Physiol*. 2002;540(Pt 1):387. doi:10.1113/JPHYSIOL.2001.013912

58. van Hall G. The Physiological Regulation of Skeletal Muscle Fatty Acid Supply and Oxidation During Moderate-Intensity Exercise. *Sports Medicine*. 2015;45(1):23-32. doi:10.1007/S40279-015-0394-8/FIGURES/2

59. Laffel L. Ketone Bodies: a Review of Physiology, Pathophysiology and Application of Monitoring to Diabetes. *Diabetes Metab Res Rev*. 1999;15(6):412-426. doi:10.1002/(SICI)1520-7560(199911/12)15:6

60. Adibi SA, Modesto TA, Morse EL, Amin PM. Amino acid levels in plasma, liver, and skeletal muscle during protein deprivation. *American Journal of Physiology*. 1973;225(2):408-414. doi:10.1152/ajplegacy.1973.225.2.408

61. Wagenmakers AJM. Protein and amino acid metabolism in human muscle. *Adv Exp Med Biol*. 1998;441:307-319. doi:10.1007/978-1-4899-1928-1_28

62. Wilkinson DJ, Piasecki M, Atherton PJ. The age-related loss of skeletal muscle mass and function: Measurement and physiology of muscle fibre atrophy and muscle fibre loss in humans. *Ageing Res Rev*. 2018;47:123-132. doi:10.1016/J.ARR.2018.07.005

63. Pisters PWT, Brennan MF. Amino acid metabolism in human cancer cachexia. *Annu Rev Nutr*. 1990;10(1):107-132. doi:10.1146/ANNUREV.NU.10.070190.000543

64. Nakamoto RK, Baylis Scanlon JA, Al-Shawi MK. The Rotary Mechanism of the ATP Synthase. *Arch Biochem Biophys*. 2008;476(1):43. doi:10.1016/J.ABB.2008.05.004

65. Rich PR. The molecular machinery of Keilin's respiratory chain. *Biochem Soc Trans*. 2003;31(Pt 6):1095-1105. doi:10.1042/BST0311095

66. Davies KJ. Oxidative stress: the paradox of aerobic life. *Biochem Soc Symp*. 1995;61:1-31. doi:10.1042/BSS0610001/50002

67. Rattan SIS. Theories of biological aging: genes, proteins, and free radicals. *Free Radic Res*. 2006;40(12):1230-1238. doi:10.1080/10715760600911303

68. Valko M, Leibfritz D, Moncol J, Cronin MTD, Mazur M, Telser J. Free radicals and antioxidants in normal physiological functions and human disease. *Int J Biochem Cell Biol*. 2007;39(1):44-84. doi:10.1016/J.BIOCEL.2006.07.001

69. Breen L, Stokes KA, Churchward-Venne TA, et al. Two weeks of reduced activity decreases leg lean mass and induces "anabolic resistance" of myofibrillar protein synthesis in healthy elderly. *J Clin Endocrinol Metab*. 2013;98(6):2604-2612. doi:10.1210/JC.2013-1502

70. McCormick R, Vasilaki A. Age-related changes in skeletal muscle: changes to life-style as a therapy. *Biogerontology*. 2018;19(6):519-536. doi:10.1007/S10522-018-9775-3

71. Gehlert S, Weinisch P, Römisch-Margl W, et al. Effects of Acute and Chronic Resistance Exercise on the Skeletal Muscle Metabolome. *Metabolites*. 2022;12(5). doi:10.3390/METABO12050445

72. Leuchtmann AB, Adak V, Dilbaz S, Handschin C. The Role of the Skeletal Muscle Secretome in Mediating Endurance and Resistance Training Adaptations. *Front Physiol*. 2021;12:1296. doi:10.3389/FPHYS.2021.709807/BIBTEX

73. Taanman JW. The mitochondrial genome: structure, transcription, translation and replication. *Biochim Biophys Acta*. 1999;1410(2):103-123. doi:10.1016/S0005-2728(98)00161-3

74. Anderson S, Bankier AT, Barrell BG, et al. Sequence and organization of the human mitochondrial genome. *Nature 1981 290:5806*. 1981;290(5806):457-465. doi:10.1038/290457a0

75. Holloszy JO. Biochemical Adaptations in Muscle: EFFECTS OF EXERCISE ON MITOCHONDRIAL OXYGEN UPTAKE AND RESPIRATORY ENZYME ACTIVITY IN SKELETAL MUSCLE. *Journal of Biological Chemistry*. 1967;242(9):2278-2282. doi:10.1016/S0021-9258(18)96046-1

76. Bruce CR, Kriketos AD, Cooney GJ, Hawley JA. Disassociation of muscle triglyceride content and insulin sensitivity after exercise training in patients with Type 2 diabetes. *Diabetologia*. 2004;47(1):23-30. doi:10.1007/S00125-003-1265-7

77. López-Lluch G, Hunt N, Jones B, et al. Calorie restriction induces mitochondrial biogenesis and bioenergetic efficiency. *Proc Natl Acad Sci U S A*. 2006;103(6):1768. doi:10.1073/PNAS.0510452103

78. Hood DA, Memme JM, Oliveira AN, Triolo M. Maintenance of Skeletal Muscle Mitochondria in Health, Exercise, and Aging. *Annu Rev Physiol*. 2019;81:19-41. doi:10.1146/ANNUREV-PHYSIOL-020518-114310

79. Wright DC, Geiger PC, Han DH, Jones TE, Holloszy JO. Calcium Induces Increases in Peroxisome Proliferator-activated Receptor γ Coactivator-1α and Mitochondrial Biogenesis by a Pathway Leading to p38 Mitogen-activated Protein Kinase Activation. *Journal of Biological Chemistry*. 2007;282(26):18793-18799. doi:10.1074/JBC.M611252200

80. Jäer S, Handschin C, St-Pierre J, Spiegelman BM. AMP-activated protein kinase (AMPK) action in skeletal muscle via direct phosphorylation of PGC-1α. *Proc Natl Acad Sci U S A*. 2007;104(29):12017. doi:10.1073/PNAS.0705070104

81. Rodgers JT, Lerin C, Haas W, Gygi SP, Spiegelman BM, Puigserver P. Nutrient control of glucose homeostasis through a complex of PGC-1α and SIRT1. *Nature 2005 434:7029*. 2005;434(7029):113-118. doi:10.1038/nature03354

82. Taherzadeh-Fard E, Saft C, Akkad DA, et al. PGC-1alpha downstream transcription factors NRF-1 and TFAM are genetic modifiers of Huntington disease. *Mol Neurodegener*. 2011;6(1):32. doi:10.1186/1750-1326-6-32

83. Sun N, Youle RJ, Finkel T. The Mitochondrial Basis of Aging. *Mol Cell*. 2016;61(5):654-666. doi:10.1016/J.MOLCEL.2016.01.028

84. Sivitz WI, Yorek MA. Mitochondrial dysfunction in diabetes: from molecular mechanisms to functional significance and therapeutic opportunities. *Antioxid Redox Signal*. 2010;12(4):537-577. doi:10.1089/ARS.2009.2531

85. IJ M. Autoimmune disease and mitochondrial dysfunction in chronic diseases. *Research on Chronic Diseases*. 2017;1(1):010–0012-. Accessed November 11, 2022. https://www.openaccessjournals.com/articles/autoimmune-disease-and-mitochondrial-dysfunction-in-chronic-diseases-12187.html

86. Ballinger SW. Mitochondrial dysfunction in cardiovascular disease. *Free Radic Biol Med*. 2005;38(10):1278-1295. doi:10.1016/J.FREERADBIOMED.2005.02.014

87. Clark EH, de la Torre AV, Hoshikawa T, Briston T. Targeting mitophagy in Parkinson's disease. *J Biol Chem*. 2021;296. doi:10.1074/JBC.REV120.014294

88. Harden A, Young W. The alcoholic ferment of yeast-juice. *Proceedings of the Royal Society of London Series B, Containing Papers of a Biological Character*. Published online 1906. doi:10.1098/rspb.1906.0029

89. Berger F, Ramírez-Hernández MH, Ziegler M. The new life of a centenarian: signalling functions of NAD(P). *Trends Biochem Sci*. 2004;29(3):111-118. doi:10.1016/J.TIBS.2004.01.007

90. Koehn CJ, Elvehjem CA. FURTHER STUDIES ON THE CONCENTRATION OF THE ANTIPELLAGRA FACTOR. *Journal of Biological Chemistry*. 1937;118(3):693-699. doi:10.1016/S0021-9258(18)74475-X

91. Katsyuba E, Romani M, Hofer D, Auwerx J. NAD+ homeostasis in health and disease. *Nat Metab*. Published online 2020. doi:10.1038/s42255-019-0161-5

92. Tedeschi PM, Bansal N, Kerrigan JE, Abali EE, Scotto KW, Bertino JR. NAD+ Kinase as a Therapeutic Target in Cancer. *Clin Cancer Res*. 2016;22(21):5189-5195. doi:10.1158/1078-0432.CCR-16-1129

93. Geiszt M. NADPH oxidases: new kids on the block. *Cardiovasc Res*. 2006;71(2):289-299. doi:10.1016/J.CARDIORES.2006.05.004

94. Fernandez-Marcos PJ, Nóbrega-Pereira S. NADPH: new oxygen for the ROS theory of aging. *Oncotarget*. 2016;7(32):50814-50815. doi:10.18632/ONCOTARGET.10744

95. Okabe K, Yaku K, Tobe K, Nakagawa T. Implications of altered NAD metabolism in metabolic disorders. *J Biomed Sci*. Published online 2019. doi:10.1186/s12929-019-0527-8

96. Fletcher RS, Ratajczak J, Doig CL, et al. Nicotinamide riboside kinases display redundancy in mediating nicotinamide mononucleotide and nicotinamide riboside metabolism in skeletal muscle cells. *Mol Metab*. Published online 2017. doi:10.1016/j.molmet.2017.05.011

97. Doig CL, Zielinska AE, Fletcher RS, et al. Induction of the nicotinamide riboside kinase NAD+ salvage pathway in a model of sarcoplasmic reticulum dysfunction. *Skelet Muscle*. 2020;10(1). doi:10.1186/S13395-019-0216-Z

98. Bieganowski P, Brenner C. Discoveries of nicotinamide riboside as a nutrient and conserved NRK genes establish a preiss-handler independent route to NAD+ in fungi and humans. *Cell*. Published online 2004. doi:10.1016/S0092-8674(04)00416-7

99. Lin H, Kwan AL, Dutcher SK. Synthesizing and Salvaging NAD+: Lessons Learned from Chlamydomonas reinhardtii. *PLoS Genet*. 2010;6(9):e1001105. doi:10.1371/JOURNAL.PGEN.1001105

100. Zhang J, Tao J, Ling Y, et al. Switch of NAD Salvage to de novo Biosynthesis Sustains SIRT1-RelB-Dependent Inflammatory Tolerance. *Front Immunol*. Published online 2019. doi:10.3389/fimmu.2019.02358

101. Dall M, Trammell SAJ, Asping M, et al. Mitochondrial function in liver cells is resistant to perturbations in NAD+ salvage capacity. *J Biol Chem*. 2019;294(36):13304-13326. doi:10.1074/JBC.RA118.006756

102. Mesquita I, Varela P, Belinha A, et al. Exploring NAD+ metabolism in host–pathogen interactions. *Cellular and Molecular Life Sciences 2015 73:6*. 2015;73(6):1225-1236. doi:10.1007/S00018-015-2119-4

103. Ryu KW, Nandu T, Kim J, Challa S, DeBerardinis RJ, Lee Kraus W. Metabolic regulation of transcription through compartmentalized NAD+ biosynthesis. *Science (1979)*. 2018;360(6389). doi:10.1126/science.aan5780

104. Cambronne XA, Stewart ML, Kim D, et al. Biosensor reveals multiple sources for mitochondrial NAD+. *Science (1979)*. Published online 2016. doi:10.1126/science.aad5168

105. Cambronne XA, Kraus WL. Location, Location, Location: Compartmentalization of NAD+ Synthesis and Functions in Mammalian Cells. *Trends Biochem Sci*. 2020;45(10):858. doi:10.1016/J.TIBS.2020.05.010

106. Cantó C, Houtkooper RH, Pirinen E, et al. The NAD+ precursor nicotinamide riboside enhances oxidative metabolism and protects against high-fat diet-induced obesity. *Cell Metab*. 2012;15(6):838. doi:10.1016/j.cmet.2012.04.022

107. Klimova N, Long A, Kristian T. Nicotinamide mononucleotide alters mitochondrial dynamics by SIRT3-dependent mechanism in male mice. *J Neurosci Res*. Published online 2019. doi:10.1002/jnr.24397

108. Luongo TS, Eller JM, Lu MJ, et al. SLC25A51 is a mammalian mitochondrial NAD+ transporter. *Nature*. 2020;588(7836):174. doi:10.1038/s41586-020-2741-7

109. Davila A, Liu L, Chellappa K, et al. Nicotinamide adenine dinucleotide is transported into mammalian mitochondria. *Elife*. Published online 2018. doi:10.7554/eLife.33246

110. Rajman L, Chwalek K, Sinclair DA. Therapeutic Potential of NAD-Boosting Molecules: The In Vivo Evidence. *Cell Metab*. 2018;27(3):529-547. doi:10.1016/J.CMET.2018.02.011

111. Rivas DA, Fielding RA. Skeletal Muscle. *Encyclopedia of Human Nutrition*. 2013;4-4:193-199. doi:10.1016/B978-0-12-375083-9.00188-4

112. Li J, Bonkowski MS, Moniot S, et al. A conserved NAD+ binding pocket that regulates protein-protein interactions during aging. *Science*. 2017;355(6331):1312. doi:10.1126/SCIENCE.AAD8242

113. Gulshan M, Yaku K, Okabe K, et al. Overexpression of Nmnat3 efficiently increases NAD and NGD levels and ameliorates age-associated insulin resistance. *Aging Cell*. 2018;17(4). doi:10.1111/ACEL.12798

114. Yeo D, Kang C, Ji LL. Aging alters acetylation status in skeletal and cardiac muscles. *Geroscience*. 2020;42(3):963. doi:10.1007/S11357-020-00171-7

115. Mao K, Chen J, Yu H, et al. Poly (ADP-ribose) polymerase 1 inhibition prevents neurodegeneration and promotes α-synuclein degradation via transcription factor EB-dependent autophagy in mutant α-synucleinA53T model of Parkinson's disease. *Aging Cell*. 2020;19(6). doi:10.1111/ACEL.13163

116. Tan A, Doig CL. NAD+ Degrading Enzymes, Evidence for Roles During Infection. *Front Mol Biosci*. 2021;8:803. doi:10.3389/fmolb.2021.697359

117. Braidy N, Berg J, Clement J, et al. Role of Nicotinamide Adenine Dinucleotide and Related Precursors as Therapeutic Targets for Age-Related Degenerative Diseases: Rationale, Biochemistry, Pharmacokinetics, and Outcomes. *Antioxid Redox Signal*. 2019;30(2):251-294. doi:10.1089/ARS.2017.7269

118. Yu HB, Jiang H, Cheng ST, Hu ZW, Ren JH, Chen J. AGK2, A SIRT2 inhibitor, inhibits hepatitis B virus replication in vitro and in vivo. *Int J Med Sci*. 2018;15(12):1356-1364. doi:10.7150/IJMS.26125

119. Doig CL, Lavery GG. PARP Inhibitors: Staying on Target? *Cell Chem Biol*. 2016;23(12):1442-1443. doi:10.1016/J.CHEMBIOL.2016.12.003

120. Mateo J, Lord CJ, Serra V, et al. A decade of clinical development of PARP inhibitors in perspective. *Ann Oncol*. 2019;30(9):1437-1447. doi:10.1093/ANNONC/MDZ192

121. Gardell SJ, Hopf M, Khan A, et al. Boosting NAD+ with a small molecule that activates NAMPT. *Nature Communications 2019 10:1*. 2019;10(1):1-12. doi:10.1038/s41467-019-11078-z

122. Duan FX, Shi YJ, Chen J, et al. Feature article: Neuroprotective effects of P7C3 against spinal cord injury in rats. *Exp Biol Med*. 2019;244(18):1680-1687. doi:10.1177/1535370219888620/ASSET/IMAGES/LARGE/10.1177_1535370219888620-FIG2.JPEG

123. Wang G, Han T, Nijhawan D, et al. P7C3 neuroprotective chemicals function by activating the rate-limiting enzyme in NAD salvage. *Cell*. 2014;158(6):1324-1334. doi:10.1016/J.CELL.2014.07.040

124. Takaso Y, Noda M, Hattori T, et al. Deletion of CD38 and supplementation of NAD+ attenuate axon degeneration in a mouse facial nerve axotomy model.

Scientific Reports 2020 10:1. 2020;10(1):1-12. doi:10.1038/s41598-020-73984-3

125. Dellinger RW, Santos SR, Morris M, et al. Repeat dose NRPT (nicotinamide riboside and pterostilbene) increases NAD+ levels in humans safely and sustainably: a randomized, double-blind, placebo-controlled study. *npj Aging and Mechanisms of Disease 2017 3:1*. 2017;3(1):1-9. doi:10.1038/s41514-017-0016-9

126. Elhassan YS, Kluckova K, Fletcher RS, et al. Nicotinamide Riboside Augments the Aged Human Skeletal Muscle NAD+ Metabolome and Induces Transcriptomic and Anti-inflammatory Signatures. *Cell Rep*. Published online 2019. doi:10.1016/j.celrep.2019.07.043

127. Martens CR, Denman BA, Mazzo MR, et al. Chronic nicotinamide riboside supplementation is well-tolerated and elevates NAD+ in healthy middle-aged and older adults. *Nature Communications 2018 9:1*. 2018;9(1):1-11. doi:10.1038/s41467-018-03421-7

128. Oakey LA, Fletcher RS, Elhassan YS, et al. Metabolic tracing reveals novel adaptations to skeletal muscle cell energy production pathways in response to NAD + depletion. *Wellcome Open Res*. 2019;3. doi:10.12688/WELLCOMEOPENRES.14898.2

129. Giroud-Gerbetant J, Joffraud M, Giner MP, et al. A reduced form of nicotinamide riboside defines a new path for NAD+ biosynthesis and acts as an orally bioavailable NAD+ precursor. *Mol Metab*. Published online 2019. doi:10.1016/j.molmet.2019.09.013

130. Yang Y, Mohammed FS, Zhang N, Sauve AA. Dihydronicotinamide riboside is a potent NAD+ concentration enhancer in vitro and in vivo. *J Biol Chem*. 2019;294(23):9295-9307. doi:10.1074/JBC.RA118.005772

131. Bai P, Cantó C, Oudart H, et al. PARP-1 inhibition increases mitochondrial metabolism through SIRT1 activation. 2011;13(4):461-468. Accessed September 17, 2021. https://pubmed.ncbi.nlm.nih.gov/21459330/

132. Pirinen E, Cantó C, Jo YS, et al. Pharmacological Inhibition of poly(ADP-ribose) polymerases improves fitness and mitochondrial function in skeletal muscle. *Cell Metab*. 2014;19(6):1034-1041. doi:10.1016/J.CMET.2014.04.002

133. Mohamed JS, Wilson JC, Myers MJ, Sisson KJ, Alway SE. Dysregulation of SIRT-1 in aging mice increases skeletal muscle fatigue by a PARP-1-dependent mechanism. *Aging*. 2014;6(10):820-834. doi:10.18632/aging.100696

134. Mukhopadhyay P, Horváth B, Rajesh M, et al. PARP inhibition protects against alcoholic and non-alcoholic steatohepatitis. *J Hepatol*. 2017;66(3):589-600. doi:10.1016/J.JHEP.2016.10.023

135. Parvin S, Ramirez-Labrada A, Aumann S, et al. LMO2 confers synthetic lethality to PARP inhibition in DLBCL. *Cancer Cell*. 2019;36(3):237. doi:10.1016/J.CCELL.2019.07.007

136. Pazzaglia S, Pioli C. Multifaceted Role of PARP-1 in DNA Repair and Inflammation: Pathological and Therapeutic Implications in Cancer and Non-Cancer Diseases. *Cells*. 2019;9(1). doi:10.3390/CELLS9010041

137. Boslett J, Helal M, Chini E, Zweier JL. Genetic deletion of CD38 confers post-ischemic myocardial protection through preserved pyridine nucleotides. *J Mol Cell Cardiol*. 2018;118:81-94. doi:10.1016/J.YJMCC.2018.02.015

138. Boslett J, Hemann C, Zhao YJ, Lee HC, Zweier JL. Luteolinidin Protects the Postischemic Heart through CD38 Inhibition with Preservation of NAD(P)(H). *J Pharmacol Exp Ther*. 2017;361(1):99-108. doi:10.1124/JPET.116.239459

139. Isatuximab, Lenalidomide, Bortezomib, and Dexamethasone in NDMM - Full Text View - ClinicalTrials.gov. Accessed January 23, 2023. https://clinicaltrials.gov/ct2/show/NCT04653246

140. Xiong X, Yu J, Fan R, et al. NAMPT overexpression alleviates alcohol-induced hepatic steatosis in mice. *PLoS One*. 2019;14(2). doi:10.1371/JOURNAL.PONE.0212523

141. Hsu CP, Oka S, Shao D, Hariharan N, Sadoshima J. Nicotinamide phosphoribosyltransferase regulates cell survival through NAD+ synthesis in cardiac myocytes. *Circ Res*. 2009;105(5):481-491. doi:10.1161/CIRCRESAHA.109.203703

142. Gerdts J, Brace EJ, Sasaki Y, DiAntonio A, Milbrandt J. SARM1 activation triggers axon degeneration locally via NAD+ destruction. *Science (1979)*. Published online 2015. doi:10.1126/science.1258366

143. Yu A, Zhou R, Xia B, Dang W, Yang Z, Chen X. NAMPT maintains mitochondria content via NRF2-PPARα/AMPKα pathway to promote cell survival under oxidative stress. *Cell Signal*. 2020;66. doi:10.1016/J.CELLSIG.2019.109496

144. Audrito V, Managò A, Gaudino F, et al. NAD-Biosynthetic and Consuming Enzymes as Central Players of Metabolic Regulation of Innate and Adaptive Immune Responses in Cancer. *Front Immunol*. Published online 2019. doi:10.3389/fimmu.2019.01720

145. Lucena-Cacace A, Otero-Albiol D, Jiménez-García MP, Peinado-Serrano J, Carnero A. NAMPT overexpression induces cancer stemness and defines a novel tumor signature for glioma prognosis. *Oncotarget*. 2017;8(59):99514. doi:10.18632/ONCOTARGET.20577

146. Wang B, Hasan MK, Alvarado E, Yuan H, Wu H, Chen WY. NAMPT overexpression in prostate cancer and its contribution to tumor cell survival and stress response. *Oncogene*. 2011;30(8):907-921. doi:10.1038/ONC.2010.468

147. Williams PA, Harder JM, Foxworth NE, et al. Vitamin B3 modulates mitochondrial vulnerability and prevents glaucoma in aged mice. *Science*. 2017;355(6326):756-760. doi:10.1126/SCIENCE.AAL0092

148. Zhai RG, Cao Y, Hiesinger PR, et al. Drosophila NMNAT Maintains Neural Integrity Independent of Its NAD Synthesis Activity. *PLoS Biol*. 2006;4(12):e416. doi:10.1371/JOURNAL.PBIO.0040416

149. Cai Y, Yu SS, Chen SR, et al. Nmnat2 protects cardiomyocytes from hypertrophy via activation of SIRT6. *FEBS Lett*. 2012;586(6):866-874. doi:10.1016/J.FEBSLET.2012.02.014

150. Chen L, Nye DM, Stone MC, et al. Mitochondria and Caspases Tune Nmnat-Mediated Stabilization to Promote Axon Regeneration. *PLoS Genet*. Published online 2016. doi:10.1371/journal.pgen.1006503

151. Liu X, Liu M, Tang C, et al. Overexpression of Nmnat improves the adaption of health span in aging Drosophila. *Exp Gerontol*. 2018;108:276-283. doi:10.1016/j.exger.2018.04.026

152. Zhu Y, Li C, Tao X, et al. Nmnat restores neuronal integrity by neutralizing mutant Huntingtin aggregate-induced progressive toxicity. *Proc Natl Acad Sci U S A*. 2019;116(38):19165-19175. doi:10.1073/PNAS.1904563116

153. Fujimura S, Hasegawa S, Shimizu Y, Sugimura T. Polymerization of the adenosine 5′-diphosphate-ribose moiety of nicotinamide-adenine dinucleotide by nuclear enzyme. *BBA Section Nucleic Acids And Protein Synthesis*. Published online 1967. doi:10.1016/0005-2787(67)90043-3

154. Chambon P, Weill JD, Mandel P. Nicotinamide mononucleotide activation of a new DNA-dependent polyadenylic acid synthesizing nuclear enzyme. *Biochem Biophys Res Commun*. Published online 1963. doi:10.1016/0006-291X(63)90024-X

155. Chambon P, Weill JD, Doly J, Strosser MT, Mandel P. On the formation of a novel adenylic compound by enzymatic extracts of liver nuclei. *Biochem Biophys Res Commun*. Published online 1966. doi:10.1016/0006-291X(66)90502-X

156. Nishizuka Y, Ueda K, Nakazawa K, Hayaishi O. Studies on the polymer of adenosine diphosphate ribose. I. Enzymic formation from nicotinamide adenine dinuclotide in mammalian nuclei. *Journal of Biological Chemistry*. Published online 1967. doi:10.1016/S0021-9258(18)95947-8

157. Doly J, Petek F. Etude de la structure d'un compose "poly(ADP-ribose" synthetise par des extraits nucleaires de foie de poulet. *C R Hebd Seances Acad Sci Ser D Sci Nat*. 1966;263:1341-1344.

158. Nishizuka Y, Ueda K, Honjo T, Hayaishi O. Enzymic adenosine diphosphate ribosylation of histone and poly adenosine diphosphate ribose synthesis in rat liver nuclei. *Journal of Biological Chemistry*. Published online 1968. doi:10.1016/S0021-9258(19)34205-X

159. Ueda K, Reeder RH, Honjo T, Nishizuka Y, Hayaishi O. Poly adenosine diphosphate ribose synthesis associated with chromatin. *Biochem Biophys Res Commun*. 1968;31(3):379-385. doi:10.1016/0006-291X(68)90486-5

160. Vyas S, Matic I, Uchima L, et al. Family-wide analysis of poly(ADP-ribose) polymerase activity. *Nat Commun*. Published online 2014. doi:10.1038/ncomms5426

161. Niere M, Mashimo M, Agledal L, et al. ADP-ribosylhydrolase 3 (ARH3), not poly(ADP-ribose) glycohydrolase (PARG) isoforms, is responsible for

degradation of mitochondrial matrix-associated poly(ADP-ribose). *Journal of Biological Chemistry*. Published online 2012. doi:10.1074/jbc.M112.349183

162. Ruiz PD, Hamilton GA, Park JW, Gamble MJ. MacroH2A1 Regulation of Poly(ADP-Ribose) Synthesis and Stability Prevents Necrosis and Promotes DNA Repair. *Mol Cell Biol*. Published online 2019. doi:10.1128/mcb.00230-19

163. Krietsch J, Rouleau M, Pic É, et al. Reprogramming cellular events by poly(ADP-ribose)-binding proteins. *Mol Aspects Med*. 2013;34(6):1066-1087. doi:10.1016/J.MAM.2012.12.005

164. Héberlé E, Amé JC, Illuzzi G, Dantzer F, Schreiber V. Discovery of the parp superfamily and focus on the lesser exhibited but not lesser talented members. *Cancer Drug Discovery and Development*. Published online 2015. doi:10.1007/978-3-319-14151-0_2

165. Bai P. Biology of Poly(ADP-Ribose) Polymerases: The Factotums of Cell Maintenance. *Mol Cell*. Published online 2015. doi:10.1016/j.molcel.2015.01.034

166. Xu F, Sun Y, Yang SZ, et al. Cytoplasmic PARP-1 promotes pancreatic cancer tumorigenesis and resistance. *Int J Cancer*. 2019;145(2):474. doi:10.1002/IJC.32108

167. Lee JH, Hussain M, Kim EW, et al. Mitochondrial PARP1 regulates NAD+-dependent poly ADP-ribosylation of mitochondrial nucleoids. *Experimental & Molecular Medicine 2022 54:12*. 2022;54(12):2135-2147. doi:10.1038/s12276-022-00894-x

168. Hopp AK, Teloni F, Bisceglie L, et al. Mitochondrial NAD+ Controls Nuclear ARTD1-Induced ADP-Ribosylation. *Mol Cell*. Published online January 14, 2021. doi:10.1016/j.molcel.2020.12.034

169. Langelier MF, Eisemann T, Riccio AA, Pascal JM. PARP family enzymes: regulation and catalysis of the poly(ADP-ribose) posttranslational modification. *Curr Opin Struct Biol*. Published online 2018. doi:10.1016/j.sbi.2018.11.002

170. Alemasova EE, Lavrik OI. Poly(ADP-ribosyl)ation by PARP1: Reaction mechanism and regulatory proteins. *Nucleic Acids Res*. Published online 2019. doi:10.1093/nar/gkz120

171. Rodríguez-Vargas JM, Oliver-Pozo FJ, Dantzer F. PARP1 and Poly(ADP-ribosyl)ation Signaling during Autophagy in Response to Nutrient Deprivation. *Oxid Med Cell Longev*. 2019;2019. doi:10.1155/2019/2641712

172. Zong W, Gong Y, Sun W, Li T, Wang ZQ. PARP1: Liaison of Chromatin Remodeling and Transcription. *Cancers 2022, Vol 14, Page 4162*. 2022;14(17):4162. doi:10.3390/CANCERS14174162

173. Gibson BA, Kraus WL. New insights into the molecular and cellular functions of poly(ADP-ribose) and PARPs. *Nature Reviews Molecular Cell Biology 2012 13:7*. 2012;13(7):411-424. doi:10.1038/nrm3376

174. Gupte R, Liu Z, Kraus WL. PARPs and ADP-ribosylation: recent advances linking molecular functions to biological outcomes. *Genes Dev*. 2017;31(2):101-126. doi:10.1101/GAD.291518.116

175. Kim DS, Challa S, Jones A, Kraus WL. PARPs and ADP-ribosylation in RNA biology: from RNA expression and processing to protein translation and proteostasis. *Genes Dev*. 2020;34(5-6):302-320. doi:10.1101/GAD.334433.119

176. Matteini F, Andresini O, Petrai S, Battistelli C, Rossi MN, Maione R. Poly(ADP-ribose) Polymerase 1 (PARP1) restrains MyoD-dependent gene expression during muscle differentiation. *Scientific Reports 2020 10:1*. 2020;10(1):1-18. doi:10.1038/s41598-020-72155-8

177. Ikejima M, Noguchi S, Yamashita R, et al. The zinc fingers of human poly(ADP-ribose) polymerase are differentially required for the recognition of DNA breaks and nicks and the consequent enzyme activation. Other structures recognize intact DNA. *Journal of Biological Chemistry*. 1990;265(35):21907-21913. doi:10.1016/S0021-9258(18)45824-3

178. Eustermann S, Videler H, Yang JC, et al. The DNA-Binding Domain of Human PARP-1 Interacts with DNA Single-Strand Breaks as a Monomer through Its Second Zinc Finger. *J Mol Biol*. 2011;407(1):149-170. doi:10.1016/J.JMB.2011.01.034

179. Langelier MF, Servent KM, Rogers EE, Pascal JM. A third zinc-binding domain of human poly(ADP-ribose) polymerase-1 coordinates DNA-dependent enzyme activation. *J Biol Chem*. 2008;283(7):4105-4114. doi:10.1074/JBC.M708558200

180. Tao Z, Gao P, Hoffman DW, Liu HW. Domain C of human poly(ADP-ribose) polymerase-1 is important for enzyme activity and contains a novel zinc-ribbon motif. *Biochemistry*. 2008;47(21):5804-5813. doi:10.1021/BI800018A/ASSET/IMAGES/LARGE/BI-2008-00018A_0009.JPEG

181. Eustermann S, Wu WF, Langelier MF, et al. Structural Basis of Detection and Signaling of DNA Single-Strand Breaks by Human PARP-1. *Mol Cell*. 2015;60(5):742-754. doi:10.1016/J.MOLCEL.2015.10.032

182. Ali AAE, Timinszky G, Arribas-Bosacoma R, et al. The zinc-finger domains of PARP1 cooperate to recognize DNA strand breaks. *Nat Struct Mol Biol*. 2012;19(7):685-692. doi:10.1038/NSMB.2335

183. Schreiber V, Molinete M, Boeuf H, de Murcia G, Menissier-de Murcia J. The human poly(ADP-ribose) polymerase nuclear localization signal is a bipartite element functionally separate from DNA binding and catalytic activity. *EMBO J*. 1992;11(9):3263-3269. doi:10.1002/J.1460-2075.1992.TB05404.X

184. Los M, Mozoluk M, Ferrari D, et al. Activation and caspase-mediated inhibition of PARP: a molecular switch between fibroblast necrosis and apoptosis in death receptor signaling. *Mol Biol Cell*. 2002;13(3):978-988. doi:10.1091/MBC.01-05-0272

185. Peng QL, Buz'Zard AR, Lau BHS. Pycnogenol® protects neurons from amyloid-β peptide-induced apoptosis. *Molecular Brain Research*. 2002;104(1):55-65. doi:10.1016/S0169-328X(02)00263-2

186. Leung CCY, Glover JNM. BRCT domains: Easy as one, two, three. *Cell Cycle*. 2011;10(15):2461. doi:10.4161/CC.10.15.16312

187. Masson M, Niedergang C, Schreiber V, Muller S, Menissier-de Murcia J, de Murcia G. XRCC1 is specifically associated with poly(ADP-ribose) polymerase and negatively regulates its activity following DNA damage. *Mol Cell Biol*. 1998;18(6):3563-3571. doi:10.1128/MCB.18.6.3563

188. Loeffler PA, Cuneo MJ, Mueller GA, Derose EF, Gabel SA, London RE. Structural studies of the PARP-1 BRCT domain. *BMC Struct Biol*. 2011;11. doi:10.1186/1472-6807-11-37

189. Buelow B, Uzunparmak B, Paddock M, Scharenberg AM. Structure/function analysis of PARP-1 in oxidative and nitrosative stress-induced monomeric ADPR formation. *PLoS One*. 2009;4(7). doi:10.1371/JOURNAL.PONE.0006339

190. Paddock MN, Buelow BD, Takeda S, Scharenberg AM. The BRCT Domain of PARP-1 Is Required for Immunoglobulin Gene Conversion. *PLoS Biol*. 2010;8(7):e1000428. doi:10.1371/JOURNAL.PBIO.1000428

191. Liu Y, Kadyrov FA, Modrich P. PARP-1 enhances the mismatch-dependence of 5′-directed excision in human mismatch repair in vitro. *DNA Repair (Amst)*. 2011;10(11):1145. doi:10.1016/J.DNAREP.2011.08.012

192. Na Z, Peng B, Ng S, et al. A small-molecule protein-protein interaction inhibitor of PARP1 that targets its BRCT domain. *Angew Chem Int Ed Engl*. 2015;54(8):2515-2519. doi:10.1002/ANIE.201410678

193. Dawicki-McKenna JM, Langelier MF, DeNizio JE, et al. PARP-1 Activation Requires Local Unfolding of an Autoinhibitory Domain. *Mol Cell*. 2015;60(5):755-768. doi:10.1016/J.MOLCEL.2015.10.013

194. Rudolph J, Mahadevan J, Dyer P, Luger K. Poly(ADP-ribose) polymerase 1 searches DNA via a 'monkey bar' mechanism. *Elife*. 2018;7. doi:10.7554/ELIFE.37818

195. Li X, Erden O, Li L, Ye Q, Wilson A, Du W. Binding to WGR Domain by Salidroside Activates PARP1 and Protects Hematopoietic Stem Cells from Oxidative Stress. *Antioxid Redox Signal*. 2014;20(12):1853. doi:10.1089/ARS.2013.5600

196. Huambachano O, Herrera F, Rancourt A, Satoh MS. Double-stranded DNA binding domain of poly(ADP-ribose) polymerase-1 and molecular insight into the regulation of its activity. *J Biol Chem*. 2011;286(9):7149-7160. doi:10.1074/JBC.M110.175190

197. Choi JR, Shin KS, Choi CY, Kang SJ. PARP1 regulates the protein stability and proapoptotic function of HIPK2. *Cell Death & Disease 2016 7:10*. 2016;7(10):e2438-e2438. doi:10.1038/cddis.2016.345

198. Langelier MF, Zandarashvili L, Aguiar PM, Black BE, Pascal JM. NAD+ analog reveals PARP-1 substrate-blocking mechanism and allosteric communication from catalytic center to DNA-binding domains. *Nat Commun*. 2018;9(1). doi:10.1038/S41467-018-03234-8

199. Steffen JD, Brody JR, Armen RS, Pascal JM. Structural Implications for Selective Targeting of PARPs. *Front Oncol*. 2013;3. doi:10.3389/FONC.2013.00301

200. Ding L, Chen X, Xu X, et al. PARP1 Suppresses the Transcription of PD-L1 by Poly(ADP-Ribosyl)ating STAT3. *Cancer Immunol Res*. 2019;7(1):136-149. doi:10.1158/2326-6066.CIR-18-0071

201. Gröschel S, Hübschmann D, Raimondi F, et al. Defective homologous recombination DNA repair as therapeutic target in advanced chordoma. *Nature Communications 2019 10:1*. 2019;10(1):1-9. doi:10.1038/s41467-019-09633-9

202. Rolli V, O'Farrell M, Ménissier-de Murcia J, de Murcia G. Random mutagenesis of the poly(ADP-ribose) polymerase catalytic domain reveals amino acids involved in polymer branching. *Biochemistry*. 1997;36(40):12147-12154. doi:10.1021/BI971055P/ASSET/IMAGES/LARGE/BI971055PF00005.JPEG

203. Krishnakumar R, Gamble MJ, Frizzell KM, Berrocal JG, Kininis M, Kraus WL. Reciprocal binding of PARP-1 and histone H1 at promoters specifies transcriptional outcomes. *Science*. 2008;319(5864):819-821. doi:10.1126/SCIENCE.1149250

204. Liu Z, Kraus WL. Catalytic-Independent Functions of PARP-1 Determine Sox2 Pioneer Activity at Intractable Genomic Loci. *Mol Cell*. 2017;65(4):589-603.e9. doi:10.1016/J.MOLCEL.2017.01.017

205. Jones A, Kraus WL. Multiomics analysis of the NAD +-PARP1 axis reveals a role for site-specific ADP-ribosylation in splicing in embryonic stem cells. *Genes Dev*. 2022;36(9-10):601-617. doi:10.1101/GAD.349335.121

206. Robaszkiewicz A, Qu C, Wisnik E, et al. ARTD1 regulates osteoclastogenesis and bone homeostasis by dampening NF-κB-dependent transcription of IL-1β. *Sci Rep*. 2016;6. doi:10.1038/SREP21131

207. Bisceglie L, Hopp AK, Gunasekera K, et al. MyoD induces ARTD1 and nucleoplasmic poly-ADP-ribosylation during fibroblast to myoblast transdifferentiation. *iScience*. 2021;24(5):102432. doi:10.1016/J.ISCI.2021.102432

208. Sharma V, Nand Pandey S, Khawaja H, Brown JK, Hathout Y, Chen YW. PARP1 Differentially Interacts with Promoter region of DUX4 Gene in FSHD Myoblasts. *J Genet Syndr Gene Ther*. 2016;7(4). doi:10.4172/2157-7412.1000303

209. Luo X, Ryu KW, Kim DS, et al. PARP-1 Controls the Adipogenic Transcriptional Program by PARylating C/EBPβ and Modulating Its Transcriptional Activity. 2017;65(2):260-271. doi:10.1016/J.MOLCEL.2016.11.015

210. Jubin T, Kadam A, Gani AR, Singh M, Dwivedi M, Begum R. Poly ADP-ribose polymerase-1: Beyond transcription and towards differentiation. *Semin Cell Dev Biol*. 2017;63:167-179. doi:10.1016/J.SEMCDB.2016.07.027

211. Azad GK, Swagatika S, Kumawat M, Kumawat R, Tomar RS. Modifying Chromatin by Histone Tail Clipping. *J Mol Biol*. 2018;430(18 Pt B):3051-3067. doi:10.1016/J.JMB.2018.07.013

212. Huletsky A, de Murcia G, Muller S, et al. The Effect of poly(ADP-ribosyl)ation on Native and H1-depleted Chromatin: A Role of Poly(ADP-ribosyl)ation on Core Nucleosome Structure. *Journal of Biological Chemistry*. 1989;264(15):8878-8886. doi:10.1016/S0021-9258(18)81875-0

213. Poirier GG, de Murcia G, Jongstra-Bilen J, Niedergang C, Mandel P. Poly(ADP-ribosyl)ation of polynucleosomes causes relaxation of chromatin structure. *Proc Natl Acad Sci U S A*. 1982;79(11):3423-3427. doi:10.1073/PNAS.79.11.3423

214. Martinez-Zamudio R, Ha HC. Histone ADP-ribosylation facilitates gene transcription by directly remodeling nucleosomes. *Mol Cell Biol*. 2012;32(13):2490-2502. doi:10.1128/MCB.06667-11

215. Gibbs-Seymour I, Fontana P, Rack JGM, Ahel I. HPF1/C4orf27 Is a PARP-1-Interacting Protein that Regulates PARP-1 ADP-Ribosylation Activity. *Mol Cell*. 2016;62(3):432-442. doi:10.1016/j.molcel.2016.03.008

216. Sutcu HH, Matta E, Ishchenko AA. Role of PARP-catalyzed ADP-ribosylation in the Crosstalk Between DNA Strand Breaks and Epigenetic Regulation. *J Mol Biol*. 2019;432(6):1769-1791. doi:10.1016/J.JMB.2019.12.019

217. Rudolph J, Roberts G, Muthurajan UM, Luger K. HPF1 and nucleosomes mediate a dramatic switch in activity of PARP1 from polymerase to hydrolase. *Elife*. 2021;10. doi:10.7554/ELIFE.65773

218. Gottschalk AJ, Trivedi RD, Conaway JW, Conaway RC. Activation of the SNF2 family ATPase ALC1 by poly(ADP-ribose) in a stable ALC1·PARP1·nucleosome intermediate. *J Biol Chem*. 2012;287(52):43527-43532. doi:10.1074/JBC.M112.401141

219. Ahel D, Hořejší Z, Wiechens N, et al. Poly(ADP-ribose)-dependent regulation of DNA repair by the chromatin remodeling enzyme ALC1. *Science*. 2009;325(5945):1240-1243. doi:10.1126/SCIENCE.1177321

220. Guetg C, Scheifele F, Rosenthal F, Hottiger MO, Santoro R. Inheritance of silent rDNA chromatin is mediated by PARP1 via noncoding RNA. *Mol Cell*. 2012;45(6):790-800. doi:10.1016/J.MOLCEL.2012.01.024

221. Matveeva EA, Al-Tinawi QMH, Rouchka EC, Fondufe-Mittendorf YN. Coupling of PARP1-mediated chromatin structural changes to transcriptional RNA polymerase II elongation and cotranscriptional splicing. *Epigenetics Chromatin*. 2019;12(1). doi:10.1186/S13072-019-0261-1

222. Matveeva EA, Mathbout LF, Fondufe-Mittendorf YN. PARP1 is a versatile factor in the regulation of mRNA stability and decay. *Sci Rep*. 2019;9(1). doi:10.1038/S41598-019-39969-7

223. Melikishvili M, Chariker JH, Rouchka EC, Fondufe-Mittendorf YN. Transcriptome-wide identification of the RNA-binding landscape of the chromatin-associated protein PARP1 reveals functions in RNA biogenesis. *Cell Discov*. 2017;3. doi:10.1038/CELLDISC.2017.43

224. Langelier MF, Planck JL, Roy S, Pascal JM. Structural basis for DNA damage-dependent poly(ADP-ribosyl)ation by human PARP-1. *Science*. 2012;336(6082):728-732. doi:10.1126/SCIENCE.1216338

225. Eleazer R, Fondufe-Mittendorf YN. The multifaceted role of PARP1 in RNA biogenesis. *Wiley Interdiscip Rev RNA*. 2021;12(2). doi:10.1002/WRNA.1617

226. Virág L, Salzman AL, Szabó C. Poly(ADP-ribose) synthetase activation mediates mitochondrial injury during oxidant-induced cell death. *J Immunol*. Published online 1998.

227. Moro L, Arbini AA, Marra E, Greco M. Mitochondrial DNA depletion reduces PARP-1 levels and promotes progression of the neoplastic phenotype in prostate carcinoma. *Cell Oncol*. 2008;30(4):307-322. doi:10.3233/CLO-2008-0427

228. Formentini L, Macchiarulo A, Cipriani G, et al. Poly(ADP-ribose) catabolism triggers AMP-dependent mitochondrial energy failure. *J Biol Chem*. 2009;284(26):17668-17676. doi:10.1074/JBC.M109.002931

229. Lehmann S, Costa AC, Celardo I, Loh SHY, Martins LM. Parp mutations protect against mitochondrial dysfunction and neurodegeneration in a PARKIN model of Parkinson's disease. *Cell Death Dis*. 2016;7(3). doi:10.1038/CDDIS.2016.72

230. Szczesny B, Brunyanszki A, Olah G, Mitra S, Szabo C. Opposing roles of mitochondrial and nuclear PARP1 in the regulation of mitochondrial and nuclear DNA integrity: implications for the regulation of mitochondrial function. *Nucleic Acids Res*. 2014;42(21):13161-13173. doi:10.1093/NAR/GKU1089

231. Gonzalez-Flores A, Aguilar-Quesada R, Siles E, et al. Interaction between PARP-1 and HIF-2α in the hypoxic response. *Oncogene*. 2014;33(7):891-898. doi:10.1038/ONC.2013.9

232. Fang EF, Scheibye-Knudsen M, Brace LE, et al. Defective mitophagy in XPA via PARP-1 hyperactivation and NAD(+)/SIRT1 reduction. *Cell*. 2014;157(4):882-896. doi:10.1016/J.CELL.2014.03.026

233. Asher G, Reinke H, Altmeyer M, Gutierrez-Arcelus M, Hottiger MO, Schibler U. Poly(ADP-ribose) polymerase 1 participates in the phase entrainment of circadian clocks to feeding. *Cell*. 2010;142(6):943-953. doi:10.1016/J.CELL.2010.08.016

234. Oliver FJ, Ménissier-de Murcia J, Nacci C, et al. Resistance to endotoxic shock as a consequence of defective NF-κB activation in poly (ADP-ribose) polymerase-1 deficient mice. *EMBO Journal*. Published online 1999. doi:10.1093/emboj/18.16.4446

235. Shou Q, Fu H, Huang X, Yang Y. PARP-1 controls NK cell recruitment to the site of viral infection. *JCI Insight*. 2019;4(12). doi:10.1172/jci.insight.121291

236. Pellat-Deceunynck C, Wietzerbin J, Drapier JC. Nicotinamide inhibits nitric oxide synthase mRNA induction in activated macrophages. *Biochemical Journal*. Published online 1994. doi:10.1042/bj2970053

237. Valdor R, Schreiber V, Saenz L, et al. Regulation of NFAT by poly(ADP-ribose) polymerase activity in T cells. *Mol Immunol*. Published online 2008. doi:10.1016/j.molimm.2007.10.044

238. Oei SL, Shi Y. Poly(adp-ribosyl)ation of transcription factor yin yang 1 under conditions of dna damage. *Biochem Biophys Res Commun*. 2001;285(1):27-31. doi:10.1006/bbrc.2001.5115

239. Szabó C, Lim LHK, Cuzzocrea S, et al. Inhibition of poly (ADP-ribose) synthetase attenuates neutrophil recruitment and exerts antiinflammatory effects. *Journal of Experimental Medicine*. Published online 1997. doi:10.1084/jem.186.7.1041

240. Lehmann M, Pirinen E, Mirsaidi A, et al. ARTD1-induced poly-ADP-ribose formation enhances PPARγ ligand binding and co-factor exchange. *Nucleic Acids Res*. 2015;43(1):129-142. doi:10.1093/NAR/GKU1260

241. Erener S, Mirsaidi A, Hesse M, et al. ARTD1 deletion causes increased hepatic lipid accumulation in mice fed a high-fat diet and impairs adipocyte function and differentiation. *The FASEB Journal*. 2012;26(6):2631-2638. doi:10.1096/FJ.11-200212

242. Jeon BT ak, Kim KE un, Heo RW on, et al. Myeloid-specific deletion of SIRT1 increases hepatic steatosis and hypothalamic inflammation in mice fed a high-fat diet. *Metab Brain Dis*. 2014;29(3):635-643. doi:10.1007/S11011-014-9542-3

243. Choi SE, Kwon S, Seok S, et al. Obesity-Linked Phosphorylation of SIRT1 by Casein Kinase 2 Inhibits Its Nuclear Localization and Promotes Fatty Liver. *Mol Cell Biol*. 2017;37(15). doi:10.1128/MCB.00006-17

244. Hans CP, Zerfaoui M, Naura AS, et al. Thieno[2,3-c]isoquinolin-5-one, a potent poly(ADP-ribose) polymerase inhibitor, promotes atherosclerotic plaque regression in high-fat diet-fed apolipoprotein E-deficient mice: effects on inflammatory markers and lipid content. *J Pharmacol Exp Ther*. 2009;329(1):150-158. doi:10.1124/JPET.108.145938

245. Morioka K, Tanaka K, Nokuo T, Ishizawa M, Ono T. Erythroid differentiation and poly(ADP-ribose) synthesis in Friend leukemia cells. *undefined*. Published online 1979. doi:10.20772/CANCERSCI1959.70.1_37

246. Francis G, Gray D, Berney J, Wing M, Guimaraes J, Hoffbrand A. Role of ADP-Ribosyl Transferase in Differentiation of Human Granulocyte-Macrophage Progenitors to the Macrophage Lineage. *Blood*. 1983;62(5):1055-1062. doi:10.1182/BLOOD.V62.5.1055.1055

247. Bhatia W, Kirkland JB, Meckling-Gill KA. Modulation of poly(ADP-ribose) polymerase during neutrophilic and monocytic differentiation of promyelocytic (NB4) and myelocytic (HL-60) leukaemia cells. *Biochem J*. 1995;308 (Pt 1)(Pt 1):131-137. doi:10.1042/BJ3080131

248. Wang Y, Zhang Y, Zhang S, et al. PARP1-mediated PARylation activity is essential for oligodendroglial differentiation and CNS myelination. *Cell Rep*. 2021;37(1). doi:10.1016/J.CELREP.2021.109695

249. Erener S, Hesse M, Kostadinova R, Hottiger MO. Poly(ADP-Ribose)Polymerase-1 (PARP1) Controls Adipogenic Gene Expression and Adipocyte Function. *Molecular Endocrinology*. 2012;26(1):79. doi:10.1210/ME.2011-1163

250. Devalaraja-Narashimha K, Padanilam BJ. PARP1 deficiency exacerbates diet-induced obesity in mice. *J Endocrinol*. 2010;205(3):243-252. doi:10.1677/JOE-09-0402

251. Oláh G, Szczesny B, Brunyánszki A, et al. Differentiation-Associated Downregulation of Poly(ADP-Ribose) Polymerase-1 Expression in Myoblasts Serves to Increase Their Resistance to Oxidative Stress. *PLoS One*. 2015;10(7):e0134227. doi:10.1371/JOURNAL.PONE.0134227

252. Klar AJS, Fogel S. Activation of mating type genes by transposition in Saccharomyces cerevisiae. *Proc Natl Acad Sci U S A*. Published online 1979. doi:10.1073/pnas.76.9.4539

253. Ivy JM, Klar AJ, Hicks JB. Cloning and characterization of four SIR genes of Saccharomyces cerevisiae. *Mol Cell Biol*. Published online 1986. doi:10.1128/mcb.6.2.688

254. Tanny JC, Dowd GJ, Huang J, Hilz H, Moazed D. An enzymatic activity in the yeast Sir2 protein that is essential for gene silencing. *Cell*. Published online 1999. doi:10.1016/S0092-8674(00)81671-2

255. Landry J, Sutton A, Tafrov ST, et al. The silencing protein SIR2 and its homologs are NAD-dependent protein deacetylases. *Proc Natl Acad Sci U S A*. Published online 2000. doi:10.1073/pnas.110148297

256. Kaeberlein M, McVey M, Guarente L. The SIR2/3/4 complex and SIR2 alone promote longevity in Saccharomyces cerevisiae by two different mechanisms. *Genes Dev*. Published online 1999. doi:10.1101/gad.13.19.2570

257. Yuan H, Marmorstein R. Structural basis for sirtuin activity and inhibition. *Journal of Biological Chemistry*. Published online 2012. doi:10.1074/jbc.R112.372300

258. Kasamatsu A, Nakao M, Smith BC, et al. Hydrolysis of O-acetyl-ADP-ribose isomers by ADP-ribosylhydrolase 3. *Journal of Biological Chemistry*. Published online 2011. doi:10.1074/jbc.M111.237636

259. Tong L, Denu JM. Function and metabolism of sirtuin metabolite O-acetyl-ADP-ribose. *Biochim Biophys Acta Proteins Proteom*. Published online 2010. doi:10.1016/j.bbapap.2010.02.007

260. Budayeva HG, Rowland EA, Cristea IM. Intricate Roles of Mammalian Sirtuins in Defense against Viral Pathogens. *J Virol*. 2016;90(1):5-8. doi:10.1128/jvi.03220-14

261. Huang JY, Hirschey MD, Shimazu T, Ho L, Verdin E. Mitochondrial sirtuins. *Biochim Biophys Acta*. 2010;1804(8):1645-1651. doi:10.1016/J.BBAPAP.2009.12.021

262. Scher MB, Vaquero A, Reinberg D. SirT3 is a nuclear NAD+-dependent histone deacetylase that translocates to the mitochondria upon cellular stress. *Genes Dev*. 2007;21(8):920-928. doi:10.1101/GAD.1527307

263. Wang C, Liu Y, Zhu Y, Kong C. Functions of mammalian SIRT4 in cellular metabolism and research progress in human cancer. *Oncol Lett*. 2020;20(4). doi:10.3892/OL.2020.11872

264. Du J, Zhou Y, Su X, et al. Sirt5 is a NAD-dependent protein lysine demalonylase and desuccinylase. *Science*. 2011;334(6057):806-809. doi:10.1126/SCIENCE.1207861

265. Feldman JL, Baeza J, Denu JM. Activation of the protein deacetylase SIRT6 by long-chain fatty acids and widespread deacylation by mammalian sirtuins. *J Biol Chem*. 2013;288(43):31350-31356. doi:10.1074/JBC.C113.511261

266. Blank MF, Grummt I. The seven faces of SIRT7. *Transcription*. 2017;8(2):67-74. doi:10.1080/21541264.2016.1276658

267. Wei W, Graeff R, Yue J. Roles and mechanisms of the CD38/cyclic adenosine diphosphate ribose/Ca 2+ signaling pathway. *World J Biol Chem*. 2014;5(1):58. doi:10.4331/wjbc.v5.i1.58

268. Glaría E, Valledor AF. Roles of CD38 in the Immune Response to Infection. *Cells*. 2020;9(1). doi:10.3390/cells9010228

269. Chini CCS, Peclat TR, Warner GM, et al. CD38 ecto-enzyme in immune cells is induced during aging and regulates NAD+ and NMN levels. *Nat Metab*. Published online 2020. doi:10.1038/s42255-020-00298-z

270. Tolomeo S, Chiao B, Lei Z, Chew SH, Ebstein RP. A Novel Role of CD38 and Oxytocin as Tandem Molecular Moderators of Human Social Behavior. *Neurosci Biobehav Rev*. 2020;115:251-272. doi:10.1016/J.NEUBIOREV.2020.04.013

271. Guedes AG, Dileepan M, Jude JA, Deshpande DA, Walseth TF, Kannan MS. Role of CD38/cADPR signaling in obstructive pulmonary diseases. *Curr Opin Pharmacol*. 2020;51:29-33. doi:10.1016/j.coph.2020.04.007

272. Quarona V, Zaccarello G, Chillemi A, et al. CD38 and CD157: a long journey from activation markers to multifunctional molecules. *Cytometry B Clin Cytom*. 2013;84(4):207-217. doi:10.1002/CYTO.B.21092

273. Luo L, Lucas RM, Liu L, Stow JL. Signalling, sorting and scaffolding adaptors for Toll-like receptors. *J Cell Sci*. Published online 2019. doi:10.1242/jcs.239194

274. Essuman K, Summers DW, Sasaki Y, Mao X, DiAntonio A, Milbrandt J. The SARM1 Toll/Interleukin-1 Receptor Domain Possesses Intrinsic NAD+ Cleavage Activity that Promotes Pathological Axonal Degeneration. *Neuron*. Published online 2017. doi:10.1016/j.neuron.2017.02.022

275. Chen YH, Sasaki Y, DiAntonio A, Milbrandt J. SARM1 is required in human derived sensory neurons for injury-induced and neurotoxic axon degeneration. *Exp Neurol*. Published online February 4, 2021:113636. doi:10.1016/j.expneurol.2021.113636

276. Viar K, Njoku D, McVoy JS, Oh U. Sarm1 knockout protects against early but not late axonal degeneration in experimental allergic encephalomyelitis. *PLoS One*. Published online 2020. doi:10.1371/journal.pone.0235110

277. Glowacki G, Braren R, Firner K, et al. The family of toxin-related ecto-ADP-ribosyltransferases in humans and the mouse. *Protein Sci*. 2002;11(7):1657. doi:10.1110/PS.0200602

278. Zolkiewska A, Nightingale MS, Moss J. Molecular characterization of NAD:arginine ADP-ribosyltransferase from rabbit skeletal muscle. *Proc Natl Acad Sci U S A*. 1992;89(23):11352-11356. doi:10.1073/pnas.89.23.11352

279. Hottiger MO, Hassa PO, Lüscher B, Schüler H, Koch-Nolte F. Toward a unified nomenclature for mammalian ADP-ribosyltransferases. *Trends Biochem Sci*. 2010;35(4):208-219. doi:10.1016/J.TIBS.2009.12.003

280. di Girolamo M, Fabrizio G. Overview of the mammalian ADP-ribosyl-transferases clostridia toxin-like (ARTCs) family. *Biochem Pharmacol*. 2019;167:86-96. doi:10.1016/J.BCP.2019.07.004

281. Paone G, Wada A, Stevens LA, et al. ADP ribosylation of human neutrophil peptide-1 regulates its biological properties. *Proc Natl Acad Sci U S A*. 2002;99(12):8231. doi:10.1073/PNAS.122238899

282. Paone G, Stevens LA, Levine RL, et al. ADP-ribosyltransferase-specific modification of human neutrophil peptide-1. *Journal of Biological Chemistry*. 2006;281(25):17054-17060. doi:10.1074/jbc.M603042200

283. Leutert M, Menzel S, Braren R, et al. Proteomic Characterization of the Heart and Skeletal Muscle Reveals Widespread Arginine ADP-Ribosylation by the ARTC1 Ectoenzyme. *Cell Rep*. 2018;24(7):1916-1929.e5. doi:10.1016/J.CELREP.2018.07.048

284. Fabrizio G, di Paola S, Stilla A, et al. ARTC1-mediated ADP-ribosylation of GRP78/BiP: A new player in endoplasmic-reticulum stress responses. *Cellular and Molecular Life Sciences*. 2015;72(6):1209-1225. doi:10.1007/s00018-014-1745-6

285. Zolkiewska A, Moss J. Integrin alpha 7 as substrate for a glycosylphosphatidylinositol-anchored ADP-ribosyltransferase on the surface of skeletal muscle cells. *Journal of Biological Chemistry*. 1993;268(34):25273-25276. doi:10.1016/S0021-9258(19)74388-9

286. Boulle N, Jones EM, Auguste P, Baird A. Adenosine diphosphate ribosylation of fibroblast growth factor-2. *Molecular Endocrinology*. 1995;9(6):767-775. doi:10.1210/MEND.9.6.8592522

287. Jones EM, Baird A. Cell-surface ADP-ribosylation of fibroblast growth factor-2 by an arginine-specific ADP-ribosyltransferase. *Biochemical Journal*. 1997;323(1):173-177. doi:10.1042/bj3230173

288. Saxty BA, Yadollahi-Farsani M, Upton PD, Johnstone SR, MacDermot J. Inactivation of platelet-derived growth factor-BB following modification by ADP-ribosyltransferase. *Br J Pharmacol*. 2001;133(8):1219-1226. doi:10.1038/sj.bjp.0704187

289. Wonigeit K, Dinkel A, Fangmann J, Thude H. Expression of the ectoenzyme RT6 is not restricted to resting peripheral T cells and is differently regulated in normal peripheral T cells, intestinal lEL, and NK cells. In: *Advances in Experimental Medicine and Biology*. Vol 419. Adv Exp Med Biol; 1997:229-240. doi:10.1007/978-1-4419-8632-0_28

290. Hong S, Brass A, Seman M, Haag F, Koch-Nolte F, Dubyak GR. Basal and inducible expression of the thiol-sensitive ART2.1 ecto-ADP-ribosyltransferase in myeloid and lymphoid leukocytes. *Purinergic Signal*. 2009;5(3):369. doi:10.1007/S11302-009-9162-2

291. Okamoto S, Azhipa O, Yu Y, Russo E, Dennert G. Expression of ADP-Ribosyltransferase on Normal T Lymphocytes and Effects of Nicotinamide Adenine Dinucleotide on Their Function. *The Journal of Immunology*. 1998;160(9).

292. Hollenberg SM, Weinberger C, Ong ES, et al. Primary structure and expression of a functional human glucocorticoid receptor cDNA. *Nature*. 1985;318(6047):635-641. doi:10.1038/318635A0

293. Oakleyt RH, Jewell CM, Yudt MR, Bofetiado DM, Cidlowski JA. The dominant negative activity of the human glucocorticoid receptor beta isoform. Specificity and mechanisms of action. *J Biol Chem*. 1999;274(39):27857-27866. doi:10.1074/JBC.274.39.27857

294. Vettorazzi S, Nalbantoglu D, Gebhardt JCM, Tuckermann J. A guide to changing paradigms of glucocorticoid receptor function—a model system for genome regulation and physiology. *FEBS J*. Published online 2021. doi:10.1111/FEBS.16100

295. Gjerstad JK, Lightman SL, Spiga F. Role of glucocorticoid negative feedback in the regulation of HPA axis pulsatility. *Stress*. 2018;21(5):403-416. doi:10.1080/10253890.2018.1470238

296. Monder C. The forms and functions of 11 beta-hydroxysteroid dehydrogenase. *J Steroid Biochem Mol Biol*. 1993;45(1-3):161-165. doi:10.1016/0960-0760(93)90136-K

297. Pratt WB, Toft DO. Regulation of signaling protein function and trafficking by the hsp90/hsp70-based chaperone machinery. *Exp Biol Med (Maywood)*. 2003;228(2):111-133. doi:10.1177/153537020322800201

298. Galigniana MD, Echeverría PC, Erlejman AG, Piwien-Pilipuk G. Role of molecular chaperones and TPR-domain proteins in the cytoplasmic transport of steroid receptors and their passage through the nuclear pore. *Nucleus*. 2010;1(4):299-308. doi:10.4161/NUCL.1.4.11743

299. Presman DM, Ganguly S, Schiltz RL, Johnson TA, Karpova TS, Hager GL. DNA binding triggers tetramerization of the glucocorticoid receptor in live

cells. *Proc Natl Acad Sci U S A*. 2016;113(29):8236-8241. doi:10.1073/PNAS.1606774113

300. Stahn C, Löwenberg M, Hommes DW, Buttgereit F. Molecular mechanisms of glucocorticoid action and selective glucocorticoid receptor agonists. *Mol Cell Endocrinol*. 2007;275(1-2):71-78. doi:10.1016/J.MCE.2007.05.019

301. Takahashi T, Kimoto T, Tanabe N, Hattori T aki, Yasumatsu N, Kawato S. Corticosterone acutely prolonged N-methyl-d-aspartate receptor-mediated Ca2+ elevation in cultured rat hippocampal neurons. *J Neurochem*. 2002;83(6):1441-1451. doi:10.1046/J.1471-4159.2002.01251.X

302. Urbach V, Walsh DE, Mainprice B, Bousquet J, Harvey BJ. Rapid non-genomic inhibition of ATP-induced Cl− secretion by dexamethasone in human bronchial epithelium. *J Physiol*. 2002;545(Pt 3):869. doi:10.1113/JPHYSIOL.2002.028183

303. Zhou J, Liu DF, Liu C, et al. Glucocorticoids inhibit degranulation of mast cells in allergic asthma via nongenomic mechanism. *Allergy*. 2008;63(9):1177-1185. doi:10.1111/J.1398-9995.2008.01725.X

304. Kong F, Liu Z, Jain VG, et al. Inhibition of IRAK1 Ubiquitination Determines Glucocorticoid Sensitivity for TLR9-Induced Inflammation in Macrophages. *J Immunol*. 2017;199(10):3654-3667. doi:10.4049/JIMMUNOL.1700443

305. Long F, Wang YX, Liu L, Zhou J, Cui RY, Jiang CL. Rapid nongenomic inhibitory effects of glucocorticoids on phagocytosis and superoxide anion production by macrophages. *Steroids*. 2005;70(1):55-61. doi:10.1016/J.STEROIDS.2004.10.004

306. Ghosh MC, Baatar D, Collins G, et al. Dexamethasone augments CXCR4-mediated signaling in resting human T cells via the activation of the Src kinase Lck. *Blood*. 2009;113(3):575-584. doi:10.1182/BLOOD-2008-04-151803

307. Löwenberg M, Verhaar AP, Bilderbeek J, et al. Glucocorticoids cause rapid dissociation of a T-cell-receptor-associated protein complex containing LCK and FYN. *EMBO Rep*. 2006;7(10):1023-1029. doi:10.1038/SJ.EMBOR.7400775

308. Demonacos C, Tsawdaroglou NC, Djordjevic-Markovic R, et al. Import of the glucocorticoid receptor into rat liver mitochondria in vivo and in vitro. *J Steroid Biochem Mol Biol*. 1993;46(3):401-413. doi:10.1016/0960-0760(93)90231-K

309. Psarra AMG, Sekeris CE. Glucocorticoids induce mitochondrial gene transcription in HepG2 cells: role of the mitochondrial glucocorticoid receptor. *Biochim Biophys Acta*. 2011;1813(10):1814-1821. doi:10.1016/J.BBAMCR.2011.05.014

310. Beaupere C, Liboz A, Fève B, Blondeau B, Guillemain G. Molecular Mechanisms of Glucocorticoid-Induced Insulin Resistance. *International Journal of Molecular Sciences 2021, Vol 22, Page 623*. 2021;22(2):623. doi:10.3390/IJMS22020623

311. Pecori Giraldi F, Pivonello R, Ambrogio AG, et al. The dexamethasone-suppressed corticotropin-releasing hormone stimulation test and the

desmopressin test to distinguish Cushing's syndrome from pseudo-Cushing's states. *Clin Endocrinol (Oxf)*. 2007;66(2):251-257. doi:10.1111/J.1365-2265.2006.02717.X

312. Löfberg E, Gutierrez A, Wernerman J, et al. Effects of high doses of glucocorticoids on free amino acids, ribosomes and protein turnover in human muscle. *Eur J Clin Invest*. 2002;32(5):345-353. doi:10.1046/J.1365-2362.2002.00993.X

313. Curtis JR, Westfall AO, Allison J, et al. Population-based assessment of adverse events associated with long-term glucocorticoid use. *Arthritis Rheum*. 2006;55(3):420-426. doi:10.1002/ART.21984

314. Gremlich S, Roduit R, Thorens B. Dexamethasone induces posttranslational degradation of GLUT2 and inhibition of insulin secretion in isolated pancreatic beta cells. Comparison with the effects of fatty acids. *J Biol Chem*. 1997;272(6):3216-3222. doi:10.1074/JBC.272.6.3216

315. Ranta F, Avram D, Berchtold S, et al. Dexamethasone induces cell death in insulin-secreting cells, an effect reversed by exendin-4. *Diabetes*. 2006;55(5):1380-1390. doi:10.2337/DB05-1220

316. Guo B, Zhang W, Xu S, Lou J, Wang S, Men X. GSK-3β mediates dexamethasone-induced pancreatic β cell apoptosis. *Life Sci*. 2016;144:1-7. doi:10.1016/J.LFS.2015.11.017

317. Avram D, Ranta F, Hennige AM, et al. IGF-1 protects against dexamethasone-induced cell death in insulin secreting INS-1 cells independent of AKT/PKB phosphorylation. *Cell Physiol Biochem*. 2008;21(5-6):455-462. doi:10.1159/000129638

318. Reich E, Tamary A, Vogt Sionov R, Melloul D. Involvement of thioredoxin-interacting protein (TXNIP) in glucocorticoid-mediated beta cell death. *Diabetologia*. 2012;55(4):1048-1057. doi:10.1007/S00125-011-2422-Z

319. Löfberg E, Gutierrez A, Wernerman J, et al. Effects of high doses of glucocorticoids on free amino acids, ribosomes and protein turnover in human muscle. *Eur J Clin Invest*. 2002;32(5):345-353. doi:10.1046/J.1365-2362.2002.00993.X

320. Curtis JR, Westfall AO, Allison J, et al. Population-based assessment of adverse events associated with long-term glucocorticoid use. *Arthritis Rheum*. 2006;55(3):420-426. doi:10.1002/ART.21984

321. Sakoda H, Ogihara T, Anai M, et al. Dexamethasone-induced insulin resistance in 3T3-L1 adipocytes is due to inhibition of glucose transport rather than insulin signal transduction. *Diabetes*. 2000;49(10):1700-1708. doi:10.2337/DIABETES.49.10.1700

322. Fain JN, Scow RO, Chernick SS. Effects of Glucocorticoids on Metabolism of Adipose Tissue in Vitro. *Journal of Biological Chemistry*. 1963;238(1):54-58. doi:10.1016/S0021-9258(19)83960-1

323. HÖPPNER W, SÜSSMUTH W, O'BRIEN C, SEITZ HJ, LUDA D, HARNEIT A. Cooperative effect of thyroid and glucocorticoid hormones on the induction of hepatic phosphoenolpyruvate carboxykinase in vivo and in cultured

hepatocytes. *Eur J Biochem*. 1986;159(2):399-405. doi:10.1111/J.1432-1033.1986.TB09882.X

324. Luan G, Li G, Ma X, et al. Dexamethasone-Induced Mitochondrial Dysfunction and Insulin Resistance-Study in 3T3-L1 Adipocytes and Mitochondria Isolated from Mouse Liver. *Molecules*. 2019;24(10). doi:10.3390/MOLECULES24101982

325. Guerriero V, Florini JR. Dexamethasone effects on myoblast proliferation and differentiation. *Endocrinology*. 1980;106(4):1198-1202. doi:10.1210/ENDO-106-4-1198

326. Han DS, Yang WS, Kao TW. Dexamethasone Treatment at the Myoblast Stage Enhanced C2C12 Myocyte Differentiation. *Int J Med Sci*. 2017;14(5):434-443. doi:10.7150/IJMS.18427

327. Lin JW, Huang YM, Chen YQ, et al. Dexamethasone accelerates muscle regeneration by modulating kinesin-1-mediated focal adhesion signals. *Cell Death Discovery 2021 7:1*. 2021;7(1):1-16. doi:10.1038/s41420-021-00412-4

328. Kun M, Mallidis C, Artaza J, Taylor W, Gonzalez-Cadavid N, Bhasin S. Characterization of 5'-regulatory region of human myostatin gene: regulation by dexamethasone in vitro. *Am J Physiol Endocrinol Metab*. 2001;281(6). doi:10.1152/AJPENDO.2001.281.6.E1128

329. Castillero E, Alamdari N, Lecker SH, Hasselgren PO. Suppression of atrogin-1 and MuRF1 prevents dexamethasone-induced atrophy of cultured myotubes. *Metabolism*. 2013;62(10):1495-1502. doi:10.1016/J.METABOL.2013.05.018

330. Schakman O, Kalista S, Barbé C, Loumaye A, Thissen JP. Glucocorticoid-induced skeletal muscle atrophy. *Int J Biochem Cell Biol*. 2013;45(10):2163-2172. doi:10.1016/J.BIOCEL.2013.05.036

331. Wang XJ, Xiao JJ, Liu L, Jiao HC, Lin H. Excessive glucocorticoid-induced muscle MuRF1 overexpression is independent of Akt/FoXO1 pathway. *Biosci Rep*. 2017;37(6). doi:10.1042/BSR20171056

332. Weinstein SP, Paquin T, Pritsker A, Haber RS. Glucocorticoid-induced insulin resistance: dexamethasone inhibits the activation of glucose transport in rat skeletal muscle by both insulin- and non-insulin-related stimuli. *Diabetes*. 1995;44(4):441-445. doi:10.2337/DIAB.44.4.441

333. Burén J, Lai YC, Lundgren M, Eriksson JW, Jensen J. Insulin action and signalling in fat and muscle from dexamethasone-treated rats. *Arch Biochem Biophys*. 2008;474(1):91-101. doi:10.1016/J.ABB.2008.02.034

334. Salamone IM, Quattrocelli M, Barefield DY, et al. Intermittent glucocorticoid treatment enhances skeletal muscle performance through sexually dimorphic mechanisms. *J Clin Invest*. 2022;132(6). doi:10.1172/JCI149828

335. Cobley JN, Sakellariou GK, Murray S, et al. Lifelong endurance training attenuates age-related genotoxic stress in human skeletal muscle. *Longev Healthspan*. 2013;2(1). doi:10.1186/2046-2395-2-11

336. Yaffe D, Saxel O. Serial passaging and differentiation of myogenic cells isolated from dystrophic mouse muscle. *Nature*. 1977;270(5639):725-727. doi:10.1038/270725A0

337. Zhu CH, Mouly V, Cooper RN, et al. Cellular senescence in human myoblasts is overcome by human telomerase reverse transcriptase and cyclin-dependent kinase 4: consequences in aging muscle and therapeutic strategies for muscular dystrophies. *Aging Cell*. 2007;6(4):515-523. doi:10.1111/J.1474-9726.2007.00306.X

338. Tan B, Dong S, Shepard RL, et al. Inhibition of Nicotinamide Phosphoribosyltransferase (NAMPT), an Enzyme Essential for NAD+ Biosynthesis, Leads to Altered Carbohydrate Metabolism in Cancer Cells. *J Biol Chem*. 2015;290(25):15812. doi:10.1074/JBC.M114.632141

339. Timmermans S, Souffriau J, Libert C. A general introduction to glucocorticoid biology. *Front Immunol*. 2019;10(JULY):1545. doi:10.3389/FIMMU.2019.01545/BIBTEX

340. Bray NL, Pimentel H, Melsted P, Pachter L. Near-optimal probabilistic RNA-seq quantification. *Nature Biotechnology 2016 34:5*. 2016;34(5):525-527. doi:10.1038/nbt.3519

341. Ritchie ME, Phipson B, Wu D, et al. limma powers differential expression analyses for RNA-sequencing and microarray studies. *Nucleic Acids Res*. 2015;43(7):e47. doi:10.1093/NAR/GKV007

342. Subramanian A, Tamayo P, Mootha VK, et al. Gene set enrichment analysis: A knowledge-based approach for interpreting genome-wide expression profiles. *Proc Natl Acad Sci U S A*. 2005;102(43):15545-15550. doi:10.1073/PNAS.0506580102/SUPPL_FILE/06580FIG7.JPG

343. Raudvere U, Kolberg L, Kuzmin I, et al. g:Profiler: a web server for functional enrichment analysis and conversions of gene lists (2019 update). *Nucleic Acids Res*. 2019;47(W1):W191-W198. doi:10.1093/NAR/GKZ369

344. Aguilan JT, Kulej K, Sidoli S. Guide for protein fold change and p-value calculation for non-experts in proteomics. *Mol Omics*. 2020;16(6):573-582. doi:10.1039/D0MO00087F

345. Veliça P, Bunce CM. A quick, simple and unbiased method to quantify C2C12 myogenic differentiation. *Muscle Nerve*. 2011;44(3):366-370. doi:10.1002/MUS.22056

346. Graeff R, Lee HC. A novel cycling assay for cellular cADP-ribose with nanomolar sensitivity. *Biochemical Journal*. 2002;361(Pt 2):379. doi:10.1042/BJ3610379

347. Braun TP, Marks DL. The regulation of muscle mass by endogenous glucocorticoids. *Front Physiol*. 2015;6(FEB):12. doi:10.3389/FPHYS.2015.00012/BIBTEX

348. Li CI, Li TC, Lin WY, et al. Combined association of chronic disease and low skeletal muscle mass with physical performance in older adults in the Sarcopenia and Translational Aging Research in Taiwan (START) study. *BMC Geriatr*. 2015;15(1). doi:10.1186/S12877-015-0011-6

349. Luongo TS, Eller JM, Lu MJ, et al. SLC25A51 is a mammalian mitochondrial NAD+ transporter. *Nature*. 2020;588(7836):174. doi:10.1038/S41586-020-2741-7

350. Wahlberg E, Karlberg T, Kouznetsova E, et al. Family-wide chemical profiling and structural analysis of PARP and tankyrase inhibitors. *Nat Biotechnol*. 2012;30(3):283-288. doi:10.1038/NBT.2121

351. Eltze T, Boer R, Wagner T, et al. Imidazoquinolinone, imidazopyridine, and isoquinolindione derivatives as novel and potent inhibitors of the poly(ADP-ribose) polymerase (PARP): a comparison with standard PARP inhibitors. *Mol Pharmacol*. 2008;74(6):1587-1598. doi:10.1124/MOL.108.048751

352. Kitamura T, Kitamura YI, Funahashi Y, et al. A Foxo/Notch pathway controls myogenic differentiation and fiber type specification. *Journal of Clinical Investigation*. 2007;117(9):2477-2485. doi:10.1172/JCI32054

353. Zhang H, Shang R, Bi P. Feedback regulation of Notch signaling and myogenesis connected by MyoD-Dll1 axis. *PLoS Genet*. 2021;17(8). doi:10.1371/JOURNAL.PGEN.1009729

354. Zhang L, Li DQ. MORC2 regulates DNA damage response through a PARP1-dependent pathway. *Nucleic Acids Res*. 2019;47(16):8502-8520. doi:10.1093/NAR/GKZ545

355. Gatti M, Imhof R, Huang Q, Baudis M, Altmeyer M. The Ubiquitin Ligase TRIP12 Limits PARP1 Trapping and Constrains PARP Inhibitor Efficiency. *Cell Rep*. 2020;32(5). doi:10.1016/J.CELREP.2020.107985

356. Fulco M, Cen Y, Zhao P, et al. Glucose restriction inhibits skeletal myoblast differentiation by activating SIRT1 through AMPK-mediated regulation of Nampt. *Dev Cell*. 2008;14(5):661-673. doi:10.1016/J.DEVCEL.2008.02.004

357. Hong J, Kim BW, Choo HJ, et al. Mitochondrial complex I deficiency enhances skeletal myogenesis but impairs insulin signaling through SIRT1 inactivation. *J Biol Chem*. 2014;289(29):20012-20025. doi:10.1074/JBC.M114.560078

358. Luo W, Ai L, Wang B fa, Zhou Y. High glucose inhibits myogenesis and induces insulin resistance by down-regulating AKT signaling. *Biomed Pharmacother*. 2019;120. doi:10.1016/J.BIOPHA.2019.109498

359. Andrabi SA, Umanah GKE, Chang C, et al. Poly(ADP-ribose) polymerase-dependent energy depletion occurs through inhibition of glycolysis. *Proc Natl Acad Sci U S A*. 2014;111(28):10209-10214. doi:10.1073/PNAS.1405158111/SUPPL_FILE/PNAS.201405158SI.PDF

360. Fouquerel E, Goellner EM, Yu Z, et al. ARTD1/PARP1 negatively regulates glycolysis by inhibiting hexokinase 1 independent of NAD+ depletion. *Cell Rep*. 2014;8(6):1819-1831. doi:10.1016/J.CELREP.2014.08.036

361. Rajamohan SB, Pillai VB, Gupta M, et al. SIRT1 promotes cell survival under stress by deacetylation-dependent deactivation of poly(ADP-ribose) polymerase 1. *Mol Cell Biol*. 2009;29(15):4116-4129. doi:10.1128/MCB.00121-09

362. Hubbard BP, Sinclair DA. Small molecule SIRT1 activators for the treatment of aging and age-related diseases. *Trends Pharmacol Sci*. 2014;35(3):146. doi:10.1016/J.TIPS.2013.12.004

363. Quattrocelli M, Barefield DY, Warner JL, et al. Intermittent glucocorticoid steroid dosing enhances muscle repair without eliciting muscle atrophy. *J Clin Invest*. 2017;127(6):2418-2432. doi:10.1172/JCI91445

364. Drazen DL, Bilu D, Edwards N, Nelson RJ. Disruption of poly (ADP-ribose) polymerase (PARP) protects against stress-evoked immunocompromise. *Molecular Medicine*. 2001;7(11):761. doi:10.1007/bf03401966

365. Trotter KW, King HA, Archer TK. Glucocorticoid Receptor Transcriptional Activation via the BRG1-Dependent Recruitment of TOP2β and Ku70/86. *Mol Cell Biol*. 2015;35(16):2799-2817. doi:10.1128/MCB.00230-15

366. Reimand J, Kull M, Peterson H, Hansen J, Vilo J. g:Profiler—a web-based toolset for functional profiling of gene lists from large-scale experiments. *Nucleic Acids Res*. 2007;35(Web Server issue):W193. doi:10.1093/NAR/GKM226

367. Martí JM, Garcia-Diaz A, Delgado-Bellido D, et al. Selective modulation by PARP-1 of HIF-1α-recruitment to chromatin during hypoxia is required for tumor adaptation to hypoxic conditions. *Redox Biol*. 2021;41:101885. doi:10.1016/J.REDOX.2021.101885

368. Caria F, Cescon M, Gualandi F, et al. Autosomal recessive Bethlem myopathy: A clinical, genetic and functional study. *Neuromuscul Disord*. 2019;29(9):657-663. doi:10.1016/J.NMD.2019.07.007

369. Wang C, Qu C, Alippe Y, et al. Poly-ADP-ribosylation-mediated degradation of ARTD1 by the NLRP3 inflammasome is a prerequisite for osteoclast maturation. *Cell Death Dis*. 2016;7(3). doi:10.1038/CDDIS.2016.58

370. Zhang D, Hu X, Li J, et al. DNA damage-induced PARP1 activation confers cardiomyocyte dysfunction through NAD+ depletion in experimental atrial fibrillation. *Nat Commun*. 2019;10(1). doi:10.1038/S41467-019-09014-2

371. Wang H, Hertlein E, Bakkar N, et al. NF-kappaB regulation of YY1 inhibits skeletal myogenesis through transcriptional silencing of myofibrillar genes. *Mol Cell Biol*. 2007;27(12):4374-4387. doi:10.1128/MCB.02020-06

372. Guttridge DC, Albanese C, Reuther JY, Pestell RG, Albert S. Baldwin Jr. NF-κB Controls Cell Growth and Differentiation through Transcriptional Regulation of Cyclin D1. *Mol Cell Biol*. 1999;19(8):5785. doi:10.1128/MCB.19.8.5785

373. Ilias I, Milionis C, Zoumakis E. An Overview of Glucocorticoid-Induced Osteoporosis. *Journal of Clinical Rheumatology*. 2022;5(5 SUPPL.). Accessed October 7, 2022. https://www.ncbi.nlm.nih.gov/books/NBK278968/

374. Cerquone Perpetuini A, Giuliani G, Reggio A, et al. Janus effect of glucocorticoids on differentiation of muscle fibro/adipogenic progenitors. *Scientific Reports 2020 10:1*. 2020;10(1):1-18. doi:10.1038/s41598-020-62194-6

375. Lawal TA, Todd JJ, Meilleur KG. Ryanodine Receptor 1-Related Myopathies: Diagnostic and Therapeutic Approaches. *Neurotherapeutics*. 2018;15(4):885. doi:10.1007/S13311-018-00677-1

376. Lee CS, Yi JS, Jung SY, et al. TRIM72 negatively regulates myogenesis via targeting insulin receptor substrate-1. *Cell Death Differ*. 2010;17(8):1254-1265. doi:10.1038/CDD.2010.1

377. Ishiwata-Endo H, Kato J, Tonouchi A, et al. Role of a TRIM72 ADP-ribosylation cycle in myocardial injury and membrane repair. *JCI Insight*. 2018;3(22). doi:10.1172/JCI.INSIGHT.97898

378. Lee C, Cederberg RA, White BR. Poly [ADP-Ribose] Polymerase-1 (PARP-1) Confers Glucocorticoid Responsiveness of the Porcine GnRH Receptor (GnRHR) Gene. *Biol Reprod*. 2011;85(Suppl_1):2-2. doi:10.1093/BIOLREPROD/85.S1.2

379. Zielinska AE, Walker EA, Stewart PM, Lavery GG. Biochemistry and physiology of hexose-6-phosphate knockout mice. *Mol Cell Endocrinol*. 2011;336(1-2):213-218. doi:10.1016/J.MCE.2010.12.004

380. Draper N, Walker EA, Bujalska IJ, et al. Mutations in the genes encoding 11β-hydroxysteroid dehydrogenase type 1 and hexose-6-phosphate dehydrogenase interact to cause cortisone reductase deficiency. *Nature Genetics 2003 34:4*. 2003;34(4):434-439. doi:10.1038/ng1214

381. White PC, Rogoff D, McMillan DR, Lavery GG. Hexose 6-phosphate dehydrogenase (H6PD) and corticosteroid metabolism. *Mol Cell Endocrinol*. 2007;265-266(SUPPL.):89-92. doi:10.1016/J.MCE.2006.12.022

382. Bujalska IJ, Hewitt KN, Hauton D, et al. Lack of Hexose-6-Phosphate Dehydrogenase Impairs Lipid Mobilization from Mouse Adipose Tissue. *Endocrinology*. 2008;149(5):2584-2591. doi:10.1210/EN.2007-1705

383. Lavery GG, Zielinska AE, Gathercole LL, et al. Lack of Significant Metabolic Abnormalities in Mice with Liver-Specific Disruption of 11β-Hydroxysteroid Dehydrogenase Type 1. *Endocrinology*. 2012;153(7):3236-3248. doi:10.1210/EN.2012-1019

384. Semjonous NM, Sherlock M, Jeyasuria P, et al. Hexose-6-Phosphate Dehydrogenase Contributes to Skeletal Muscle Homeostasis Independent of 11β-Hydroxysteroid Dehydrogenase Type 1. *Endocrinology*. 2011;152(1):93-102. doi:10.1210/EN.2010-0957

385. Zielinska AE, Fletcher RS, Sherlock M, Doig CL, Lavery GG. Cellular and genetic models of H6PDH and 11β-HSD1 function in skeletal muscle. *Cell Biochem Funct*. 2017;35(5):269. doi:10.1002/CBF.3272

386. Aguilar CA, Shcherbina A, Ricke DO, et al. In vivo Monitoring of Transcriptional Dynamics After Lower-Limb Muscle Injury Enables Quantitative Classification of Healing. *Scientific Reports 2015 5:1*. 2015;5(1):1-17. doi:10.1038/srep13885

387. Imai S ichiro. “Clocks” in the NAD World: NAD as a Metabolic Oscillator for the Regulation of Metabolism and Aging. *Biochim Biophys Acta*. 2010;1804(8):1584. doi:10.1016/J.BBAPAP.2009.10.024

388. Nakahata Y, Sahar S, Astarita G, Kaluzova M, Sassone-Corsi P. Circadian control of the NAD+ salvage pathway by CLOCK-SIRT1. *Science*. 2009;324(5927):654-657. doi:10.1126/SCIENCE.1170803

389. Cartwright DM. Investigating the physiological and functional roles of the nicotinamide riboside kinase pathway in skeletal muscle. Published online 2021. Accessed December 21, 2022. http://etheses.bham.ac.uk//id/eprint/11685/

390. Aprile-Garcia F, Antunica-Noguerol M, Budziñski ML, Liberman AC, Arzt E. Novel insights into the neuroendocrine control of inflammation: the role of GR and PARP1. *Endocr Connect*. 2014;3(1):R1. doi:10.1530/EC-13-0079

391. Kamaletdinova T, Fanaei-Kahrani Z, Wang ZQ. The Enigmatic Function of PARP1: From PARylation Activity to PAR Readers. *Cells*. 2019;8(12). doi:10.3390/CELLS8121625

392. Sun Y, Chen J, Huang S yin N, et al. PARylation prevents the proteasomal degradation of topoisomerase I DNA-protein crosslinks and induces their deubiquitylation. *Nature Communications 2021 12:1*. 2021;12(1):1-16. doi:10.1038/s41467-021-25252-9

393. Wallace AD, Cidlowski JA. Proteasome-mediated Glucocorticoid Receptor Degradation Restricts Transcriptional Signaling by Glucocorticoids. *Journal of Biological Chemistry*. 2001;276(46):42714-42721. doi:10.1074/jbc.M106033200

394. Challa S, Ryu KW, Whitaker AL, Abshier JC, Camacho C v., Kraus WL. Development and characterization of new tools for detecting poly(ADP-ribose) in vitro and in vivo. *Elife*. 2022;11. doi:10.7554/ELIFE.72464

395. Knezevic CE, Wright G, Remsing Rix LL, et al. Proteome-wide profiling of clinical PARP inhibitors reveals compound-specific secondary targets. *Cell Chem Biol*. 2016;23(12):1490. doi:10.1016/J.CHEMBIOL.2016.10.011

396. Ménissier De Murcia J, Niedergang C, Trucco C, et al. Requirement of poly(ADP-ribose) polymerase in recovery from DNA damage in mice and in cells. *Proc Natl Acad Sci U S A*. 1997;94(14):7303. doi:10.1073/PNAS.94.14.7303

397. Zhang N, Zhang Y, Qian H, Wu S, Cao L, Sun Y. Selective targeting of ubiquitination and degradation of PARP1 by E3 ubiquitin ligase WWP2 regulates isoproterenol-induced cardiac remodeling. *Cell Death Differ*. 2020;27(9):2605-2619. doi:10.1038/S41418-020-0523-2

398. Qian H, Zhang N, Wu B, et al. The E3 ubiquitin ligase Smurf2 regulates PARP1 stability to alleviate oxidative stress-induced injury in human umbilical vein endothelial cells. *J Cell Mol Med*. 2020;24(8):4600-4611. doi:10.1111/JCMM.15121

399. Cui Z, Hwang SM, Gomes A v. Identification of the Immunoproteasome as a Novel Regulator of Skeletal Muscle Differentiation. *Mol Cell Biol*. 2014;34(1):96. doi:10.1128/MCB.00622-13

400. Sun Q, Gatie MI, Kelly GM. Serum-dependent and -independent regulation of PARP2. *Biochem Cell Biol*. 2019;97(5):600-611. doi:10.1139/BCB-2018-0345

401. Miwa M, Ida C, Yamashita S, et al. In Vivo Level of Poly(ADP-ribose). *Challenges 2018, Vol 9, Page 23*. 2018;9(1):23. doi:10.3390/CHALLE9010023